Neuronal and ionic mechanisms of oxaliplatin-induced hypersensitivities and paraesthesias

Saleque, Nurjahan

Awarding institution:
King's College London

Neuronal and ionic mechanisms of oxaliplatin-induced hypersensitivities and paraesthesias

Thesis submitted for the degree of

Doctor of Philosophy

King's College London

Nurjahan Saleque

Wolfson Centre for Age-Related Diseases

Institute of Psychiatry, Psychology & Neuroscience

King's College London

2016-2021

Abstract

Oxaliplatin is an effective anti-cancer drug for the treatment of colorectal cancer and other solid tumours. However, the compound is associated with dose-limiting effects. Uniquely for oxaliplatin, patients report acute cold-evoked paraesthesias and cold allodynia during or immediately after infusion of the drug. In addition, everyday tasks such as buttoning shirts, fastening zips and touching cool surfaces is associated with discomfort and pain. A chronic neuropathy develops over repeated cycles of treatment with a stocking-and-glove distribution. The aim of my project was to identify novel neuronal and ionic mechanisms in acute oxaliplatin-induced hypersensitivities and paraesthesias. The six resulting chapters focus on *in vivo*, *in vitro* and *ex vivo* mechanistic studies of oxaliplatin-induced neuropathy.

We examined the effects of oxaliplatin *in vivo* and established a translational mouse model. From this, we were able to isolate DRG neurons for mechanistic *in vitro* studies using $[Ca^{2+}]_i$ imaging. We observed a modestly increased cold sensitivity in isolated neurons from treated mice, and in naïve DRG neurons treated with oxaliplatin. Oxaliplatin also directly activated a very small proportion of neurons. However, these effects appeared unlikely to accurately reflect the proportion of neurons responsible for the symptoms observed in mice *in vivo* or those reported by patients in the clinic. Therefore, we used the skin-saphenous nerve preparation to record the activity of single afferent nerve fibres stimulated at the peripheral nerve terminal.

Acute and direct oxaliplatin treatment sensitised all A fibre classes to cold ramps and notably, resulted in cold-evoked action potential bursts. In addition, novel cold-evoked responses were seen in normally cold-insensitive C fibres. Oxaliplatin also changed the adaptation

properties of all A fibres, such that impulses and action potential bursts were displayed outside mechanical application periods. Interestingly, the acute effects of oxaliplatin at the nerve terminal level was different to recordings made in fibres from oxaliplatin-treated mice. Here, we showed increased spontaneous activity and C fibres being most affected by cold ramps, rather than A fibres. It is likely that differences in the duration and effective concentration of oxaliplatin exposure may explain at least part of these differences.

In order to identify novel ion channel targets involved in oxaliplatin evoked hyperexcitability, we used a multielectrode array in a 48-well assay format to study cultured cortical neurons. Oxaliplatin produced a concentration-dependent increase in network bursts in these cultures. In addition, we identified a novel voltage-gated potassium channel ($K_v2.1$) that is required for oxaliplatin-induced excitability. We demonstrate that inhibition of $K_v2.1$ fully reversed oxaliplatin-induced cold hypersensitivity *in vivo* and in single fibre recordings in naïve and treated preparations. Oxaliplatin also directly produced a hyperpolarising shift of the $K_v2.1$ channel activation kinetics by ~9 mV, in patch-clamp experiments of *Kcnb1* transfected HEK293 cells. Finally, we report that oxaliplatin produced reversible and irreversible oxidation of cysteine residues in the model protein, human serum albumin. We hypothesise that such covalent modification are likely to be central for the side effects produced by oxaliplatin, and may also be responsible for the positive modulation of $K_v2.1$ described here. However, further experiments are required to confirm this. We have comprehensively assessed the effect of oxaliplatin acute and chronic treatment on peripheral sensory neurons and identified possible mechanisms that underlie acute neuropathy.

Acknowledgements

I would like to thank David, my primary supervisor for this PhD opportunity and for the many pep talks along this journey. I have loved being part of the Andersson/Bevan labs and feel grateful to have worked alongside such a great team. I would also like to thank Stuart for welcoming me into this lab 6 years ago! I have learned so much under your guidance and mentorship, which have shaped my personal and professional development. Clive, I want to thank you for always making me laugh on tough days and for all your help with behavioural assays. I will miss your stories about weird and wonderful people you've met in research, and hope that I can be one of them! I would also like to thank Anne-Marie and Anna for their support and guidance during my time spent at Evotec.

A special shoutout and thank you to my good friend and mentor, Nisha, for her patience and calm when teaching me the skin-nerve dissection. I could not have done this without you and I thank you for your kindness and support in science and life. I would like to thank my good friend and fellow biscuit, Tilly, for her patience, unrelenting support and keen interest in driving this project into new and exciting directions. Thank you for helping me with experiments and my thesis. You deserve a very long break, my friend! Omar, Ulku, Runisha, Yaz and Vin, I had the best PhD experience with you all as my dear friends. Thank you for the laughs, coffee and memories! Eva, I can't believe our four years together have come to an end. We made it! I wish you all the best in the future. Ivona and Margot thank you for making the office and lab a positive place to work in and for all the snacks! Thank you to Talisia for being my friend and for your support in the early years of my PhD.

I would like to thank my friends, Manal, Saf, Anisah and Tam for keeping me sane over the years and always believing in me. I could not have done it without you all. A big thank you to my siblings, Sharmin, Qaiyum and Hamida for all the love and free entertainment throughout the years. You all are the best! To Nasif Ismail Mugisha (full name just for you), thank you for always believing in me and for being my best friend. Your unwavering support and kindness makes me feel like I can achieve anything.

Finally, my heartfelt thanks to my parents, Rowshan and Abdus, to whom I dedicate my thesis. Without you, none of this would have been possible. Thank you for your endless love, support and sacrifice. Everything I am, I owe to you both.

Table of Contents

Table of Figures

Table of Tables

Table of Schematics

1. General Introduction

1.1 Introduction to sensation

The ability to detect and respond to external stimuli is crucial for an organism's survival. Aristotle first characterised the five exteroceptive senses in humans in De Anima, book II. These five senses include sight, hearing, smell, touch and taste (Damann et al., 2008). In addition to sensing the outside world, humans can also perceive sensations which arise internally through interoceptive senses. The third major function of the somatosensory system is proprioception, for the perception and control of body position and balance (Abraira and Ginty, 2013).

1.2 The somatosensory nervous system

Sensory nerves detect stimuli within internal and external environments and convey this information to the central nervous system (CNS) for a range of sensory modalities. Mechanical sensations such as touch, pressure and vibration and additional sensations such as temperature and pain are all processed by the somatosensory nervous system.

The anatomical organisation of the somatosensory nervous system consists of a pathway of three orders of neurons. The first order neuron or primary afferent neuron innervates target organs in the periphery. The second order neuron is located within the spinal cord or brainstem and relays information to a third order neuron within the brain.

1.3 The primary afferent neuron

Primary afferent neurons are pseudounipolar and are composed of two axonal branches (Figure 1-1), a branch which innervates target tissue distally and a central branch which synapses onto second order neurons located within the dorsal horn of the spinal cord or the brainstem. The cell bodies of primary afferent neurons which innervate the body are located

within the dorsal root ganglia (DRG). In contrast, sensory neurons which innervate the face, head and neck regions have cell bodies located within the trigeminal ganglia (TG).

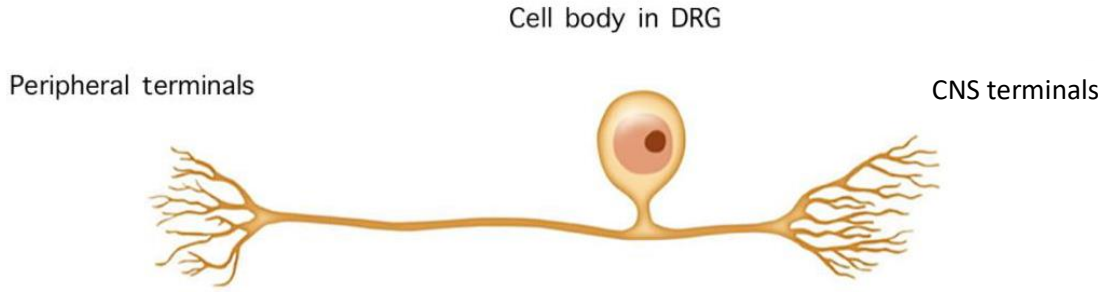

Figure 1-1 The pseudo-unipolar sensory neuron.

The pseudo-unipolar sensory neuron has its cell body (soma) located inside the DRG from where an axon projects and splits into two branches, a central branch that goes to the spinal cord level (CNS) to form synapses with other neurons, and a peripheral branch that forms the peripheral nerve terminals at the target organ level (i.e. skin, joint, muscle). Modified from Monica Schroeder/Science source.

1.3.1 Sensory modalities

Charles Bell (1774-1842), a Scottish physician in the nineteenth century was amongst the first in a group of scientists to propose the idea that sensory nerves were modality specific. The concept of specificity of cutaneous sensation was developed further by Johannes Müller (1801-1858) when he formulated the 'law of specific energies.' This law stated that the perception of a sense was determined by the pathway which carried it, rather than the stimulus which evoked it (Norrsell et al., 1999).

Further work into understanding cutaneous sensation was conducted by Magnus Blix, Alfred Goldscheider and Henry Donaldson. All three researchers independently published papers in the 1880's describing their work on the discoveries of distinct cutaneous spots which were selective for specific sensory modalities such as pain, touch, warm and cool (Norrsell et al., 1999). This work was supported by the Austrian-German physiologist Max Von Frey (1852-1932) who mapped out these punctate cutaneous spots on the skin and studied their density in various places on the body (Norrsell et al., 1999). It is now understood that different primary afferent neurons are sensitive to one or more sensory modalities. Nerve fibres are classified according to the sensory modalities that they transduce and can as a result be broadly categorised as mechanoreceptors, thermoreceptors and nociceptors.

1.3.2 Primary afferent nerve fibre types

Primary afferent fibres are classified based on their degree of myelination, axonal conduction velocities, cell body size and axon diameter (Abraira and Ginty, 2013; Bessou and Perl, 1969; Li et al., 2011; Smith and Lewin, 2009; Zimmermann et al., 2009). Many studies have shown that primary afferent fibres can be grouped into distinct functional subpopulations (Figure 1-

2) on the basis of their receptive field properties (Koltzenburg et al., 1997). This is supported by the human experience of distinct sensations such as light touch, vibration, pressure and pain when axons of functionally different subpopulations of sensory neurons are stimulated electrically (Koltzenburg et al., 1997; Torebjörk et al., 1987).

Aα fibres have very large-diameter (15-20 μm), thickly myelinated axons, which are responsible for signalling proprioceptive information. Aβ fibres are large-diameter (5-15 μm), myelinated axons that have low mechanical thresholds and respond to innocuous mechanical stimuli such as light touch (Abraira and Ginty, 2013). Aβ fibres have fast conduction velocities which vary across species and is ~50 m/s in humans and > 10 m/s in mice (Koltzenburg et al., 1997). Aδ fibres are thinly myelinated, medium-diameter (1-5 μm) afferents and have a slower conduction velocity than Aβ fibres. Aδ fibres are involved in thermosensing, nociception, and mechanosensation.

C fibres are unmyelinated, small-diameter (< 1 μm) axons fibres and have very slow conduction velocities. C fibres are principally involved in the detection of temperature and pain, and are commonly described as polymodal receptors (Basbaum et al., 2009; Purves et al., 2001). C fibres are sensitive to mechanical and heat stimuli (CMH), or mechanical and cold stimuli (CMC) or even mechanical, heat and cold stimuli (CMHC). There is also a population of C fibres that are insensitive to mechanical or thermal stimuli under normal physiological conditions, but can become sensitised during various pathophysiological changes e.g. inflammatory sensitisation (Dubin and Patapoutian, 2010).

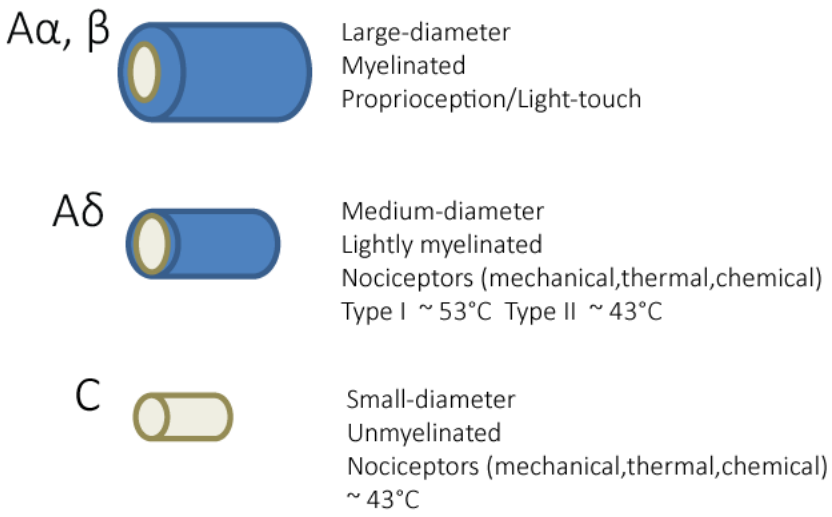

Figure 1-2 Three classes of primary afferent nerve fibres expressed in mice.

The properties of Aβ, Aδ and C primary afferent nerve fibres. Adapted from (Julius and Basbaum, 2001).

Although Aδ and C fibres are commonly classified as nociceptors, there is a proportion of low threshold mechanoreceptors in each of the sensory fibre classes; the Down-hair (D-hair) and C-low-threshold mechanoreceptor (C-LTMR) respectively. These fibres are sensitive to innocuous stimuli, mainly light touch (Brown and Iggo, 1967). C-LTMRs are activated by brush and tactile stimuli. They are particularly important in responding to pleasurable touch sensations such as caressing and stroking (Olausson et al., 2010; Reynders et al., 2015; Seal et al., 2009). C-LTMRs also contribute to touch hypersensitivity after injury (Delfini et al., 2013; Reynders et al., 2015; Seal et al., 2009). Recent findings have also shown that D-hair fibres can become sensitised to influence or produce pain in pathophysiological states (Dawes et al., 2018).

1.3.3 Psychophysical studies characterising the properties of primary afferent neurons

In 1894, Max Von Frey discovered discrete pain points in the human skin by probing subjects at varying intensities. This led to the mapping of distinct spots in the human skin which were responsible for detecting different sensory modalities and this specificity was attributed to the existence of specific receptors beneath these spots. Further to these findings, Von Frey also suggested that the sensation of pain was associated with unencapsulated free nerve endings (Norrsell et al., 1999). Sherrington corroborated these findings in his own work and showed that these free nerve endings were either thinly myelinated or unmyelinated.

In 1922, Gasser and Erlanger successfully recorded the compound action potential (CAP) for the first time (Gasser and Erlanger, 1922). They later went onto describing the relationship between the diameter of a nerve fibre and its conduction velocity in the CAP, which won them the Nobel Prize (Gasser and Erlanger, 1927). Studies on the CAP revealed that larger fibres

required lower electrical threshold for activation and had faster conduction velocities when compared to smaller fibres (Gasser and Erlanger, 1927, 1929a). This led to the full characterisation and roles of different sized afferent fibres, with large-diameter fibres being associated with tactile sensation and small-diameter fibres being important in temperature and pain sensations (Kruger et al., 1981).

Major advancements were made by Adrian and Zotterman in 1926, who demonstrated a novel method to record from single afferent nerve fibres in the cat (Adrian and Zotterman, 1926). This allowed the properties of fibres to be investigated, including adaptation properties and frequency of discharges to various mechanical stimuli (Adrian and Zotterman, 1926). Since this, many studies have investigated the properties of afferent neurons. It is possible to record from individual afferent fibres and characterise them according to their adaptation properties and responses to electrical and thermal stimuli (Reeh, 1986).

Substantial investigations of cutaneous sensation were conducted by Edward Perl and colleagues in the late 1960s and early 1970s. Electrophysiological recordings made in cats and primates characterised the properties of nociceptors, that were activated upon application of noxious stimuli but remained inactive to innocuous stimuli (Burgess and Perl, 1967; Perl, 1968). This work was particularly important in distinguishing the unique properties such as very slow conduction velocities, high mechanical thresholds and temperature sensitivity of unmyelinated C fibres from known classes of nociceptive and non-nociceptive myelinated fibres (Bessou and Perl, 1969; Brown and Iggo, 1967; Burgess and Perl, 1967; Perl, 1968).

1.4 Mammalian glabrous vs hairy skin

The skin is the largest organ and mediates our sense of touch. The skin is neurophysiologically complex as it is innervated by a plethora of sensory neuron subtypes including nociceptors, pruriceptors, which convey itch, thermoreceptors and low-threshold mechanoreceptors (LTMRs) (Abraira and Ginty, 2013; Lumpkin et al., 2010; Reynders et al., 2015; Zimmerman et al., 2014). The sense of touch allows mammals to recognise and manipulate objects. Anatomically, there are a multitude of skin type specialisations that are innervated by a wide array of sensory neuron subtypes, creating a diversity of functions of touch neurons (Lumpkin et al., 2010; Owens and Lumpkin, 2014; Zimmerman et al., 2014).

Mammalian skin can be divided into hairy and glabrous (non-hairy) skin (Figure 1-3). Glabrous skin is predominantly found on the hands and feet of mammals and is specialised for discriminative touch, determining texture and shape to recognise objects which then provides feedback to the CNS to provide the required responses such as grip control and locomotion (Zimmerman et al., 2014). Hairy skin covers most of the body surface (90 %) and also has a discriminative touch role, but with lower spatial acuity compared to glabrous skin. Hairy skin is particularly important for affective touch – touch that evokes an emotional responses such as during nurturing (Abraira and Ginty, 2013; Lumpkin et al., 2010).

There are four types of mechanosensory end organs located within the glabrous skin: Pacinian corpuscles, Ruffini endings, Meissner corpuscles and Merkel's discs. Hair follicles are also considered to be specialised mechanosensory organs (Abraira and Ginty, 2013). Three major hair types have been identified in mouse hairy skin including zigzag, awl/auchene and guard cells which differ in their abundance, length and LTMR subtype innervation (Li et al., 2011).

Importantly, glabrous and hairy skin are comprised of morphologically distinct but highly specialised mechanosensory organs which are capable of mediating unique aspects of touch.

1.4.1 Cutaneous mechanoreceptors

LTMRs are a heterogeneous group of sensory neurons and are divided into subtypes according to their sensitivities, conduction velocities and adaptation properties to sustained mechanical stimulation (Zimmerman et al., 2014). There are two main types of Aβ LTMRs; slowly adapting (SA) and rapidly adapting (RA). SA touch receptors are indentation detectors and fire continuously during a sustained stimulus, whereas RA touch receptors are velocity detectors that respond only to the onset and offset of mechanical stimuli (Zimmerman et al., 2014). The population of LTMRs in the glabrous skin is different to those that are found in the hairy skin due to the anatomical structures present and the physiological functions required from these mechanoreceptors. Hairy skin is important in affective touch, whereas glabrous skin, which has a thicker epidermal layer, and is more important for discriminative touch (Ackerley et al., 2014; McGlone and Reilly, 2010).

More recently, Schwann cells which form a mesh-like network in the subepidermal layer of the skin have been discovered to be inherently mechano-sensitive (Abdo et al., 2019). Due to their intimate association with unmyelinated nociceptive neurons, they are able to convey noxious mechanical and thermal information to the nerves (Abdo et al., 2019).

1.4.1.1 Glabrous skin LTMRs

In the glabrous skin, the two Aβ LTMR populations can be subdivided further to give two types of SA-LTMRs: SA1- and SA2-LTMRs and two types of RA-LTMRs: RA1- and RA2-LTMRs.

SA1-LTMRs innervate Merkel cells, named after the anatomist Friedrich Sigmund Merkel (1875), who was the first to histologically describe an epidermal cell cluster forming contacts with afferent nerve fibres in vertebrate skin (Abraira and Ginty, 2013). They respond to sustained indentation with a sustained and slowly adapting discharge which is linearly correlated with the indentation depth and duration (Johnson, 2001). SA1-LTMRs exhibit high spatial acuity and are sensitive to points, edges and curvature (Abraira and Ginty, 2013; Johnson, 2001). Due to these two properties, SA1-LTMRs are capable of transmitting an acute spatial neural image of a tactile stimulus (Johnson, 2001). The SA1 receptors are Merkel-neurite complexes which involve Merkel cells in the basal epidermis of the skin that enfold and encompass the unmyelinated ends of SA1 axons (Johnson, 2001; Ogawa, 1996). Piezo2 ion channels expressed in Merkel cells contribute to the mechanotransduction in SA1 fibres and have been demonstrated to be the principal Merkel-cell mechanotransduction channel *in vivo* (Nakatani et al., 2015; Woo et al., 2014). Additionally, studies in *Krt14Cre;Atoh1*^{CKO} animals, which completely lack epidermal Merkel cells in their skin, show similar SA1 firing deficits as Piezo2 conditional knockout mice in skin–nerve recordings. Thus, Merkel cells themselves are mechanosensitive (Woo et al., 2014). Merkel cells cluster in groups to form 'touch domes' in hairy skin (Iggo and Muir, 1969), and associate exclusively with guard hairs in hairy skin (Li et al., 2011). Overall, SA1 responses are in highly touch sensitive skin structures such as the fingertips and whisker follicles.

SA2-LTMRs also generate a sustained response to skin indentation like SA1-LTMRs, but differ in their inter-spike intervals, with SA2 feedback being more uniform than those in SA1-LTMRs (Li et al., 2011). SA2-LTMR responses are thought to arise from Ruffini endings, after histologist and embryologist, Angelo Ruffini (1894), but direct evidence is still lacking (Chambers et al., 1972). Ruffini endings which later became known as Ruffini corpuscles are small, encapsulated nerve endings in the dermis. SA2-LTMRs innervate the skin less densely than SA1-LTMRs and their receptive fields are ~5 times larger (Johansson and Vallbo, 1979). They are particularly important in transmitting information about skin stretch and changes in hand and finger shape as well as detection of object motion, particularly when the movement produces skin stretch (Abraira and Ginty, 2013). The ability of SA2-LTMRs to sense mechanical stretch applied to Ruffini endings has been suggested to be due to collagen fibres (Maeda et al., 1999). However, Ruffini corpuscles or Ruffini-like endings have not been identified in rodents and therefore it is thought to be unlikely that these structures give rise to SA2 responses (Abraira and Ginty, 2013). Therefore, the morphological and physiological functions of SA2-LTMRs in different animal species remains unknown.

RA1-LTMRs in the glabrous skin innervate Meissner's corpuscles in rodents and primates. These corpuscles were first discovered by anatomist, Georg Meissner (1852) and are made up of flattened lamellar cells which are arranged horizontally in connective tissue. Meissner's corpuscles are localised to dermal papillae in the glabrous skin, found in fingerprint skin and the soles of feet of humans (Owens and Lumpkin, 2014). The anatomical arrangement of lamellar cells and nerve terminals within the Meissner corpuscle is critical in determining the physiological properties of RA1-LTMRs. Following indentation of the glabrous skin, collagen fibres that connect the basal epidermis to lamellar cells of the corpuscle provide the

mechanical force required to deform the corpuscle and trigger action potentials, which rapidly adapt due to the nature of RA1-LTMRs (Li et al., 2011; Rutlin et al., 2014). The corpuscle regains its original shape upon removal of the stimulus and in doing so induces another volley of action potentials, giving the distinctive on-off responses of RA1-LTMRs (Abraira and Ginty, 2013). One of the first functions ascribed to RA1-LTMRs was detection and scaling of low-frequency vibrations (Torebjörk and Ochoa, 1980). RA1-LTMRs are more sensitive than SA1-LTMRs and respond consistently and with very short latencies to skin stimulation. This makes them well suited to respond quickly to minute motions which may be essential for sensing when a gripped object slips (Abraira and Ginty, 2013). In this way, RA1- and SA1-LTMRs play complementary roles in discriminating tactile stimuli.

RA2-LTMRs innervate Pacinian corpuscles and are highly sensitive and responsive to high frequency vibration transmitted through objects held in the hand (Park et al., 2016). RA2-LTMRs are more sensitive than RA1-LTMRs and often respond to motions in the nanometre range (Lynn, 1971). Pacinian corpuscles, discovered by the anatomist, Filippo Pacini (1835) are phasic receptors and are important for the detection of gross pressure changes and vibrations in the skin. The corpuscles are located deep in the dermis and their receptive fields are large, often encompassing the whole hand. This, coupled with the extreme sensitivity means that RA2 afferents display little spatial acuity (Abraira and Ginty, 2013). Overall, RA2-LTMRs are likely to mediate the perception of transmitted vibrations from manipulating objects in our hands (Lumpkin et al., 2010; Owens and Lumpkin, 2014; Rutlin et al., 2014).

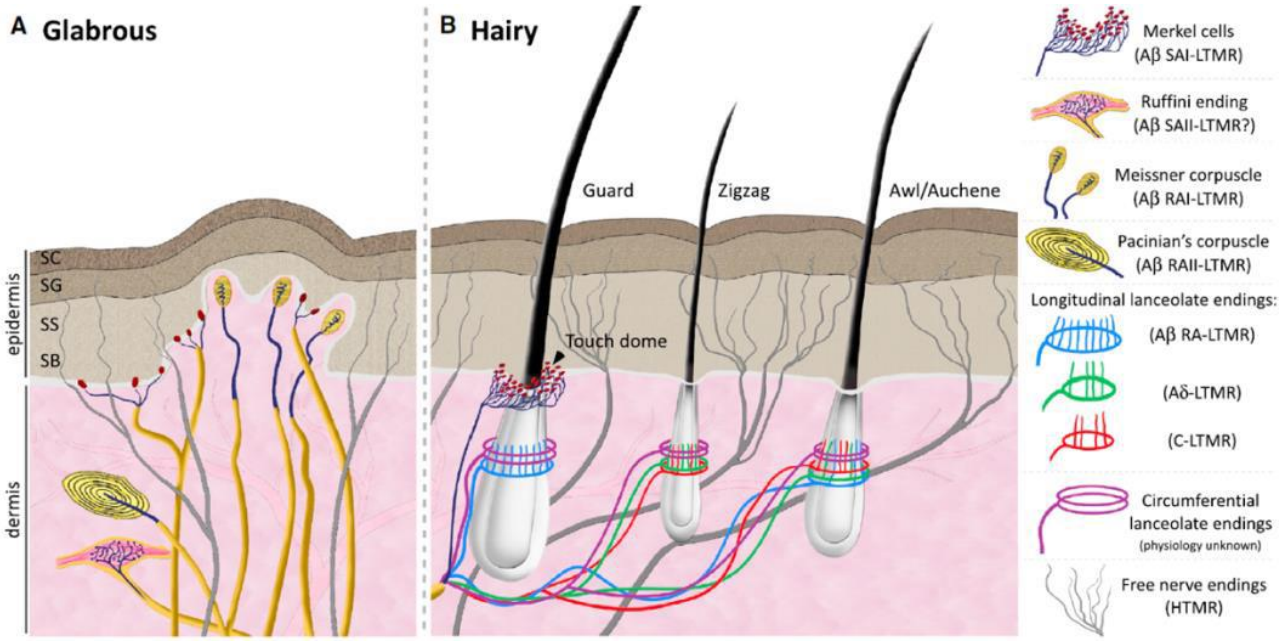

Figure 1-3 Cutaneous mechanoreceptors expressed in glabrous vs. hairy skin in mice.

(A) Four types of LTMR fibres which exist in the glabrous skin to mediate touch. Aβ fibre end organs can be Pacinian corpuscles, Ruffini endings or Meissner's corpuscles. Merkel cells form synapse-like associations with enlarged nerve terminal branching from a single Aβ fibre. (B) In hairy skin, LTMRs have longitudinal lanceolate endings around the hair follicles. Both glabrous and hairy skin are comprised of Aβ, Aδ and C-LTMRs. (Abraira and Ginty, 2013).

1.4.1.2 Hairy skin LTMRs

Hairy skin is important in body temperature regulation, protection from the environment and in the sense of touch. Hairy skin is innervated by several LTMRs which are categorised into Aβ, Aδ and C-LTMRs according to their conduction velocities. These LTMRs are physically and functionally associated with hair follicles, which fall into three distinct types according to length, thickness and presence of kinks in the hair shaft (Schlake, 2007).

Similar to glabrous skin, hair follicle innervating Aβ-LTMRs are divided into two groups according to their firing adaptation rates; SA- and RA-LTMRs. Hairy skin SA1-LTMRs are also associated with the Merkel cell complex, found within the epidermal/dermal junction surrounding the mouths of guard hairs (Abraira and Ginty, 2013). In fact, SA1-LTMRs are exclusively associated with guard hairs in the hairy skin (Li et al., 2011) and the properties are similar to those recorded from their counterparts in the glabrous skin (Woodbury and Koerber, 2007). SA2 response properties have been identified in the rodent hairy skin, however, the anatomical correlate of SA2 units remains controversial (Wellnitz et al., 2010). In contrast, Aβ RA-LTMRs are well characterised in the hairy skin and have been classified extensively across species and different hair follicle types (Brown and Iggo, 1967). RA-LTMR responses arise from lanceolate endings that surround hair follicles (Lechner and Lewin, 2013; Li et al., 2011; Rutlin et al., 2014). In the mouse, these lanceolate endings associate with guard hairs and awl/auchene hair follicles (Li et al., 2011). The physiological properties of RA-LTMRs are well characterised. These afferents do not respond to thermal stimuli (Abraira and Ginty, 2013). In addition, their response to hair follicle movement is linearly correlated with the velocity and final amplitude of displacement. Finally, the size of RA-LTMR receptive fields can vary across the body (Abraira and Ginty, 2013).

The second group of hair follicle associated LTMRs are classified as Aδ-LTMRs/down (D-) hair mechanoreceptors. Studies in the cat and mouse reveal that D-hair LTMRs exhibit some of the lowest mechanical thresholds and highest dynamic sensitivity to any other LTMR, making them the most sensitive mechanoreceptor in skin (Brown and Iggo, 1967; Burgess and Perl, 1967; Koltzenburg et al., 1997). Indeed, the force thresholds required to activate D-hairs are at least ten times lower than those of Aβ-LTMRs in multiple species (Lechner and Lewin, 2013). D-hair receptor responses are elicited following the movement of multiple hair types, particularly hair deflection (Brown and Iggo, 1967; Burgess et al., 1968; Rutlin et al., 2014). D-hair LTMRs respond to rapid cooling of the skin e.g. 40-30 °C and 30-20 °C in 2 seconds, but not to warming of the skin (Brown and Iggo, 1967; Li et al., 2011). Genetic labelling studies have revealed similarities between RA-LTMR and D-hair LTMR anatomical associations with hair follicles, in that they both form longitudinal lanceolate endings around hair follicles. However, Aδ-LTMR lanceolate endings are found around awl/auchene and zigzag, but not guard hair follicles (Li et al., 2011).

Though C fibres are often associated with painful stimuli, mechanoreceptors with conduction velocities within the C fibre range were described in the cat to be associated with tickling sensations (Zotterman, 1939). Later research confirmed that not all C fibre afferents are involved in relaying noxious information (Iggo, 1960). C-LTMRs are extremely sensitive to skin indentation and are maximally activated by stimuli that move slowly across their receptive field (Li et al., 2011; Olausson et al., 2010; Reynders et al., 2015). Notably, C-LTMRs display an intermediately adapting current and show a modest sustained discharge during a maintained mechanical stimulus (Abraira and Ginty, 2013). Unlike other hairy skin LTMRs, C-LTMRs commonly exhibit after-discharge, which can be up to a few seconds after the stimulus has

been removed. Similar to cold responses seen in some Aδ-LTMRs, C-LTMRs are activated by rapid cooling, but not warming of the skin. C-LTMRs are exclusively expressed in hairy skin and are thought to be important in mediating affective touch (Vallbo et al., 1993). Like all other hairy skin LTMRs, C-LTMRs form longitudinal lanceolate endings around hair follicles, and similar to Aδ-LTMRs, these develop around awl/auchene and zigzag hair follicles (Lechner and Lewin, 2013; Li et al., 2011). Multiple expression markers have been identified for C-LTMRs including tyrosine hydroxylase (TH), vesicular glutamate transporter (VGLUT3) and MRGPRB4 in non-peptidergic C fibres. These C fibres all contribute to the perception of light touch and are found only in hairy skin.

1.4.1.3 Schwann cells

Cutaneous Schwann cells have been shown to be expressed close to the dermal/epidermal border in both glabrous and hairy skin (Abdo et al., 2019). In addition, they are closely associated with or attached to ascending nociceptive nerve fibres in some mouse strains. Interestingly, this study also revealed that nerve terminals emerged from the soma of Schwann cells located near the border of the epidermis. Subepidermal nerves branched with radial Schwann cells and in intraepidermal endings, smaller parts of the nerve terminals were in contact with glia processes. Mechanical stimulation of nociceptive Schwann cells produced a transient depolarisation (Abdo et al., 2019). They were able to respond to both positive and negative changes in force. Both the response and adaptation properties were rapid. This suggests very fast gating mechanisms of the mechanoreceptor current which differs to that which has been described in sensory neurons (Poole et al., 2014). In addition, these nociceptive Schwann cells convey noxious thermal stimuli. The discovery that most or all types of nociceptors being able to contribute to this glio-neural complex is important. It may

provide an explanation for the apparent heterogeneity in cell receptor types mediating different aspects of thermal and mechanical nociceptive transduction.

1.4.2 Cutaneous thermoreceptors

The existence of distinct cold and warm sensory spots in the skin was described in psychophysical studies conducted by Blix, Goldscheider and Donaldson (Norrsell et al., 1999). The discovery of temperature sensitive afferent fibres in the lingual nerve of the cat was an important landmark made by Zotterman in 1935 (reviewed by Iggo, 1984). Subsequent studies have investigated the firing patterns of warm and cold fibres in multi-unit and single fibre recordings and detailed the properties of these receptors (Hensel and Boman, 1960; Hensel et al., 1960; Iggo, 1984). In such studies, warm and cold thermoreceptors have been shown to continuously discharge impulses over a narrow range of temperatures, the rate of which is dependent on the temperature. Thermoreceptors are maximally excited at innocuous temperatures and have dynamic sensitivity. The rate of impulse discharge depends on the rate of temperature change, but is always higher than the rate at constant temperatures (Iggo, 1984). Nearly always, a reduced continuous discharge from CC fibres may signal warmth. Thermoreceptors have a high degree of specificity for temperature and cannot be readily activated by non-thermal stimuli. These afferent fibres are typically mechanically insensitive (Hensel et al., 1960; Torebjörk and Schmelz, 2005). However, for cold pain, responses are still evoked and persist after the skin surface has been numbed by cooling. Skin sensations were inhibited by noxious cold temperatures and returned upon rewarming between 16-26 °C (Klement and Arndt, 1992). Cutaneous receptors are therefore unlikely to be mediators of cold pain. Instead, cold pain occurred and disappeared at the same temperature as vein walls. In addition, the pain intensity was proportional to vein wall

temperatures. Intravenous block by procaine inhibited cold pain evoked by surface cooling, whereas perivenous procaine application reduced, but did not abolish pain during skin cooling. The authors contend that nociceptors of the vein wall are likely mediators of cold pain (Klement and Arndt, 1991, 1992).

Electrophysiological recordings have been performed in human subjects and conduction velocities from cold and warm thermoreceptors have been discovered to appear in the Aδ and C fibre ranges (Hensel and Boman, 1960; Serra et al., 1999). Warm sensation has been attributed to C afferents, whereas cold detection is a function of both Aδ and C fibres (Hensel and Schafer, 1984; Torebjörk and Schmelz, 2005). The properties of cold-sensitive afferents are similar across species including cat, dog, primates and humans. An example of this is that cold-sensitive fibres discharge impulses as bursts upon cooling. This is a phenomenon reported in cold fibres in cat lingual nerves, monkey skin nerves, perioral units in dogs and scrotal skin of rats (Bade et al., 1979; Hensel and Boman, 1960; Hensel et al., 1960; Iggo, 1969; Torebjörk and Schmelz, 2005). Cold-sensitive fibres from these species do differ in the proportion of cold fibres that discharge impulses as bursts to cooling.

In microneurography studies in the hairy skin of human volunteers, it was found that 40 % of C-mechano (CM) fibres are responsive to cold temperatures, with a threshold of ~10 °C (Cain et al., 2001; Campero et al., 1996). The proportion of cold-sensitive fibres reported is different between studies. This population of CMC fibres is thought to be important in the detection of cold pain.

1.4.3 Nociceptors

Over a century ago, Charles Sherrington (1857-1952) proposed the existence of the nociceptor, a primary sensory neuron that is gated by noxious stimuli (Julius and Basbaum, 2001). This group of primary sensory neurons can be distinguished from other classes as a result of their sensitivity to noxious heat, intense pressure or irritant chemicals (Burgess and Perl, 1967). Nociceptors however, are not activated by warming (innocuous) or light touch. The receptive properties of these fibres are tuned for the detection of pain that arises from actual or threatened damage to non-neural tissue (nociceptive pain) that is critical to an organism's survival.

Nociceptors are composed of Aδ and C primary afferent nerve fibres which innervate peripheral tissues as free nerve endings. Aδ fibres typically respond either only to noxious mechanical forces (Aδ mechano-sensitive nociceptors) or to both noxious mechanical and thermal stimuli (Aδ mechano-thermal nociceptors), whereas C fibres typically are polymodal (Julius and Basbaum, 2001; Purves et al., 2001). Aδ fibres are responsible for mediating acute and fast/first pain, made possible by the intermediate conduction velocities in these thinly myelinated fibres. In contrast, C fibres mediate a second phase of delayed, longer lasting, and dull pain due to the slower conduction velocities in these unmyelinated fibres.

1.5 Central projections of primary afferent neurons

The central terminals of primary afferent nerve fibres from peripheral target organs innervate the dorsal horn of the spinal cord (Basbaum et al., 2009). Different types of sensory nerve fibres project to a different level within the dorsal horn (Figure 1-4). Large, myelinated Aβ tactile afferents that innervate hair follicles terminate deep within the dorsal horn (laminae

III-V). In contrast, small-diameter, unmyelinated C fibres terminate in the superficial layers of the dorsal horn (laminae I-II). Medium-diameter, nociceptive Aδ fibres terminate in the superficial (laminae I) and deeper layers of the dorsal horn (laminae II-III).

Second order neurons synapse with central terminals of primary afferent neurons in the dorsal horn, which then project to and synapse with third order neurons in the brain to elicit the perception of pain. The distinction between nociception and pain was made by Woodworth and Sherrington in 1904. Experiments were conducted using decerebrate animal preparations in which brain structures were removed. The pain behaviours were measured in these preparations and it was concluded that the cortex was essential to perception of pain (Woodworth and Sherrington, 1904).

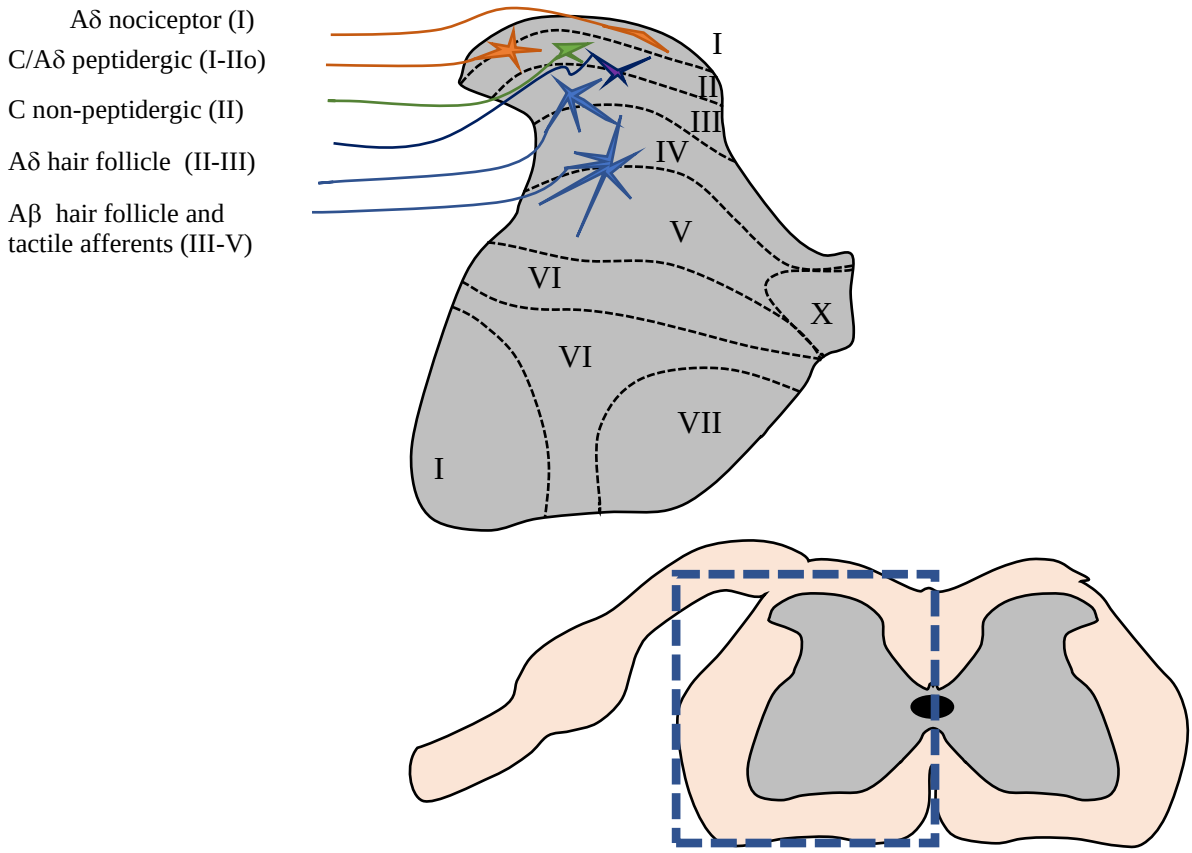

Figure 1-4 Different classes of primary afferent fibres project to distinct area of the dorsal horn.

Nociceptive nerve fibres (Aδ and C fibres) terminate within the superficial layers (lamina I-II) of the dorsal horn of the spinal cord. In contrast, non-nociceptive fibres (Aβ-fibres) terminate deeper within the dorsal horn (lamina III-IV).

1.6 The molecular basis of sensation

Primary afferent neurons respond to changes in the physiochemical environment. Different types of neurons detect changes in temperature, the presence of hormones, mediators and various chemicals and metabolites in the extracellular fluid. The sensory properties of different neurons are defined by the expression of ion channels and receptors that act as transduction molecules. Transduction channels are expressed at the terminal as well as along the axons of primary afferent neurons.

1.6.1 Thermosensation

1.6.1.1 Heat

Sensory neurons respond to both innocuous warmth and noxious heat, with a distinct threshold for the latter at around 43 °C (Basbaum et al., 2009). The search for the molecular receptor for capsaicin, the pungent ingredient in chilli peppers, which was also known to cause activation of nociceptive sensory neurons (Bevan and Szolcsányi, 1990; Szolcsányi, 1977; Wood et al., 1988a) and a sensation of 'burning pain' led to the discovery (Bevan et al., 2014; Kirschstein et al., 1997; Reichling and Levine, 1997), and the subsequent cloning of Transient receptor potential Vanilloid 1 (TRPV1) (Caterina et al., 1997). TRPV1 is activated by capsaicin and noxious heat, with the activation threshold for the channel being ~43 °C (Basbaum et al., 2009; Caterina et al., 1997, 2000; Reichling and Levine, 1997). TRPV1 is expressed in the majority of heat-sensitive sensory neurons, therefore making it a strong candidate as the molecular sensor of noxious heat (Caterina et al., 1997, 2000). Studies using mice lacking functional TRPV1 (*Trpv1*$^{-/-}$) reported that mice fully lacked the cellular and behavioural responses to capsaicin, however they still exhibited robust pain responses to heat in the hot-plate and tail immersion assays, albeit with an increased withdrawal latency

compared to wildtype (WT) animals (Caterina et al., 2000; Davis et al., 2000). A key finding was that the loss of heat hypersensitivity induced by inflammation is more pronounced. Other studies have shown that TRPV1 expressing neurons are essential for the detection of noxious heat. In one study, silencing of TRPV1-positive neurons through TRPV1-mediated permeation of the voltage-gated sodium channel blocker, QX-314 rendered animals temporarily insensitive to radiant heat (Binshtok et al., 2007). In studies where TRPV1 was ablated from the central terminals of sensory neurons, there was a substantial reduction in inflammatory thermal hypersensitivity (Cavanaugh et al., 2009; Jeffry et al., 2009). These studies indicate that TRPV1 plays an important role in both acute noxious heat sensing and heat-induced pain and hypersensitivity. Ablation shows that TRPV1 containing neurons are essential to heat sensing, but knockout studies show more of a modest role for TRPV1. However, the residual heat sensitivity may be explained by the existence of other molecular heat transducers.

Other members of the TRPV subfamily have been proposed as potential heat transducers that may function alongside TRPV1 (Figure 1-5). TRPV2, a capsaicin-insensitive TRPV1 homologue expressed in medium- to large-diameter sensory neurons, is activated by hot temperatures with a temperature activation threshold of ~52 °C (Caterina et al., 1999). However, studies using *Trpv2*$^{-/-}$ and *Trpv1*$^{-/-}$ / *Trpv2*$^{-/-}$ mice have shown that TRPV2 is not essential for sensing noxious hot temperatures, with the response in the double knockout mice being similar to *Trpv1*$^{-/-}$ mice (Park et al., 2011). In addition, TRPV3 and TRPV4 have been identified as sensors of warm innocuous temperatures. TRPV3 has been reported to be activated at temperature thresholds between 31-39 °C (Peier et al., 2002a; Smith et al., 2002; Xu et al., 2002). TRPV3 is predominantly expressed in mouse keratinocytes (Chung et al., 2004; Peier et al., 2002a), although also expressed in sensory nerve ganglia of primates with an overlap with TRPV1

expression (Smith et al., 2002; Xu et al., 2002). Although heat-evoked TRPV3 currents occur at innocuous temperatures, currents continue to increase when temperatures are raised into the noxious range (Peier et al., 2002a). Currents are progressively sensitised over time at elevated temperatures (Peier et al., 2002a). This adds to the dynamic threshold of this channel. Behavioural studies using *Trpv3*$^{-/-}$ mice have shown that these mice display a reduced preference for innocuous warm temperatures on the two plate preference test compared to WT counterparts (Moqrich et al., 2005). *Trpv3*$^{-/-}$ mice also displayed increased latencies in the tail immersion assay when the water bath was set to 50 °C and 52 °C and to paw withdrawal latency on a 55 °C hot plate (Moqrich et al., 2005). However, the role of TRPV3 in heat sensation has been disputed in a study which reported no significant changes in thermal preference or noxious heat sensitivity between TRPV3$^{-/-}$ and WT mice (Huang et al., 2011).

In addition, TRPV4 is activated by ambient temperatures with a temperature activation threshold of 25-34 °C (Güler et al., 2002; Watanabe et al., 2002). This channel is activated by hypotonic solutions and, consistent with this finding, hypoosmotic solutions potentiate heat-evoked responses whilst hyperosmotic solutions inhibit them (Güler et al., 2002). Like TRPV3, TRPV4 channels are expressed by skin keratinocytes, where they are thought to be responsible for the majority of heat-evoked currents (Chung et al., 2004). Indeed the current most commonly observed in keratinocytes and attributed to TRPV4 is diminished in *Trpv4*$^{-/-}$ keratinocytes and re-established by transfection of WT TRPV4 (Chung et al., 2004). Whilst these results suggest that TRPV4 is required for the majority of heat sensing in keratinocytes, behavioural studies using *Trpv4*$^{-/-}$ mice suggest that TRPV4 is not required for noxious heat sensing (Liedtke and Friedman, 2003). Moreover, *Trpv3*$^{-/-}$/ *Trpv4*$^{-/-}$ mice display no

impairments to noxious or innocuous heat sensing. This demonstrates that compensatory heat-sensing by TRPV1 channels is not masking a deficit in the double knockout mice, suggesting that neither TRPV3 nor TRPV4 channels are required for heat sensing (Huang et al., 2011).

Another member of the TRP channel family, TRP Melastatin 3 (TRPM3), is important for noxious heat detection. TRPM3 is expressed in DRG and TG neurons at levels comparable to other important TRP channels including TRPV1, TRPM8 and TRPA1 (Vriens et al., 2011). This channel is activated by the endogenous neurosteroid pregnenolone sulphate (PS), which has been used as a pharmacological tool for the channel characterisation and as a probe for TRPM3 expression (Wagner et al., 2008). Vriens *et al.* showed that heat (40 °C) evoked increases in $[Ca^{2+}]_i$ in HEK293 cells transiently expressing TRPM3. In addition, there was a synergistic effect between chemical and thermal activation of TRPM3. The TRPM3 agonist PS, shifted the activation of TRPM3 to lower temperatures. Conversely, it was demonstrated that increasing the temperature from room temperature to 37 °C strongly potentiated PS responses (Vriens et al., 2011). Furthermore, *Trpm3*$^{-/-}$ mice exhibit altered temperature preferences, compromised behavioural responses to noxious heat and fail to develop heat hyperalgesia associated with inflammation (Vriens et al., 2011). However, recent investigations in our lab have found that heat sensitivity in DRG neurons from *Trpm3*$^{-/-}$ mice respond similarly to WT mouse DRG neurons (data not published). In contrast, we reported that established FCA-evoked heat hypersensitivity was reduced by a TRPM3 antagonist, as well as proalgesic agents, bradykinin (BK) and PGE_2 (Alkhatib et al., 2019). Surprisingly, BK and PGE_2 also inhibited heat sensitivity produced by TRPM3 agonists in the same study.

Finally, TRPM2 has also been identified as a potential sensory neuron heat transducer. TRPM2 responses to temperatures > 35 °C were first reported in pancreatic islet cells (Togashi et al., 2006). TRPM2 is co-expressed with insulin in islet beta cells, and mild heating evokes an increase in cytosolic Ca^{2+} and insulin release (Togashi et al., 2006). Heat also potentiates the TRPM2 response to its ligands, nicotinamide adenine dinucleotide (β-NAD^{+}) and adenosine 5'-diphosphoribose (ADPR) (Togashi et al., 2006). These responses and the heat-evoked release of insulin are inhibited by 2-aminoethoxydiphenyl borate (2-APB) (Togashi et al., 2008). In addition, TRPM2 is required for sensitivity to warmth in sensory neurons (Tan and McNaughton, 2016). The proportion of heat-sensitive neurons isolated from *Trpm2*$^{-/-}$ mice was significantly reduced, despite the fact that sensitivity to agonists of the TRP channels reported to contribute to heat sensing remained the same as WT mice (Tan and McNaughton, 2016). In addition, heat-sensitive neurons express TRPM2 mRNA. In the thermal place preference assay, there was a marked increase in the time that *Trpm2*$^{-/-}$ mice spent on a plate set at non-noxious warm (38 °C) temperatures compared to WT mice (Tan and McNaughton, 2016). This suggests that TRPM2 is an important and constitutive heat sensor, unlike TRPM3 which may be more important during inflammatory-induced heat hyperalgesia.

Ion channels which do not belong to the TRP channel family have also been implicated in heat transduction mechanisms. The calcium-activated chloride channel (CaCC), anoctamin 1 (ANO1) has been reported to be activated by heat with a threshold temperature of ~44 °C (Cho et al., 2012; Vriens et al., 2011). ANO1 is expressed within the nociceptive subpopulation of sensory neurons with a high level of co-expression of TRPV1 (~80 %). In experiments conducted by Cho and colleagues, WT DRG neurons were co-treated with a TRPV1 antagonist and the CaCC blocker, mefloquine which abolished heat-evoked currents. Mefloquine also

blocked heat responses in *Trpv1*$^{-/-}$ neurons (Cho et al., 2012). However, these findings remain unclear, since we found that mefloquine produced Ca^{2+} responses in a large percentage of DRG neurons and therefore thought it unusable for $[Ca^{2+}]_i$ measurements (data not published). In addition, both WT and *Trpv1*$^{-/-}$ mice were intrathecally injected with small interfering RNA (siRNA) specific for ANO1 and displayed significantly increased tail and paw withdrawal latencies in the tail immersion (50-54 °C) and hot plate assays. *Ano1*$^{-/-}$ mice also showed deficits in noxious heat detection (Cho et al., 2012), showing that ANO1 is a promising heat sensor in nociceptive sensory neurons.

1.6.1.2 Cold

Several mechanisms for the transduction of cold stimuli have been proposed: direct activation of cold-gated ion channels, inhibition of background two-pore domain (K_{2P}) or voltage-gated Ca^{2+} channels, and inhibition of the Na^+/K^+ ATPase (Foulkes and Wood, 2007). It is likely that all these events occur during cooling but there is still debate around the relative contribution of each in mechanisms for the transduction of noxious cold. The sensation of innocuous cooling is distinct from cold pain. Cold temperatures are reported to feel painful when they fall below 15 °C. However, according to DFNS guidelines for quantitative sensory testing (QST) studies, cold pain in control subjects varies. In these studies, the skin was challenged with a probe, and the temperature ramped down by 1 °C/s (Rolke et al., 2006; Wasner et al., 2004). The reading was taken when the subject pressed a button to report pain or discomfort. Therefore, only the temperature of the probe is known, and it is difficult to ascertain what the actual tissue temperature is when the pain is reported. These thresholds can change during pathophysiological states to a wider range of cold temperatures (0-28 °C), which can be perceived as painful (McKemy, 2013).

Cold-mediated inhibition of the Na^+/K^+ pump is one of the earliest theories to be proposed for the signalling of cold sensation (Pierau et al., 1974). Cold temperature was the first means used to block the pump and stop ATPase activity. Ouabain, an inhibitor of the Na^+/K^+ ATPase was used in recordings of cold-sensitive afferents and was shown to alter the activity of these fibres (Pierau et al., 1974). The notion that an electrogenic sodium pump is responsible for temperature sensitivity of cold receptors was later refuted by Reid and Flonta as ouabain was unable to indirectly depolarise the majority of cold-sensitive DRG neurons or the depolarisation level was insufficient to trigger action potential firing (Reid and Flonta, 2001). Thus, the inhibition of the Na^+/K^+ pump is not thought to be the principal mechanism of cold transduction.

Members of the TRP superfamily are cation-permeable transduction channels, many of which are thermosensitive. The discovery and functional characterisation of TRP Melastatin 8 (TRPM8), a channel activated by cold temperatures and cooling compounds has been fundamental to the study of the molecular basis of cooling (McKemy, 2007; McKemy et al., 2002; Peier et al., 2002b). TRPM8 is expressed in a small subset of TG and DRG neurons that are sensitive to cooling and cooling agents such as menthol and icilin (Viana and Voets, 2020). This channel has been extensively studied and there is compelling evidence through pharmacological and genetic studies that TRPM8 is a critical sensor for innocuous cold temperatures. Thus, animals lacking TRPM8 are unable to discriminate between 30 and 20 °C compared to their WT counterparts (Bautista et al., 2007; Colburn et al., 2007; Dhaka et al., 2007). However, TRPM8-deficient mice are still able to sense and avoid temperatures below 10-15 °C, indicating that there are additional sensors for noxious cold (Bautista et al., 2007; Viana and Voets, 2020).

Many studies show that TRPM8 is critical in acute noxious cold detection (Gentry et al., 2010; Knowlton et al., 2010). In addition, studies in healthy human volunteers have shown that the application of menthol to the skin induced a cooling sensation and augmented cold-evoked pain, suggesting a possible role of TRPM8 expressing fibres in cold pain and hyperalgesia (Hatem et al., 2006; Namer et al., 2008). In patients, the selective TRPM8 antagonist, PF-05105679 significantly inhibited pain in the cold pressor test with efficacy equivalent to oxycodone (Andrews et al., 2015; Winchester et al., 2014). However, it should be noted that menthol is not a selective agonist for TRPM8, but also activates TRP Ankyrin 1 (TRPA1). Therefore, the sensory effects of menthol may not be fully explained by TRPM8 activation. An additional level of complexity comes from the fact that that TRPM8 has been implicated in cooling-induced analgesia in mice (Proudfoot et al., 2006). This study demonstrated that topical application of icilin to the paws of neuropathic mice reversed sensitisation to mechanical and thermal stimuli. This suggests that a single molecular sensor may have multiple functions.

The sensation of noxious cold has also been attributed to TRPA1, a TRP channel that is usually co-expressed with TRPV1 in a subpopulation of nociceptive sensory neurons (Story et al., 2003). However, there is no consensus on TRPA1 channel's role in cold sensing (Basbaum et al., 2009; McKemy, 2013; Sexton et al., 2014). TRPA1 has been identified as the receptor that is activated by pungent food including allyl isothiocyanate (AITC), cinnamaldehyde and allicin (Bandell et al., 2004; Bautista et al., 2005, 2006; Jordt et al., 2004). Jordt *et al.* showed that the majority (96 %) of AITC responsive cultured TG neurons from rats were insensitive to cold (Jordt et al., 2004). In fact, cooling from 22-6 °C led to a reduction of AITC-evoked responses in TRPA1-expressing oocytes. These findings were corroborated by Bautista *et al.* who found

that cold activation of TG neurons is unchanged in cultures from *Trpa1*$^{-/-}$ mice when compared to WT counterparts (Bautista et al., 2006). However, these findings have been disputed in other studies which have shown a reduction in the number of cold-sensitive TG neurons from *Trpa1*$^{-/-}$ mice compared to WT (Karashima et al., 2009). In addition, *Trpa1*$^{-/-}$ mice showed decreased responsiveness to noxious cold temperatures on a cold plate and reduced sensitivity to acetone application when compared with WT mice (Kwan et al., 2006). However, thermal place preference is unchanged in *Trpa1*$^{-/-}$ mice (McKemy, 2013), unlike responsiveness in assays of noxious cold (Andersson et al., 2009; Gentry et al., 2010). Finally, most cold-sensitive DRG neurons do not express the channel (Munns et al., 2007), thus indicating that TRPA1 is unlikely to be involved directly in noxious cold sensing.

The third TRP channel that has been proposed to play a role in cold sensation is TRP Canonical 5 (TRPC5). There is however, minimal expression of the channel in DRG neurons according to RNA sequencing data (Liang et al., 2019; Lopes et al., 2017). The role is also somewhat unclear as TRPC5 currents increased as temperatures were decreased below 37 °C, with maximal currents at 25 °C when the channel was expressed in a recombinant cell line (Zimmermann et al., 2011). However, *Trpc5*$^{-/-}$ mice displayed similar behavioural responses to cool temperatures as their WT counterparts (Zimmermann et al., 2011). Therefore TRPC5 may contribute to innocuous cold sensation alongside TRPM8, but may also provide an explanation for cold sensation in the population of sensory neurons that are unresponsive to agonists of TRPM8 or TRPA1 (Alloui et al., 2006).

Ion channels including potassium and sodium channels have also been implicated in cold transduction mechanisms (Lolignier et al., 2016). Potassium channels are critical for setting

the membrane potential and also control neuronal excitability, repetitive firing activity and spike threshold and duration (Lolignier et al., 2016). Primary sensory neurons express a repertoire of potassium channels that can modulate their transduction properties and shape their excitability (Belmonte and Viana, 2008; Tsantoulas and McMahon, 2014). Most of the potassium currents, and therefore channels have been confirmed in patch-clamp studies (Gold and Gebhart, 2010; Gold et al., 1996). This diversity of potassium channel expression in DRG neurons was confirmed at the single cell transcriptome level (Usoskin et al., 2015). Many studies have proposed a role of potassium channels in cold sensitivity and either described altered expression levels or functional changes in response to neuronal injury. Consequently, different potassium channels have been shown to contribute to hyperexcitability in nociceptors and produce sensory abnormalities such as cold and mechanical allodynia (Descoeur et al., 2011; Pereira et al., 2014; Tsantoulas and McMahon, 2014).

Several members of the K_{2P} potassium channel family have been shown to play a key modulatory role in cold sensation. These channels are important in mediating voltage-independent background leak K^+ currents and are critical in setting the resting membrane potential (Chemin et al., 2003). Some channels within the K_{2P} family are highly temperature sensitive. The most extensively studied of these channels include TREK-1, TREK-2, TRAAK and TASK-3, all of which have been shown to have a role in cold sensitivity. TREK-1 and TREK-2 are abundantly expressed in DRG neurons, but TRAAK and TASK-3 expression is limited. Use of TREK- and TRAAK-deficient mice has revealed the roles that each of the channels may have in thermal and mechanical sensitivity (Alloui et al., 2006; Noël et al., 2009a; Pereira et al., 2014). Interestingly, *KCNK10*$^{-/-}$ (TREK2) mice show enhanced responses to cool temperatures but no signs of abnormal cold pain, whereas *KCNK2*$^{-/-}$ (TREK1) and *KCNK4*$^{-/-}$ (TRAAK) mice show

greater responses to noxious cold. The expression of all three of these channels was found to be significantly reduced in a mouse model of oxaliplatin-induced cold hypersensitivity (Descoeur et al., 2011; Pereira et al., 2014). Therefore it may be the case that in neuropathic conditions, reduced background K^+ leak current may contribute to cold hypersensitivity (Lolignier et al., 2016). TASK-3 has been found to be selectively expressed in TRPM8-expressing cold thermoreceptive neurons. Pharmacological inhibition of TASK-3 shifted the temperature threshold of cold-sensitive TRPM8-expressing DRG neurons to warmer temperatures (Morenilla-Palao et al., 2014). In addition, TASK3 null mice revealed a greater sensitivity to cooling and augmented responses to electrical and thermal stimulations (Morenilla-Palao et al., 2014).

Voltage-gated potassium channels (K_v) including K_v1 and $K_v7.2/7.3$ (KCNQ2/3) have a role in the physiology of cold sensing and in the pathophysiology of cold pain (Lolignier et al., 2016). The delayed potassium current (I_{KD}) current composed of $K_v1.1$ and $K_v1.2$ subunits is a slowly inactivating, dendrotoxin- and 4-aminopyridine-sensitive current that is differentially expressed in TRPM8-expressing cold-sensitive neurons, and plays a major role in modulating threshold temperatures to cold stimuli (Madrid et al., 2009; Viana et al., 2002a). Activation of I_{KD} counters the depolarising effect of the cold activated TRPM8-dependent current, which results in a reduced overall response to temperature decreases and a shift towards colder temperature thresholds in individual neurons (Madrid et al., 2009). Furthermore, the local blockade of I_{KD} in the hind paw of mice causes nocifensive behaviours in response to normally innocuous stimuli, suggesting that the I_{KD} current is important in acting as an excitability brake to cold stimuli *in vivo* (Madrid et al., 2009). $K_v7.2/7.3$, the molecular components of the M-current also work in synergy with TRPM8 channels to modulate the response of nociceptors

to cold. Pharmacological blockade of the M-current sensitises a large proportion of C fibres in response to cold that require the activation of TRPM8 channels (Vetter et al., 2013).

The most abundantly expressed voltage-gated sodium channels (Na_v) in peripheral afferent fibres are $Na_v1.7$ - 1.9. Channelopathies in each of these isoforms is associated with distinct inherited pain disorders, ranging from congenital pain insensitivity ($Na_v1.7$) to severe neuropathic pain syndromes ($Na_v1.8$ and $Na_v1.9$) (Cummins et al., 2004; Dib-Hajj et al., 2005, 2007; Huang et al., 2019; Waxman et al., 1999). The tetrodotoxin-resistant (TTX-r) channels, $Na_v1.8$ (gene: *Scn10a*) and $Na_v1.9$ (gene: *Scn11a*) are expressed in nociceptors and are functionally important for afferent cold-responsiveness. The inactivation of $Na_v1.8$ is relatively cold resistant (Foulkes and Wood, 2007; Luiz et al., 2019; Zimmermann et al., 2007). This means that unlike other isoforms of the channel, $Na_v1.8$ can continue to generate action potentials at very low temperatures. Indeed, *Scn10a*$^{-/-}$ mice display decreased sensitivity to noxious cold, as well as heat and mechanical stimuli (Akopian et al., 1999; Zimmermann et al., 2007). $Na_v1.9$ has a largely similar expression pattern with $Na_v1.8$ in DRG neurons and is important in the perception of pain in response to noxious cold (Lolignier et al., 2015). Nociceptors from *Scn11a*$^{-/-}$ mice show a decreased activation in response to cooling and behaviourally, these mice have an increased tolerance to noxious cold (Lolignier et al., 2015). Cold-sensitive nociceptors have a substantial $Na_v1.9$ current which amplifies subthreshold depolarisations provided by cold transduction channels, the identity of which is unclear. Interestingly, the majority of $Na_v1.9$ positive neurons do not express either TRPA1 or TRPM8 (Lolignier et al., 2015). In addition, $Na_v1.9$ has been shown to play a role in oxaliplatin-induced cold hypersensitivity (Lolignier et al., 2015). Thus, the inactivation kinetics of both TTX-r

isoforms of Na_v channels are functionally suited to contributing to action potential initiation in cold-sensitive fibres at low temperatures.

In addition, $Na_v1.6$ (gene: *Scn8a*) has been shown to play a role in the pathophysiology of cold pain. This channel is TTX-sensitive (TTX-s) and expressed primarily on myelinated axons. $Na_v1.6$ has been implicated in oxaliplatin-induced cold hypersensitivity as post-stimulus discharges, normally present in WT mice in response to oxaliplatin treatment, are completely absent in *Scn8a*$^{-/-}$ null mice (Sittl et al., 2012). Two key studies have demonstrated that $Na_v1.6$ is important for the activity of oxaliplatin and cold allodynia induced by oxaliplatin (Deuis et al., 2013; Sittl et al., 2012). In addition, another study showed that there were increased levels of $Na_v1.6$ mRNA and protein in oxaliplatin-treated rats compared to naïve rats (Li et al., 2019). The microRNA gene, mIR-30b-5p negatively regulates the *Scn8a* expression by binding to *Scn8a* three prime untranslated region (3'UTR) in a cell line (Li et al., 2019). The same study demonstrated a marked increase in the ratio of $Na_v1.6$-positive DRG neurons in oxaliplatin-treated rats compared to control rats. Thus, there is strong evidence to suggest that oxaliplatin alters the expression of and interacts with $Na_v1.6$ in peripheral sensory neurons.

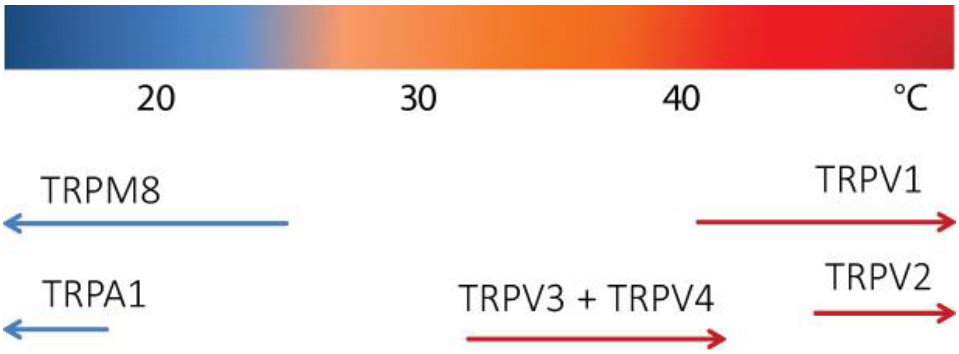

Figure 1-5 Temperature activation ranges for thermosensitive TRP channels.

Temperature activation ranges for TRPM8, TRPA1, TRPV1-4. TRPA1's role as a noxious cold sensor remains controversial. TRPV2 was originally demonstrated as a noxious heat sensor in the cloned rat channel (Caterina et al., 1999), but later studies of the human homologue found no activation (Neeper et al., 2007). Adapted from (Tominaga, 2007).

1.6.2 Mechanosensation

In contrast to the substantial number of thermosensitive ion channels that have been identified, very few mechano-sensitive channels have been studied. Principally, mechanical force opens excitatory, cation permeable channels which leads to the depolarisation of the nerve terminal and generates receptor potential (Delmas et al., 2011).

1.6.2.1 Model organisms

Acid-sensing ion channels (ASICs) belong to a proton-gated subgroup of degenerin-epithelial Na^+ channel family of cation channels (Delmas et al., 2011) and have been proposed as candidate mechanotransducer channels. ASICs were initially implicated in mechanotransduction following the discovery of invertebrate homologues of these channels (MEC subunits) in *Caenorhabditis elegans* (*C. elegans*) that were essential to the perception of touch (Delmas et al., 2011). ASIC 1, 2 and 3 are expressed in sensory neurons of the DRG and nodose ganglia (Page et al., 2005). Deletion of ASIC1 has been shown to increase the mechanical sensitivity of afferents innervating the gut, but does not alter the function of cutaneous mechanoreceptors (Page et al., 2004). A similar finding was reported for ASIC2, where deletion of this channel had no effect on cutaneous mechanoreceptors, but increased mechanical sensitivity in gut mechanoreceptors (Page et al., 2004; Roza et al., 2004). In contrast, in ASIC3-null mice, mechanosensitivity is decreased in the majority of afferent fibres innervating the gut (Page et al., 2005). In addition, mechanosensitivity of AM- nociceptive fibres is decreased in the absence of ASIC3 (Price et al., 2001). However, these findings were disputed by Drew *et al.*, who demonstrated that neither ASIC2 nor ASIC3 played roles in mechanically activated currents in sensory neuron ganglia (Drew et al., 2004). Thus, the role of ASICs in mechanotransduction is not fully characterised.

In addition, the *osm-9* gene in C. elegans encodes a six transmembrane domain protein which is similar to TRP channels in *Drosophila* (Colbert et al., 1997). It is expressed in sensory neurons that mediate osmosensory, mechanosensory and chemosensory functions. In particular, *osm-9* is required for the mechanosensory response to nose touch (Colbert et al., 1997).

Finally, the *Drosophila* TRP channel TRPN1/NompC is a putative mechano-sensitive channel that affects fly locomotion (Cheng et al., 2010). Loss-of-function mutations in the *nompc* gene abolishes mechanoreceptor potentials in fly bristles and a missense mutation alters adaptation of mechanoreceptor potentials (Walker et al., 2000). In addition, *nompc* controls the pace of larval crawling (Cheng et al., 2010).

1.6.2.2 Piezo channels

The discovery of two proteins, Piezo1 and Piezo2, as long sought after molecular carriers of an excitatory mechanically activated (MA) current found in many cells was ground-breaking. Since their discovery, further investigations have revealed a critical role for these ion channels in a wide range of physiological functions. Piezo1 and Piezo2 are large transmembrane proteins which form homo-multimers and function as pore-forming non-selective cation channels (Coste et al., 2010; Volkers et al., 2015). Expressing Piezo1 and/or Piezo2 in a variety of mammalian cell lines induces large MA cationic currents (Coste et al., 2010). Piezo2 is expressed in 20 % of all DRG neurons, as it is detected at across all subsets of neurons (Coste et al., 2010). Coste and colleagues have demonstrated a role for Piezo2 in rapidly adapting MA currents in somatosensory neurons (Coste et al., 2010). Therefore, Piezo2 has a potential role in touch and pain sensation. Indeed, knockdown of Piezo2 in zebrafish embryos abolished

light touch-evoked responses (Faucherre et al., 2013). Piezo2 has also been shown to be important in gentle touch sensing through its expression in the Merkel cell-neurite complex (Ikeda et al., 2014; Maksimovic et al., 2014; Woo et al., 2014). Use of Piezo2-GFP reporter mice demonstrate Piezo2 expression in both Merkel cells and apposed nerve terminals (Woo et al., 2014). Specific knockdown of Piezo2 in Merkel cells revealed that this channel is responsible for mediating mechanically activated currents in Merkel cells (Woo et al., 2014). This activity contributes to behavioural tactile responses in rats (Ikeda et al., 2014) and mice (Woo et al., 2014). The role of Piezo2 has also been studied in humans carrying a loss-of-function mutation in *PIEZO2*. Piezo2 deficient patients displayed loss of tactile discriminative touch perception and serious loss of joint proprioception, resulting in a compromised balance (Chesler et al., 2016). Gain-of-function mutations in Piezo2 channels in humans results in a form of distal arthrogryposis (Coste et al., 2013). This condition involves multiple congenital contractures in patients, specifically limited eye movements and restrictive lung movement. Thus, Piezo channels are thought to play an important and direct role in mechanotransduction.

1.6.3 Chemosensation

Primary afferent nerve fibres are also chemosensitive and can be activated by an array of chemical mediators such as purines, amino acids and pungent food compounds (Wood and Docherty, 1997). The chemical activation of sensory neurons through ligand-gated ion channels is vital for the function of the visual, olfactory and somatosensory systems (Wood and Docherty, 1997).

The majority of sensory neurons in culture respond to the purine, adenosine 5'-triphosphate (ATP) by an increase in $[Ca^{2+}]_i$ or depolarisation (Burnstock, 2000). ATP activates sensory neurons by binding to ionotropic P2X receptors, which can exist as homo- or hetero-multimeric channel complexes. There are seven members of the P2X family, $P2X_{1-7}$ and six of these $P2X_{1-6}$ are expressed in sensory neurons of the DRG, TG and nodose ganglia (Burnstock and Wood, 1996). However, $P2X_3$ is selectively expressed in nociceptive sensory neurons and raises the possibility that ATP might be important in nociceptor activation (Burnstock, 2000; Chen et al., 1995). Indeed, ATP has been identified to have a role in pain. Studies have demonstrated analgesia in neuropathic and inflammatory pain by knockdown and functional downregulation of $P2X_3$ (Barclay et al., 2002; Dorn et al., 2004). $P2X_2$ and $P2X_3$ homomers or heteromers are responsible for the purinergic response in sensory neurons (Cockayne et al., 2005).

Sensory neurons are also activated by the neurotransmitter, 5-Hydroxytryptamine (5-HT), which can activate ~40 % of cultured DRG neurons (Robertson and Bevan, 1991). The direct activation of primary afferent neurons by 5-HT is elicited by binding mainly to the ligand-gated ion channel $5\text{-}HT_3$. However, other receptor subtypes can be activated and affect neuronal sensitivity due to modulation of intracellular pathways (Wood and Docherty, 1997).

Other chemoreceptors expressed in sensory neurons include nicotinic and muscarinic receptors for acetylcholine (Genzen et al., 2001; Nandigama et al., 2010; Reeh, 1994) and ionotropic and metabotropic receptors for glutamate (Carlton and Hargett, 2007; Sato et al., 1993; Willcockson and Valtschanoff, 2008). These excitatory chemical mediators excite peripheral nerve terminals and DRG neurons isolated in culture.

In addition, sensory neurons can be activated by pungent compounds found in food and some of these molecules have been of central importance for studies of sensory neuron transduction mechanisms. Capsaicin from chilli peppers and piperine from black pepper activates TRPV1 expressed on sensory neurons (Caterina et al., 1997; McNamara et al., 2005; Wood et al., 1988b). Compounds found in cinnamon, mustard oil and garlic activate sensory neurons in a TRPA1-dependent manner and the cooling compound from the mint plant, menthol, activates sensory neurons predominantly through activation of TRPM8 (Bautista et al., 2005; Jordt et al., 2004; McKemy, 2007; Peier et al., 2002b).

Sensory neurons expressing TRPA1 can also be activated by environmental irritants such as acrolein and by oxidants and products of oxidative stress, such as H_2O_2, 4-HNE and 4-ONE (Andersson et al., 2008; Bautista et al., 2006). Additionally, hydrogen sulphide (H_2S), 15d-PGJ_2 and methylglyoxal activate sensory neurons in a TRPA1-dependent manner (Andersson et al., 2008, 2013; Eberhardt et al., 2014; Streng et al., 2008). Moreover, TRPV1 channels can be activated by the endogenous cannabinoid lipid, anandamide (Zygmunt et al., 1999) as well as the related lipid, 2-acylglycerol (Zygmunt et al., 2013). TRPA1 is activated by THC, the active principle in cannabis, and several other cannabinoids (Jordt et al., 2004; Zygmunt et al., 2002).

1.7 Pain and inflammatory sensitisation

High threshold 'painful' stimuli activate sensory transduction channels expressed on nociceptive nerve fibres resulting in the sensation of pain. Acute pain serves as a defence mechanism as it alerts the body to environmental stimuli which could cause tissue damage (Basbaum et al., 2009). However, there are circumstances in which the pain pathway becomes sensitised long after the original insult or injury has resolved, leading to pain hypersensitivity (Basbaum et al., 2009). In this chronically hypersensitive state, pain no longer serve as a useful

warning signal. Chronic pain is often associated with heightened responses to noxious stimuli (hyperalgesia), and sometimes allodynia, a state in which stimuli that are not usually perceived as painful produce pain or paraesthesias. Pain hypersensitivity is a secondary effect of tissue injury and inflammation (inflammatory pain) or following sensory nerve damage (neuropathic pain) (Basbaum et al., 2009; Julius and Basbaum, 2001)

Tissue injury, and the resulting inflammatory response, leads to sensitisation of peripheral sensory nerve afferents. Pro-inflammatory agents and cells infiltrate the site of tissue injury and the area surrounding the terminals of sensory nerves (Basbaum et al., 2009). Chemical mediators are released from cells which have been disrupted by injury, and are secreted from immune cells which have infiltrated the site of injury or by the activity of inflammatory enzymes (Woolf and Ma, 2007). The resulting mixture referred to as the 'inflammatory soup' (Figure 1-6) includes peptides (CGRP, substance P, bradykinin), lipid mediators (prostaglandins, thromboxanes, leukotrienes and endocannabinoids), cytokines, chemokines, growth factors, protons and ATP (Basbaum et al., 2009; Julius and Basbaum, 2001; Woolf and Ma, 2007). These inflammatory agents act on sensory nerve terminals, thereby increasing their sensitivity to other stimuli, and in some cases, can depolarise the afferents directly.

The sensitisation of primary afferent nerve fibres occurs as a result of inflammatory agents interacting with specific receptors. Some inflammatory mediators such as protons and ATP can directly activate ion channels expressed on peripheral nerve terminals (Dawes and McMahon, 2013). This results in an influx of cations following the opening of the ion channel and evokes depolarisation of the membrane and an increase in action potential firing. In contrast, other inflammatory agents such as prostaglandins, bradykinin, histamine and

chemokines exert their effects by activating GPCRs (Ji et al., 2014). Activation of GPCRs by inflammatory mediators results in the activation of a heteromeric G protein and induction of a biochemical signalling cascade which is dependent on the class of G-protein activated. Both Gq and Gs signalling pathways result in the activation of protein kinases (PKA, PKC), which can modulate the activity of transduction channels such as TRPV1 and TRPA1, and ion channels which are important for excitability (HCN2, $Na_v1.7$-1.9). This lowers the action potential threshold and promotes increased neuronal firing (Emery et al., 2011; Ji et al., 2014).

Neurotransmitters such as substance P and CGRP are released from nociceptive nerve fibre terminals when activated by noxious stimuli (Holzer, 1998; Massaad et al., 2004). The release of these neurotransmitters results in vasodilation and plasma extravasation, as well as activation of non-neuronal cells such as mast cells and neutrophils (Brain and Williams, 1985, 1988; Holzer, 1998). This is referred to as neurogenic inflammation.

Neurotrophic factors including nerve growth factor (NGF), glial cell-derived neurotrophic factor (GDNF) and brain-derived neurotrophic factor (BDNF), elicit effects by binding to receptor tyrosine kinases (Chao, 2003). Upon activation of these receptors, the monomers dimerise and activate downstream signalling cascades. This can affect the transcription of pain and inflammation-related proteins, and can also acutely modulate the activity of ion channels expressed at the nerve terminal (Basbaum et al., 2009). In addition, pro-inflammatory cytokines such as TNF-α and IL-1 bind to their receptors to induce signalling cascades which can modulate neuronal function.

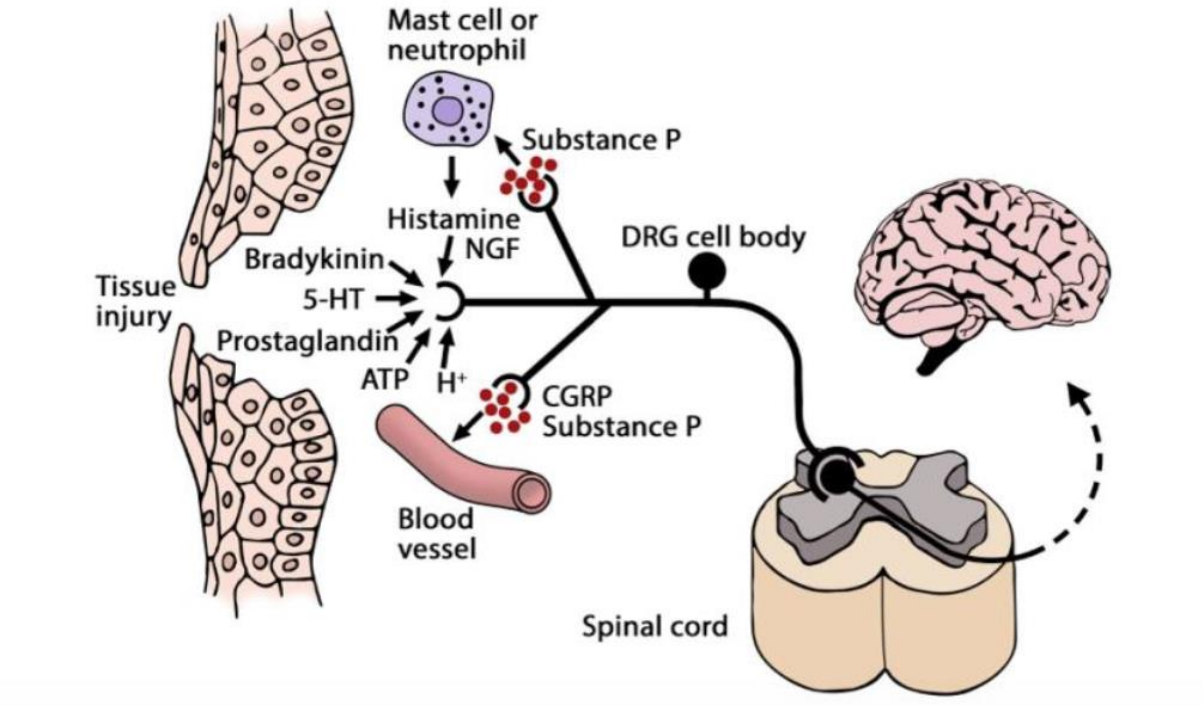

Figure 1-6 Inflammatory sensitisation at the site of tissue injury.

Following tissue injury, sensitisation of primary afferent nerve terminals can occur when mediators from the 'inflammatory soup' activate their receptors. Some mediators, such as protons and ATP, can activate ion channels directly on primary afferent nerve terminals and depolarise the membrane to cause action potential firing. Other mediators such as bradykinin, 5-HT and prostaglandins rely on the activation of GPCRs and intracellular signalling pathways to sensitise transduction channels and ion channels in sensory neurons. Neurotransmitters such as substance P and CGRP are released from nociceptive nerve terminals after activation by noxious stimuli. These neurotransmitters result in vasodilation by exerting their effects on nearby blood vessels and plasma extravasation as part of neurogenic inflammation. Finally, neurotrophic factors such as NGF activate tyrosine kinase receptors. This causes dimerization of the receptor and results in downstream signalling cascades which result in transcriptional changes. This can affect inflammatory-related proteins and modulate the activity of ion channels expressed at the nerve terminal. Modified from (Julius and Basbaum, 2001; Yam et al., 2018).

1.8 Neuropathic pain

The term 'neuropathy' was first coined in 1827 and used to describe nerve dysfunction/damage and abnormal nerve activity. Neuropathy can lead to chronic pain or loss of sensation. Neuropathic pain is caused by a lesion or disease of the somatosensory system, including peripheral fibres and neurons and affects 7-10 % of the general population (Colloca et al., 2017). The incidence of neuropathic pain has been increasing over recent years due to increased incidence of diabetes mellitus and improved survival from cancer after chemotherapy (Colloca et al., 2017). Neuropathic pain symptoms include paraesthesias (pins and needles), electric shocks, burning sensations and pain evoked by light touching (Colloca et al., 2017). Patients can also experience spontaneous pain.

1.8.1 Nerve Injury

Nerve damage can occur by traumatic injury, metabolic or infectious disease or after chemotherapy treatment. Various animal models of peripheral nerve injury have been established in order to study the underlying mechanism(s) for neuropathic pain. A commonly used model is spare nerve injury (SNI), a classic denervation model involving lesions in two of three terminal branches from the sciatic nerve (tibial and common peroneal nerves) (Decosterd and Woolf, 2000). This model produces robust mechanical allodynia after one day post-operation and can last for up to 28 days. In the same study by Decosterd and Woolf, the SNI model resulted in increased sensitivity to mechanical stimuli as assessed by von Frey hairs and thermal (heat and cold) stimuli in mice. Other models of nerve injury have been developed to target different regions in the mouse in order to elicit different symptoms and sensory changes in the animal. They include the partial sciatic nerve injury (PNI) (Seltzer et

al., 1990), the spinal nerve ligation (SNL) (Ho Kim and Mo Chung, 1992) and the sciatic nerve chronic constriction injury (CCI) models (Bennett and Xie, 1988).

1.8.2 Diabetic neuropathy

Diabetic neuropathy is the most common complication of diabetes mellitus, often leading to mortality as well as a great economic burden for diabetes care (Vinik et al., 2013). With the incidence of diabetes being predicted to double between 2000 and 2030 (Juster-Switlyk and Smith, 2016), accordingly the incidence of diabetic neuropathy will increase. The pathogenesis of diabetic peripheral neuropathy is marked by both metabolic and vascular factors (Cameron et al., 2001). Hyperglycaemia is only one of the key metabolic events known to cause axonal and microvascular injury, but there are also other factors at play (Juster-Switlyk and Smith, 2016).

Between 20-50 % of patients with diabetic neuropathy develop neuropathic pain (Juster-Switlyk and Smith, 2016; Themistocleous et al., 2016). This pain is typically localised to the feet but can spread proximally with disease progression. However, the pathophysiology of neuropathic pain in diabetic neuropathy is complex and not yet fully understood. Initially, there is a 'dying back' axonopathy principally affecting sensory neurons, which are believed to become hyperexcitable due to altered gene expression and posttranslational modification of key ion channels (Lauria et al., 2014; Themistocleous et al., 2016). Sensory hyposensitivity affects patients with painful and painless diabetic sensory neuropathy equally and is a major clinical problem as it facilitates development of ulcers, foot complications and amputations.

Diabetes has been induced in mice models in order to study the mechanisms of the disease and its complications. The streptozocin (STZ) model is very commonly used as it results in the

destruction of pancreatic islet β-cells leading to diabetic mice. Single fibre recordings using the STZ mice model have revealed that there is a decreased proportion of Aβ fibres that innervate the diabetic skin, and that diabetes severely impaired the function of cutaneous C and Aβ fibres. This correlated with mice behavioural changes of mechanical hypoalgesia in diabetic mice (Lennertz et al., 2011). However, it has been shown that STZ generates peroxynitrite, which produces sensory abnormalities by stimulating TRPA1 directly (Andersson et al., 2015). As a result, sensory loss is established within an hour of STZ administration and 2-3 days before mice become diabetic. Therefore, the introduction of models that more closely translate the pathophysiology of diabetic neuropathy like the *Ins2*$^{+/Akita}$ model are important for mechanistic studies. Vastani and colleagues showed that Akita mice develop hyposensitivity to noxious mechanical and heat stimulation *in vivo*. In addition, there was a marked loss of heat sensitivity in DRG neurons in culture and reduced activity in mechanonociceptors, whereas low threshold Aβ fibres were unaffected (Vastani et al., 2018).

1.8.3 Chemotherapy induced peripheral neuropathy

Chemotherapy induced peripheral neuropathy (CIPN) is a common dose-limiting side effect of anticancer drugs. Symptoms of CIPN are regularly so severe that it limits or leads to the cessation of treatment and can drastically impact patients' quality of life both during and following therapy (Boyette-Davis et al., 2013, 2015; Quasthoff and Hartung, 2002). The effects of CIPN can also persist after the cessation of treatment in a phenomenon known as 'coasting' (Quasthoff and Hartung, 2002). The type of neuropathy which develops in patients depends on the substance used, with platinum-based agents resulting in a pure sensory and painful neuropathy and vincristine and taxanes resulting in a mixed sensorimotor neuropathy

(Quasthoff and Hartung, 2002). The severity of neurotoxicity is related both to the cumulative dose and type of drug used. However, neuropathic pain can also develop even after a single round of drug treatment either during or immediately after treatment (Quasthoff and Hartung, 2002). A greater predisposition for CIPN has been observed in nerves previously damaged by diabetes, alcohol or inherited neuropathy (Quasthoff and Hartung, 2002). The mechanisms for CIPN are poorly understood. However, it is well known that primary afferent neurons are most susceptible to the effects of these anticancer drugs as most sensory symptoms start at the tips of the toes and fingers and then advance proximally in a 'stocking-glove' distribution (Binder et al., 2007; Boyette-Davis et al., 2011, 2013). Symptoms including pain, tingling and numbness are typically observed in patients' fingers and toes. QST studies have provided greater analysis and detail of the symptoms experienced by patients before and after treatment in the case of specific anticancer agents.

1.9 Oxaliplatin as an anticancer therapy

Oxaliplatin is a third generation platinum based chemotherapeutic drug that is primarily used to treat colorectal cancer, but can also used for other solid tumours (Avan et al., 2015; Carozzi et al., 2015; Deuis et al., 2013; Di Francia et al., 2013; McWhinney et al., 2009). Its introduction as a therapeutic agent followed the earlier platinum based anticancer drugs cisplatin and carboplatin, which were approved to treat ovarian and testicular cancer (Avan et al., 2015; McWhinney et al., 2009). Patients with advanced colorectal cancer are commonly prescribed oxaliplatin in combination with 5-Fluorouracil (5-FU) and Leucovorin (LV) which is often referred to as the FOLFOX4 treatment regimen (Saif and Reardon, 2005; Tsai et al., 2016). This

combination therapy is the first line therapy for advanced colorectal cancer (Lehky et al., 2004; Saif and Reardon, 2005; Wilson et al., 2002).

Although the use of oxaliplatin and other platinum based chemotherapeutic agents has proven to be efficacious in the treatment of various cancers, their use is often compromised by serious side effects such as peripheral sensory neuropathies (Avan et al., 2015; Boyette-Davis et al., 2015). Indeed, around 85 % of patients treated with oxaliplatin are affected by acute or chronic sensory neuropathies (Avan et al., 2015). The acute neurotoxicity is unique to oxaliplatin and can be triggered and/or exacerbated by cold (Deuis et al., 2013; Nassini et al., 2011; Park et al., 2009; Zhao et al., 2012). However, the degree to which oxaliplatin-induced cold hypersensitivity and pain are manifested depends on the cumulative dose of the drug and the frequency with which the drug is administered (Di Francia et al., 2013; Park et al., 2009).

1.9.1 Metabolism of oxaliplatin

Oxaliplatin undergoes rapid non-enzymatic biotransformation in the body in the presence of water and nucleophiles such as chloride, glutathione and methionine (Figure 1-7) (Han et al., 2017a). The two metabolites formed from this reaction include oxalate (leaving group) and a reactive electrophilic species of dichloro (1, 2-diaminocyclohexane) platinum (Pt (DACH)) (Ehrsson et al., 2002; Han et al., 2017a; Jerremalm et al., 2009; Screnci et al., 2000). The most common reactive species formed include monoaqua/monochloro-, diaqua and dichloro-DACH (Han et al., 2017a; Jerremalm et al., 2009). Oxalate is a modest affinity chelator of calcium and magnesium and has been proposed to underlie acute cold allodynia but not mechanical allodynia following oxaliplatin administration (Sakurai et al., 2009; Zhao et al.,

2012). Calcium and magnesium ions accelerate the decomposition of oxaliplatin in chloride-containing solutions *in vitro* and its clearance *in vivo* (Han et al., 2017a). It has been suggested that oxalate is also able to alter the kinetics of voltage gated sodium channels in the acute phase of neurotoxicity caused by oxaliplatin use (Avan et al., 2015; Sakurai et al., 2009). Although few papers report the half-life of oxaliplatin, Ehrsson and co-workers initially demonstrated that the mean half-life of oxaliplatin degradation was 45 minutes *in vivo* (Ehrsson et al., 2002) but later conducted more sensitive spectrophotometric experiments to show that the half-life is 15 minutes *in vivo* (Jerremalm et al., 2009b). Han *et al.* have shown that after 30 minutes in saline, ~85 % of oxaliplatin degrades *in vitro* (Han et al., 2017a). This compares to 100 % degradation after an hour in water. This demonstrates that although Cl^- may accelerate oxaliplatin decomposition, it proceeds relatively slowly *in vitro*.

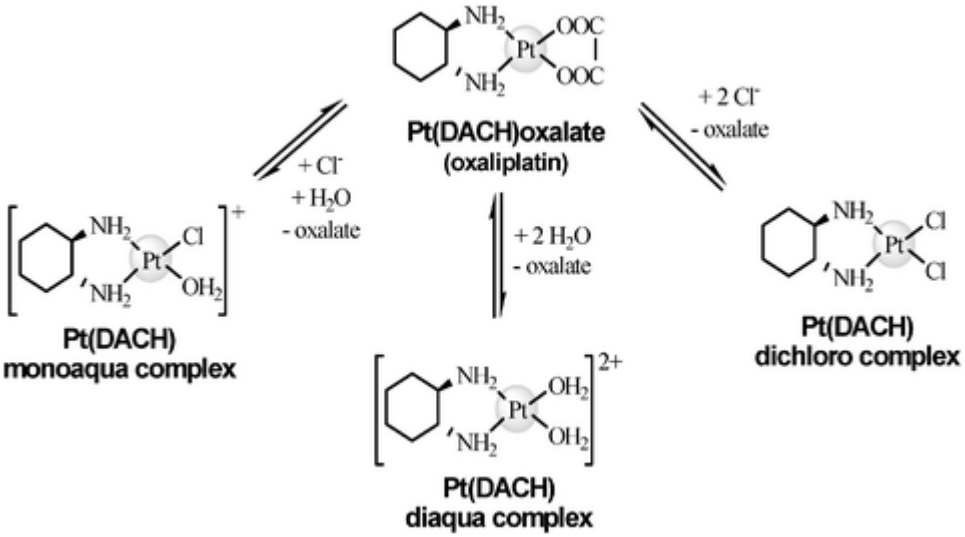

Figure 1-7 Decomposition of oxaliplatin.

Oxaliplatin is thought to undergo spontaneous non-enzymatic biotransformation in the presence of water and nucleophiles such as chloride, glutathione and methionine. This reaction displaces oxalate (leaving group) and results in the formation of reactive species including mononaqua-, diaqua and dichloro-Pt(DACH). The most common product is the dichloro form. (Esteban-Fernández et al., 2010).

1.9.2 Clinical side effects of oxaliplatin

QST studies performed in colorectal cancer patients before and after they received oxaliplatin have revealed acute sensory abnormalities with rapid onset. Baseline readings were also compared against healthy volunteers. A QST study by Barbosa *et al.* was able to link the changes seen in various parameters of sensory modality tests to the primary afferent fibre subtypes that are affected. This study reported loss of textural detection and light touch in Aβ fibres in colorectal cancer patients compared to healthy volunteers using the bumps detection and touch detection test. These deficits were exacerbated in patients after oxaliplatin treatment (Barbosa et al., 2014). In addition, oxaliplatin shifted the cold pain threshold to warmer temperatures as expected from the well-recognised cold allodynia (Barbosa et al., 2014; Binder et al., 2007). Other QST studies have reported a significant reduction in mechanical pain thresholds as assessed by pinprick stimuli, warm hypoesthesia and even heat hyperalgesia, although the last symptom remains controversial (Binder et al., 2007; Krøigård et al., 2014). QST studies capture the adverse clinical symptoms reported by patients on oxaliplatin treatment well and have been particularly useful to translate the symptomatic presentation in patients to mice. In addition, some studies have indicated which subset of primary afferent neurons are affected to explain the symptoms (Barbosa et al., 2014; Forstenpointner et al., 2018). Although several ion channels have been proposed, there is nothing to suggest that these would be preferentially expressed in the longest afferents which innervate the hands and feet.

1.9.3 Mechanisms for oxaliplatin-induced cold hypersensitivity and paraesthesias

Numerous ion channels have been proposed to mediate oxaliplatin-induced cold hypersensitivity and paraesthesias, based on investigations *in vivo*, and electrophysiological and molecular biology studies *in vitro*. MacDonald and colleagues have recently reported cold sensitivity in previously cold-insensitive large-diameter sensory neurons (MacDonald et al., 2021). This shed light on the population of sensory neurons which are affected by oxaliplatin. However, there is no consensus supporting any single target or mechanism. A discussion of some of the proposed ion channels follows below.

1.9.3.1 Na^+ channels and currents

Na_v channels have been longstanding candidate channels in the mechanism for acute effects of oxaliplatin. Many studies have shown that mutations in these Na_v channels can result in marked pain phenotypes and diseases (Cummins et al., 2007; Deuis et al., 2013; Levinson et al., 2012; Waxman and Zamponi, 2014; Waxman et al., 1999; Wood et al., 2004) and alterations in their kinetics can lead to hyperexcitability (Adelsberger et al., 2000; Lehky et al., 2004; Waxman and Zamponi, 2014; Wilson et al., 2002).

Following injury, neurons and axons have been shown to have abnormal expressions of Na_v channels which leads to the development of hyperexcitability and pain (Waxman et al., 1999; Zhang et al., 2020). Thus, the dysregulated expression of sodium channels in primary sensory neurons are thought to contribute to various forms of chronic pain. DRG neurons are known to express numerous sodium channels, which are both TTX-s and TTX-r (Lolignier et al., 2015; Waxman et al., 1999; Wood et al., 2004). The gene expression of these channels has been

shown to be altered following injuries which significantly influences the triggering of pain (Cummins et al., 2007; Waxman and Zamponi, 2014; Waxman et al., 1999).

$Na_v1.7$ has attracted particular attention as a consequence of diseases associated with both gain and loss-of-function mutations in the channel (Cummins et al., 2007; Deuis et al., 2013; Levinson et al., 2012; Waxman and Zamponi, 2014; Wood et al., 2004). Gain-of-function mutations result in hyperexcitability due to repetitive firing and altered inactivation kinetics (Liu and Wood, 2011). However, the $Na_v1.7$-selective blocker, BIIB074 failed clinically despite a promising first enriched trial (Zakrzewska et al., 2017), suggesting that this isoform cannot be targeted successfully, and that blocking it alone is not effective. Other isoforms have been shown to be involved in the transmission of pain signals including the TTX-r isoforms, $Na_v1.8$ and $Na_v1.9$ (Liu and Wood, 2011). Blocking these isoforms has been shown to be effective in ameliorating pain in mice (Cummins et al., 2007; Liu and Wood, 2011). Both $Na_v1.8$ and $Na_v1.9$ are important in noxious cold sensing as discussed above, and have for this reason been proposed to play some role in oxaliplatin-induced cold hypersensitivity (Lolignier et al., 2015; MacDonald et al., 2020a). $Na_v1.9$ has also been implicated in the transmission of pain in some rodent models (Deuis et al., 2013). In *Scn11a*$^{-/-}$ mice, there were no signs of cold allodynia following oxaliplatin administration compared to WT (Lolignier et al., 2015). Furthermore, calcium imaging studies showed that the proportion of cold-sensitive neurons isolated from oxaliplatin-treated mice were significantly reduced in *Scn11a*$^{-/-}$ mice compared to WT (Lolignier et al., 2015).

Studies in mice also indicate that $Na_v1.6$ is important for oxaliplatin-induced cold allodynia. Deuis and colleagues used a pharmacological approach to demonstrate that the symptoms of oxaliplatin-evoked hypersensitivities can be alleviated by sodium channel blockers.

Tetrodotoxin (TTX) and $Na_v1.6$-selective μ-Conotoxins almost completely reversed the effects of oxaliplatin. Intra-plantar injections of TTX in oxaliplatin treated mice inhibited nocifensive responses when exposed to cool surfaces (Deuis et al., 2013), suggesting that a TTX-s subtype of sodium channels was involved in the mechanism. Patch-clamp investigations of mouse DRG neurons demonstrated that oxaliplatin produced cold-evoked action potential bursts, by reducing the inactivation of $Na_v1.6$ (Sittl et al., 2012). The effects of cooling during oxaliplatin treatment were abolished in *Scn8a*$^{med/med}$ mice, which lack functional $Na_v1.6$ channels (Sittl et al., 2012).

1.9.3.2 Potassium channels and currents

The involvement of potassium channels as cold sensors has been suggested due to changes in their kinetics caused by cooling. The blockade of potassium currents which normally serve as excitability brakes to depolarisation could be important in causing nerve firing to cold stimuli (McKemy, 2013; Viana et al., 2002a). The voltage-dependent 4-AP-sensitive potassium current I_{KD} and the two-pore potassium channels including TRAAK, TREK-1 and TREK-2 channels are attractive targets since the latter are not voltage-sensitive and all can remain open constitutively and set the membrane potential and neuronal excitability.

It has been shown that cold-sensitive neurons are activated by cooling once there is closure of a background potassium current and firing (Viana et al., 2002a). This current referred to as the I_{KD} is important in functioning as excitability brakes and is particularly important in preventing activation of cold-insensitive neurons to cooling (Viana et al., 2002a). In a later study, it was concluded that cold-sensitive closed K^+ current, may set the threshold for neuronal firing (Madrid et al., 2009). Thus, inhibition of this current may be important in

sensitising the cold-insensitive neuronal population, a phenomenon which may help to explain neuropathic pain and hypersensitivity induced by cold (Viana et al., 2002a).

K_{2P} channels are activated by thermal, mechanical and lipid stimuli (Pereira et al., 2014). TREK-2 is expressed in rodent primary nociceptive afferents of the DRG and also innervate the skin (Pereira et al., 2014). TREK-2 is one of the major background potassium currents that has a complementary role with TREK-1 and TRAAK channels to regulate depolarising currents (Pereira et al., 2014). This channel has been implicated in cold allodynia, a key feature seen in patients taking oxaliplatin over a prolonged period (Pereira et al., 2014). A marked decrease in TREK1 and TRAAK transcripts were observed in mice that were treated with oxaliplatin (Descoeur et al., 2011), suggesting that these channels have an important regulatory role for excitability in neurons. Furthermore, mice lacking TREK1/TRAAK (*KCNK2/KCNK4*$^{-/-}$) showed tonic intolerance to noxious cold and developed cool allodynia which resembled that seen in WT mice injected with oxaliplatin (Descoeur et al., 2011). Therefore, this suggests that altered kinetics in background potassium channels and currents in neurons can increase the excitability in these cells. Furthermore, this could activate a cold-insensitive population of neurons, which may cause oxaliplatin-induced cold hypersensitivity.

1.9.3.3 TRP channels

The role of TRP channels in oxaliplatin-induced cold and mechanical hyperalgesia has also been investigated. It has been predicted that there may be more than one TRP channel involved in the mechanism for the development of peripheral neuropathic pain symptoms. Studies have shown that the mRNA expression for TRPV1, TRPA1 and TRPM8 increase significantly following treatment with Pt-containing chemotherapeutics (Anand et al., 2010;

Carozzi et al., 2015; Deuis et al., 2013; Mizuno et al., 2014; Park et al., 2015; Zhao et al., 2012). However, since cold sensitivity appears so quickly, expression changes cannot be responsible for the acute effects of oxaliplatin. Therefore, the importance of these channels is unclear.

TRPM8, which is activated by cool temperatures (30-15 °C), cooling agents such as menthol and icilin, and is an osmosensor (Peier et al., 2002b; Quallo et al., 2015), has been suggested to be a key transduction channel in oxaliplatin-induced cold hypersensitivity. Permanent inactivation of the channel result in deficits in the ability of mice to develop cold allodynia following oxaliplatin treatment (Descoeur et al., 2011; Mizuno et al., 2014). A potentially related finding was that TRPM8 mRNA expression was increased in DRG neurons following treatment with oxaliplatin (Gauchan et al., 2009; Mizuno et al., 2014).

TRPA1 is another TRP channel that has been studied due to its possible role in oxaliplatin-induced cold and mechanical hypersensitivity (Nassini et al., 2011; Park et al., 2015; Zhao et al., 2012). It is activated by pungent compounds including allyl isothiocyanate (AITC) and cinnamaldehyde (Bandell et al., 2004; Bautista et al., 2005). It is known to be activated by chemicals produced as a result of oxidative stress and irritants such as H_2O_2 and acrolein, which can cause neurogenic inflammation (Andersson et al., 2008; Nassini et al., 2011; Park et al., 2015). There is controversy surrounding whether TRPA1 is a sensor of noxious cold, as discussed above. However, some studies have demonstrated a role for TRPA1 in oxaliplatin-induced cold hypersensitivity. Park *et al.* showed that there was a significantly increased TRPA1 mRNA expression when mice were treated with oxaliplatin compared to control groups (Park, Chae et al. 2015). However, cold sensitivity induced by oxaliplatin *in vivo* appears before any transcriptional effect can be relevant. In addition, blocking TRPA1 or use

of *Trpa1*$^{-/-}$ mice reduces sensitivity to noxious cold and mechanical stimuli without oxaliplatin administration (Andersson et al., 2009; Gentry et al., 2010). Thus, it is unclear whether TRPA1 contributes specifically to oxaliplatin-induced cold hypersensitivity.

Similar to TRPA1 and TRPM8, the expression of TRPV1 is upregulated in DRG neurons following treatment with oxaliplatin (Anand et al., 2010; Ta et al., 2010). However, whether TRPV1 is involved in the development of oxaliplatin evoked sensory neuropathy remains uncertain. Mizuno and colleagues showed that nocifensive behaviours were not increased when the specific TRPV1 agonist capsaicin was administered in the hind paw of oxaliplatin treated rats (Mizuno et al., 2014). In contrast, Anand *et al.* reported that TRPV1 in DRG neurons was sensitised by oxaliplatin, as measured by increased calcium responses to capsaicin (Anand et al., 2010). However, these conclusions are not clear given the small sample size of neurons used. The potential role of TRP channels in the pathophysiology of oxaliplatin-induced pain remains to be clarified.

Studies of transgenic mice with selective knockout of individual TRP channels have been used to strengthen the role of these channels in the mechanism of oxaliplatin-induced cold and mechanical hypersensitivity. Descoeur and colleagues showed that *Trpm8*$^{-/-}$ mice failed to develop cold hypersensitivity after oxaliplatin treatment (Descoeur et al., 2011). Gauchan and colleagues showed that TRPM8 mRNA levels were significantly increased in mice injected with a single 3 mg/kg injection of oxaliplatin (Gauchan et al., 2009). Nassini and colleagues have demonstrated that mechanical and cold hyperalgesia caused by oxaliplatin were absent in *Trpa1*$^{-/-}$ mice (Nassini et al., 2011). In addition, findings from Zhao *et al.* confirmed TRPA1 involvement by use of a selective pharmacological antagonist (HC-030031) and genetic

ablation of TRPA1 (Zhao et al., 2012). However, it should be noted that *Trpa1*$^{-/-}$ mice display a reduced sensitivity in all pain models examined so far, as well as in the naïve state as mentioned above (Zygmunt and Högestätt, 2014). Thus, the role of this channel is not clear in oxaliplatin-induced cold pain.

1.10 Aims and objectives

Proposed mechanisms for oxaliplatin-induced cold hypersensitivity and paraesthesias have been investigated intensely for many years, no consensus has been reached and much remains unexplained.

The aims of this project were first to establish the effects of oxaliplatin on sensory neurons at the level of the DRG and peripheral terminals (Chapters 3 and 5). Single fibre recordings were conducted to elucidate the fibre type and subpopulations of primary afferent fibres that are affected by direct application of oxaliplatin to the receptive fields of single fibres (Chapter 5). This was important in providing a greater understanding of the cellular mechanisms which underlie oxaliplatin-induced cold hypersensitivity and paraesthesias.

Following on from this, we aimed to identify an ion channel that could be targeted to prevent the effects of oxaliplatin in sensory neurons. Multielectrode array (MEA) assays were used to provide a high throughput system in order to find candidate ion channels (Chapter 6). Novel target candidates were then studied further using behavioural and electrophysiological approaches (Chapter 7).

2 The effects of oxaliplatin *in vivo*

2.1 Introduction

Oxaliplatin-induced cold-evoked paraesthesias and acute neuropathic pain are common dose-limiting effects in the clinic (Binder et al., 2007; Grothey, 2003; Saif and Reardon, 2005). Chronic neuropathy develops with repeated treatment cycles and cold allodynia is commonplace (Saif and Reardon, 2005). Patients report that everyday tasks become increasingly difficult and touching cool surfaces is painful or unpleasant (Grothey et al., 2011). In order to model this in animals, the effects of different dose regimens have been examined *in vivo* in an attempt to faithfully recapitulate the clinical symptoms (Descoeur et al., 2011; Deuis et al., 2013; Mizuno et al., 2014; Nagasaka et al., 2017; Sakurai et al., 2009). Descoeur and colleagues showed that a single systemic dose of oxaliplatin (6 mg/kg) is sufficient to induce a behavioural phenotype in mice that mimics patient cold hypersensitivities (Descoeur et al., 2011). Studies of transgenic mice, electrophysiological and pharmacological investigation of ion channels and expression analysis, have identified several ion channels as potential candidates for oxaliplatin-induced sensory abnormalities (Descoeur et al., 2011; Deuis et al., 2013; Gauchan et al., 2009; Kono et al., 2012; Nassini et al., 2011; Sittl et al., 2010, 2012).

TRPM8, the principal mammalian cold transduction channel, is activated by cool temperatures between the range of 15-32 °C and cooling agents such as menthol and icilin (McKemy et al., 2002; Peier et al., 2002b). Studies of *Trpm8*$^{-/-}$ mice suggest that the channel may be involved in oxaliplatin-induced cold hypersensitivity (Descoeur et al., 2011; Gauchan et al., 2009; Kono et al., 2012; Mizuno et al., 2014). In addition, TRPM8 mRNA expression was increased in DRG neurons isolated from oxaliplatin-treated mice (Descoeur et al., 2011; Gauchan et al., 2009). However, the latter finding cannot explain the acute cold

hypersensitivity induced by oxaliplatin, since this is established within minutes of administration, before any expressional changes can occur.

Here we have used a single systemic dose of oxaliplatin (Descoeur et al., 2011) to induce the behavioural phenotype and explored the role of TRPM8 in this model of oxaliplatin-induced cold and mechanical allodynia.

2.2 Aims

The aim of this chapter was to establish a model of oxaliplatin-induced peripheral neuropathy in mice, using a single dose of the compound. The effect of oxaliplatin on nociception was examined *in vivo*, and the importance of TRPM8 was determined using *Trpm8*$^{-/-}$ mice. Importantly, we aim to demonstrate that the model, which reflects what is dosed in the clinic, could produce sensory abnormalities akin to those seen in patients.

2.3 Methods

Behavioural experiments were carried out according to the U.K. Home Office Animal Procedures (1986) Act. All procedures were approved by the King's College London Animal Welfare and Ethical Review Body. All mice used in this study were of the C57BL/6J background. Adult male and female mice were used in all experiments, mice were 8-12 weeks old and weighed between 20-25 g.

All behavioural experiments presented in this chapter were conducted by Clive Gentry. The experimenter was unblinded to all treatment groups, however, all experiments were performed in a randomised manner.

2.3.1 Drugs used *in vivo*

Oxaliplatin (product Y0000271, Sigma-Aldrich) was dissolved in 5 % glucose solution. Mice were dosed with a single (6 mg/kg) intraperitoneal (i.p.) injection of oxaliplatin or vehicle (5 % glucose). The effect of oxaliplatin on nociception was monitored for up to 7 days after administration and mice were thereafter killed by cervical dislocation.

2.3.2 Mechanical allodynia assessed using Randall-Selitto paw pressure test

The Randall-Selitto paw pressure test (Randall and Selitto, 1957) was performed using an Analgesy-meter (Ugo Basile, Gemonio, Italy). Mice were kept in their holding cages to acclimatise (10-15 minutes) to the experimental room. Individual mice were lightly restrained by the experimenter and a constantly increasing pressure stimulus was applied to the dorsal surface of the hind paw using a blunt conical probe. The nociceptive threshold was defined as the force in grams at which the mouse withdrew its paw. A force cut off value of 150 g was used to avoid tissue injury. Mice which responded at cut off value were excluded from analyses.

2.3.3 Cold nociception assessed using cold plate (10 °C)

Cold nociception was assessed using a cold plate (Ugo Basile) set to 10 °C to measure the paw withdrawal latency. Mice were lightly restrained and one hind paw was placed in contact with the surface of the cold plate (Gentry et al., 2010). The time taken for a withdrawal response was recorded. A latency cut off value of 30 seconds was used to avoid tissue injury. Mice which responded at cut off value were excluded from analyses.

Further behavioural assessments were performed to assess changes in temperature sensitivity between vehicle- and oxaliplatin-treated mice at day 3 after injection. Paw withdrawal latencies were compared at 10-20 °C and 35-55 °C at 5 °C increments.

2.3.4 Assessing the role of TRPM8 in oxaliplatin-induced hypersensitivity *in vivo*

Trpm8$^{-/-}$ mice (n = 6) were obtained from Jackson Laboratories, and were developed by David Julius and colleagues (Bautista et al., 2007). Wildtype (WT) mice (n = 6) used in these experiments were not littermates of the *Trpm8*$^{-/-}$ mice.

The Randall-Selitto paw pressure test and cold plate assay tests were performed in WT and *Trpm8*$^{-/-}$ mice to assess the role of the channel in oxaliplatin-induced hypersensitivity *in vivo*. In addition, tactile sensitivity was assessed using von Frey filaments (0.008–2 g) according to the up-down method of Chaplan *et al.* (Chaplan et al., 1994). Animals were placed in a Perspex chamber with a metal grid floor allowing access to their plantar surface and were acclimatised for 60 minutes prior to the start of the experiment. The von Frey hairs were applied to the plantar surface of the hind paw with enough force to allow the filament to bend and were held static for ∼2 – 3 seconds. The stimulus was repeated up to five times at

intervals of several seconds. The stimulus interval was adapted to allow for the resolution of any behavioural responses to previous stimuli. A positive response was noted if the paw was sharply withdrawn or if the mouse flinched upon removal of the hair. Any movement of the mouse, such as walking or grooming, was deemed an unclear response, and in such cases the stimulus was repeated. If no response was noted, a higher force hair was tested and the filament producing a positive response was recorded as the threshold. This was tested before treatment and 1 day after treatment.

2.3.5 Statistical analysis

A Two-way repeated measures (RM) ANOVA was performed in experiments involving two treatment groups or genotypes over time courses. When comparing data between groups, Sidak's *post-hoc* analysis was used and when data within groups were compared, Dunnett's *post-hoc* analysis was performed. An unpaired *t* test was used to analyse data between treatment groups at a single time point.

2.4 Results

2.4.1 Oxaliplatin induces mechanical and cold hypersensitivity *in vivo*

Patients treated with oxaliplatin in the clinic often experience dose-limiting effects and sensory abnormalities which include cold-evoked paraesthesias, cold allodynia and mechanical hypersensitivities (Deuis et al., 2013; Grothey, 2003; Pachman et al., 2015; Saif and Reardon, 2005; Sittl et al., 2012; Wilson et al., 2002). Intraperitoneal injection of oxaliplatin (6 mg/kg) produced significant cold and mechanical hypersensitivities in mice within 3 hours (Figure 2-1 and 2-2). This was followed by a complete remission 1 day after oxaliplatin injection. Thereafter, a more sustained phase of hypersensitivity to cold and mechanical stimulation developed.

Patients report altered abnormal sensations to mechanical stimuli including paraesthesias and tactile allodynia after oxaliplatin treatment (Grothey, 2003; Johnston et al., 2017; Kawashiri et al., 2011; Webster et al., 2005). We found that oxaliplatin reduced the paw withdrawal thresholds significantly after 3 hours and on days 2 and 3 compared to vehicle-treated mice (Figure 2-1). In addition, oxaliplatin treatment reduced the paw withdrawal thresholds at the same time points when compared to baseline (Figure 2-1). In addition, oxaliplatin-induced paraesthesias and cold allodynia are the most common adverse effects experienced by patients in the clinic after acute treatment with the compound (Barbosa et al., 2014; Deuis et al., 2013; Saif and Reardon, 2005).

Oxaliplatin treatment in mice significantly reduced paw withdrawal latencies to a cold plate (10 °C) after 3 hours and 3 days when compared to vehicle-treated mice (Figure 2-2). There was also a trend towards increased cold sensitivity in oxaliplatin-treated mice at days 2, 4 and

7 compared to vehicle-treated mice. Oxaliplatin-treated mice showed a marked reduction in paw withdrawal latencies to cold plate after 3 hours, and on days 3 and 7 when compared to the baseline (Figure 2-2).

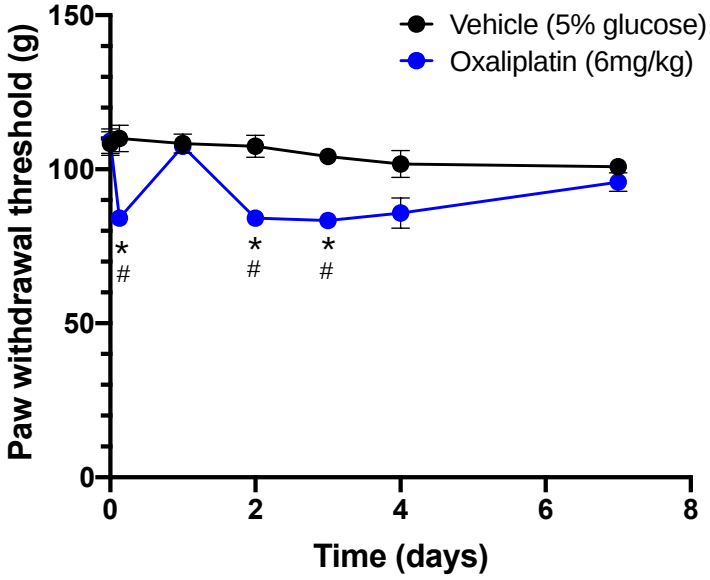

Figure 2-1 Oxaliplatin treatment causes mechanical hyperalgesia in mice.

Oxaliplatin reduced the paw withdrawal threshold after 3 hours, and on days 2 and 3 after treatment when compared to vehicle-treated mice. In addition, oxaliplatin reduced the paw withdrawal threshold at 3 hours, and on days 2 and 3 after treatment when compared to baseline. Data presented as mean ± S.E.M. $^{*}P < 0.05$ between treatment groups, Two-way RM ANOVA followed by Sidak's *post-hoc* test. $^{\#}P < 0.05$ compared to the naïve, pre-injection value, Two-way RM ANOVA followed by Dunnett's *post hoc* test.

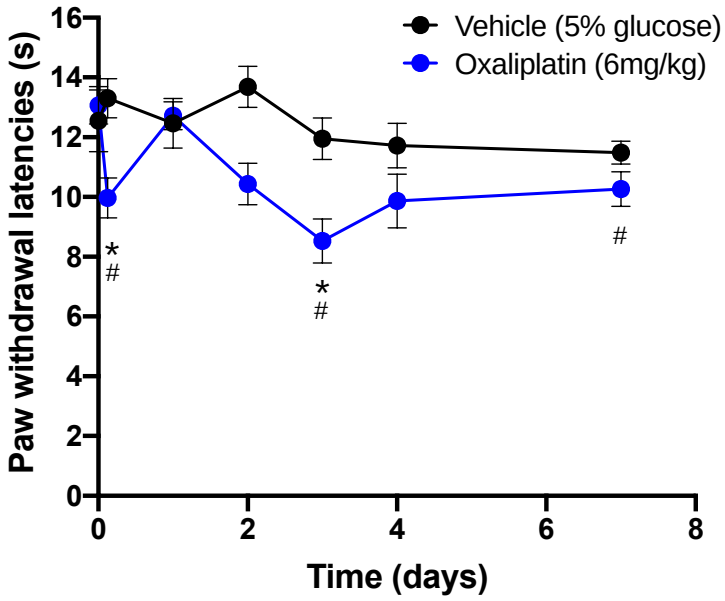

Figure 2-2 Oxaliplatin treatment causes cold allodynia in mice.

Oxaliplatin reduced the paw withdrawal latencies after 3 hours and 3 days when compared to vehicle-treated mice. In addition, oxaliplatin treatment reduced the paw withdrawal latencies after 3 hours, 3 and 7 days after treatment when compared to baseline. Data presented as mean ± S.E.M. $^{*}P < 0.05$ between treatment groups, Two-way RM ANOVA followed by Sidak's *post-hoc* test. $^{\#}P < 0.05$ compared to the naïve, pre-injection value, Two-way RM ANOVA followed by Dunnett's *post hoc* test.

2.4.2 Oxaliplatin increases the sensitivity to noxious cold, but not heat

Oxaliplatin has been reported to produce hypersensitivity to heat, as well as mechanical and cold stimulation (Attal et al., 2009; Binder et al., 2007). We examined the behavioural sensitivity over a range of innocuous and noxious temperatures 3 days after vehicle or oxaliplatin treatment. This marked maximal hypersensitivity after oxaliplatin treatment. Oxaliplatin did not reduce the heat withdrawal threshold in mice (35-55 °C) when compared vehicle-treated mice (Figure 2-3). However, we observed a significant reduction in the paw withdrawal latencies between oxaliplatin-treated and vehicle-treated mice at 10 °C, but not to other cool temperatures (15, 20 °C).

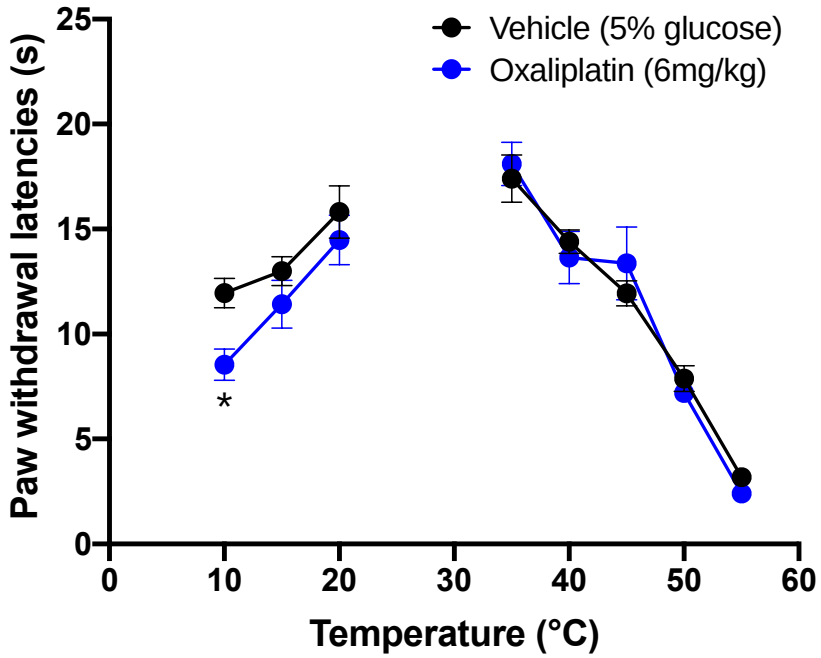

Figure 2-3 Oxaliplatin increases sensitivity to noxious cold, but not heat.

Oxaliplatin significantly reduced the paw withdrawal latencies at 10 °C when compared to vehicle-treated mice. Oxaliplatin-treated mice did not show increased sensitivity to heat (35-55 °C) when compared to vehicle-treated mice. Data presented as mean ± S.E.M. *$P < 0.05$ between genotypes, unpaired *t* test.

2.4.3 The onset of cold allodynia is delayed in *Trpm8*$^{-/-}$ mice

TRPM8 is the principal mammalian cold sensor (McKemy et al., 2002; Peier et al., 2002b). Earlier studies have shown that use of *Trpm8*$^{-/-}$ mice prevents the development of oxaliplatin-induced cold hypersensitivity and that the chemotherapeutic increases TRPM8 mRNA expression (Gauchan et al., 2009; Kono et al., 2012). Here we examined the effect of oxaliplatin (6 mg/kg, i.p.) on cold and mechanical sensitivity in WT and *Trpm8*$^{-/-}$ mice.

In naïve mice, before administration of oxaliplatin, the paw withdrawal latency to a cold plate at 10 °C was longer in *Trpm8*$^{-/-}$ mice compared to WT mice (Figure 2-4). Oxaliplatin increased the cold sensitivity in mice of both genotypes, but *Trpm8*$^{-/-}$ mice consistently remained significantly less sensitive than WT. Our results further indicate that the onset of cold hypersensitivity may be delayed in *Trpm8*$^{-/-}$ mice, since their responsiveness was unaltered 1 day after administration. Mice of both genotypes remained hypersensitive for at least 2 weeks. Interestingly, oxaliplatin treatment caused a significant reduction in the paw withdrawal latency after 1 day in WT mice, the same point at which there was a remission in previous experiments.

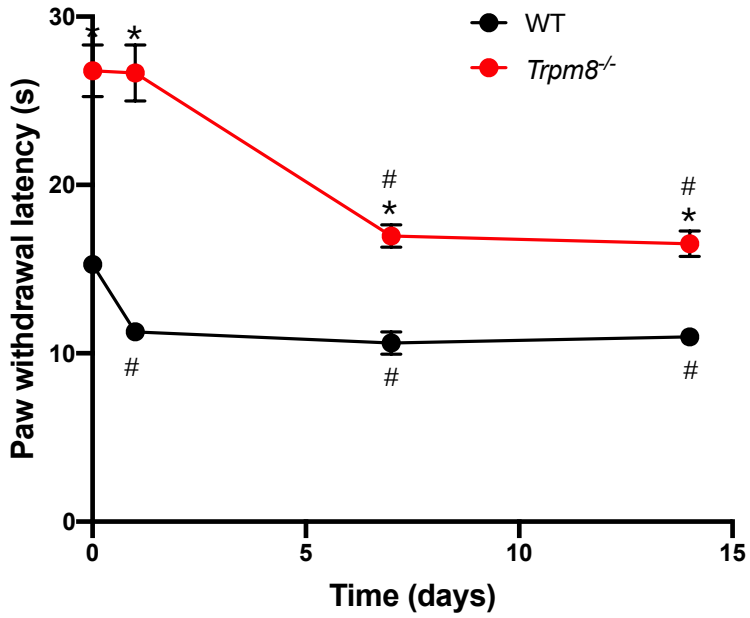

Figure 2-4 Oxaliplatin-induced cold allodynia in Trpm8$^{-/-}$ and WT (Trpm8$^{+/+}$) mice

Oxaliplatin reduced the paw withdrawal latency to a cold plate (10 °C) in *Trpm8*$^{-/-}$ and WT (*Trpm8*$^{+/+}$) mice. There was a delayed onset of cold hypersensitivity in *Trpm8*$^{-/-}$ mice. The paw withdrawal latency was unaltered after 1-day oxaliplatin treatment in *Trpm8*$^{-/-}$ mice. Data presented as mean ± S.E.M. *$P < 0.05$ between genotypes, Two-way RM ANOVA followed by Sidak's *post-hoc* test. $^{\#}P < 0.05$ compared to the naïve, pre-injection value, Two-way RM ANOVA followed by Dunnett's *post hoc* test.

2.4.4 Mechanical hypersensitivity was absent in *Trpm8*$^{-/-}$ mice

In the clinic, patients have reported experiencing dynamic and tactile allodynia following oxaliplatin treatment (Johnston et al., 2017; Kawashiri et al., 2011; Pachman et al., 2015). In addition, they experience increased pressure pain (Gamelin et al., 2002, 2004; Grothey et al., 2011; Saif and Reardon, 2005). We used the Randall-Selitto test to assess sensitivity to mechanical stimuli over the entire surface of the hind paw. In WT mice, oxaliplatin caused a significant reduction in paw withdrawal thresholds at days 1, 7 and 14 when compared to baseline (Figure 2-5). In contrast, *Trpm8*$^{-/-}$ mice did not develop acute oxaliplatin-induced mechanical hypersensitivity. Instead, oxaliplatin treatment caused a reduction in paw withdrawal threshold only at day 14 in this group (Figure 2-5).

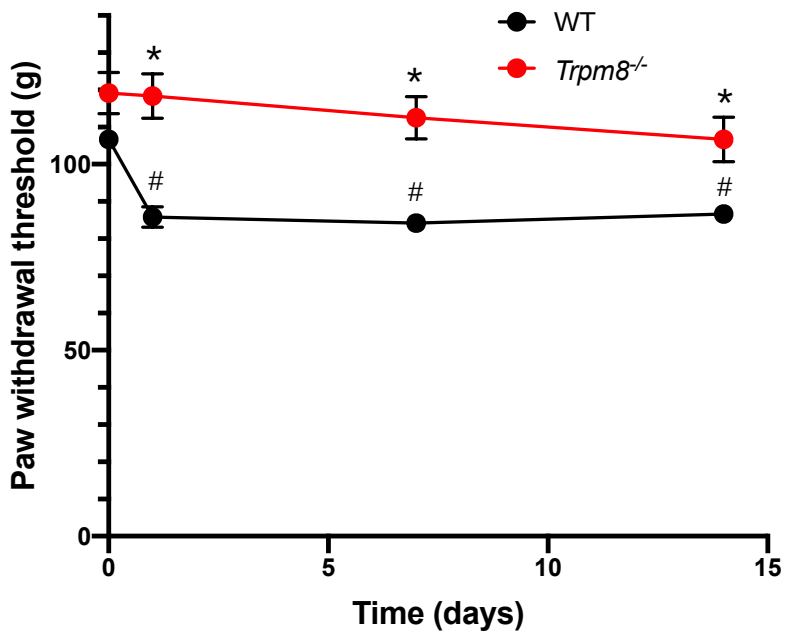

Figure 2-5 Trpm8$^{-/-}$ mice failed to develop acute oxaliplatin-induced mechanical hypersensitivity.

Oxaliplatin reduced the paw withdrawal threshold in the Randall-Selitto test in WT (*Trpm8*$^{+/+}$) mice only. Oxaliplatin did not affect the mechanical sensitivity in *Trpm8*$^{-/-}$ mice. Data presented as mean ± S.E.M. **P* < 0.05 between genotypes, Two-way RM ANOVA followed by Sidak's *post-hoc* test. $^{\#}P$ < 0.05 compared to the naïve, pre-injection value, Two-way RM ANOVA followed by Dunnett's *post hoc* test.

2.4.5 Oxaliplatin-induced tactile allodynia is reduced in *Trpm8*$^{-/-}$ mice

Patients develop oxaliplatin-induced paraesthesias and tactile allodynia (Saif and Reardon, 2005). We examined the role of TRPM8 in the development of oxaliplatin-induced tactile allodynia using von Frey filaments, before and 1 day after administration of the compound. The paw withdrawal threshold was reduced in WT mice 1 day after oxaliplatin treatment when compared to baseline (Figure 2-6). Oxaliplatin did not affect the paw withdrawal thresholds of *Trpm8*$^{-/-}$ mice 1 day after treatment when compared to baseline (Figure 2-6). As a result, there was a marked difference between the genotypes after oxaliplatin treatment.

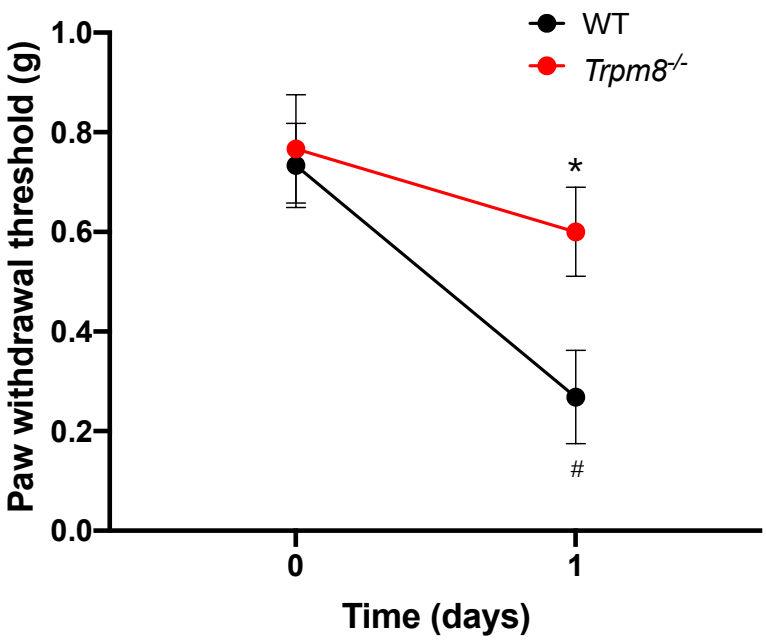

Figure 2-6 Trpm8$^{-/-}$ mice failed to develop acute oxaliplatin-induced tactile allodynia.

Oxaliplatin significantly reduced the paw withdrawal threshold to von Frey filaments 1 day after treatment when compared to baseline in WT (*Trpm8*$^{+/+}$) mice. However, the paw withdrawal thresholds were unaffected in *Trpm8*$^{-/-}$ mice after oxaliplatin treatment. Data presented as mean ± S.E.M. **P* < 0.05 between genotypes, Two-way RM ANOVA followed by Sidak's *post-hoc* test. $^{\#}P$ < 0.05 compared to the naïve, pre-injection value, Two-way RM ANOVA followed by Dunnett's *post hoc* test.

2.5 Discussion

The results presented in this chapter demonstrate that oxaliplatin, administered as a single systemic dose resulted in cold allodynia and mechanical hyperalgesia in mice. In this study, we show that oxaliplatin caused acute increased sensitivity in WT mice in the Randall-Selitto and cold plate assays. This was followed by a sustained period of abnormality in both modalities of sensation. Finally, in WT mice oxaliplatin increased sensitivity to noxious cold but not heat in mice. This is in contrast to QST studies which have reported oxaliplatin-induced heat hyperalgesia and allodynia in patients (Attal et al., 2009; Binder et al., 2007). Whilst the cold-plate test was effective at showing cold-hypersensitivity, it did not fully translate the patient experience which is often more severe and occurs at cool temperatures in addition to colder ones.

Previous studies have identified a role for TRPM8, the principal mammalian cold sensor in oxaliplatin-induced cold hypersensitivity (Anand et al., 2010; Gauchan et al., 2009; Kawashiri et al., 2012; Kono et al., 2012). We demonstrate that oxaliplatin-induced cold allodynia was delayed in its onset in mice lacking the functional *TRPM8 channel*, in agreement with earlier studies (Gauchan et al., 2009; Kono et al., 2012). Interestingly, there was an absence of acute mechanical hyperalgesia and tactile allodynia in *Trpm8*$^{-/-}$ mice after oxaliplatin treatment (Descoeur et al., 2011; Yamamoto et al., 2018).

Acute oxaliplatin-induced neuropathy occurs in almost all patients and manifests as distal sensory and/or motor disturbances including paraesthesias, dysaesthesias and muscle fasciculations (Deuis et al., 2013; Saif and Reardon, 2005; Webster et al., 2005). These symptoms are triggered and exacerbated by exposure to cold and there is a significant reduction in cold pain thresholds (Attal et al., 2009; Binder et al., 2007). Over time, patients

can experience functional impairment as paraesthesias become more severe. This can interfere with daily activities (Grothey et al., 2011; Saif and Reardon, 2005).

The plasma concentration of oxaliplatin in patients after a high dose (130 mg/m^2) of the drug is reported to be between 0.83-1.31 mg/L (Culy et al., 2000). However, systemic doses of between 3.5 mg/kg and 40 mg/kg of oxaliplatin in mice have been shown to have comparable plasma concentrations of the compound as in patients (Marmiroli et al., 2017; Sprowl et al., 2013). In addition, 6 mg/kg of oxaliplatin is a therapeutic dose of the drug (Descoeur et al., 2011). In this study, we investigated the acute effects of oxaliplatin *in vivo*. We showed that mice developed a behavioural phenotype that recapitulated some aspects of patient symptoms. The acute phase of hypersensitivity and sensory abnormalities can occur between hours to days after treatment, with up to 95 % of patients being affected (Ramirez et al., 2018). We also found that the maximal hypersensitivity occurred at day 3 after treatment for both paw withdrawal latencies to cold and in the paw pressure test. This faithfully translated the findings of a clinical trial for oxaliplatin-induced neuropathy, which found that the acute adverse effects of oxaliplatin peaked at day 3, and persisted for up to a week after treatment (Pachman et al., 2015). Many dose regimens have been used to recapitulate the clinical symptoms of oxaliplatin. Intra-plantar administration of oxaliplatin is effective and requires smaller doses of the drug to evoke the same responses (Deuis et al., 2013, 2014). It also allows comparison between the treated and untreated hind paws. However, since oxaliplatin undergoes spontaneous decomposition after injection, we sought to use a systemic dosing regimen to translate the clinical situation more closely.

The pathophysiological basis of acute oxaliplatin-induced neuropathy, particularly cold allodynia is not fully understood. This is in part due to the limited number of animal models which accurately capture the neuropathic symptomatology clinically, particularly the rapid onset of cold allodynia (Deuis et al., 2013). The different behavioural models used may explain some of the discrepancies in the literature. Many investigators have used tail immersion assays or the acetone test, which may not accurately reflect the clinical setting (Descoeur et al., 2011; Mizuno et al., 2014). The acetone drop is localised to just the central portion of the paw and its application also exerts some mechanical stimulation. In addition, the behavioural assays are conducted after a day of treatment at the earliest, which means that the acute phase of cold allodynia is usually missed. However, in one study which reported the onset of cold allodynia after minutes of injection, it has been suggested that oxaliplatin administration *in vivo* exerts a direct excitatory effect on peripheral sensory nerve endings (Deuis et al., 2013).

The authors suggest that ion channel modulation of voltage-gated sodium and potassium channels are the reason for oxaliplatin-induced hyperexcitability (Deuis et al., 2013). However, they cannot be sure that there are no additional transduction processes that elicit activity. Our study also demonstrates the acute effects of oxaliplatin *in vivo*. There was a significant reduction in the withdrawal latencies to cold and thresholds to mechanical stimuli after 3 hours of drug application. Therefore, oxaliplatin directly acts on voltage-gated ion channels in sensory neurons as cold and mechanical hypersensitivities are present before any transcriptional changes can occur. This is in agreement with Deuis and colleagues. Although, transcriptional changes may also be a direct consequence of oxaliplatin during the later stages of hypersensitivity.

TRPM8 is the principal mammalian cold sensor (McKemy et al., 2002) and when the channel is inhibited pharmacologically (Andrews et al., 2015) or is genetically inactivated (Colburn et al., 2007; Dhaka et al., 2007; Knowlton et al., 2010), mice show impaired detection to cool temperatures. We examined the importance of TRPM8 for acute oxaliplatin-induced neuropathy. As expected, *Trpm8*$^{-/-}$ mice had longer paw withdrawal latencies to the cold plate when compared to WT counterparts. Although *Trpm8*$^{-/-}$ mice displayed a markedly reduced cold sensitivity at all time points, oxaliplatin caused increased sensitivity at days 7 and 14. These mice failed to develop acute cold hypersensitivity on day 1 after oxaliplatin treatment. Our findings agree with those of earlier studies, which have shown that inhibition of TRPM8 pharmacologically and genetically prevents acute oxaliplatin-induced cold allodynia (Descoeur et al., 2011; Kono et al., 2012; Zhao et al., 2012). However, our results may also indicate TRPM8 independent mechanisms, as oxaliplatin still increased sensitivity to cold in these mice. Studies investigating the role of $Na_v1.6$ indicate that A fibres are likely candidates which may be directly affected by oxaliplatin (Deuis et al., 2013, 2014; Sittl et al., 2012). TRPM8 is preferentially expressed in very small-diameter neurons, which are not likely to give rise to A fibres (Deuis et al., 2013; Koltzenburg et al., 1997). In addition, spinal integration of input from constitutively active TRPM8-positive cold fibres and A fibres may both be important. This is plausible because without TRPM8, cold fibres lose their impulse activity (Belmonte and Gallar, 2011; McKemy, 2007; Parra et al., 2010; Tajino et al., 2011).

We also found that *Trpm8*$^{-/-}$ mice failed to develop acute oxaliplatin-induced mechanical hypersensitivity in the Randall-Selitto test and tactile allodynia to von Frey filaments. This is in contrast to other studies which have shown no role for TRPM8 in oxaliplatin-induced

mechanical hypersensitivity (Descoeur et al., 2011). However, some TRPM8-positive fibres have been shown to be insensitive to mechanical stimulation (Belmonte and Gallar, 2011). The human hairy skin is innervated by cold-sensitive and mechano-insensitive C fibres which have low activation thresholds to cold (Campero et al., 2001). In addition, the cold search method in skin-nerve preparations was developed to identify cold-sensitive, yet mechano-insensitive C fibres (Zimmermann et al., 2011). Our results suggest that spinal integration of tonic input from cold-sensitive, TRPM8 expressing afferent fibres regulates the sensitivity to noxious mechanical stimulation. However, in a study conducting recordings in skin-saphenous nerve preparation from WT and *Trpm8*$^{-/-}$ mice, two populations of TRPM8-expressing neurons were identified. The first being cold-sensitive and mechanically-insensitive, and the second group responding to high threshold mechanical deformation of the skin (Jankowski et al., 2017). In addition, a further study showed encoding deficits in mechano-cold C fibres (CMC) from *Trpm8*$^{-/-}$ mice (Winter et al., 2017).

We observed a remission in oxaliplatin-induced cold and mechanical hypersensitivity 1 day after compound application in some experiments. Whilst this was unexpected, it may be explained by the fact that the day 1 timepoint reading was conducted at different times during the 24 hour period post injection. Whilst the compound is unlikely to disappear from the site of action, circadian changes can affect pharmacokinetic parameters during the initial distribution phase of oxaliplatin (Boughattas et al., 1994). Platinum levels in plasma ultrafiltrate can be undetectable for up to 24 hours after oxaliplatin, but sustained levels were found after the 24 hour time point (Boughattas et al., 1994). This may explain the consistent and long-term effects of the compound *in vivo*.

In summary, we have demonstrated that oxaliplatin evokes long-lasting mechanical and cold hypersensitivity after a single injection. The behavioural phenotype in mice is akin to the symptoms presented by patients in the clinic. Thus, offering translational opportunities for the study of mechanisms. In addition, we identified 3 days after injection as time point of reliable and maximal hypersensitivity, which was important for planned *ex vivo* experiments (Chapter 5). Finally, we found that TRPM8 is involved in acute oxaliplatin-induced cold and mechanical hypersensitivity. Further investigations into the acute cellular and molecular mechanisms for oxaliplatin-induced neuropathy is required. We explored this using *in vitro* and *ex vivo* techniques. Using these findings, we were able to investigate the role of target ion channels *in vivo* as demonstrated in Chapter 7.

3 The acute and long-term effects of oxaliplatin on the excitability of DRG neurons *in vitro*

3.1 Introduction

Oxaliplatin treatment *in vivo* in C57BL/6J mice resulted in a behavioural phenotype that faithfully recapitulated some of the symptoms experienced by patients in the clinic (Chapter 2) (Barbosa et al., 2014; Saif and Reardon, 2005). Mice treated with oxaliplatin developed acute cold hypersensitivity within hours of oxaliplatin administration. Clinically, most of the symptoms that affect patients are sensory in nature and include paraesthesias, cold and mechanical hyperalgesia and allodynia, as well as shooting pain (Barbosa et al., 2014; Grothey, 2003; Saif and Reardon, 2005; Wilson et al., 2002). We sought to determine whether the effects of oxaliplatin *in vitro*, to facilitate mechanistic investigations in isolated neurons and other tissue preparations. Oxaliplatin increases the excitability of DRG neurons in culture (Adelsberger et al., 2000; Anand et al., 2010; Descoeur et al., 2011; Gauchan et al., 2009; Zhao et al., 2012). However, most studies in the literature have focused on the longer term effects of oxaliplatin by isolating DRG neurons from treated mice (Descoeur et al., 2011; Gauchan et al., 2009; Kono et al., 2012). Few studies have examined the acute effects of the drug on sensory neurons (Adelsberger et al., 2000; Anand et al., 2010; Nassini et al., 2011; Sittl et al., 2012). Both approaches may provide important insights into the underlying mechanisms of acute and chronic oxaliplatin-induced cold and mechanical hypersensitivities.

Administration of oxaliplatin *in vivo* (Chapter 2) was important for providing tissue and neurons for mechanistic studies using *in vitro* and *ex vivo* methods. To determine whether the altered excitability induced by oxaliplatin are maintained *in vitro*, we studied isolated DRG neurons using the intracellular calcium ($[Ca^{2+}]_i$)-sensitive dye, Fura 2-AM. Using $[Ca^{2+}]_i$-measurements at modest magnification (10x objective), we analysed large numbers of neurons rapidly. $[Ca^{2+}]_i$ imaging studies permits the measurement of various modalities in neurons, i.e. temperature and chemosensitivity, by measuring the change in the $[Ca^{2+}]_i$. In

contrast, patch-clamp recordings made in individual neurons from a culture makes it possible to investigate the parameters which govern excitability changes. Earlier studies have shown that oxaliplatin dramatically increases excitability in DRG neurons by modulating the activity of ion channels including Na^+, K^+ and Ca^{2+} (Adelsberger et al., 2000; Schulze et al., 2011; Sittl et al., 2010, 2012). Oxaliplatin can also sensitise neurons so that thresholds are shifted to hyperpolarised membrane potentials. Neurons display repetitive and high frequency impulse discharges, which can even be seen as bursting patterns of discharges (Sittl et al., 2012). The acute effects of oxaliplatin are explained by the compound's interaction with voltage-gated ion channels. The longer term effects (days to weeks) are more likely to be explained by transcriptional changes (Descoeur et al., 2011). We studied the effects of oxaliplatin in populations of sensory neurons to assess whether a particular subset of neurons was impacted by both acute and long-term exposure to oxaliplatin.

3.2 Aims

To study the mechanistic basis of oxaliplatin-induced cold hypersensitivity, neurons were isolated from WT mice treated with vehicle and oxaliplatin. Next, we investigated isolated neurons from *Trpm8*$^{-/-}$ mice and compared the response with WT mice. Finally, we directly applied oxaliplatin to naïve DRG neurons to assess acute effects of the compound.

3.3 Methods

3.3.1 Drugs and Reagents

All reagents were purchased from Sigma-Aldrich unless otherwise stated. The extracellular solution (ECS) used in all Ca^{2+} imaging experiments contained (in mM) 140 NaCl, 5 KCl, 10 glucose, 10 HEPES, 2 $CaCl_2$ and 1 $MgCl_2$. Reagents used during experiments (in μM) 300 Oxaliplatin, 1 Icilin, 5 1-7 (Wei, 2018), 100 allyl isothiocyanate (AITC) and 1 capsaicin. Other reagents used included potassium chloride (KCl; 50 mM), Fura 2-AM ester (2.5 μM; Invitrogen, CA, USA) and probenecid (1 mM).

3.3.2 Cell culture

The cell culture methods were performed as previously described (Bevan and Winter, 1995). Adult male or female C57BL/6J mice were killed by cervical dislocation, as approved by schedule 1 methods by the United Kingdom Home Office, and ganglia were removed from all levels of the spinal cord using aseptic methods. Ganglia were incubated in 0.25 % collagenase Type IV (Worthington, NJ, USA) in serum-free minimum essential medium (MEM; Invitrogen) containing 1 % penicillin and streptomycin for 3 hours at 37 °C in a humidified incubator gassed with 5 % CO_2 in air.

The ganglia were subsequently incubated with 0.25 % trypsin (Sigma-Aldrich, CA, USA) in MEM for 20 minutes before being mechanically dissociated via trituration using flame polished Pasteur pipettes to obtain a single cell suspension. Trypsin was removed by addition of MEM containing 10 % fetal bovine serum (FBS) followed by centrifugation at ~168 g (1000 rpm) for 10 minutes. The cell pellet containing the ganglia was re-suspended in MEM containing 1 % penicillin and streptomycin, 10 % FBS and 0.05 % DNase

(Worthington) before being layered onto a 2 ml cushion of sterile 15 % bovine serum albumin in MEM. The layered mixture was then centrifuged at ~168 g (1000 rpm) for 10 minutes. The cell pellet, containing the neurons was then re-suspended in an appropriate volume of MEM containing 10 % FBS, 50 ng ml^{-1} nerve growth factor (NGF; Promega, WI, USA) and 10 μM cytosine arabinoside (Sigma-Aldrich) to prevent the growth of non-neuronal cells.

Isolated neurons were plated on poly-D-lysine coated coverslips and maintained at 37 °C in an incubator gassed with 5 % CO_2 in air and supplemented with MEM containing 10 % FBS, 50 ng ml^{-1} NGF and 10 μM cytosine arabinoside for up to 24 hours before experimentation.

3.3.3 Calcium Imaging

Live cell calcium imaging was used to study the intracellular calcium concentration of individual DRG neurons. Cells were loaded with Fura 2, a ratiometric calcium indicator dye, by incubation with the membrane permeant acetoxymethyl (AM) ester form of the dye (Fura 2-AM). Fura 2-AM passively diffuses into the cells where intracellular esterases cleave ester bonds to liberate the membrane impermeant (Fura-2) form of the dye inside the cells (Oakes et al., 1988). The dye loading ECS contained 2.5 μM Fura 2-AM with 1 mM probenecid to inhibit efflux of Fura 2 through anion transporters. Cells were incubated with the Fura 2-AM solution for *ca*. 1 hour at 37 °C.

Fura 2 is excited at 340 nm and 380 nm and the ratio of emissions at these wavelengths directly reflects intracellular Ca^{2+} levels. Emission after excitation at 380 nm is reduced by

increasing Ca^{2+}, and emission following excitation at 340 nm is increased by increasing Ca^{2+} levels. The emission spectrum of Fura 2 has a maximum at *ca*. 510 nm.

For $[Ca^{2+}]_i$-imaging, coverslips were mounted in a chamber (volume ~0.4 ml) and viewed using a Nikon Diaphot microscope with a 10x, 0.5NA objective. Images of a group of cells were captured (typically 300-500 millisecond duration exposures) with 1 second intervals between each pair of measurements using a CoolSnap CCD camera with alternate excitation at 340 and 380 nm (± 2.5 nm slit width) controlled by a DeltaRamX monochromator (PTI, New Jersey). Emission was measured at > 520 nm using a dichroic mirror and a longpass optical filter. Analyses of emission intensity ratios at 340 nm/380 nm excitation (R, in individual cells) were performed with the ImageMaster suite of software. Cells were superfused with ECS (rate ~3 ml per min) delivered from a fine tube positioned close to the cells under study with the ECS removed by suction. The temperature of the ECS perfusate was measured by a thermistor attached to the exit of the super-perfusion tube. ECS temperature was maintained or altered by a Peltier device controlled by a programmed power supply (Marlow Industries, Tx, USA). For cold ramps the temperature was changed at 8-10 °C/minute.

Experiments were designed to stimulate cells with a single cold ramp (35-10 °C) following a pre-incubation period (10-,30- or 120 minutes) at 37 °C in the absence and presence of oxaliplatin (300 µM). We assessed the direct effects of oxaliplatin on DRG neurons. These experiments involved perfusion of oxaliplatin (300 µM) for 5, 10 and 15 minutes to cultured neurons in calcium imaging experiments. In other experiments, DRG neurons were isolated from oxaliplatin-treated (6 mg/kg, i.p.) and vehicle-treated (5 % glucose, i.p.) from wildtype (WT) and TRPM8 knockout (*Trpm8*$^{-/-}$) mice. These neurons were stimulated with two cold

ramps (35-10 °C). Icilin (1 µM) or 1-7 (5 µM) were used to characterize TRPM8 expressing neurons, capsaicin (1 µM) and AITC (100 µM) identified TRPV1 and TRPA1 expressing neurons respectively in certain experiments. The total number of viable DRG neurons present was determined by exposure to 50 mM KCl which depolarized the neurons and evoked calcium entry via voltage-gated calcium channels.

3.2.4 Calculating temperature thresholds in calcium imaging experiments

During calcium imaging, the time points which corresponded to each 2 °C decrease in temperature during cold ramps in the experiments were marked. In addition, the start temperature (35 °C) and the temperature at the end of the cold ramp (10 °C) were noted. Plots of temperature vs Fura 2 ratio were created in Origin Software 7.5 to calculate each temperature threshold from generated graphs of time vs. Fura 2 ratio.

3.2.5 Whole-cell current-clamp of dorsal root ganglion cells treated with oxaliplatin

Current-clamp recordings were obtained using a Axopatch 200B amplifier (Molecular Devices, Sunnyvale, CA, USA) and digitised using an Axon Digidata 1550B (Molecular Devices) (acquired at 25 kHz and filtered at 10 kHz with a low-pass Bessel filter). For all recordings the ECS contained (mM); 140 NaCl, 3 KCl, 2 $MgCl_2$, 2 $CaCl_2$, 10 HEPES, 10 dextrose (pH and osmolarity adjusted as above). Intracellular solution contained (mM); 140 KCl, 0.5 EGTA, 5 HEPES, 10 dextrose (pH adjusted to 7.3 with KOH, osmolarity adjusted to 310 with sucrose). A Narashige PC-10 (puller was used to manufacture patch pipettes from borosilicate glass (Warner Instruments, MA, USA) with a resistance between 1–2 MΩ and fire polished (Microforge MF830, Narashige). Whole-cell configuration of medium- to large-diameter DRG neurons (>

30 micron) were obtained in voltage-clamp prior to proceeding to current-clamp mode. Cells with a stable RMP, recorded for 30 s and found to have an RMP ≤-55 mV, were recorded from. Input resistance was determined by hyperpolarising current steps at 10 pA increments between -10 to -60 pA and fitted to linear regression. Current threshold was determined to be the first action potential elicited after serial depolarising current injections in 10 pA increments. Repetitive firing was assessed by increasing current injection from 0 – 3 nA over 5 seconds. Action potential characteristics were analysed offline using Clampfit (Molecular Devices, version 8). After-hyperpolarisation potential was defined as the D between resting membrane potential and the maximum trough. Data was analysed offline with Excel (Microsoft) and plotted using GraphPad Prism software (Version 7, La Jolla, CA).

All current-clamp experiments were performed by Dr. Mathilde Israel.

3.2.6 Statistical analysis

Differences in the proportions of cold-sensitive neurons were analysed using a Fisher's exact test, two-sided. All temperature threshold data was first tested for normality. Unpaired *t* tests or Mann-Whitney *U* tests were then used to compare treatment groups. All average threshold temperatures are presented as mean ± S.E.M.

3.4 Results

3.4.1 Oxaliplatin treatment *in vivo* increases the proportion of cold-sensitive isolated DRG neurons

DRG neurons were isolated from treated mice 3 days after injection, since our behavioural experiments indicate that the hypersensitivity to cold reaches its peak at this time point. This was to assess whether the hypersensitivity *in vivo* could be reflected functionally *in vitro*. We found that that a greater proportion of DRG neurons isolated from oxaliplatin-treated mice responded to cooling. The increased responsiveness to cold in neurons from these mice was significant during the first and second cold ramps when compared to DRG neurons from vehicle-treated mice (Table 3-1). The proportion of cold-sensitive neurons remained unchanged between the first and second challenges in both groups, indicating that the cold sensitivity was not subject to a marked sensitisation or desensitisation.

Table 3-1 Proportion of cold-sensitive DRG neurons isolated from mice 3 days after treatment with a single i.p. injection of vehicle (5 % glucose) and oxaliplatin (6 mg/kg)

	Vehicle (5 % glucose)		Oxaliplatin (6 mg/kg)		Fisher's exact test
	Population of cold-sensitive neurons	**% of cold-sensitive neurons**	**Population of cold-sensitive neurons**	**% of cold-sensitive neurons**	
Cold ramp 1	131/2681 neurons	4.9 %	180/2679 neurons	6.7 %	*P* = 0.004 **
Cold ramp 2	141/2681 neurons	5.3 %	193/2679 neurons	7.2 %	*P* = 0.003 **

3.4.2 increased AITC sensitivity in cold-sensitive neurons from oxaliplatin-treated mice

In order to identify the population of DRG neurons which oxaliplatin sensitised to cold, three TRP channel agonists were used. This was based on the findings in previous studies which identified TRPM8, TRPA1 and TRPV1 as potential targets in oxaliplatin-induced hyperexcitability (Anand et al., 2010; Gauchan et al., 2009; Kono et al., 2012; Nassini et al., 2011; Zhao et al., 2012). 1-7 (Wei, 2018; Yang et al., 2018) is an unpublished TRPM8 agonist, AITC is a TRPA1 agonist and capsaicin, a TRPV1 agonist. Oxaliplatin treatment *in vivo* did not increase the proportion of TRPM8 expressing neurons that responded to cold compared to vehicle treatment *in vivo* during either cold ramp (Table 3-2 A, B). In addition, there was no increase in the TRPV1-expressing population of DRG neurons after oxaliplatin treatment when compared to vehicle treatment *in vivo* during both cold stimulations (Table 3-2 A, B). However, the proportion of AITC sensitive neurons was significantly increased in cultures from mice treated with oxaliplatin compared to vehicle during both cold ramps (Table 3-2 A, B). A subset of neurons (20 %) from both vehicle- and oxaliplatin-treated mice did not respond to the TRP channel agonists, which is slightly lower than, but in agreement with another study (Munns et al., 2007).

Table 3-2 Functional selectivity of cold-sensitive neurons isolated from vehicle- or oxaliplatin-treated mice (6 mg/kg, i.p.)

A. Cold ramp 1

	Vehicle (5 % glucose)	Oxaliplatin (6 mg/kg)	Fisher's exact test
1-7	66/131 (50 %)	88/180 (48 %)	*P* = 0.819
AITC	26/131 (20 %)	58/180 (32 %)	*P* = 0.019 *
Capsaicin	54/131 (41 %)	68/180 (37 %)	*P* = 0.558
None	29/131 (22 %)	42/180 (23 %)	*P* = 0.891

B. Cold ramp 2

	Vehicle (5 % glucose)	Oxaliplatin (6 mg/kg)	Fisher's exact test
1-7	73/141 (52 %)	90/193 (47 %)	*P* = 0.377
AITC	27/141 (19 %)	65/193 (34 %)	*P* = 0.004 **
Capsaicin	53/141 (38 %)	77/193 (40 %)	*P* = 0.733
None	28/141 (19 %)	51/193 (26 %)	*P* = 0.193

3.4.3 Reduced cold sensitivity in neurons isolated from *Trpm8*$^{-/-}$ mice

TRPM8 is the principal mammalian cold sensor (McKemy et al., 2002; Peier et al., 2002b). Behaviourally, we showed that *Trpm8*$^{-/-}$ mice have a delayed onset to oxaliplatin-induced cold hypersensitivity (Chapter 2, Figure 2-4). We therefore assessed whether the cold sensitivity of DRG neurons isolated from *Trpm8*$^{-/-}$ mice treated with oxaliplatin was altered *in vitro* compared to that of DRG neurons isolated from oxaliplatin-treated WT mice. The proportion of cold-sensitive neurons was unchanged in oxaliplatin-treated *Trpm8*$^{-/-}$ mice compared to WT during the first cold ramp (Table 3-3). However, the proportion of cold-sensitive neurons was significantly reduced in oxaliplatin-treated *Trpm8*$^{-/-}$ mice compared to WT during the second cold ramps (Table 3-3). The proportion of cold-sensitive neurons did not change between cold ramps in neurons from either genotype.

Table 3-3 Proportion of cold-sensitive DRG neurons isolated from oxaliplatin-treated WT and *Trpm8*$^{-/-}$ mice

	WT		Trpm8$^{-/-}$		Fisher's exact test
	Population of cold-sensitive neurons	**% of cold-sensitive neurons**	**Population of cold-sensitive neurons**	**% of cold-sensitive neurons**	
Cold ramp 1	100/1977	5 %	65/1746	3.7 %	*P* = 0.055
Cold ramp 2	127/1977	6.4 %	70/1746	4 %	*P* = 0.001 **

3.4.4 Oxaliplatin lowered the threshold temperatures of activation in neurons isolated from WT and *Trpm8*$^{-/-}$ mice

DRG neurons taken from oxaliplatin-treated mice showed a shift towards colder threshold temperatures of activation when compared to neurons isolated from vehicle-treated mice, in response to the first cold ramp (vehicle 25.8 ± 1.2 °C; oxaliplatin 23.9 ± 0.5 °C, Mann-Whitney *U* test, $P < 0.05$, n = 131 and 180 neurons respectively) (Figure 3-1 A). However, the threshold temperatures of activation were unchanged between treatment groups during the second cold ramp (vehicle 24.8 ± 0.5 °C; oxaliplatin 23.7 ± 0.5 °C, Mann-Whitney *U* test, $P > 0.05$, n = 141 and 193 neurons respectively) (Figure 3-1 B).

In addition, oxaliplatin-treated *Trpm8*$^{-/-}$ mice had threshold temperatures of activation at even colder temperatures during cold stimulations, when compared to neurons isolated from WT mice during the first cold ramp (WT 24.0 ± 0.6 °C; *Trpm8*$^{-/-}$ 20.9 ± 0.6 °C, Mann-Whitney *U* test, $P < 0.05$, n = 100 and 65 neurons respectively) (Figure 3-1 C). A similar phenomenon was seen during the second cold ramp (WT 23.9 ± 0.5 °C; *Trpm8*$^{-/-}$ 21.2 ± 0.7 °C, Mann-Whitney *U* test, $P < 0.05$, n = 127 and 70 neurons respectively) (Figure 3-1 D).

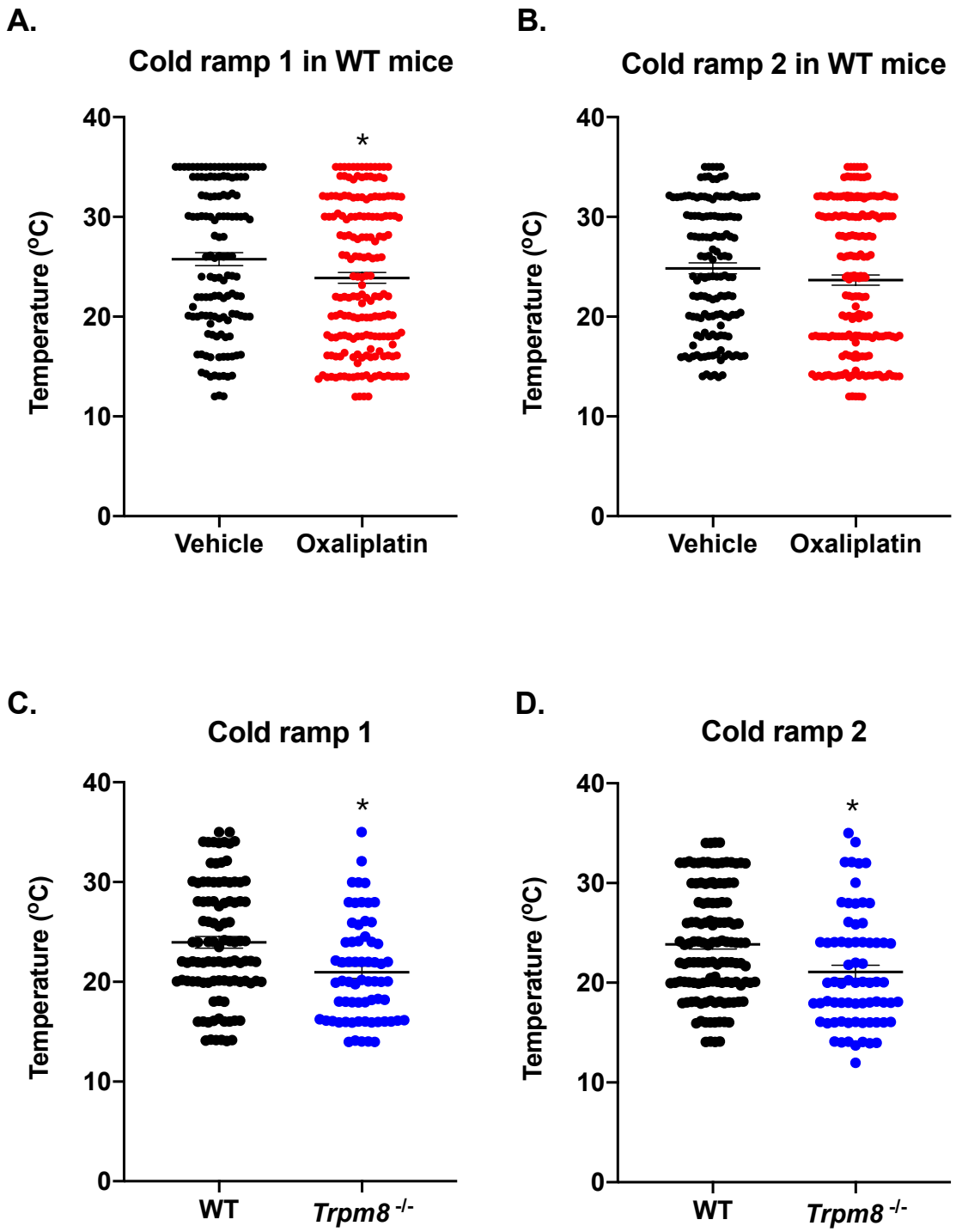

Figure 3-1 Threshold temperatures of activation in cold-sensitive neurons isolated from vehicle-treated and oxaliplatin-treated in WT and Trpm8$^{-/-}$ mice.

Mice were injected with vehicle (5 % glucose) or oxaliplatin (6 mg/kg) i.p. and DRG neurons were isolated at day 3 following treatment. A) Oxaliplatin (red circles) significantly shifted the threshold temperatures towards colder temperatures when compared to vehicle (black circles) in WT mice during the first cold ramp (vehicle 25.8 ± 1.2 °C; oxaliplatin 23.9 ± 0.5 °C, Mann-Whitney *U* test, $P < 0.05$, n = 131 and 180 neurons respectively). B) Oxaliplatin did not

significantly shift the average threshold temperature when compared to vehicle (black circles) in WT mice during the second cold ramp (vehicle 24.8 ± 0.5 °C; oxaliplatin 23.7 ± 0.5 °C, Mann-Whitney *U* test, $P > 0.05$, n = 141 and 193 neurons respectively). C) There was a significant shift towards colder threshold temperatures in neurons from oxaliplatin-treated *Trpm8*$^{-/-}$ mice (blue circles) when compared to WT treated mice (black circles) during the first cold ramp (WT 24.0 ± 0.6 °C; *Trpm8*$^{-/-}$ 20.9 ± 0.6 °C, Mann-Whitney *U* test, $P < 0.05$, n = 100 and 65 neurons respectively). D) There was also a significant shift towards colder threshold temperatures in neurons from oxaliplatin-treated *Trpm8*$^{-/-}$ mice (blue circles) when compared to WT treated mice (black circles) during the second cold ramp (WT 23.9 ± 0.5 °C; *Trpm8*$^{-/-}$ 21.2 ± 0.7 °C, Mann-Whitney *U* test, $P < 0.05$, n = 127 and 70 neurons respectively).

3.4.5 Oxaliplatin activates a small subset of DRG neurons directly

We next examined whether oxaliplatin could directly active DRG neurons. Naïve DRG neurons were treated with oxaliplatin (300 μM) for 5, 10 and 15 minutes to determine the proportion of direct responders to the compound. Oxaliplatin did not increase the proportion of neurons activated when compared to vehicle after 5 minutes (Table 3-4). A very small number of neurons displayed a spontaneously increased $[Ca^{2+}]_i$ with ECS for 5, 10 and 15 minutes (Table 3-4). However, oxaliplatin modestly increased the percentage of direct responders when compared to vehicle treatment after 10 minutes (Table 3-4). Oxaliplatin also increased the proportion of neurons, although not significantly activated after 15 minutes when compared to vehicle (Table 3-4). Interestingly, neurons that were directly activated by oxaliplatin often showed oscillations in their responses. The very low percentages are approximate, and some comparisons may have strengthened by an increased sample size. Nevertheless, it is clear that the proportion produced $[Ca^{2+}]_i$.

Table 3-4 Percentage of neurons activated by direct agonism to vehicle or oxaliplatin

	Vehicle (ECS)		Oxaliplatin (300 µM)		Fisher's exact test
Direct application (minutes)	**Population of cold-sensitive neurons**	**% of cold-sensitive neurons**	**Population of cold-sensitive neurons**	**% of cold-sensitive neurons**	
5	9/566 neurons	1.6 %	14/777 neurons	1.8 %	*P* = 0.834
10	9/567 neurons	1.6 %	25/630 neurons	4.0 %	*P* = 0.014 *
15	13/231 neurons	5.6 %	29/395 neurons	7.3 %	*P* = 0.508

3.4.6 Incubation with oxaliplatin significantly increased the proportion of cold-sensitive neurons

Here, to determine whether pre-treatment of oxaliplatin influenced cold sensitivity, we next investigated whether neurons incubated in the presence of oxaliplatin displayed an altered sensitivity to stimulation with cold. DRG neurons were incubated with or without oxaliplatin for 10-, 30- and 120-minutes and thereafter challenged with a cold ramp. Oxaliplatin increased the proportion of cold-sensitive neurons after a 120-minute incubation modestly, but significantly, compared to vehicle (Table 3-5). Oxaliplatin did not sensitise neurons to cold stimuli after a 10-minute or 30-minute pre-treatment period when compared to vehicle (Table 3-5).

Table 3-5 Proportion of cold-sensitive DRG neurons after incubation with vehicle and oxaliplatin

	Vehicle (ECS)		Oxaliplatin (300 µM)		Fisher's exact test
Pre-treatment (minutes)	**Population of cold-sensitive neurons**	**% of cold-sensitive neurons**	**Population of cold-sensitive neurons**	**% of cold-sensitive neurons**	
10	30/489 neurons	6.1 %	33/598 neurons	5.5 %	*P* = 0.697
30	20/529 neurons	3.8 %	33/579 neurons	5.7 %	*P* = 0.159
120	30/597 neurons	5.0 %	84/1064 neurons	7.9 %	*P* = 0.026 *

3.4.7 Functional classification of cold-sensitive neurons

We used the same selection of TRP channel agonists as described above, to identify sensory neuron subpopulations that were affected by oxaliplatin. Oxaliplatin treatment did not influence the subset of neurons which were recruited as novel cold responders. The proportion of cold-sensitive neurons that were TRPM8-positive did not differ between oxaliplatin and vehicle treated neurons after 10- (Table 3-6 A), 30- (Table 3-6 B) or 120-minutes incubation (Table 3-6 C). Oxaliplatin did not alter the proportion of TRPA1 cold-sensitive neurons at 10- (Table 3-6 A), 30- (Table 3-6 B) and 120-minutes (Table 3-6 C) compared to vehicle. Furthermore, the proportion of cold-sensitive neurons that responded to capsaicin did not differ and was not significantly changed by incubation with oxaliplatin for 10, 30 or 120 minutes (Table 3-6 A-C). The number of cold-sensitive neurons studied was limited overall, and the effect size would have to be substantial to be detected. Comparable to previous findings, there were a subset of cold-responsive neurons in both treatment groups after all incubation times which were not functionally expressing TRPM8, TRPA1 or TRPV1 channels (Table 3-6). Whilst there was a greater range (15-40 %) in this proportion of neurons compared to our earlier experiments, it was in agreement with another study (Munns et al., 2007).

Table 3-6 Functional selectivity of cold-sensitive neurons isolated from vehicle- or oxaliplatin-treated mice (single i.p. injection)

A. 10 minutes

	Vehicle (5 % glucose)	Oxaliplatin (6 mg/kg)	Fisher's exact test
Icilin	6/30 (20 %)	12/27 (44 %)	*P* = 0.085
AITC	4/30 (13 %)	6/27 (22 %)	*P* = 0.492
Capsaicin	12/30 (40 %)	12/27 (44 %)	*P* = 0.792
None	12/30 (40 %)	8/27 (30 %)	*P* = 0.579

B. 30 minutes

	Vehicle (5 % glucose)	Oxaliplatin (6 mg/kg)	Fisher's exact test
Icilin	8/20 (40 %)	10/33 (30 %)	*P* = 0.555
AITC	8/20 (40 %)	7/33 (21 %)	*P* = 0.209
Capsaicin	8/20 (40 %)	11/33 (33 %)	*P* = 0.769
None	3/20 (15 %)	13/33 (39 %)	*P* = 0.009 **

C. 120 minutes

	Vehicle (5 % glucose)	Oxaliplatin (6 mg/kg)	Fisher's exact test
Icilin	13/30 (43 %)	28/84 (33 %)	*P* = 0.378
AITC	8/30 (26 %)	22/84 (26 %)	*P* = 0.999
Capsaicin	17/30 (56 %)	47/84 (56 %)	*P* = 0.999
None	6/30 (20 %)	18/84 (21 %)	*P* = 0.999

3.4.8 Oxaliplatin-induced cold-sensitive neurons had unchanged threshold temperatures

Further analysis into the threshold temperatures of activation and the cell size of individual neurons was conducted. This was to identify any cellular mechanisms in oxaliplatin-induced novel cold-sensitive neurons. Oxaliplatin pre-treatment for 10 minutes did not significantly shift the threshold temperature of activation when compared to vehicle (vehicle 21.3 ± 1.2 °C; 23.6 ± 1.2 °C, Mann-Whitney *U* test, $P > 0.05$, n = 30 and 33 neurons respectively) (Figure 3-2 A). In addition, oxaliplatin did not alter the threshold temperature of activation after longer incubation periods. Indeed, the average threshold temperature of activation did not differ between vehicle and oxaliplatin (vehicle 25.8 ± 1.6 °C; oxaliplatin 25.0 ± 1.2 °C, unpaired *t* test, $P > 0.05$, n = 20 and 33 neurons respectively) after a 30-minute incubation period (Figure 3-2 B). Consistent with our previous findings, oxaliplatin shifted the threshold temperatures of activation towards colder temperatures, although not significantly when compared to vehicle following a 120-minute incubation period (vehicle 25.8 ± 1.2 °C; 24.7 ± 0.8 °C, Mann-Whitney *U* test, $P > 0.05$, n = 30 and 84 neurons respectively) (Figure 3-2 C).

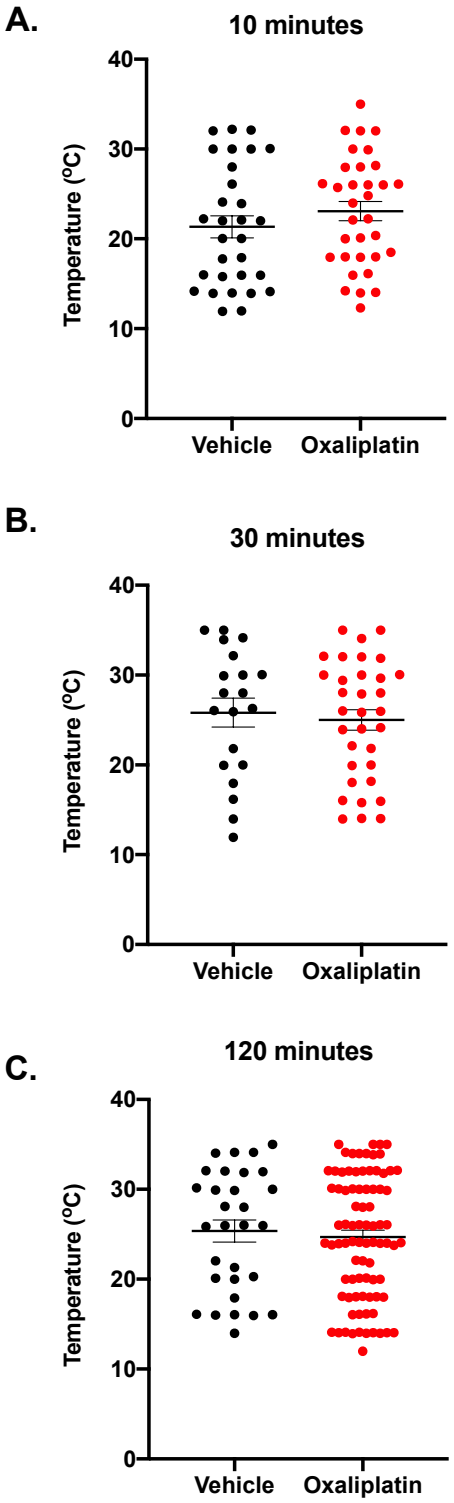

Figure 3-2 Acute oxaliplatin treatment did not sensitise temperature thresholds of cold-sensitive neurons.

Threshold temperatures were calculated for all cold-sensitive neurons. This was to identify the subset of neurons which were recruited as novel cold responders after acute oxaliplatin treatment. A) Oxaliplatin (red circles) showed a trend towards warmer threshold temperatures when compared to vehicle (black circles) after a 10-minute pre-treatment period. B) Oxaliplatin (red circles) did not affect threshold temperatures when compared to

vehicle (black circles) after a 30-minute pre-treatment period. C) Oxaliplatin (red circles) showed a trend towards warmer threshold temperatures when compared to vehicle (black circles) after a 120-minute pre-treatment period.

3.4.9 Oxaliplatin incubation did not change action potential characteristics *in vitro*

Current clamp experiments were conducted on cultured DRG neurons incubated with vehicle (0.5% glucose) or oxaliplatin (100 μM). DRG neurons were patched based on their size (> 30 μm) and there was no difference found between the treatment groups (vehicle, 1179 ± 370 μm^2; Oxaliplatin 955 ± 161 μm^2, $P > 0.05$, n = 9 - 12) (Figure 3-3A). The average amount of current required to elicit a single action potential (rheobase) was 1130 ± 260 pA in oxaliplatin-treated neurons compared to 1410 ± 340 pA in vehicle treated neurons (Figure 3-3C). While slightly reduced, this was not statistically significant ($P > 0.05$). In line with this, the input resistance (input R) was higher on average in oxaliplatin-treated neurons (110.1 ± 15.6 mΩ) when compared vehicle-treated neurons (74.4 ± 15.8 mΩ), although not stastistically significant (Figure 3-3 D). Other parameters that were assessed in current clamp recordings included the resting membrane potential (RMP), action potential half-width, afterhyperpolarisation (AHP) of neurons treated with vehicle or oxaliplatin. There was no difference in the RMP of neurons after oxaliplatin incubation (-66.5 ± 1.2 mV) when compared with vehicle-treated neurons (-65.6 ± 1.4 mV, Figure 3-3B). Oxaliplatin incubation did not alter the action potential half-width (Figure 3-3 E) (Vehicle, 0.75 ± 0.08 ms; oxaliplatin, 0.8 ± 0.1 ms). In addition, oxaliplatin treatment resulted in a more pronounced AHP (-11.0 ± 2.2), although this was not significant when compared to vehicle-treated neurons (-6.0 ± 1.6, $P > 0.05$, unpaired *t* test, Figure 3-3 F). In addition to passive neuronal properties and action potential parameters, large-diameter neurons were challenged with a 5 second, 3 nA ramp to assess repetitive action potential firing. Large-diameter neurons typically resist repetitive firing, this is reflected in our findings (19/21 neurons patched fired 1 action potential or less during ramp stimulus) and there was no significant difference between vehicle control and oxaliplatin groups (vehicle, 1 ± 1 APs; oxaliplatin 2 ± 1 APs).

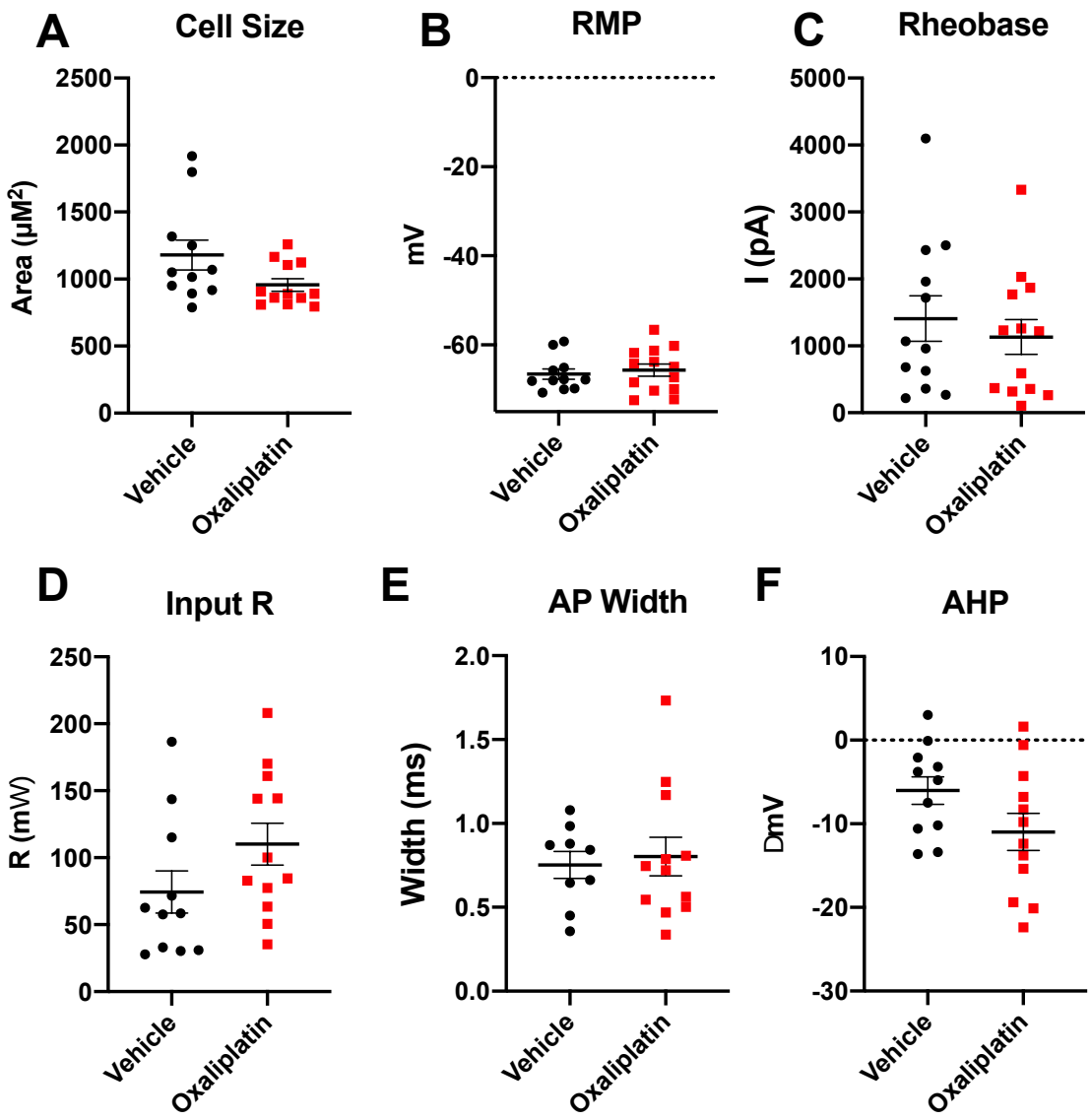

Figure 3-3 Oxaliplatin did not cause hyperexcitability of medium- to large-diameter neurons.

Current-clamp recordings of isolated medium – large DRG neurons incubated with oxaliplatin (1 hr, 100 μM) or vehicle control (0.5% glucose). A) DRG neurons were chosen based on size vehicle, 1179 ± 370 micron^2; oxaliplatin 955 ± 161 micron^2. B) Passive neuronal parameters such as resting membrane potential (RMP) were not signficantly different after oxaliplatin incubation (-66.5 ± 1.2 mV) compared to vehicle control (-65.6 ± 1.4 mV). C) Rheobase was not significantly altered by oxaliplatin 1410 ± 340 pA ; control, 1130 ± 260 pA D) Input resistance (input R) was not signficantly increased by oxaliplatin (110.1 ± 15.6 mΩ) when compared vehicle-treated neurons (74.4 ± 15.8 mΩ). E) Action potential half-width (AP width) Vehicle, 0.75 ± 0.08 ms; oxaliplatin, 0.8 ± 0.1 ms were similarly unchanged. F) Afterhyperpolarisation potential (AHP) measured as changed from resting membrane potential to trough was not signficantly hyperpolarised (oxaliplatin, -11.0 ± 2.2; control 6.0 ± 1.6, P > 0.05, unpaired *t* test) n = 11 and 12.

3.5 Discussion

In this chapter, we show that oxaliplatin caused very small changes in cold sensitivity of DRG neurons in culture. This was seen after acute and long-term application of the compound *in vitro* and *in vivo*. In addition, oxaliplatin did not consistently alter the chemo-sensitive profiles of DRG neurons that were cold responsive. This suggested that oxaliplatin did not exert its effects selectively on a single subset of neurons, and that the affected neurons may instead have other intrinsic properties. Oxaliplatin does not act specifically on 1-7/icilin, AITC or capsaicin sensitive neurons to cause Ca^{2+} influx. Finally, oxaliplatin did not change passive neuronal properties, increase excitability or change action potential characteristics of large-diameter neurons in culture.

Oxaliplatin increased the proportion of cold-sensitive DRG neurons after acute and long-term oxaliplatin treatment. In experiments using DRG neurons isolated from treated mice, we showed that cold sensitivity is maintained *in vitro*. We report that 4-8 % of DRG neurons are cold-sensitive after sustained oxaliplatin treatment *in vivo*. This is in line with the findings from another study (Descoeur et al., 2011). The proportion of cold-sensitive neurons between vehicle and oxaliplatin were quite similar across all experiments, and the effect of oxaliplatin was modest. This is unlikely to accurately reflect the functional impact of oxaliplatin *in vivo* (Descoeur et al., 2011; Deuis et al., 2013; Saif and Reardon, 2005, 2005; Tofthagen et al., 2013a). Oxaliplatin treatment, for several hours and days causes transcriptomics changes in DRG neurons (Starobova and Vetter, 2017). This may explain the changes in cold-sensitivity in neurons isolated from oxaliplatin-treated mice and during the 120-minute incubation period. In contrast, acute oxaliplatin-induced cold hypersensitivity develops when the compound acts directly at $K_v1.1$, $K_v1.2$, $Na_v1.8$ and $Na_v1.9$ channels, as well as TREK and TRAAK

channels found in small-diameter neurons (Lolignier et al., 2015, 2016; MacDonald et al., 2020b). In addition, oxaliplatin alters $Na_v1.6$ activity in large-diameter A fibres (Deuis et al., 2013, 2014; Sittl et al., 2012). Whilst there was a significant reduction in the proportion of cold-sensitive neurons in oxaliplatin-treated *Trpm8*$^{-/-}$ mice when compared to WT mice, vehicle-treated *Trpm8*$^{-/-}$ mice were not included. Therefore, it is difficult to assess the full role of the channel. However, it is likely that there are TRPM8-independent mechanisms involved, as there are multiple cold-sensitive ion channels expressed in DRG neurons, including TREK, TRAAK, $K_v1.1$ and $K_v1.2$ and $Na_v1.6$ (Alloui et al., 2006; Madrid et al., 2009; Noël et al., 2009a; Sittl et al., 2012; Viana et al., 2002b). Overall, our results for oxaliplatin-induced cold sensitivity *in vitro* was limited, suggesting other models are necessary to reveal molecular mechanisms.

In a previous study conducted by Gauchan and colleagues, oxaliplatin treatment in mice increased TRPM8 mRNA expression in DRG neurons on day 3 post administration (Gauchan et al., 2009). However, we did not find enhanced responses to icilin or an increase in the number of TRPM8-expressing neurons. We show that there is no change in the proportion of 1-7 and icilin sensitive neurons after both oxaliplatin treatment *in vivo* and pre-treatment *in vitro*. Our results are supported by investigations conducted by Descoeur *et al.*, who reported that oxaliplatin did not modify TRPM8 transcript expression (Descoeur et al., 2011). In addition, oxaliplatin did not affect the amplitude response to WS-12, a selective TRPM8 agonist in treated DRG neurons in a separate $[Ca^{2+}]_i$ study (Anand et al., 2010).

TRPA1 and TRPV1 have also been reported to play a role in oxaliplatin-induced cold responses. Oxaliplatin did not sensitise cold-sensitive neurons to capsaicin responses in our experiments including both acute and chronic treatment of the compound. Interestingly, an

increased proportion of oxaliplatin-treated cold-sensitive neurons responded to AITC, compared to vehicle-treated neurons. Previous studies have reported similar findings that oxaliplatin pre-treatment is able to sensitise AITC responses (Zhao et al., 2012). In addition, oxaliplatin evoked a calcium response in mouse TRPA1 CHO cells (Nassini et al., 2011) and increased TRPA1 mRNA expression (Descoeur et al., 2011). However, this contrasts with our own observations that oxaliplatin does not directly or exclusively activate TRPA1-expressing neurons. Whilst some studies predict a direct role of oxaliplatin on TRPA1 (Descoeur et al., 2011; Zhao et al., 2012), others hypothesise indirect roles via superoxides (Nassini et al., 2011). Oxaliplatin did not sensitise AITC responses in our pre-treatment experiments. In fact, the proportion of neurons that were AITC responsive were between 20-40 %. It is expected that up to 50 % of DRG neurons express TRPA1, and are mainly co-localised with TRPV1 (Hjerling-Leffler et al., 2007). Another study has reported that 25-30 % DRG neurons respond to TRPA1 agonists (Andersson et al., 2008). Our findings show that in some cases, the percentage of cold-sensitive neurons that responded to AITC, were lower than reported in the literature. It is unclear whether TRPA1 expressing neurons are crucial for oxaliplatin-induced cold hypersensitivity based on our findings.

Acute oxaliplatin incubation did not significantly increase cold sensitivity in DRG neurons in culture. We observed an increase in the proportion of cold-sensitive neurons after incubation with oxaliplatin for 120-minutes, but not after 10- and 30- minutes. This is similar to the results of other studies which showed hyperexcitability of DRG neurons following oxaliplatin pre-treatment for at least an hour (Sittl et al., 2010, 2012; Zhao et al., 2012). This suggests that following oxaliplatin decomposition *in vitro*, the compound causes cellular changes that take time (Ehrsson et al., 2002; Han et al., 2017b). Oxaliplatin might be activating cold-

sensitive channels via indirect mechanisms such as oxidation (Carozzi et al., 2015; Di Cesare Mannelli et al., 2012; Nassini et al., 2011). To characterise the population of neurons affected by acute oxaliplatin treatment, we calculated the cell diameter of neurons.

We found that the majority of cold-sensitive neurons were of a small- to medium-diameter (data not shown) (Daniels et al., 2009; Dhaka et al., 2008). This is perhaps indicative of sensitisation of nociceptors by oxaliplatin which may be important in explaining clinical symptoms. In particular, cold allodynia may occur as a result of oxaliplatin sensitisation of nociceptive neurons that are not normally cold-sensitive. Indeed, it has previously been reported that oxaliplatin sensitises C fibre responses to cold, heat and mechanical stimuli (Baron, 2006; Binder et al., 2007; Joseph et al., 2008). These changes have been proposed to be due to peripheral sensitisation as a result of hyperexcitability of C fibres following abnormal expression of sodium and TRP channels (Baron, 2006; Binder et al., 2007). However, later studies have reported direct effects of oxaliplatin on large-diameter A fibres (Deuis et al., 2013, 2014; Forstenpointner et al., 2018; Sittl et al., 2012). The effects of oxaliplatin are shown to be mediated by $Na_v1.6$, which is expressed exclusively in large-diameter A fibres (Deuis et al., 2013, 2014; Sittl et al., 2012).

We performed current-clamp experiments in large-diameter neurons because they were not captured in Ca^{2+}-imaging studies and due to the role of $Na_v1.6$ in cold-sensitivity in large-diameter A fibres. Oxaliplatin treatment (1 hr) did not significantly increase the excitability or alter action potential characteristics in DRG neurons. However, oxaliplatin-treated DRG neurons displayed a shift towards more negative potentials in afterhyperpolarisation (AHP) when compared to vehicle-treated neurons. Oxaliplatin-induced changes to AHP have been reported in an earlier study in the sciatic nerve of adult rats, and is explained by the

malfunction of voltage-gated potassium channels (K_v) (Kagiava et al., 2008). It is difficult to ascertain exactly which component of the AHP, fast, medium or slow is most affected by oxaliplatin as more detailed analysis is required. Each component is governed by different ion channels, with the first being dependent on the activity of K_v channels and the medium and slow AHP phases being governed by calcium-dependent and voltage-independent potassium (SK) channels (Bond et al., 2004). This does indicate that potassium channels are involved in oxaliplatin-induced hyperexcitability, which has been shown (Descoeur et al., 2011; González et al., 2017; Sittl et al., 2010). Future studies should focus on K_V channel dysfunction after oxaliplatin treatment. To what extent are these K+ currents changed by cooling in the presence of oxaliplatin remains unknown.

In summary, we show that oxaliplatin-induced cold sensitivity is limited in DRG neurons. Although a modest phenotype can be detected *in vitro* after sustained oxaliplatin treatment *in vivo*, it does not fully reflect what happens *in vivo*. Oxaliplatin can directly activate a small proportion of neurons and sensitise others to cold ramps. We predicted that these neurons could be small-diameter neurons expressing TRPM8, TRPA1 and TRPV1 channels. In addition, large-diameter neurons were studied in current-clamp experiments. We did not find that oxaliplatin activated a particular subset of neurons. Finally, acute pre-treatment with oxaliplatin only sensitised cold-evoked responses after 120-minutes. Overall, examining the effects of oxaliplatin *in vitro* using DRG neurons was limited in providing insight into the mechanistic basis for cold hypersensitivity. We therefore explored the effects of oxaliplatin on nerve terminals in the skin-saphenous nerve preparation, instead of somata for further investigations (Chapter 5).

4 Single fibre recordings in naive C57BL/6J mice

4.1 Introduction

The mammalian skin-saphenous nerve preparation was developed in the guinea pig and rat by Peter Reeh in the 1980's (Reeh, 1986) and later adapted for mice (Koltzenburg et al., 1997). The advantage of this technique over single-unit recordings *in vivo* or human microneurography is that it enables experimental control over external variables which could interfere with the physiology of the receptors. The *ex vivo* skin-nerve preparation also allows receptive fields of individual units to be directly stimulated by electrical, mechanical, thermal and chemical stimuli in a non-invasive, controlled manner. In addition, due to the lack of time related changes in fibre excitability patterns and spontaneous activity, recordings can reliably be made for up to 8 hours after dissection. Here, I have exploited the opportunity to apply oxaliplatin directly to the receptive field of individual fibres.

The studies presented in this chapter and in chapter 5 were conducted to determine the functional changes to primary afferent neurons in response to cold and mechanical stimulation following local and acute application of oxaliplatin to the receptive field of single-units. Cold allodynia is the hallmark of oxaliplatin-induced neuropathic pain (Attal et al., 2009; Barbosa et al., 2014) and most patients experience cold-evoked paraesthesias and pain in response to tasks such as holding cutlery, drinking cool drinks and opening the fridge (Lehky et al., 2004). Although recent studies have shown that oxaliplatin predominantly affects A fibres (Deuis et al., 2013; Forstenpointner et al., 2018; Sittl et al., 2010, 2012), the specific categories of A fibres most affected by oxaliplatin have not been identified. In this chapter, all classes of A fibres and two classes of C fibres were identified and characterised to establish a reference for the functional properties of these fibre classes. This enabled comparisons to be made between fibres after topical acute oxaliplatin treatment to the receptive field with

those under normal physiological conditions in naïve C57BL/6J mice. In addition, the effects of oxaliplatin *in vivo* have been presented in chapter 2 and show that a single systemic dose of oxaliplatin is sufficient to cause acute cold and mechanical hypersensitivity in mice which is also seen in patients in the clinic. In chapter 5, this was followed up by performing single- and multi-unit recordings in skin-nerve preparations taken from oxaliplatin-treated animals to investigate whether functional changes could be seen at the terminal level of peripheral afferent nerve fibres days after injection to provide an explanation for the behavioural phenotype.

4.2 Aims

The aim of the present study was to determine the properties of mechanically sensitive afferent nerve fibre classes in naïve C57BL/6J mice. Single-units were categorised as Aβ, Aδ and C fibres according to their conduction velocities. Mechanical and cold thresholds and evoked patterns of impulse activity in response to mechanical and cold stimuli in different fibre types were analysed and enabled full characterisation of individual fibres.

4.3 Methods

4.3.1 Animals

8-12 week old C57BL/6J male and female mice were used. Mice were culled by cervical dislocation and the hind paw skin was shaved.

4.3.2 Skin-nerve preparation and set-up

The saphenous nerve and the dorsal hind paw skin that it innervates was dissected free to the lumbosacral plexus to ensure that a sufficient length of nerve was available for recording. After dissection, the preparation was placed 'inside up' or 'outside down' in a bath chamber to facilitate the oxygenation through the corium side of the skin and the preparation was superfused with an oxygen saturated modified synthetic interstitial fluid (SIF) solution set at 31 ± 1 °C containing (in mM): 108 NaCl, 3.5 KCl, 0.7 $MgSO_4.7H_2O$, 26.2 Na_2CO_3, 1.65 $NaH_2PO_4.2H_2O$, 9.6 sodium gluconate, 5.55 glucose, 7.6 sucrose and 1.53 $CaCl_2$. The skin was left to equilibrate in the organ bath for an hour in order to avoid spontaneous firing from fibres.

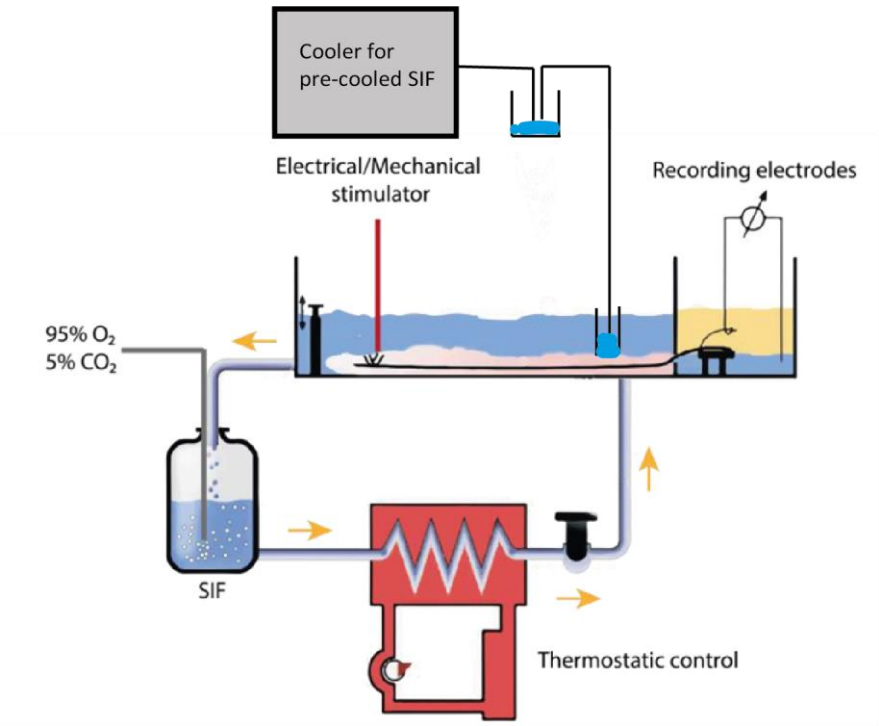

Figure 4-1 Experimental set-up for single-fibre recordings.

The skin-saphenous nerve preparation is pinned down in a bath chamber circulated with oxygenated and warmed SIF. The nerve is passed through a small gap into the adjacent recording chamber where oil isolates the nerve from the SIF. The tip of the nerve is always placed on a mirror to enable it to be desheathed and teased into thinner filaments for recordings. Modified from (Zimmermann et al., 2009).

4.3.3 Recording technique

The skin was pinned down using insect pins before the start of recordings and the saphenous nerve was pulled through into the adjacent smaller recording chamber and placed on a mirror. The recording chamber including the mirror, gold recording electrode with the saphenous nerve inside was covered with paraffin oil to enable electrical isolation. The nerve was desheathed and subsequently teased into fine filaments with watchmakers forceps using a microscope. During the recordings, nerve filaments were placed on the gold electrode in the oil phase, and the reference electrode was positioned nearby, but in the aqueous phase. Single fibres were identified with a mechanical search stimulus (manual probing to the skin using a blunt glass rod) and were recorded extracellularly using a low-noise differential amplifier. The conduction velocity of each axon was determined by electrically stimulating the most sensitive area of the receptive field with square-wave pulses (1 millisecond duration every 2 or 4 seconds for A and C fibres respectively) using a microelectrode and a Digitimer stimulator (Figure 4-2). In accordance with earlier studies and recordings in the mouse, a cut-off of 1.2 m/s was used to distinguish between myelinated and unmyelinated fibres. Fibres with a conduction velocity > 10 m/s were classified as Aβ fibres and those with a conduction velocity > 1.2 m/s and < 10 m/s were classified as Aδ fibres. Fibres were further categorised into subclasses of populations based on responses to mechanical and cold stimulation following calculation of conduction velocity.

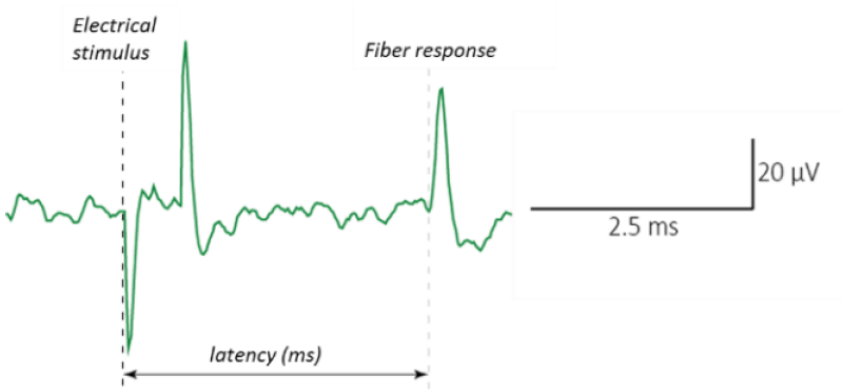

Figure 4-2 Electrical stimulation of fibre.

All fibres were electrically stimulated to evoke an action potential. The response time is defined as latency and measured in milliseconds (ms). Diagram prepared by Ulku Cuhadar (Cuhadar thesis, 2019).

4.3.4 Mechanical stimulation

A mechanical stimulating probe (1 mm diameter) connected to a force transducer was placed in the same position as the electrical microelectrode and controlled via the Spike2 programme (Cambridge Electronic Design (CED)). Forces (in g) were applied to the receptive field following conversion from an input value (in mV). The mechanical threshold was determined for each fibre by applying 2 second step waveform pulses. Forces were applied iteratively until the threshold, defined as the minimum force that could evoke two action potentials was determined. Following this, fibres were mechanically stimulated with step and ramp protocols to enable more detailed characterisation of single-units based on their adaptation properties. A 10 second step-shaped force was applied at a low force (4 g) and high force (15 g) (Figure 4-4) with a two-minute interval between to enable recovery of the fibre and to prevent tachyphylaxis. Step protocols were particularly important in allowing low- and high- threshold mechanoreceptors (LTMR and HTMR respectively) to be distinguished. Ramp protocols were applied to characterise the coding properties of HTMRs including AM and CM fibres which encode applied forces with a linear increase in the evoked impulse rate. A 20 g ramp was applied for 15 seconds in order to characterise fibre adaptation properties further.

4.3.5 Cold stimulation

After the mechanical characterisation, each fibre was additionally challenged with cold. The cold sensitivity of all fibres was assessed by sealing off receptive fields of individual units with a metal ring (6 mm diameter). Vaseline was applied to the underside of the ring to create a tight seal and prevent any leakages. The bath solution within the ring was manually removed with a syringe and a thermocouple was gently applied to measure the intracutaneous

temperature. Cold ramps lasting 60 seconds (Figure 4-6) were applied by delivery of pre-cooled SIF via a separate circulation system.

4.3.6 Data Acquisition

The extracellular potentials were recorded using World Precision Instruments (WPI) low-noise head stage DAM80 AC differential amplifier which amplified the signal (gain of 10^4) and was connected to a ground connection. The signal was filtered with a low pass (300 Hz) and a high pass (10 KHz) filter. The differential amplifier was connected to a CED 1401 acquisition board. The output of the signal was visualised on an oscilloscope, recorded on a PC and made audible via speakers. All data was acquired using the Spike2 programme.

4.3.7 Data Analysis

Action potentials were analysed in Spike2 by creating a template using the waveform of the fibre in each recording (Figure 4-3). A separate channel was created with action potentials for these waveforms at each event (stimulation period) during the recording. This was duplicated and the channel draw mode function was used to convert this into action potentials/second (Hertz) to visualise discharge rates as a histogram (Figure 4-4). For analysis, the period during mechanical and cold stimuli were scanned for events. Action potentials were exported as numerical text data into Excel (Figure 4-5). Data were exported in 1 second time bins and basic analysis was performed to assess total number of spikes, peak firing frequency and threshold (temperature for cold) of activation for cold and mechanical stimulations in Spike2, Excel and GraphPad Prism (Version 8.3, CA, USA). In addition, the firing pattern of fibres during the cold and mechanical stimulation periods were plotted.

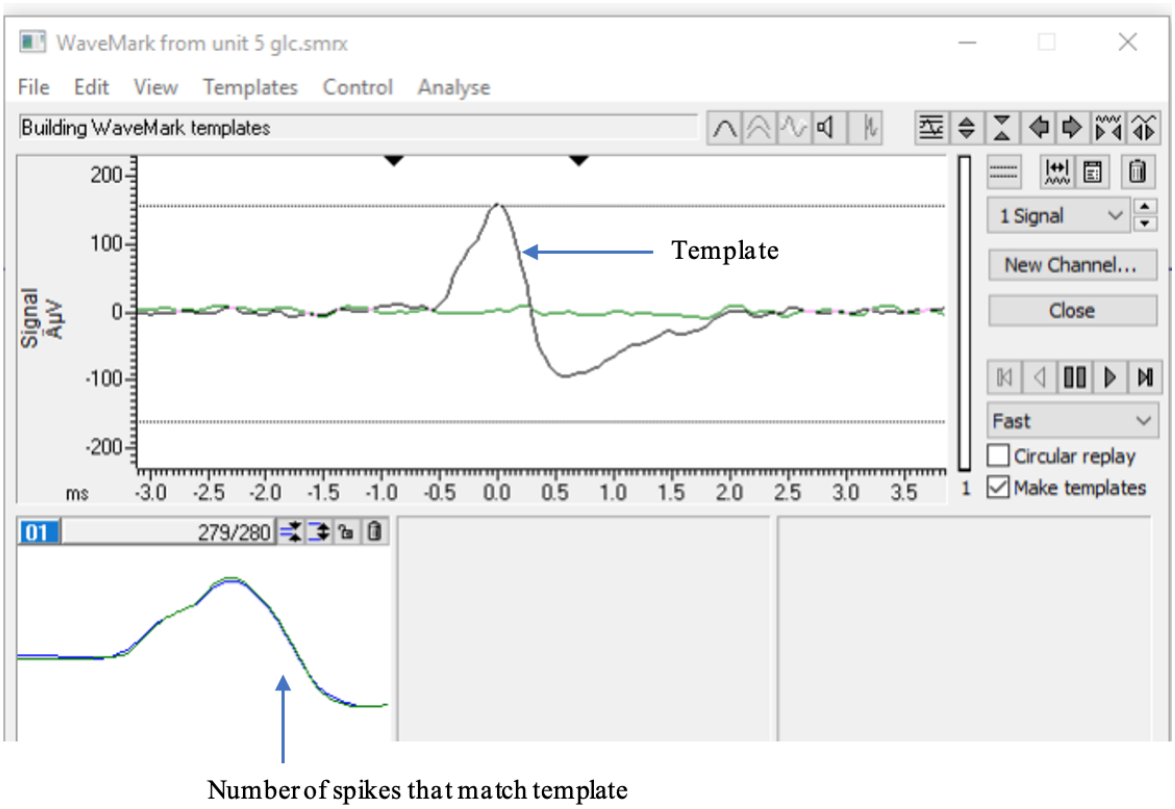

Figure 4-3 Generating templates for analysis.

Once impulses from the selected fibre were identified in the recording, a template was created to allow spike discrimination and selection. Spike events that matched the waveform template were extracted for further analysis.

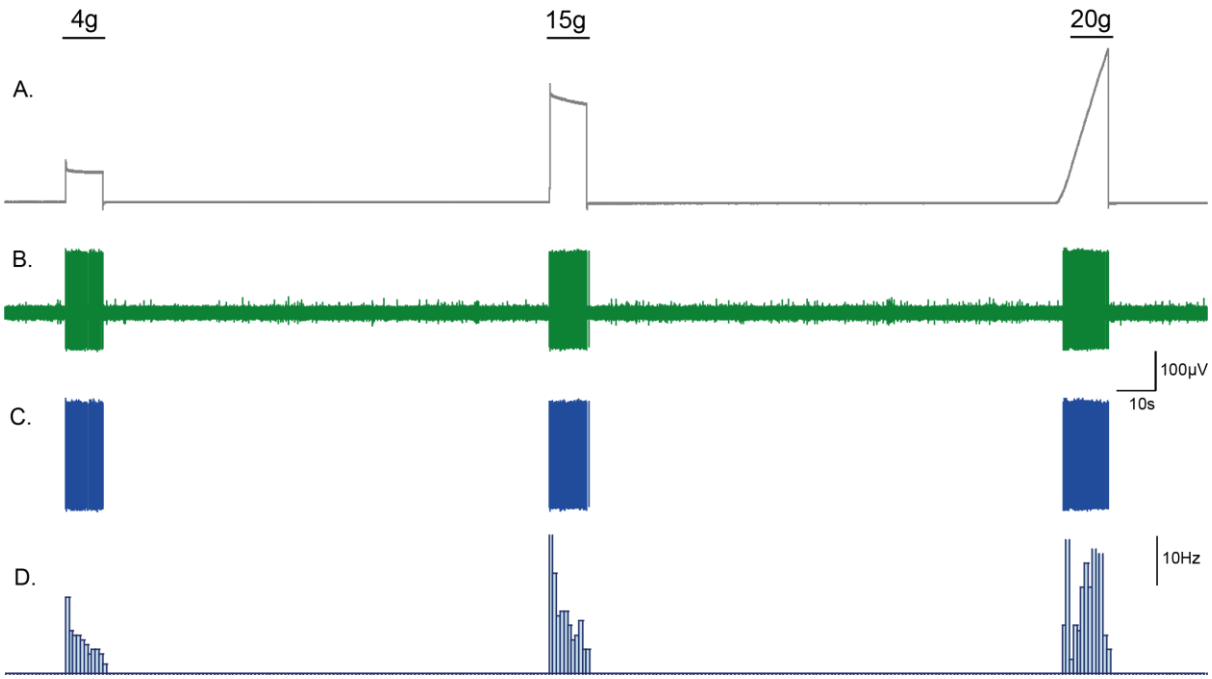

Figure 4-4 Mechanical force steps and ramps with single-unit impulse responses.

A) The mechanical forces and types applied to individual fibres. B) The green trace shows action potentials triggered by mechanical force from recordings. C) In blue are the impulses generated from the template in a new channel. D) The histograms (bottom trace) represent fibre impulse frequency (events/sec or Hertz).

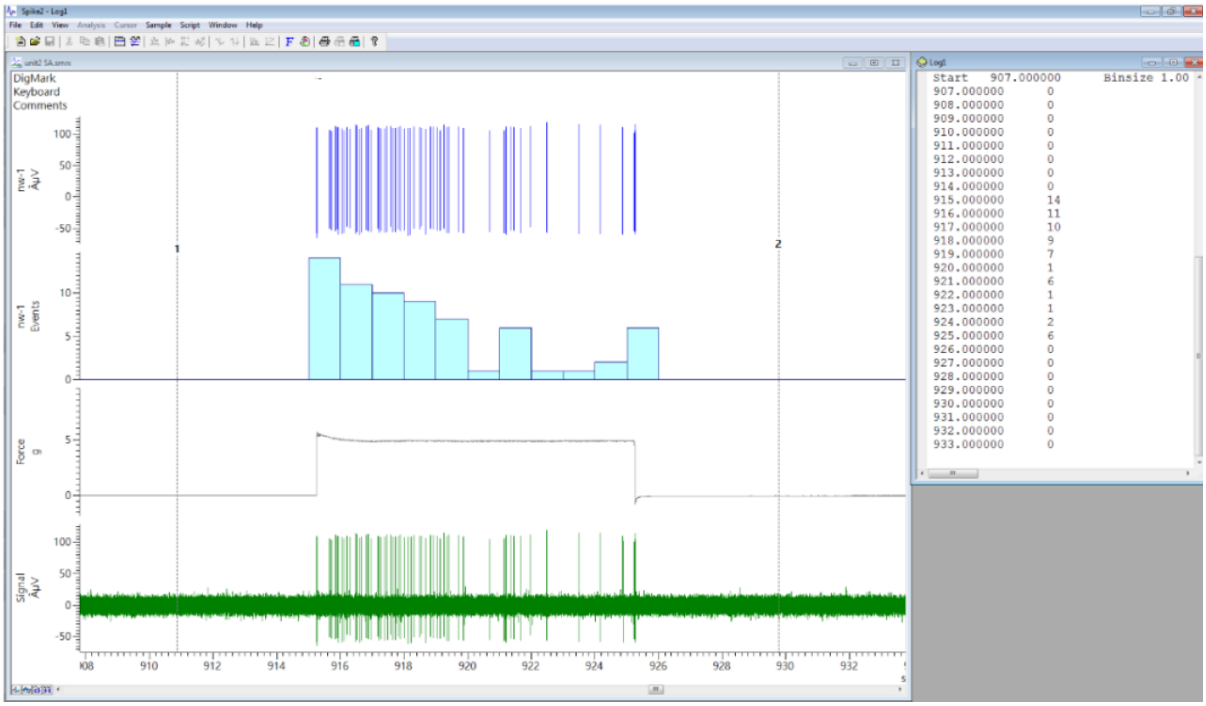

Figure 4-5 Analysis of impulses evoked by mechanical stimulation using Spike2.

In the three channels displayed, the top channel with spikes in blue has been created after the template has been run in the recording to discriminate the fibre of choice. The second channel displayed as a histogram is a representation of spikes as events/sec. The last channel in green shows the original fibre activity recording. Cursors 1 and 2 determine the period scanned for events. The window on the right indicates the number of action potentials occurring during each 1-second bin which was exported into Excel for further analysis.

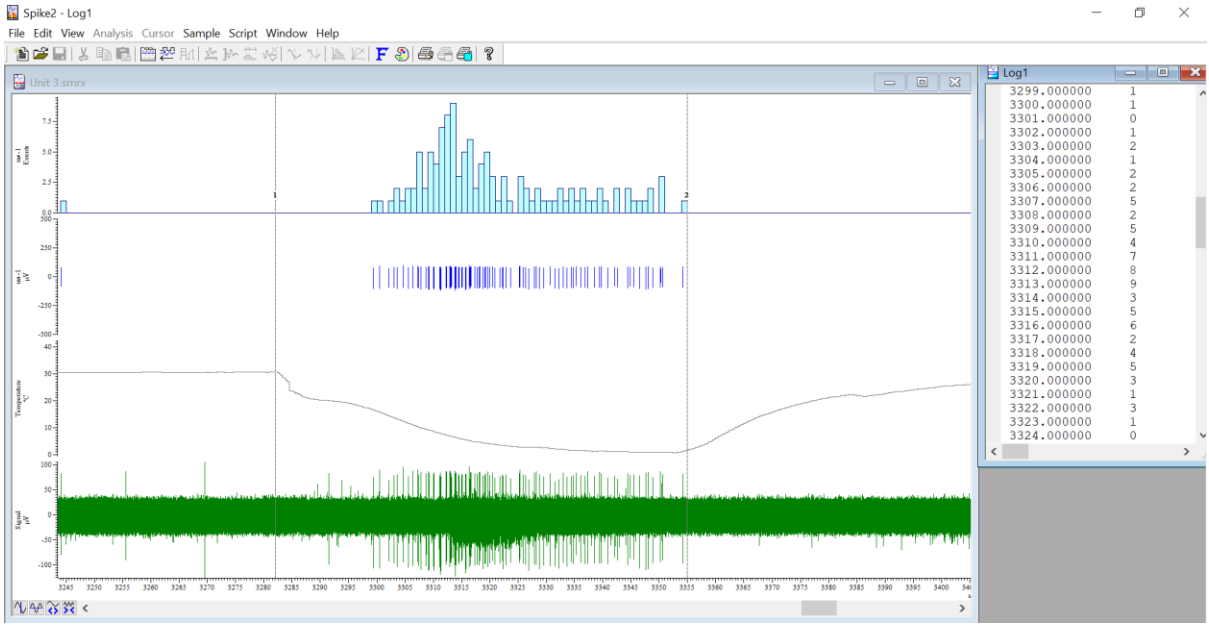

Figure 4-6 Analysis of cold responses using Spike2.

Data during cold ramps was exported in the same way as mechanical responses. The cursors marked the start and end of the cold ramp and the number of action potentials occurring during each 1-second bin were exported into Excel for further analysis. The threshold was determined by identifying the second action potential fired by the fibre during the cold ramp to mitigate the risk of impulses unrelated to the stimulus influencing the estimated temperature thresholds.

4.4 Results

A total of 234 fibres, n = 133 from naïve C57BL/6J male and female mice, 51 treated with acute oxaliplatin treatment and 50 treated with acute vehicle (glucose) treatment which were mechanically sensitive from the hairy hind paw skin were recorded and classified according to their conduction velocity, mechanical and cold threshold and impulse discharge properties.

4.4.1 Types of mechanically sensitive fibres in the hairy skin of naïve mice

Table 4-1 Naïve mice fibres mechanical threshold and conduction velocity

Class	Fibre type	n	Average Mechanical threshold (g)	SEM	Average conduction velocity (m/s)	SEM
Aβ	SA	23	0.5	0.1	13.9	2.2
	RA	26	0.3	0.1	14.8	1.2
Aδ	DH	16	0.4	0.1	6.5	0.6
	AM	31	3.9	0.6	4.4	0.4
C	CM	17	3.8	0.7	0.5	0.1
	CMC	20	3.0	0.6	0.4	0.1

Fibres in preparations from naïve C57BL/6J mice before treatment with glucose or oxaliplatin were studied as a control group for their properties. This served as a reference group for comparison of functional properties of fibres after treatment. The saphenous nerve from the isolated skin-nerve preparation was dissected into progressively thinner filaments and the receptive field of the fibre innervating the skin was identified mechanically. Once the receptive field was identified, the conduction velocity of the fibre and its mechanical threshold were determined. In addition, the response to mechanical forces and cold ramps were recorded.

Mechano- and cold-sensitive fibres were categorised into six different fibre types. Fibres were classified into three main classes: Aβ, Aδ and C according to their conduction velocities (Koltzenburg et al., 1997). In accordance with earlier studies and recordings in the rat, a cut-off of 1.2 m/s was used to distinguish between myelinated and unmyelinated fibres. Fibres with a conduction velocity > 10 m/s were classified as Aβ fibres and those with a conduction velocity > 1.2 m/s and < 10 m/s were classified as Aδ fibres. Fibres were further categorised into subclasses based on their responses to mechanical and cold stimulation.

Aβ fibres were divided into two types, rapidly adapting (RA) and slowly adapting (SA) fibres according to their response to sustained mechanical stimuli. Aβ fibres that discharged briefly at the beginning and again at the end to a constant force stimulus were classified as RA fibres (Figure 4-9), whereas Aβ fibres that responded with a sustained pattern of impulses were classified as SA fibres (Figure 4-8). Both RA and SA fibres discharged impulses for very low forces (Table 4-1). Neither of the two fibre types responded to cold stimuli. These findings were in agreement with earlier studies (Koltzenburg et al., 1997).

Aδ fibres were also categorised into two types, based on their mechanical activation thresholds. Aδ fibres with low mechanical activation thresholds were classified as D-hair fibres (DH) and those with high force thresholds for activation were classified as Aδ-mechanoreceptor (AM) fibres (Table 4-1). DH fibres had an activation threshold (0.41 ± 0.08 g) that was similar to that of RA (0.3 ± 0.1 g) and SA (0.5 ± 0.1 g) fibres. Furthermore, like RA fibres, DH fibres discharged impulses briefly at the beginning and end to a constant force application (Figure 4-7). In contrast, AM fibres had a higher average mechanical threshold (3.9 ± 0.6 g). The response profile for AM fibres differs to DH fibres as they respond throughout

the full duration of a constant force application (Figure 4-10). In the case of a ramp stimulation, which apply increasing forces gradually, AM fibres showed increasing firing with increasing force, thereby encoding the force (Figure 4-10 C). This is in contrast with DH and Aβ fibres which do not encode force with a linear increase in the impulse frequency.

Mechanically sensitive C (CM) and mechanically and cold-sensitive C (CMC) fibres were also recorded. Both classes of C fibres had very low conduction velocities and high activation thresholds (CM fibres 3.8 ± 0.7 g; CMC 3.0 ± 0.6 g) in response to mechanical stimulation (Table 4-1). CM and CMC fibres displayed similar impulse discharge patterns to AM nociceptors in response to mechanical stimulation and were able to encode increasing force with a corresponding increase in the impulse discharge rate (Figure 4-11). CMC fibres had the additional capability of responding to cold ramps.

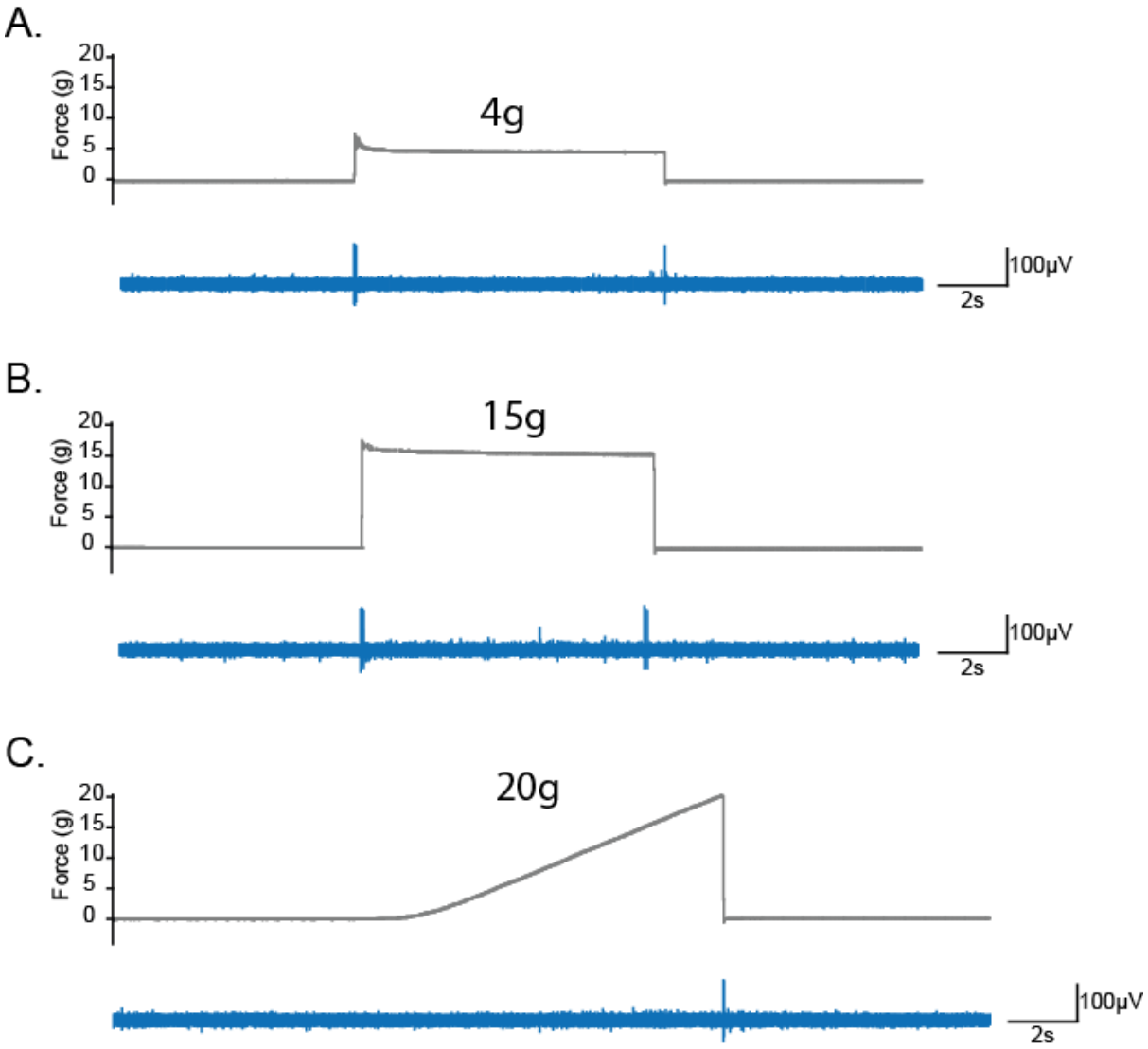

Figure 4-7 Example traces of naïve Aδ DH responses to step and ramp stimuli.

A) Response to non-noxious 4 g force step. DH fibres only discharge impulses at the start and end of a mechanical stimulation. B) Response to noxious 15 g force step. Same pattern of firing seen as in the 4 g force step. C) Response to 20 g ramp. DH fibres are non-nociceptors and therefore cannot encode ramps which have increasing forces over time. The classic DH response to a ramp is shown here as they only discharge impulses once the ramp has ended.

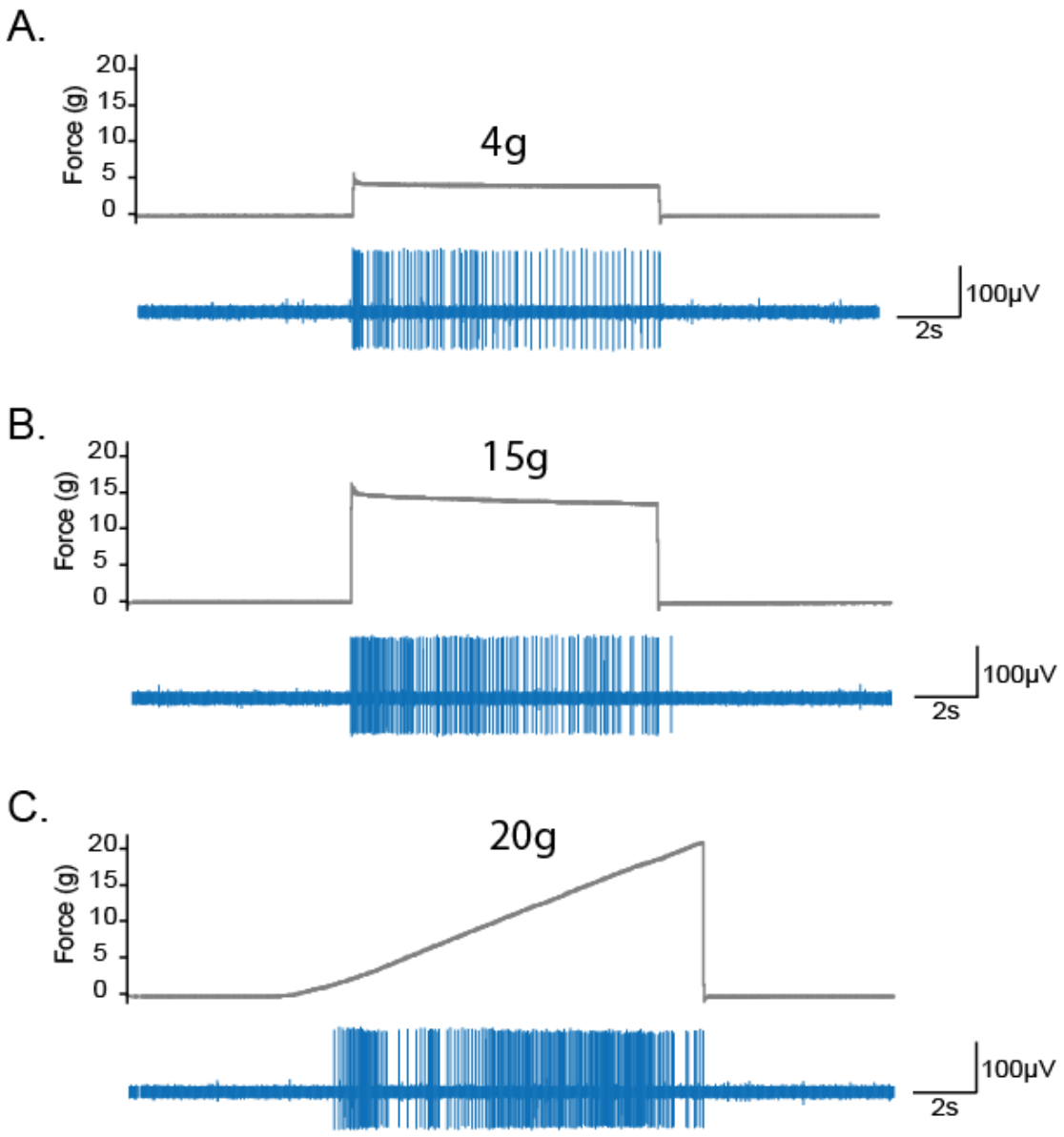

Figure 4-8 Example traces of naïve Aβ SA responses to step and ramp stimuli.

A) Response to non-noxious 4 g force step. SA fibres sustain discharge impulses throughout mechanical stimulation. B) Response to noxious 15 g force step. Same sustained pattern of firing seen as in the 4 g force step but less regular firing. C) Response to 20 g ramp. SA fibres are non-nociceptors and therefore cannot encode ramps which have increasing forces over time. The classic SA response to a ramp is shown here as there is sustained firing throughout but the discharge impulses are not encoding the increasing forces.

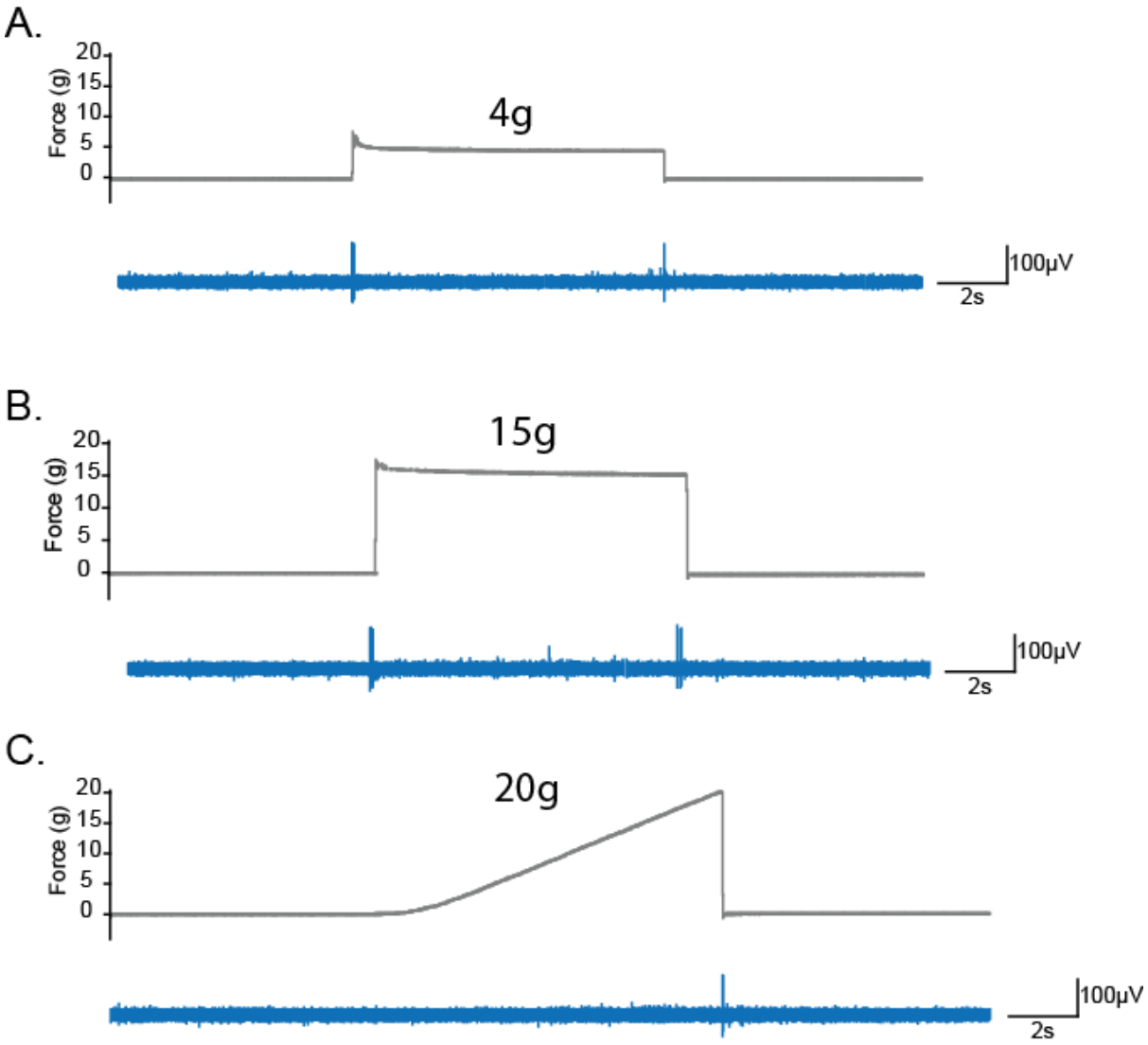

Figure 4-9 Example traces of naïve Aβ RA responses to step and ramp stimuli.

A) Response to non-noxious 4 g force step. RA fibres, like DH fibres only discharge impulses at the start and end of a mechanical stimulation. B) Response to noxious 15 g force step. Same pattern of firing seen as in the 4 g force step. C) Response to 20 g ramp. RA fibres are non-nociceptors and therefore cannot encode ramps which have increasing forces over time. The classic RA response to a ramp is shown here and is identical to that of DH fibres, with discharge impulses seen just at the end of the ramp.

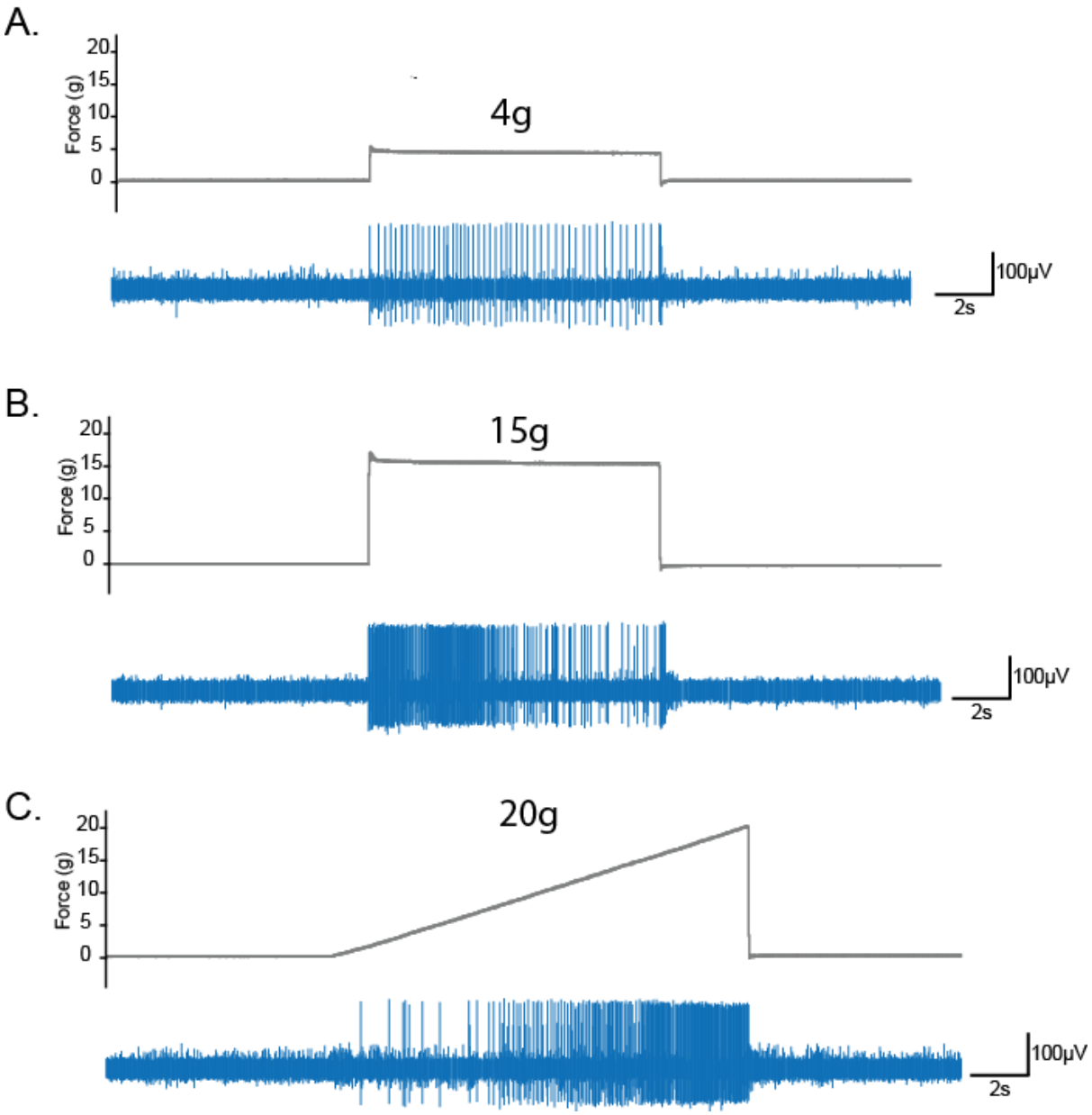

Figure 4-70 Example traces of naïve Aδ AM responses to step and ramp stimuli.

A) Response to non-noxious 4 g force step. AM fibres show very regular patterns of discharge impulses to low force mechanical stimulation. B) Response to noxious 15 g force step. Increased rate of discharge impulses with regular and sustained firing throughout stimulation. C) Response to 20 g ramp. A mechanical ramp stimulus were used to display encoding properties of AM fibres to increasing forces. AM fibres are nociceptors and encode an increasing stimulus intensity with an increasing impulse rate. This is demonstrated by the greater number of action potentials fired at higher forces.

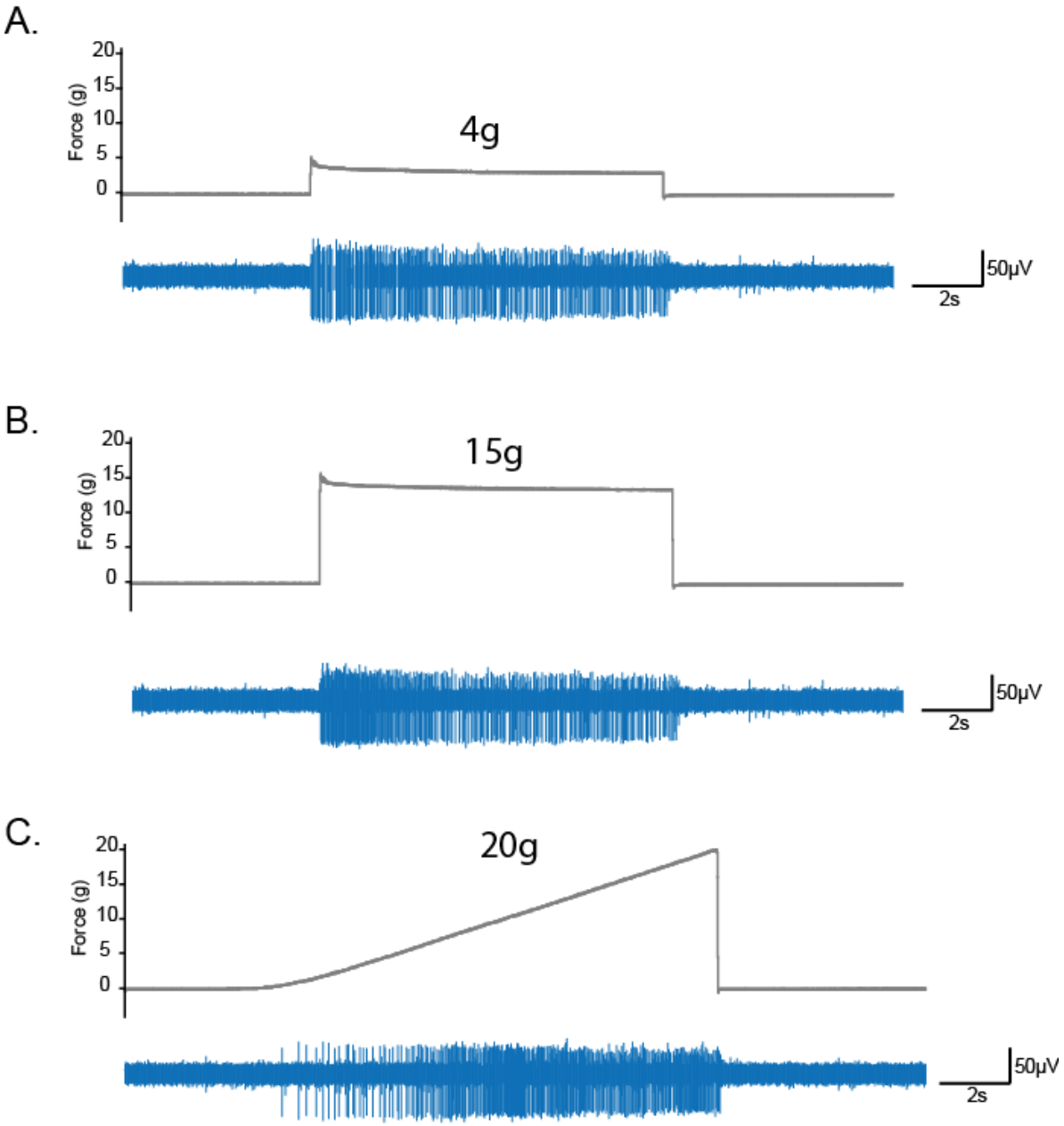

Figure 4-11 Example traces of naïve CM responses to step and ramp stimuli.

A) Response to non-noxious 4 g force step. Majority of CM fibres show very regular patterns of discharge impulses to low force mechanical stimulation. B) Response to noxious 15 g force step. Increased rate of discharge impulses with regular and sustained firing throughout stimulation. C) Response to 20 g ramp. A mechanical ramp stimulus used to show encoding properties of fibres to increasing forces. CM fibres are nociceptors and therefore encode ramps which have increasing forces over time. This is shown by a greater number of action potentials fired at higher forces.

4.4.2 Conduction velocity of mechanically sensitive fibres

The conduction velocity of each fibre was determined by electrically stimulating the receptive field with a square-wave electrical pulse (duration 1 millisecond, with inter-stimulus intervals of 2 or 4 seconds) as described in the methods above (section 4.3). Classification of fibres was made as previously described (Koltzenburg et al., 1997). The mean conduction velocity of Aβ fibres recorded from naïve mice was 14.4 ± 1.2 m/s (n = 49). The mean conduction velocity for Aδ fibres was 5.1 ± 0.4 m/s (n = 47) and 0.4 ± 0.0 m/s (n = 37) for C fibres.

Similar to previous studies, the conduction velocities were not normally distributed (Figure 4-12), which can be explained by the heterogenous and diverse population of fibres (Koltzenburg et al., 1997). There was a clear distinction between myelinated A fibres and unmyelinated C fibres based on the conduction velocities of fibres, but not between Aβ and Aδ fibres. Whilst conduction velocities were used as a starting point to classify fibres, impulse discharge patterns to mechanical and cold stimulations were used to fully characterise fibres.

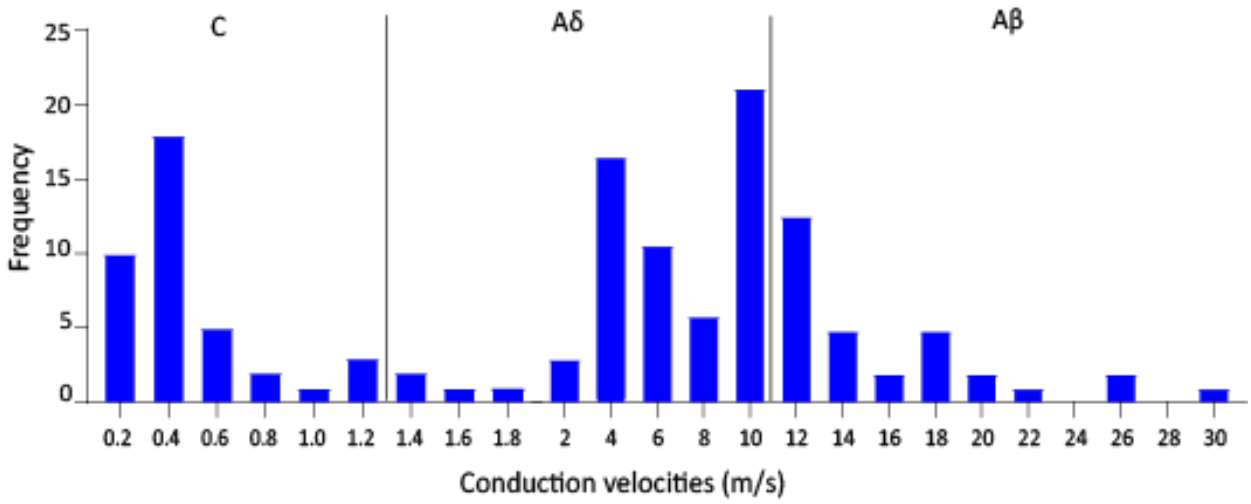

Figure 4-12 Bin distribution of the fibre conduction velocity (m/s).

Fibre conduction velocity (CV) varies according to the fibre class. C fibres are the slowest with CV values between 0.2 and 1.2 m/s. Aδ fibres have intermediate CV values between 2 and 10 m/s and Aβ fibres have the greatest CV range (> 10 m/s). The lines within the graph indicate the limits of each fibre class according to their CV (Koltzenburg et al., 1997).

4.4.3 Analysis of impulse discharge patterns of fibres to mechanical stimulation

After recording the fibre conduction velocity, fibres were stimulated with mechanical force for 2s and their activation threshold identified iteratively (methods, section 4.3). RA, SA and DH fibres are low threshold mechano-sensitive receptors (LTMRs), so are activated at lower forces when compared with mechano-nociceptors. The mean mechanical force thresholds for these LTMRs are shown in Table 4-1 and Figure 4-13 A.

In contrast, AM and CM (and therefore CMC) fibres are high threshold mechano-sensitive receptors (HTMRs) and therefore require greater force stimulation to evoke a response in these fibres (Table 4-1 and Figure 4-13 B). This is due to the nociceptive nature of these fibres when compared with LTMRs, which are non-nociceptors.

A feedback-controlled mechanical stimulator was used to investigate responses evoked by stimulation of suprathreshold forces. Sustained steps at 4 g and 15 g forces were used to study the mechanical adaptation properties of RA, SA, DH, AM, CM and CMC fibres. In the case of HTMRs, an additional mechanical ramp stimulus at 20 g force was applied to show encoding properties. All impulse discharge patterns at all forces were analysed.

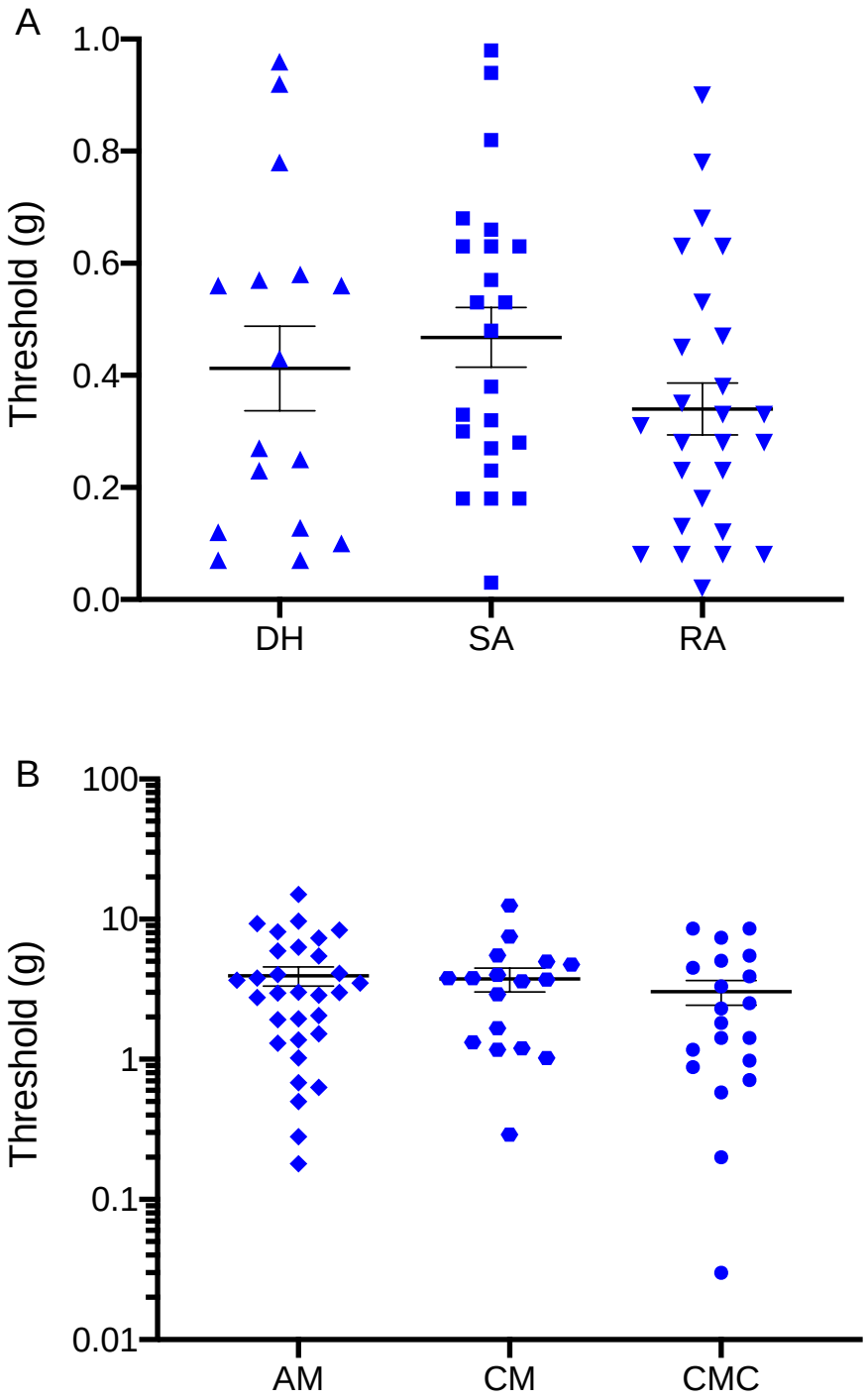

Figure 4-13 Activation threshold of mechanically sensitive hairy-skin nerve fibres in naïve C57BL/6J mice.

A) Low threshold mechano-sensitive receptors (LTMRs): DH, SA, RA fibres all have a similar and low mechanical threshold of activation. B) High threshold mechano-sensitive receptors (HTMRs): AM, CM and CMC fibres are all nociceptors with a higher mechanical threshold of activation compared to LTMRs. All data are presented as mean ± S.E.M.

A typical recording from an SA fibre is displayed in Figure 4-8. At the non-noxious 4 g force application, there was on average 84 ± 19 imp/s. There was an increase in the average number of impulse discharges (111 ± 16 imp/s) at the noxious 15 g force application. As seen in the example in Figure 4-8 B, there was a slight increase in the adaptation rate when compared to Figure 4-8 A, seen by less regular impulse discharges in the second half of the 15 g force application. The classic response of SA fibres to steps is that they discharge impulses throughout the constant force stimulation. Although this is also seen in response to a 20 g ramp (Figure 4-8 C), SA fibres cannot encode the ramp stimulus, therefore there is no increase in discharge impulses with increasing force.

Despite having similar conduction velocities, RA fibres can be distinguished from SA fibres due to their different discharge pattern in response to mechanical stimuli. As shown in Figure 4-9, RA fibres discharge impulses at the very beginning and end of the step stimulus. The mean impulse discharge rate at the non-noxious 4 g step was 7 ± 1 imp/s and the mean impulse discharge rate at the noxious 15 g step was 9 ± 1 imp/s. This revealed a lower overall peak impulse discharge rate in RA fibres compared to SA fibres during a constant force application. This can be explained by the rapid mechanical adaptation properties shown by RA fibres when compared to SA fibres. Again, RA fibres cannot encode increasing forces, therefore the typical response of RA fibres to a ramp stimulation is seen in Figure 4-9 C.

Although DH fibres belong to the Aδ fibre class, they display discharge patterns that are identical to RA fibres (Figure 4-7). They responded only at the beginning and at the end of the stimulus and remained silent during the remainder of the mechanical challenges. The average impulse discharge rate was 4 ± 1 imp/s and 7 ± 1 imp/s in response to the 4 g step and 15 g

step respectively. The inability of these fibres to encode increasing forces is shown in Figure 4-7 C.

AM fibres showed a regular pattern of firing in response to step stimuli and sustained impulse discharges throughout constant force stimulations (Figure 4-10). The total number of action potentials and the impulse rate were positively correlated with the intensity of the step stimulus. The mean impulse discharge rate was 53 ± 23 imp/s in response to the 4 g step and 89 ± 16 imp/s in response to the 15 g step. It was typical for AM fibres to discharge impulses at higher frequencies in the first 5 seconds of the 10s 15 g force step stimulation as shown in Figure 4-10 B. The highest total number of action potentials generated was recorded for the highest force, 20 g. The mean discharge rate was 101 ± 20 imp/s in response to the 20 g ramp. Stimulation of AM fibres with the 20 g ramp stimulus generated an increasing impulse discharge rate throughout the stimulation period. A maximal impulse discharge rate was reached towards the end of the ramp stimulus (Figure 4-10 C).

CM and CMC fibres had a similar firing pattern to AM fibres in response to step and ramp stimuli (Figure 4-11). In comparison to AM fibres, CM and CMC fibres displayed a lower peak discharge and a lower total number of action potentials to all stimuli. The mean impulse discharge rate to the 4 g step was 16 ± 6 imp/s and 23 ± 4 imp/s for CM and CMC fibres respectively. The total number of action potentials increased with increased step stimuli and the mean impulse discharge rate was 51 ± 18 imp/s for CM and 76 ± 18 imp/s for CMC fibres in response to the 15 g step. Like AM fibres, the greatest number of action potentials was fired in response to the 20 g ramp for CM and CMC fibres. The mean discharge rate was 57 ± 22 imp/s for CM and 75 ± 15 imp/s for CMC fibres in response to the 20 g ramp. Like AM

nociceptors, CM and CMC nociceptors reliably encoded increasing impulse rates (Figure 4-11 C).

4.4.4 Analysis of impulse discharge patterns of HTMRs to cold stimulation

Following characterisation of fibres using mechanical stimulations, all fibre types were exposed to a single cold ramp. The receptive field of the fibre being recorded from was sealed off with a metal ring (6 mm diameter). The bath solution within the ring was manually removed with a syringe and a thermocouple was gently applied to measure the intracutaneous temperature (31 ± 1 °C). Cold ramps lasting 60 seconds were applied by delivery of pre-cooled SIF via a separate circulation system (methods, section 4.3).

As expected, there was no cold-evoked firing seen in the majority of fibres from naïve mice. In fact, there was no response to cold ramps seen in any LTMRs. In contrast, HTMR nociceptors were capable of discharging impulses in response to cold ramps. In accordance with earlier studies, there was a small percentage (~10 %) of cold-sensitive AM nociceptors in recordings. It was typical for AMC fibres to discharge few impulses throughout the duration of the cold ramp, as shown in the example trace (Figure 4-14). However, just 2 AMC fibres were found in our study overall.

Like AMC fibres, CMC nociceptors faithfully responded throughout cold ramps. It was also typical for CMC fibres to have a low peak discharge as shown in the example trace in Figure 4-15. The mean total number of action potentials during the cold ramp was 52 ± 23 imp/s. The mean peak firing frequency was 4 ± 1 imp/s and the mean threshold temperature of activation was 17.4 ± 1.9 °C. The impulse discharge pattern was regular, with no high frequency firing or bursting pattern of action potentials.

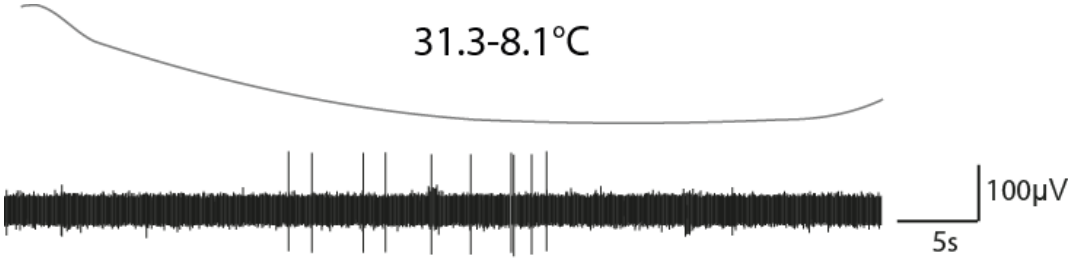

Figure 4-14 Example trace of naïve AMC fibre response to cold ramp.

Cold-evoked discharge impulses seen in a small proportion of AM nociceptors. Typically, there are not many action potentials seen during the cold ramp and the firing pattern is regular.

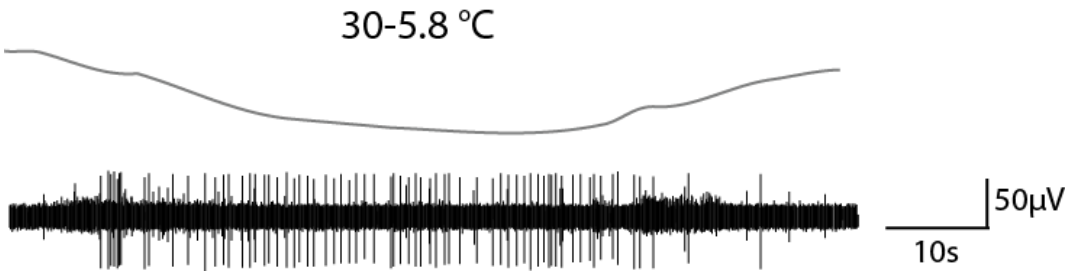

Figure 4-15 Example trace of naïve CMC fibre response to cold ramp.

Cold-evoked discharge impulses seen in a proportion of C fibres. These cold and mechano-sensitive C nociceptors typically fire few action potentials throughout the cold ramp.

4.5 Discussion

In this chapter, the properties of myelinated A and unmyelinated CM and CMC fibres innervating the hairy skin of naïve C57BL/6J mice were characterised.

4.5.1 LTMRs

Aβ and DH fibres are all characterised as LTMRs due to their activation to light touch. Aβ fibres from hairy skin displayed either rapidly adapting (RA) or slowly adapting (SA) properties in response to constant force stimulation to their receptive fields. Early studies in cat, monkey and human hairy and glabrous skin have all characterised and identified the role of these fibres (Burgess et al., 1968; Johansson and Vallbo, 1979). Both Aβ fibre types are well suited to convey fine spatial information as they have small receptive fields and densely innervate the distal finger pads where tactile acuity is high (Bensmaïa et al., 2006; Johansson and Vallbo, 1979).

4.5.1.1 Rapidly adapting (RA) LTMRs

Hairy skin RA-LTMRs are not spontaneously active and they do not respond to thermal stimuli (Abraira and Ginty, 2013). Their responses arise from longitudinal lanceolate endings that surround hair follicles and RA fibres are extremely sensitive to hair follicle deflection, with putative sites for mechanotransduction located between the nerve fibre and hair follicle keratinocytes (Abraira and Ginty, 2013; Halata, 1993). RA fibres are associated with perception of high frequency and dynamic events, such as slipping and gripping of objects (Park et al., 2016). These fibres can be further divided into RA type I and II, with the latter being exclusively able to detect transient events such as vibration (Park et al., 2016).

4.5.1.2 Slowly adapting (SA) LTMRs

In recordings in cat hairy skin, direct mechanical stimulation to the skin activated two type of slowly adapting fibres; SA type I and II (Burgess et al., 1968). SA type I-LTMRs are widely expressed in hairy skin, and are associated with the Merkel cell complex found within the epidermal/dermal junction surrounding the mouths of guard hairs of rodents and they generate a sustained response to skin indentation (Abraira and Ginty, 2013; Bensmaïa et al., 2006). In contrast, SA II LTMRs are less densely populated in the rodent hairy skin, although their response properties have been identified. However, the anatomical correlate for SA type II-LTMRs in the rodent hairy skin remains controversial (Abraira and Ginty, 2013). SA type II fibres respond to stretch and may function as proprioceptors (Park et al., 2016). The properties of RA and SA fibres displayed in this chapter were similar to those previously reported in single fibre recordings in the mouse (Koltzenburg et al., 1997).

4.5.1.3 Down-hair (DH) LTMRs

In single-unit recordings from cats and rabbits, it was shown that movement of guard hairs led to the activation of thickly myelinated Aβ fibres, whereas thinly myelinated A fibres were activated by finer, zig zag hairs, the D-hair (down hair receptors) (Brown and Iggo, 1967). D-hair (DH) mechanoreceptors have been shown to be extremely sensitive to mechanical stimulation and display fast adaptation to mechanical displacement of the hair (Burgess et al., 1968). Notable differences in DH adaptation properties have been identified between species, with primate DH receptors showing slow adaptation when stimulated mechanically (Perl, 1968). However, single-unit recordings in healthy human volunteers have revealed a population of low threshold Aδ mechanoreceptors with similar properties to DH fibres identified earlier in cats and rabbits (Adriaensen et al., 1983). Thirty years after the

characterisation of DH fibres in the cat, Koltzenberg and colleagues studied DH properties in the mouse (Koltzenburg et al., 1997) and their findings were in accordance with those presented in this chapter. It should be noted that our study and the one by Koltzenburg *et al.* stimulated RA and DH fibres on the corium side of the skin rather than by deflecting hair cells, which is the physiological basis of activating these fibres.

4.5.2 HTMRs

4.5.2.1 Aδ-mechanonociceptors (AM)

High threshold mechanoreceptors (HTMRs) with myelinated axons that responded to noxious stimuli were first described in cats, monkeys and humans (Adriaensen et al., 1983; Burgess and Perl, 1967; Burgess et al., 1968; Perl, 1968). In recordings from monkey hairy and glabrous skin, the HTMRs that were described to be specifically activated by high pressure applied to the skin, but not to noxious cold or heat (Perl, 1968) correspond with AM fibres that were identified in recordings from naïve C57BL/6J mice in this chapter. These HTMRs in the monkey displayed slow adaptation properties when a constant noxious force was applied to cause deformation of the skin (Perl, 1968). AM nociceptor axons terminate in unspecialised nerve endings which penetrate the epidermal/dermal interface, at which point, they become unmyelinated (Kruger et al., 1981; Purves et al., 2001). In earlier studies in the rat and mouse, thinly myelinated AM fibres have been shown to have higher activation thresholds in comparison to thickly myelinated Aβ fibres (Koltzenburg et al., 1997; Smith et al., 2013). Furthermore, AM HTMRs have been shown here and in previous studies to encode the intensity of force stimuli, a key feature of nociceptors (Banik and Brennan, 2008).

4.5.2.2 C-mechanonociceptors (CM)

Unmyelinated C fibres have been classified according to their responses to mechanical and thermal stimuli. There are two main groups of C fibres; mechanically sensitive (CM) and mechanically insensitive C fibres. Mechanically sensitive C fibres can be further subdivided into two populations, those with low thresholds (C-LTMRs) likely to be non-nociceptors and those with high thresholds (CM), classified as nociceptors. Mechanically insensitive fibres are thermoreceptors, which respond to innocuous warm and cool temperatures. There are also mechanically insensitive fibres that behave like nociceptors as they respond to heat and capsaicin (Ringkamp et al., 2001). They can become sensitised after injury (Wooten et al., 2014). In the current study, single-unit recordings from only CM fibres were conducted. C-LTMRs were not encountered due to their anatomical distribution which primarily localises them to hairy back skin, rather than innervating the mouse paw hairy skin (Li et al., 2011). In humans, C-LTMRs are distributed widely in the forearm rather than in the hands (Vallbo et al., 1999).

Like AM nociceptors, CM fibres were activated by high mechanical thresholds and encoded the intensity of force stimuli (Koltzenburg et al., 1997). The mean number of action potentials to constant step and increasing ramp stimuli was lower in CM fibres compared to AM fibres, but it increased with the increase in force stimuli.

4.5.3 Cold sensitivity in HTMRs

4.5.3.1 Aδ-mechano-cold nociceptors (AMC)

The majority of the Aδ fibres in this study were AM nociceptors, which was in accordance with earlier studies (Koltzenburg et al., 1997; Stucky et al., 1999). Within this class of fibres,

further subdivisions can be made according to the response of AM fibres to noxious heat and cold stimuli. Whilst we did not stimulate fibres with noxious heat stimuli, we characterised and identified a population of AM fibres that were cold-sensitive (Aδ-mechanocold (AMC)). Previous studies in the glabrous skin, showed that approximately a third of all AM fibres that were studied were of the AMC classification and that these fibres displayed a wide range of threshold temperatures of activation in response to cold application (Cain et al., 2001). The present study shows a smaller proportion of AMC fibres (10 %), which is in line with single-unit recordings made previously in mouse hairy skin (Koltzenburg et al., 1997; Stucky et al., 1999). All AMC fibres showed a regular and low peak impulse discharge rate and the threshold temperatures of activation varied between fibres.

4.5.3.2 C-mechano-cold nociceptors (CMC)

Like AM nociceptors, CM fibres can be functionally subclassified according to their thermal sensitivity. In this study, CM fibres were stimulated with cold ramps and a proportion of CMC (C-mechano-cold) nociceptors were identified. We found 54 % of all CM fibres to be cold-sensitive, which is slightly higher than what has been previously reported in single-unit recordings in the mouse (Koltzenburg et al., 1997; Stucky et al., 1999). These CMC fibres varied in the number of action potentials they fired in response to the cold ramps but generally displayed a regular pattern of firing, with no bursting in accordance with earlier studies (Zimmermann et al., 2009). However, CMC fibres responded more vigorously to cold stimuli when compared to AMC fibres.

Typically C thermoreceptors are mechanically insensitive and have been reported to be spontaneously active and responsive primarily to cooling to their receptive field (Cain et al., 2001; Koltzenburg et al., 1997). They display a basal activity at resting temperatures and

respond strongly to changes in temperatures. This class of C fibres was first described in *in vitro* preparations of guinea pig cornea (Brock et al., 1998; Carr et al., 2002, 2003) and then studied more extensively in the cat *in vivo* (Bade et al., 1979; Duclaux et al., 1980; Hensel and Schäfer, 1982). The major characteristic of these fibres is to fire at ambient temperatures with burst-like discharge (Zimmermann et al., 2009). In the present study, all fibres were first identified using a mechanical search stimulus to their receptive field, therefore none of the fibres presented in this chapter were of the thermoreceptor mechano-insensitive subpopulation of C fibres, which are typically non nociceptive in function (Cain et al., 2001).

4.5.4 Summary

Fibre properties from six different classes of fibres in hairy skin of naïve C57BL/6J mice were described in this chapter. This provides a reference for comparison to functional changes in fibre properties after direct and acute application of oxaliplatin and glucose to the receptive field of individual fibres in the following chapter.

5. Effects of oxaliplatin in *in vitro* skin-nerve preparations

5.1 Introduction

The dose-limiting effects of oxaliplatin commonly affects sensory neurons. Acute oxaliplatin-induced neuropathic pain and cold-evoked distal dysaesthesias and paraesthesias are symptoms that occur after rapid onset of the drug (Deuis et al., 2013; Saif and Reardon, 2005). Other symptoms including cold-dependent muscular contractions of the extremities or the jaw can occur (Lehky et al., 2004; Wilson et al., 2002). Initially, these symptoms are transient and can be mild. However, over time, a cumulative sensory neuropathy develops and eventually causes sensory ataxia and functional impairment (Grolleau et al., 2001; Saif and Reardon, 2005). Everyday tasks such as fastening zips and buttoning shirts become difficult (Grothey et al., 2011), this tactile allodynia suggests that there is a large fibre neuropathy.

Quantitative sensory testing (QST) and nerve conduction studies in oxaliplatin-treated patients have provided information into the functional impairment of different classes of sensory neurons. The earliest changes in QST parameters are seen in the vibration detection thresholds and cold pain thresholds (Krøigård et al., 2020). This captures the initial cold hypersensitivity and tingling experienced by patients in the clinic (Barbosa et al., 2014). This is followed by deficits in mechanical detection thresholds after 6 months of oxaliplatin treatment (Barbosa et al., 2014; Krøigård et al., 2020). Some studies have also reported increased sensitivity to warm and heat detection thresholds (Barbosa et al., 2014; Binder et al., 2007). In addition, sural nerve conduction velocities and action potentials are significantly reduced over the course of treatment (Krøigård et al., 2020). This may, in part be linked to reductions in intraepidermal nerve fibre densities (IENFD) (Burakgazi et al., 2011). However, it is clear that the acute effects of systemic oxaliplatin result in increased hypersensitivities at

the extremities (Deuis et al., 2013; Grolleau et al., 2001; Saif and Reardon, 2005). Therefore, it is prudent to study the effects of the compound at the peripheral nerve terminals.

Direct application of oxaliplatin to cultured DRG neurons isolated from naïve mice and DRG neurons isolated from oxaliplatin-treated mice had a limited effect on cold sensitivity excitability at level of the DRG (Chapter 3). Oxaliplatin directly interacts with sensory afferents and has been shown to preferentially modulate the activity of A fibres over C fibres (Forstenpointner et al., 2018; Sittl et al., 2012). However, no studies have reported which subpopulations of fibres are modulated by oxaliplatin directly. In doing so, it may be possible to facilitate identification of both a cellular and molecular basis for oxaliplatin-induced cold hypersensitivity and paraesthesias. The *ex vivo* skin-nerve preparation allows the receptive fields of individual units to be directly stimulated by electrical, mechanical and thermal stimuli in a precise, controlled manner, before and after drug application. This allows the experimenter to study the function of sensory afferents in their anatomical context independently of the CNS and before and after chemical applications.

5.2 Aims

In this chapter, we aim to investigate the effects of direct application of oxaliplatin to the receptive fields of single fibres in naïve skin-nerve preparations. We studied the functional properties of six classes of fibres to mechanical and cold stimuli before and after oxaliplatin and vehicle (5 % glucose) application. In addition, we investigated how the properties of individual fibres and multi-units were affected by oxaliplatin treatment *in vivo*.

5.3 Methods

5.3.1 Experimental protocol

The experimental set-up was the same as previously described (Chapter 4). Oxaliplatin (product Y0000271, Sigma-Aldrich) was dissolved in 5 % glucose solution (278 mOsm/L, B. Braun). The vehicle used was 5 % glucose solution. The protocol was created to allow comparison of excitation properties of single fibres to mechanical and thermal stimuli before and after drug application, using either 600 µM oxaliplatin or vehicle. Oxaliplatin solution was kept at room temperature with carbogen bubbling through it before application. Drugs were applied into the metal ring which sealed off the receptive field for cold stimulations. The bath solution was removed, and the drug solutions were applied until the ring was filled completely. Drugs were incubated for 20-minutes. The drug was removed at the end of the incubation period, before challenging the receptive fields with cold ramps.

5.3.2 Mechanical and cold stimulation

The first cold ramp was applied after the initial mechanical characterisation of the unit and used as a control (conducted in SIF) measurement. This was followed by a 20-minute incubation period with either oxaliplatin (600 µM) or its vehicle (5 % glucose). The drug was removed at the end of the incubation period from the metal ring and was superfused with SIF and challenged with the first cold ramp. The next cold ramp after drug application was applied after a two-minute interval (schematic 1). Mechanical stimuli were applied again after these two cold stimuli following drug application.

5.3.3 Recordings in preparations taken from treated animals

In a separate set of experiments, skin-nerve preparations were taken from mice that were treated with a single systemic dose of oxaliplatin (6 mg/kg) or vehicle (5 % glucose) as described in Chapter 2. Preparations were taken after adult male and female mice were culled on days 1, 2 and 4 after oxaliplatin injection. The proportion of cold-sensitive fibres were compared between preparations from oxaliplatin- and glucose-treated mice (day 4 only). In all experiments, a cold search stimulus (ice cold SIF) was used to locate cold-sensitive fibres rather than using the traditional mechanical search probe. This enabled comparisons in the proportion of cold-sensitive fibres to be made between treatment groups. Once fibres were identified as cold-sensitive using the ice-cold SIF, cold ramps were applied. Two cold ramps were applied in these experiments (schematic 2). Fibres were later characterised for the electrical latencies and mechanical thresholds (where possible). The single-unit recordings were all classified as A or C fibres based on their conduction velocities after their responses to cold ramps were recorded. It was only possible in some cases for full mechanical characterisation to be completed. In preparations from treated mice, only multi-unit recordings were possible in some cases due to the generally increased spontaneous level of activity in preparations.

5.3.4 Statistical Analysis

The data was analysed to assess the differences in the total number of action potentials discharged, peak firing frequency and thresholds for mechanical and cold stimulation periods before and after drug applications. Normality tests were performed on the data to check the distribution of the data and further statistical analyses were conducted based on the outcome. If data was normally distributed at all points, a paired *t* test was used to compare

responses before and after drug application. Unpaired *t* tests were used to compare data that was normally distributed between treatment groups. If the data failed to pass normality tests at any point (before or after), then a Wilcoxon test was performed within treatment groups and a Mann-Whitney *U* test for non-parametric tests between treatment groups. Fisher's exact test, two-sided was conducted to compare population data before and after oxaliplatin and vehicle (5 % glucose) treatment.

Naïve preparations

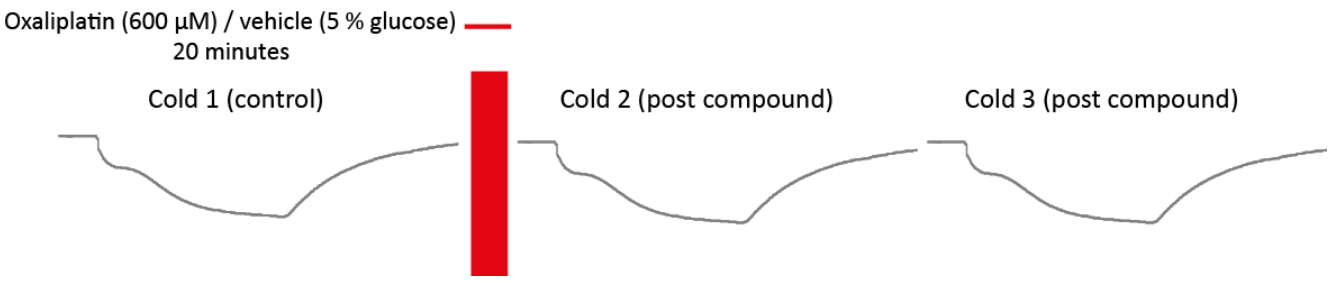

Schematic 1 Experimental protocol for cold stimulations applied in naïve skin-nerve preparations.

Treated preparations

Schematic 2 Experimental protocol for cold stimulations applied in skin-nerve preparations taken from vehicle- and oxaliplatin-treated mice.

5.4 Results

5.4.1 Properties of fibres prior to treatment in naïve preparations

All mechanical thresholds were recorded before the application of either oxaliplatin (600 µM) or vehicle (5 % glucose) to the receptive field of single-units. The consistent properties of fibres indicate that these studies are unlikely to be unduly influenced by differences in the quality or characteristics of the units allocated to treatment with vehicle or oxaliplatin. However, 6/10 CMC fibres used in experiments with oxaliplatin treatment had mechanical thresholds between 4.5 - 8.5 g (Figure 5-1 B), which was significantly higher (unpaired *t* test, *P* = 0.0047, n = 10 fibres) than mechanical thresholds in fibres which were later treated with glucose (Table 5-1).

Table 5-1 Single-unit recordings made in naïve skin-nerve preparations treated with acute and direct application of oxaliplatin (600 µM) or vehicle (5 % glucose) at the receptive field

Fibre class	Fibre Type	Treatment	n	Mean Mechanical threshold (g)	SEM	P value	Mean CV (m/s)	SEM	P value
Aβ	RA	Glucose	9	0.30	0.07	*P* = 0.518	13.80	1.12	*P* = 0.735
		Oxaliplatin	7	0.29	0.11		16.93	1.67	
	SA	Glucose	10	0.40	0.06	*P* = 0.253	12.08	0.62	*P* = 0.735
		Oxaliplatin	12	0.52	0.09		15.80	4.28	
Aδ	DH	Glucose	4	0.26	0.11	*P* = 0.806	6.19	1.16	*P* = 0.601
		Oxaliplatin	3	0.29	0.14		4.83	1.24	
	AM	Glucose	10	3.18	1.04	*P* = 0.661	4.24	0.71	*P* = 0.923
		Oxaliplatin	10	3.33	0.78		4.34	0.74	
C	CM	Glucose	7	3.00	0.63	*P* = 0.404	0.53	0.17	*P* = 0.984
		Oxaliplatin	10	4.27	1.14		0.43	0.10	
	CMC	Glucose	10	1.43	0.34	*P* = 0.0047	0.37	0.02	*P* = 0.669
		Oxaliplatin	10	4.65	0.94		0.44	0.04	

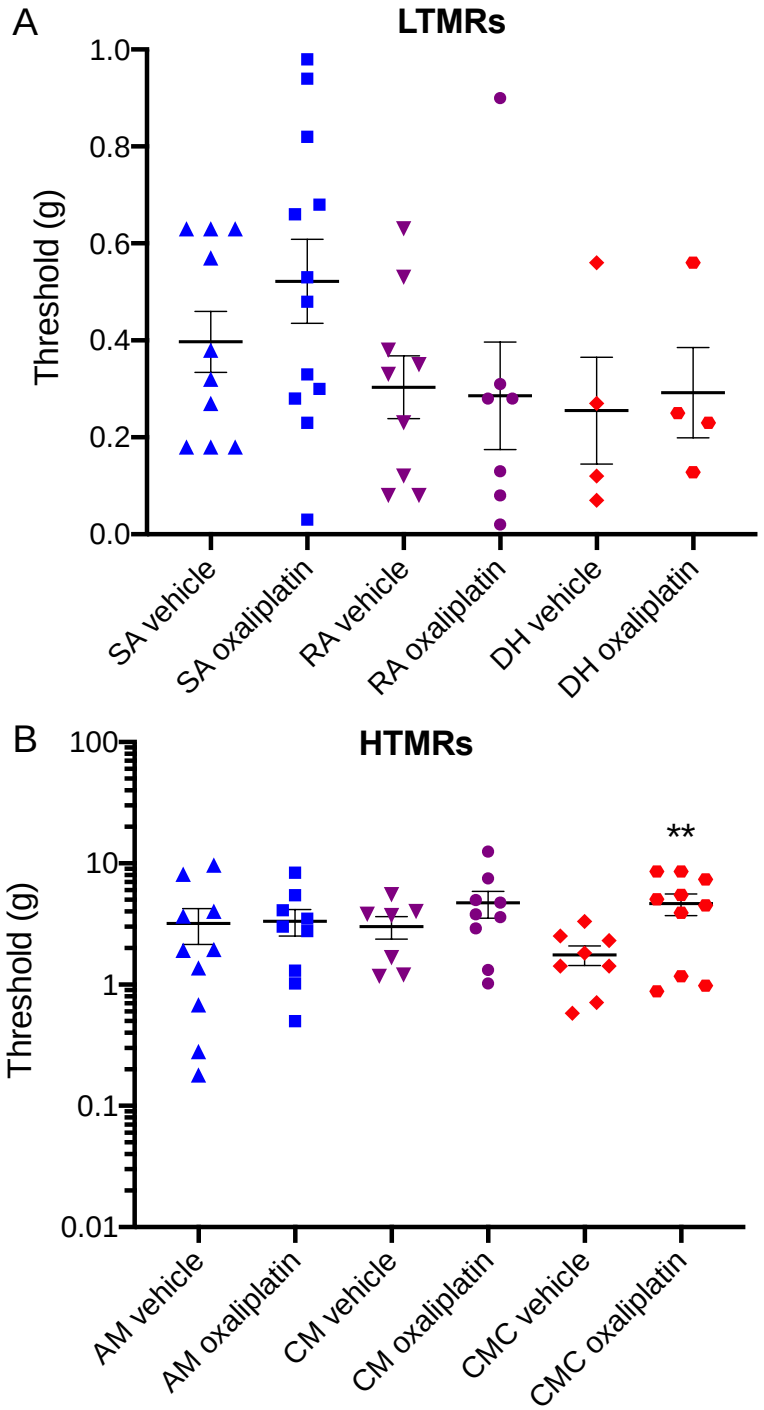

Figure 5-1 Activation threshold of mechanically sensitive hairy-skin nerve fibres in naïve C57BL/6J mice before treatment with vehicle (5 % glucose) and oxaliplatin.

A) Low threshold mechano-sensitive receptors (LTMRs): DH, SA, RA fibres all have a similar and low mechanical threshold of activation. B) High threshold mechano-sensitive receptors (HTMRs): AM, CM and CMC fibres are all nociceptors with a higher mechanical threshold of activation compared to LTMRs. CMC fibres that went on to be treated with oxaliplatin had a greater mechanical threshold at the start of experiments compared to vehicle counterparts (unpaired *t* test, $P = 0.0047$, n = 10 fibres). All data are presented as mean ± S.E.M.

5.4.2 Effect of oxaliplatin on A-LTMRs

5.4.2.1 DH-LTMRs

The receptive fields of DH units were incubated with oxaliplatin (600 µM) for 20 minutes. Notably, these low threshold mechanoreceptors were not robust in withstanding the long protocol (> 20 minutes) and were therefore difficult to locate using a mechanical search stimulus following vehicle and oxaliplatin treatment. For this reason, comparisons were only made between and within treatment groups on fibres that remained responsive to mechanical stimulations after treatment. This significantly reduces the number of viable DH fibres (n = 3 - 4 fibres) in these studies.

The number of action potentials elicited by mechanical stimulation with 4 or 15 g did not change after oxaliplatin (Figure 5-2 A, C), neither compared to vehicle (4 g: vehicle 4 ± 1 APs; oxaliplatin 2 ± 1 APs, 15g: vehicle 5 ± 2 APs; oxaliplatin 4 ± 1 APs) nor naïve response, before incubation (4 g: before oxaliplatin 4 ± 1 APs; after oxaliplatin 2 ± 1 APs, 15 g: before oxaliplatin 7 ± 2 APs; after oxaliplatin 4 ± 1 APs). However, the very small number of DH units studied here makes these conclusions uncertain.

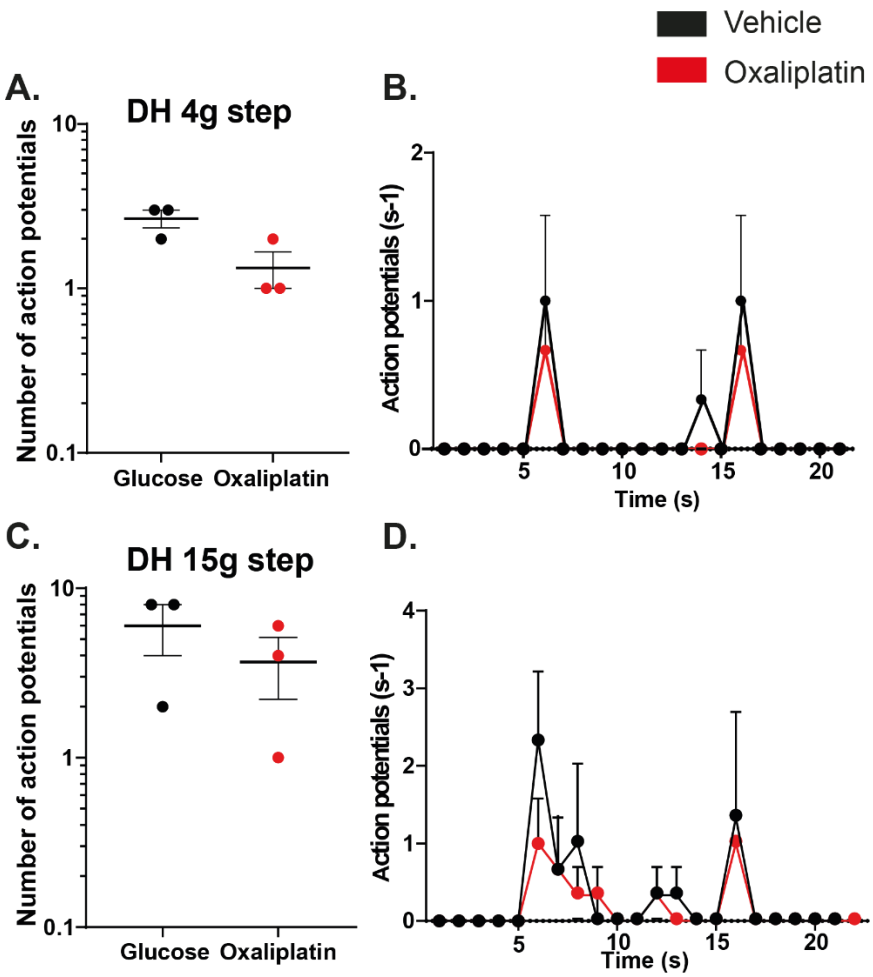

Figure 5-2 Oxaliplatin does not change adaptation in DH fibres.

A) Oxaliplatin did not alter the number of action potentials during 4 g force steps when compared to vehicle. B) No significant difference seen in the average impulse discharge rates of DH fibres treated with oxaliplatin (red circles) compared to vehicle (black circles). C) Oxaliplatin did not alter the number of action potentials during 15 g force steps when compared to vehicle. D) Both vehicle and oxaliplatin treatment altered the adaptation of DH fibres to 15 g force step, which is likely to indicate that the force was too high for these fibres.

5.4.2.2 RA-LTMRs

Oxaliplatin altered the responses of rapidly adapting (RA) fibres to suprathreshold 4 g and 15 g mechanical forces (Figure 5-3 A, C). Oxaliplatin did not change the number of action potentials discharged during a 4 g force step when compared to vehicle treatment (Figure 5-3 A). In contrast, oxaliplatin treatment increased the total number of action potentials during a 15 g mechanical stimulation when compared to vehicle treatment (vehicle 5 ± 1 APs; oxaliplatin 149 ± 67 APs, unpaired *t* test, $P = 0.026$, n = 7 - 9 fibres) (Figure 5-3 C).

Typically, RA fibres respond to mechanical forces with an on-off pattern of firing (Chapter 4, Figure 4-9). However, oxaliplatin changed the adaptation properties in a subpopulation of RA fibres, particularly during 15 g force steps (Figure 5-3 D, 5-4). In these fibres, the response to mechanical stimulation appeared very similar to that typical of SA fibres and outlasted the stimulation period (Figure 5-4). These changes were also seen during 4 g force steps, where RA fibres discharged impulses throughout and after the mechanical stimulation period (Figure 5-3 B). However, this was more dramatic during the 15 g force step (Figure 5-3 D, 5-4).

Oxaliplatin also increased the total number of action potentials compared to before treatment during the 15 g force step. Among 7 RA fibres, 4 changed to the SA appearance, while 3 did not. In contrast, oxaliplatin treatment had little effect on the number of action potentials discharged during a 4 g force step when compared to before treatment (before oxaliplatin 5 ± 1 APs; after oxaliplatin 3 ± 1 APs). Overall, acute oxaliplatin treatment affected the adaptation responses of RA fibres to mechanical forces, most dramatically at 15 g forces. These changes likely to be important clinically and may provide a cellular basis for oxaliplatin-induced paraesthesias.

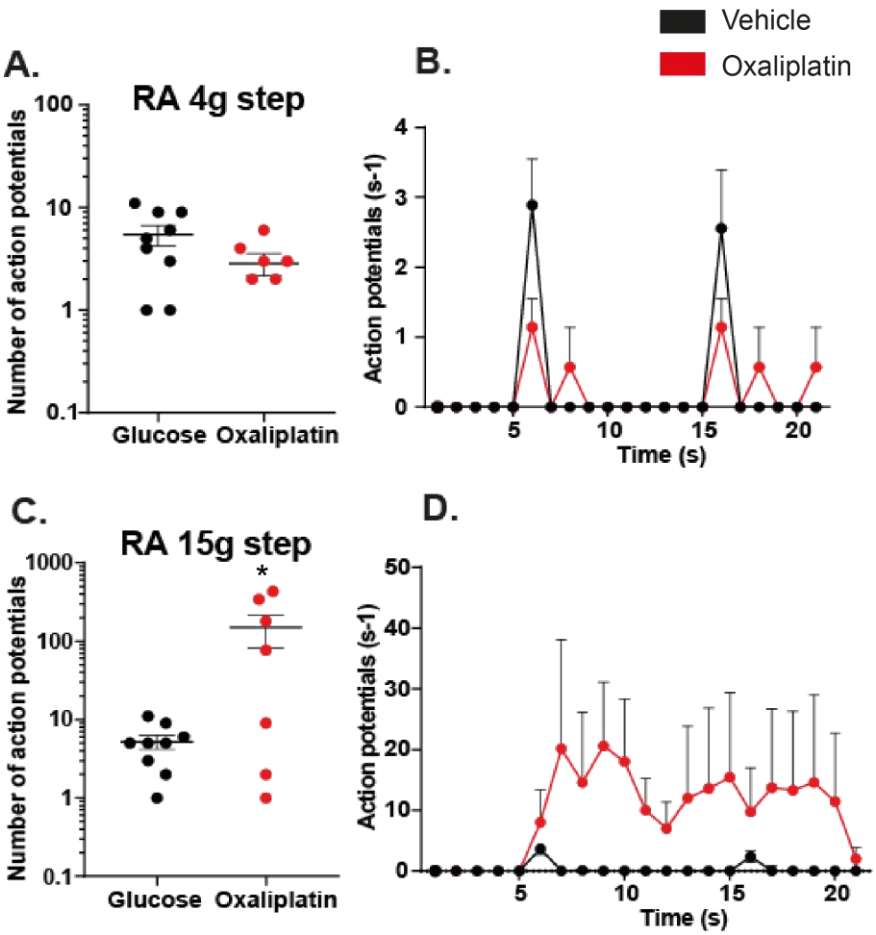

Figure 5-3 Oxaliplatin disrupts adaptation in some RA fibres.

A) Oxaliplatin did not alter the number of action potentials during 4 g force steps when compared to vehicle. B) No significant difference seen in the average impulse discharge rates of RA fibres treated with oxaliplatin (red circles) compared to vehicle (black circles). However, some fibres displayed activity outlasting the stimulation period. C) Oxaliplatin (red circles) significantly increased the number of action potentials discharged during 15 g force step compared to vehicle treatment (black circles). D) Oxaliplatin (red circles) dramatically altered the impulse discharge rate and pattern of firing in RA fibres compared to vehicle (black circles). Some RA fibres displayed activity outlasting the stimulation period.

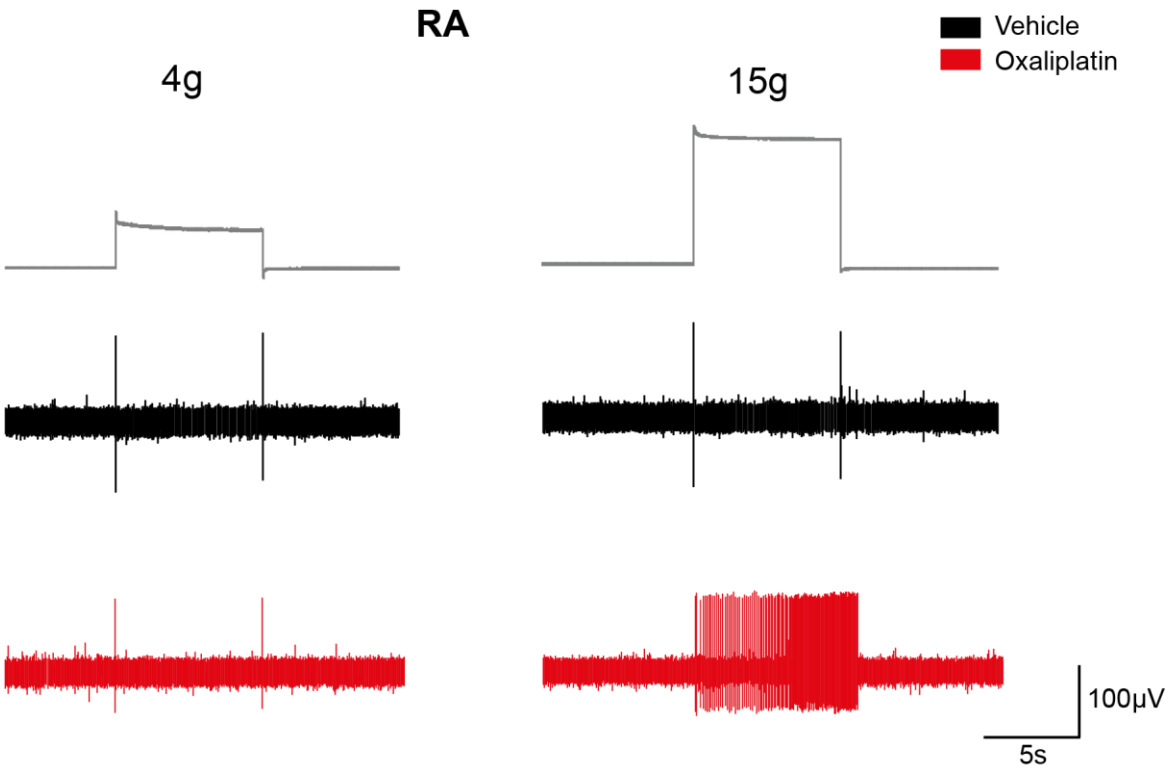

Figure 5-4 Oxaliplatin changes the firing pattern of a subset of RA fibres to noxious stimuli.

Example RA fibre responses to 4 g and 15 g force steps after vehicle (black) and oxaliplatin (red) application to the receptive field of single-units. Oxaliplatin changed the adaptation properties of some RA fibres during high forces, making them respond like SA fibres as shown above.

5.4.2.3 SA-LTMRs

Notably, oxaliplatin sensitised slowly adapting (SA) fibres evoked by both 4 g and 15 g force steps (Figure 5-5 A, C). Oxaliplatin significantly increased the total number of action potentials discharged during a 4 g step when compared to vehicle treatment (vehicle 29 ± 6 APs; oxaliplatin 166 ± 51 APs, unpaired *t* test, $P = 0.025$, n = 10 - 12 fibres) (Figure 5-5 A). Oxaliplatin treatment did not significantly increase the number of action potentials during a 15 g force step when compared to vehicle (vehicle 53 ± 19 APs; oxaliplatin 330 ± 129 APs, n = 10 - 12 fibres) (Figure 5-5 C). The rate of impulse discharge was dramatically increased during 4 g and 15 g forces after oxaliplatin treatment when compared to vehicle treatment (Figure 5-5 B, 5-5 D).

In contrast, oxaliplatin did not significantly affect the impulse discharges evoked during 4 g and 15 g force steps when compared to naïve responses, before treatment. Overall, oxaliplatin sensitised SA fibre responses during 4 g force application periods which may reflect the mechanical hypersensitivity reported in the clinic.

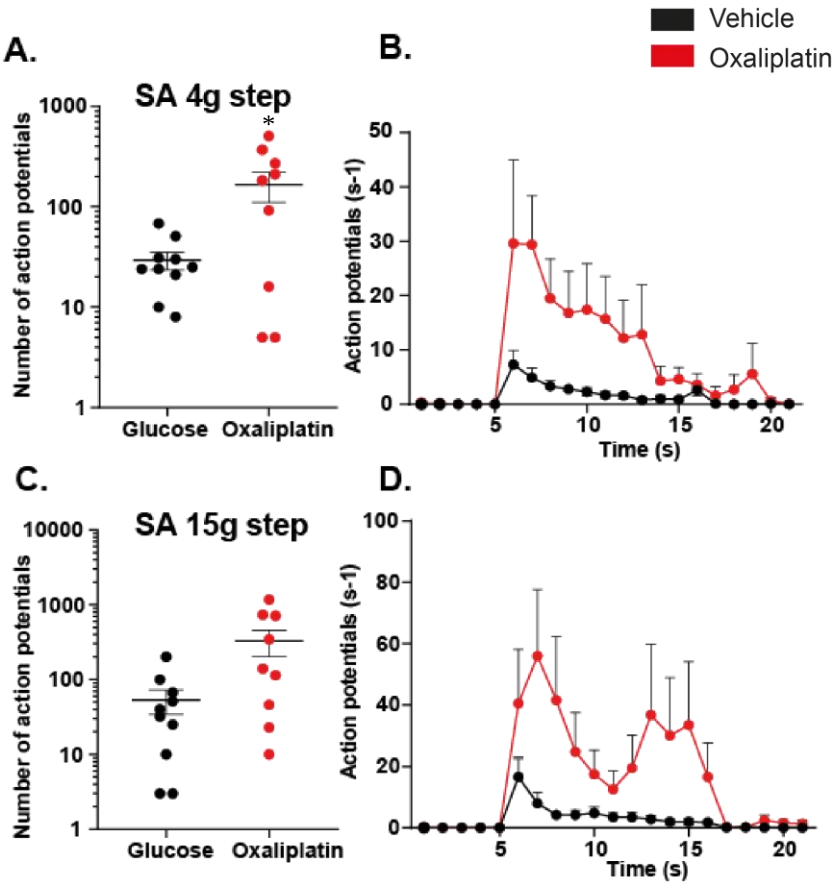

Figure 5-5 Oxaliplatin sensitised SA fibre responses to mechanical stimulation.

A) Oxaliplatin (red circles) significantly increased the number of action potentials discharged during 4 g force steps when compared to vehicle (black circles). B) Oxaliplatin (red circles) markedly increased the impulse discharge rate during the mechanical stimulation period when compared to vehicle treatment (black circles). Some fibres displayed activity outlasting the stimulation period. C) Oxaliplatin did not alter the number of action potentials discharged during 15 g force step when compared to vehicle treatment (black circles). D) Oxaliplatin (red circles) dramatically increased the impulse discharge rate compared to vehicle (black circles).

5.4.3 Oxaliplatin sensitised AM nociceptors to innocuous mechanical forces

Oxaliplatin significantly increased the number of action potentials in AM fibres elicited by a 4 g force step compared to vehicle (vehicle 20 ± 7 APs; oxaliplatin 308 ± 137 APs, Mann-Whitney *U* test, *P* = 0.0014, n = 10 fibres) (Figure 5-6 A, 5-7 A). On average, the impulse discharge rate was increased by at least 10-fold in AM fibres exposed to oxaliplatin treatment compared to those that were treated with vehicle (Figure 5-6 B). Some fibres also displayed activity outlasting the stimulation period. This result demonstrated a marked sensitisation of AM fibre responses to mechanical stimulation at low forces.

Interestingly, oxaliplatin did not alter the impulse discharge rate at higher mechanical step forces overall (Figure 5-6 C). Only a subset of AM fibres showed increased activity at these forces. There was ~3-fold increase in the impulse discharge rate during the 15 g step (Figure 5-6 D). Some fibres displayed activity outlasting the stimulation period. In addition, oxaliplatin did not alter the impulse discharge number during a 20 g ramp when compared to the vehicle treatment (Figure 5-6 E). However, the impulse discharge rate was increased, although not dramatically (Figure 5-6 F).

Oxaliplatin also significantly increased the impulse discharge number in AM fibres during 4 g steps when compared to naïve responses, before treatment (before oxaliplatin 23 ± 6 APs; after oxaliplatin 308 ± 137 APs, Wilcoxon test, *P* = 0.008, n = 10 fibres) (Figure 5-7 A). In addition, oxaliplatin significantly increased the total number of action potentials during a 15 g step when compared to baseline (before oxaliplatin 66 ± 17 APs; after oxaliplatin 239 ± 102 APs, Wilcoxon test, *P* = 0.037, n = 10 fibres) (Figure 5-7 A). Oxaliplatin did not, however, affect the number of impulses discharged during 20 g ramps when compared to baseline (Figure 5-

7 A). AM nociceptors were sensitised to lower mechanical forces, indicating a basis for mechanical hyperalgesia. The responses to higher mechanical forces affected a subset of AM fibres and saturated the responses in other fibres, showing no alteration overall. It is clear from these results that oxaliplatin affected different subsets of AM fibres in different ways.

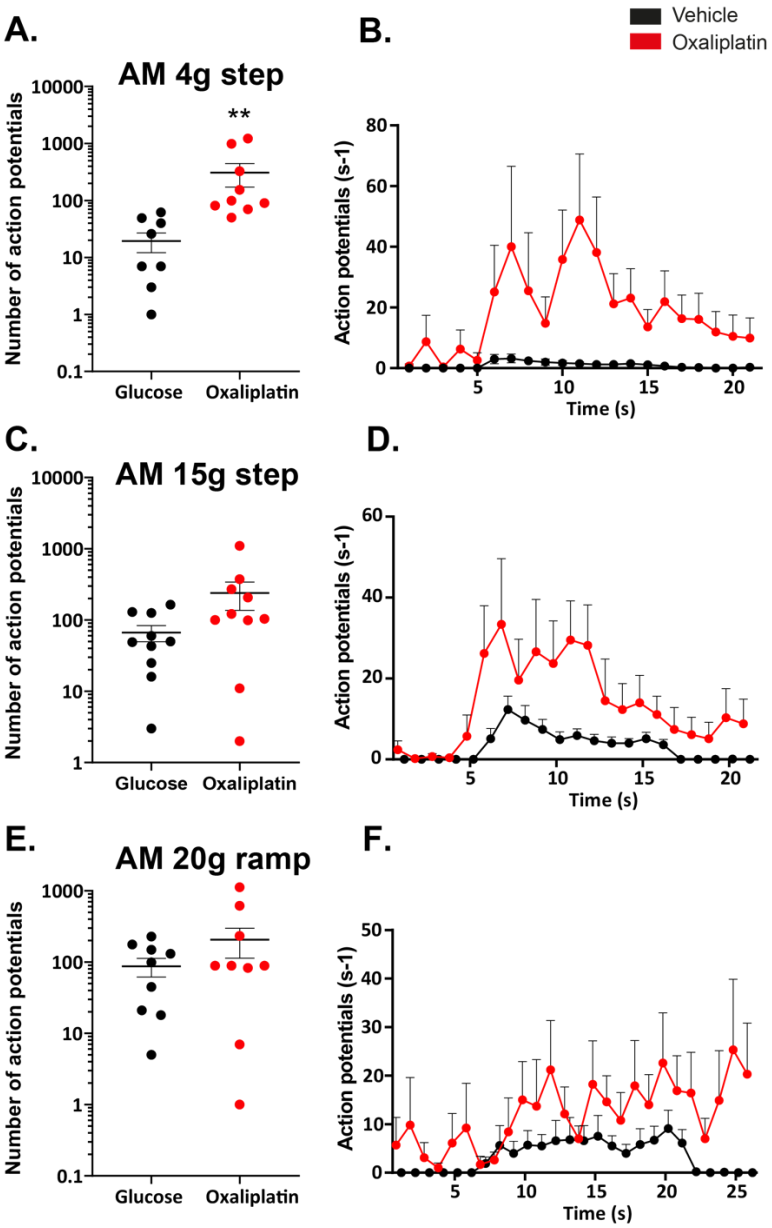

Figure 5-6 Oxaliplatin sensitised AM fibre responses to innocuous mechanical forces.

A) Oxaliplatin (red circles) significantly increased the number of action potentials discharged during 4 g force steps when compared to vehicle (black circles). B) Oxaliplatin (red circles) markedly increased the impulse discharge rate during the mechanical stimulation period when compared to vehicle treatment (black circles). In some fibres, activity outlasted the stimulation period. C) Oxaliplatin did not alter the number of action potentials during 15 g force steps when compared to vehicle. D) Oxaliplatin (red circles) dramatically increased the impulse discharge rate compared to vehicle (black circles). Some fibres displayed activity outlasting the stimulation period. E) Oxaliplatin did not alter the number of action potentials during a 20 g ramp when compared to vehicle (black circles). F) Oxaliplatin (red circles) did not alter the impulse discharge rate dramatically when compared to vehicle (black circles).

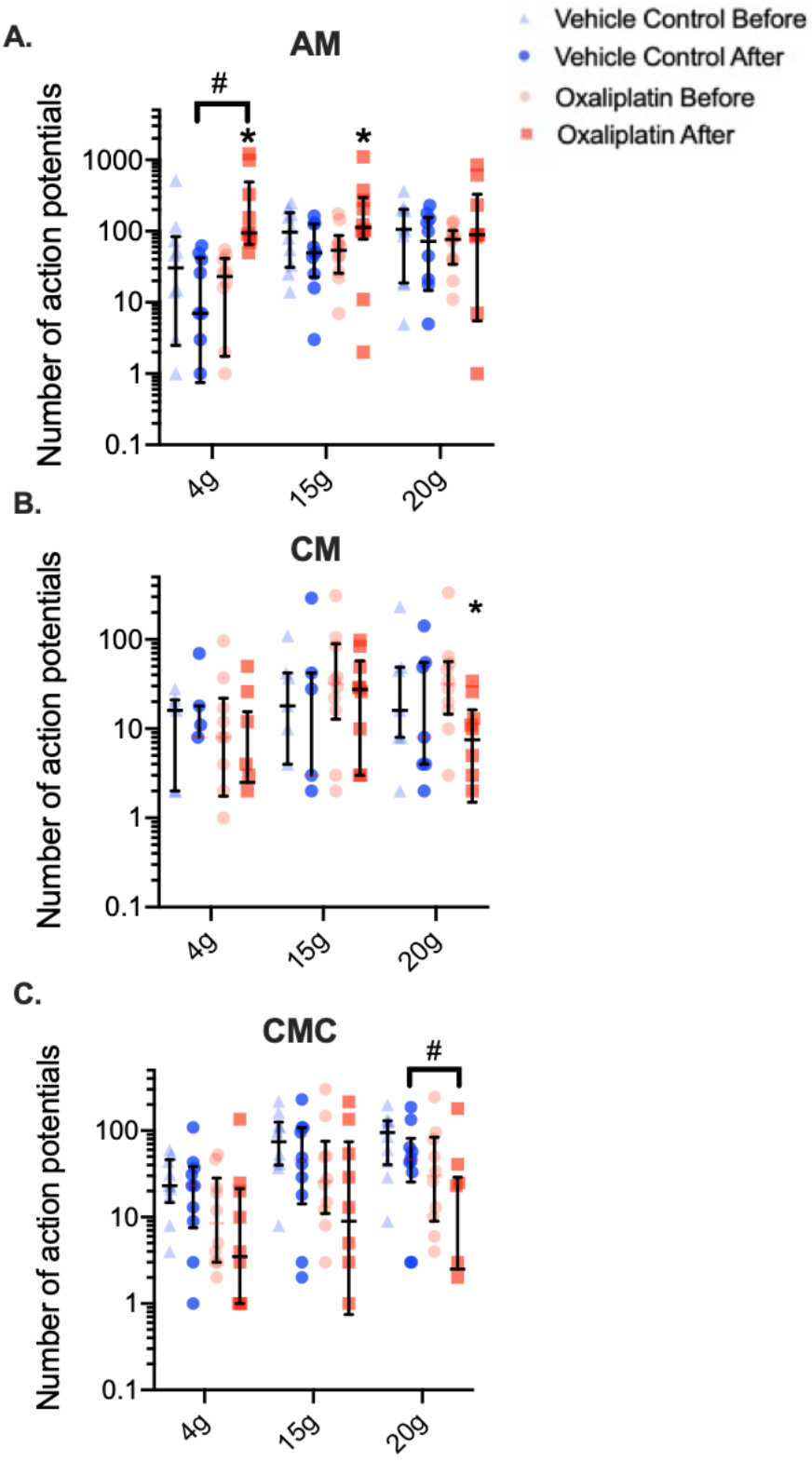
A.
AM
Vehicle Control Before
Vehicle Control After
Oxaliplatin Before
Oxaliplatin After
Number of action potentials
1000
100
10
1
0.1
#
*
*
4g
15g
20g
B.
CM
Number of action potentials
100
10
1
0.1
*
4g
15g
20g
C.
CMC
Number of action potentials
100
10
1
0.1
#
4g
15g
20g

Figure 5-7 Oxaliplatin increases action potentials discharged in AM-HTMRs, but has opposite effects in C-HTMR fibres.

A) Oxaliplatin (pink squares) significantly increased (denoted by #) the number of action potentials discharged in AM fibres during 4 g force steps when compared to vehicle (dark blue circles). In addition, oxaliplatin (pink squares) significantly increased (denoted by *) the impulse discharge number when compared to baseline (light pink circles) during 4 g and 15 g force steps. B) Oxaliplatin (pink squares) caused a significant reduction (denoted by *) in the number of action potentials discharged during 20 g ramps in CM fibres when compared to baseline (light pink circles). C) Oxaliplatin (pink squares) caused a significant reduction (denoted by #) in the impulse discharge number during 20 g ramps in CMC fibres when compared to vehicle (dark blue circles).

5.4.4 Oxaliplatin reduced the encoding properties in C fibres

C fibres were stimulated mechanically in the same way as A fibres using a 10 second 4 g and 15 g force step. All nociceptors (AM and C fibres) were additionally challenged with a 20 g ramp mechanical stimulus to compare encoding properties to increasing forces between treatment groups.

In CM fibres, oxaliplatin significantly decreased the total number of action potentials discharged in response to a 20 g ramp compared to before treatment (before oxaliplatin 61 ± 31 APs; after oxaliplatin 10 ± 4 APs, Wilcoxon test, P = 0.019, n = 10 fibres) (Figure 5-7 B). Oxaliplatin did not significantly alter the number of impulses discharged during 4 g and 15 g steps when compared to naïve responses, before treatment (Figure 5-7 B). However, it appears that there are two subsets of CM fibres, some which do show a reduction in their activity after oxaliplatin treatment, and others which remain unaffected. In addition, there were no differences in the number of action potentials discharged between oxaliplatin and vehicle treatments at any of the mechanical forces (Figure 5-7 B).

Oxaliplatin did not alter the impulse discharges evoked by any of the mechanical stimuli in CMC fibres when compared to naïve responses, before treatment (Figure 5-6 C). However, oxaliplatin significantly reduced the total number of action potentials discharged during the 20 g ramp when compared to vehicle treatment (vehicle 60 ± 18 APs; oxaliplatin 28 ± 18 APs, Mann-Whitney U test, P = 0.011, n = 10 fibres) (Figure 5-7 C). Oxaliplatin did not change the number of action potentials discharged during 4 g and 15 g steps compared to vehicle treatment (Figure 5-7 C). This indicates that small nociceptive fibres were less affected by acute oxaliplatin treatment, which is reflected in the clinical symptom profile.

5.4.5 Oxaliplatin-induced post-stimulus discharges seen in A fibres

We observed that some classes of A fibres displayed activity which outlasted the mechanical stimulation after oxaliplatin treatment. This was predominantly seen in recordings for AM, SA and RA fibres. We analysed the number of fibres that showed post-stimulus discharges in the oxaliplatin treatment groups and compared them to vehicle treatment. The number of AM fibres that continued to discharge impulses after the end of the mechanical stimulation period was markedly increased in response to 4 g force after oxaliplatin when compared to vehicle treatment (vehicle 2/10 fibres; oxaliplatin 8/10 fibres, Fisher's exact test, two-sided, $P = 0.023$, n = 10 fibres). An example trace is demonstrated below (Figure 5-8). Oxaliplatin treatment did not significantly increase the number of AM fibres that displayed post-stimulus discharges at 15 g step and 20 g ramp forces.

Oxaliplatin significantly increased the number of RA fibres which displayed post-stimulus discharges after the 15 g force step when compared to vehicle treatment (vehicle 0/9 fibres; oxaliplatin 4/7 fibres, Fisher's exact test, two-sided, $P = 0.019$, n = 7 - 9 fibres). This, however, was not the case following the 4 g force step (Figure 5-9). Furthermore, some SA fibres exhibited impulse discharges outside of mechanical stimulation periods. However, this was not significant at either 4 g or 15 g forces. An example of an SA fibre exhibiting high frequency firing after the ending of 4 g and 15 g forces is shown (Figure 5-10).

Overall, the post-stimulus discharges lasted a minimum of a few seconds and up to a few minutes after mechanical stimulation. At times, there were fibres in the background that continued to discharge impulses for the remainder of the recording. Interestingly, post stimulus discharges were often displayed as action potential bursts, suggesting changes to the adaptation properties of fibres. However, there were populations of AM, SA and RA fibres

that were also unchanged after oxaliplatin treatment. This may be explained by the functional classes consisting of fibres with distinct structural or molecular properties.

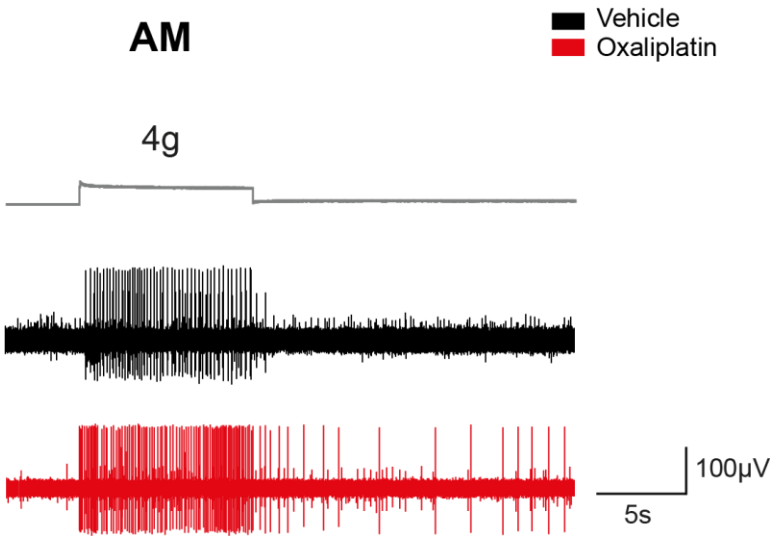

Figure 5-8 Oxaliplatin-induced post-stimulus impulse activity in AM fibres.

Example AM fibre responses to 4 g force steps after vehicle (black) or oxaliplatin (red) direct application to the receptive field of single-units. Oxaliplatin changed the adaptation properties of some AM fibres. Action potentials were discharged outside of the mechanical stimulation period which lasted for seconds.

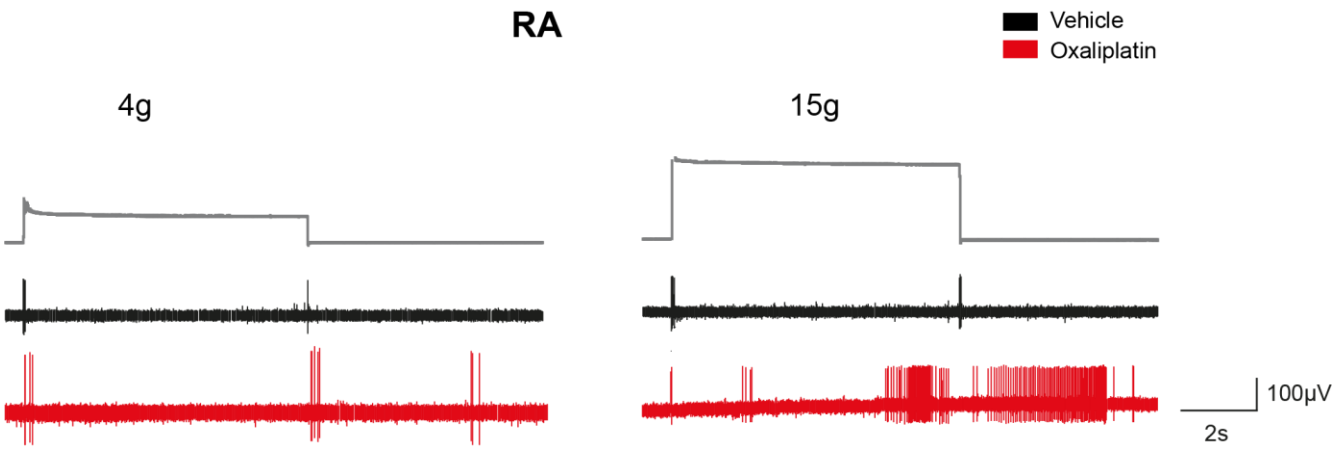

Figure 5-9 Oxaliplatin-induced post-stimulus discharges in RA fibres.

Example RA fibre responses to 4 g and 15 g force steps after vehicle (black) or oxaliplatin (red) direct application to the receptive field of single-units. Oxaliplatin changed the adaptation properties of some RA fibres very dramatically. Action potentials were discharged outside of the mechanical stimulation period which lasted for seconds. RA fibres also displayed action potential bursts at higher mechanical forces (15 g) as shown.

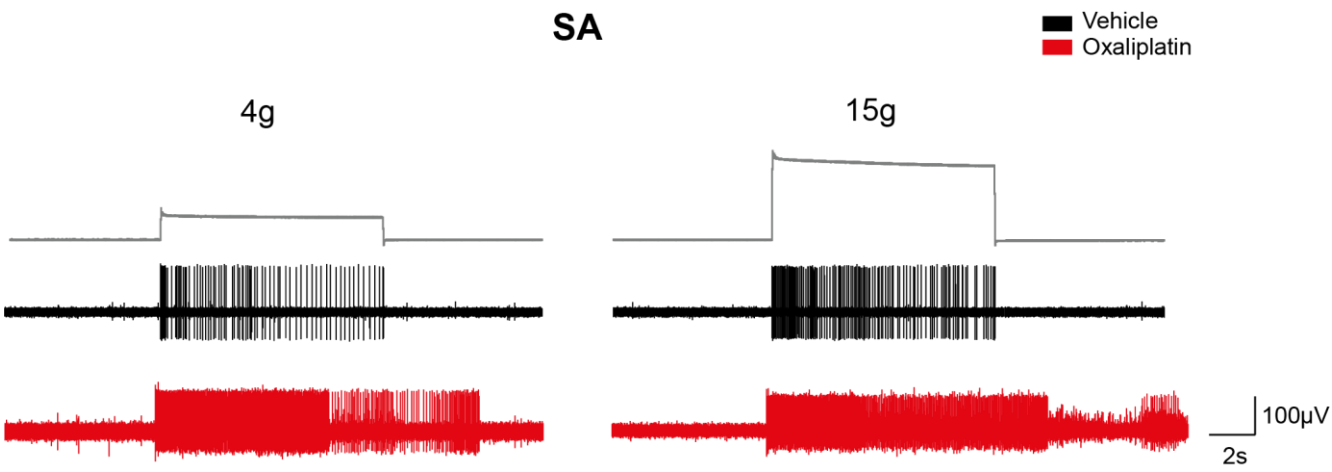

Figure 5-10 Oxaliplatin-induced post-stimulus discharges in SA fibres.

Example SA fibre responses to 4 g and 15 g force steps after vehicle (black) or oxaliplatin (red) application to the receptive field of single-units. Oxaliplatin changed the adaptation properties of some SA fibres very dramatically. Action potentials were discharged outside of the mechanical stimulation period which lasted for seconds to minutes. At both 4 g and 15 g force steps, SA fibres displayed action potential bursts.

5.4.6 Paradoxical oxaliplatin-induced desensitisation to mechanical stimuli

Paradoxically, oxaliplatin caused desensitisation to responses during mechanical stimuli in some fibres. This was seen in two ways; either by a reduction in the total number of action potentials during the stimulation period or by no response to any stimuli after oxaliplatin treatment. In order to determine whether this was a unique phenomenon resulting from oxaliplatin treatment to the receptive field of single-units rather than a time dependent effect, we compared the number of fibres that were 'silenced' after oxaliplatin treatment with those that were 'silenced' after vehicle treatment.

Oxaliplatin significantly increased the number of silenced AM fibres when compared to vehicle treatment (vehicle 0/10 fibres; oxaliplatin 12/22 fibres, Fisher's exact test, two-sided, $P = 0.004$). This effect was also marked in RA fibres where there was a significant increase in the number of silenced fibres after oxaliplatin treatment compared with vehicle treatment (vehicle 1/10 fibres; oxaliplatin 9/16 fibres, Fisher's exact test, two-sided, $P = 0.037$). For DH fibres, 7/10 fibres were no longer responsive to either mechanical or cold stimuli after oxaliplatin treatment compared to 1/5 fibres after vehicle treatment, although not significant due to the low numbers of DH fibres recorded. SA single-unit recordings were more robust than other A fibres after oxaliplatin treatment as there was a minimal degree of desensitisation when compared to vehicle counterparts (vehicle 0/10 fibres; oxaliplatin 1/13 fibres).

Interestingly, both CM and CMC fibres display a reduction in the total number of action potentials discharged in response to a 20 g mechanical stimulus but did not become silenced completely after oxaliplatin treatment.

5.4.7 Novel cold sensitivity seen in all A fibre classes after oxaliplatin application

Acute application of oxaliplatin to the receptive field of single fibres made these normally temperature insensitive fibres cold activated in all subpopulations of A fibres. Oxaliplatin often induced action potential bursts in A fibres both during and after cold stimulation. We investigated this abnormal cold-sensitivity further by challenging receptive fields with two consecutive cold ramps (~31-7 °C) after oxaliplatin treatment (referred to as oxaliplatin 1 and 2). The gain of cold responsiveness in normally cold-insensitive fibres may provide insights into the neuronal basis of oxaliplatin-induced cold-evoked paraesthesias and dysaesthesias.

5.4.7.1 AM fibres

In AM fibre recordings, oxaliplatin significantly increased the number of cold-sensitive fibres seen during the first (oxaliplatin 1: 5/10 fibres, vehicle: 0/10 fibres, Fisher's exact test, two-sided, $P = 0.021$, n = 10 fibres) and second cold ramps (oxaliplatin 2: 7/10 fibres, vehicle: 0/10 fibres, Fisher's exact test, two-sided, $P = 0.0006$, n = 10 fibres) compared to control. The total number of action potentials discharged during the second cold ramp after oxaliplatin treatment was significantly greater than control (control: 0 APs; oxaliplatin 2: 1801 ± 1004 APs, Wilcoxon test, $P = 0.016$, n = 7 fibres) (Figure 5-11 A). In addition, oxaliplatin significantly increased the number of action potentials discharged during the second cold ramp compared to the first (oxaliplatin 1: 789 ± 473 APs; oxaliplatin 2: 1801 ± 1004 APs, Wilcoxon test, $P = 0.031$, n = 5 - 7 fibres). Oxaliplatin also increased the peak discharge frequency during the second cold ramp after treatment compared to control (control 0 APs; oxaliplatin 2: 106 ± 39 APs, Wilcoxon test, $P = 0.016$, n = 7 fibres) (Figure 5-11 B). Often, oxaliplatin treatment induced cold-evoked action potential bursts (trace in Figure 5-12). In AM fibre recordings,

there were multiple fibres that exhibited action potential bursts (Figure 5-13 A). This occurred during cold ramps and outlasted stimulation periods.

Furthermore, oxaliplatin significantly increased the average threshold temperature for AM fibres during both cold ramps compared to control (control: n/a; oxaliplatin 1: 14.0 ± 4.4 °C; oxaliplatin 2: 26.4 ± 1.2 °C, paired *t* test, $P = 0.018$ and $P < 0.0001$ respectively, n = 5 -7 fibres). The average threshold temperature was also significantly shifted towards warmer temperatures between cold ramps after oxaliplatin treatment (oxaliplatin 1: 14.0 ± 4.4 °C; oxaliplatin 2: 26.4 ± 1.2 °C, paired *t* test, $P = 0.042$, n = 5 -7 fibres) (Figure 5-11 C, 5-12). We demonstrated that acute oxaliplatin treatment to the receptive fields of AM single-units is sufficient to sensitise these fibres to cold ramps. This gain of cold function is undoubtedly important in helping explain behavioural, and possibly clinical symptoms of the drug.

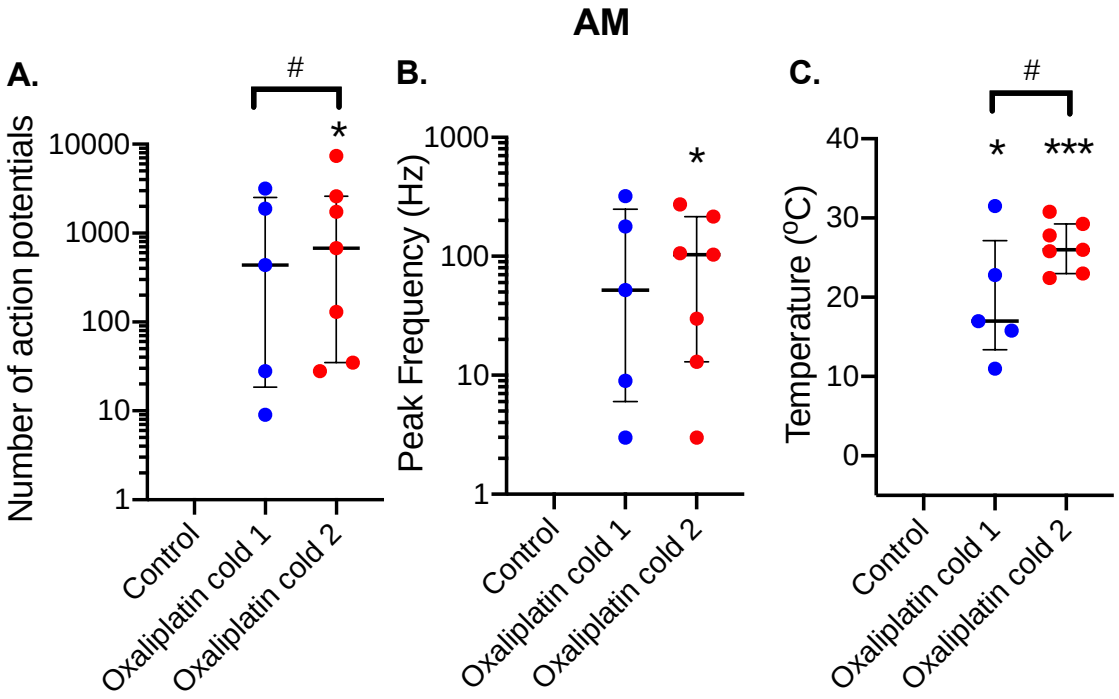

Figure 5-11 Oxaliplatin causes novel cold responses in AM fibres.

A) There was a significant increase in the number of action potentials discharged during the second cold ramp after oxaliplatin (oxaliplatin 2; red circles) when compared to control (denoted by *) (control: 0 APs; oxaliplatin 2: 1801 ± 1004 APs, Wilcoxon test, *P* = 0.016, n = 7 fibres). In addition, oxaliplatin sensitised the impulse discharge number during the second cold ramp (red circles) compared to the first cold ramp (blue circles) (denoted by #) (oxaliplatin 1: 789 ± 473 APs; oxaliplatin 2: 1801 ± 1004 APs, Wilcoxon test, *P* = 0.031, n = 5 -7 fibres). B) Oxaliplatin increased the peak discharge frequency during the second cold ramp (red circles) compared to control (denoted by *) (control: 0 APs; oxaliplatin 2: 106 ± 39 APs, Wilcoxon test, *P* = 0.016, n = 7 fibres). C) Oxaliplatin significantly increased the average threshold temperature for AM fibres during both cold ramps (blue and red circles) compared to control (denoted by *) (control: n/a; oxaliplatin 1: 14.0 ± 4.4 °C; oxaliplatin 2: 26.4 ± 1.2 °C, paired *t* test, *P* = 0.018 and *P* < 0.0001 respectively, n = 5 -7 fibres). In addition, there was a marked increase in the average threshold temperatures between the cold ramps after oxaliplatin treatment (denoted by #) (oxaliplatin 1: 14.0 ± 4.4 °C; oxaliplatin 2: 26.4 ± 1.2 °C, paired *t* test, *P* = 0.042, n = 5 -7 fibres).

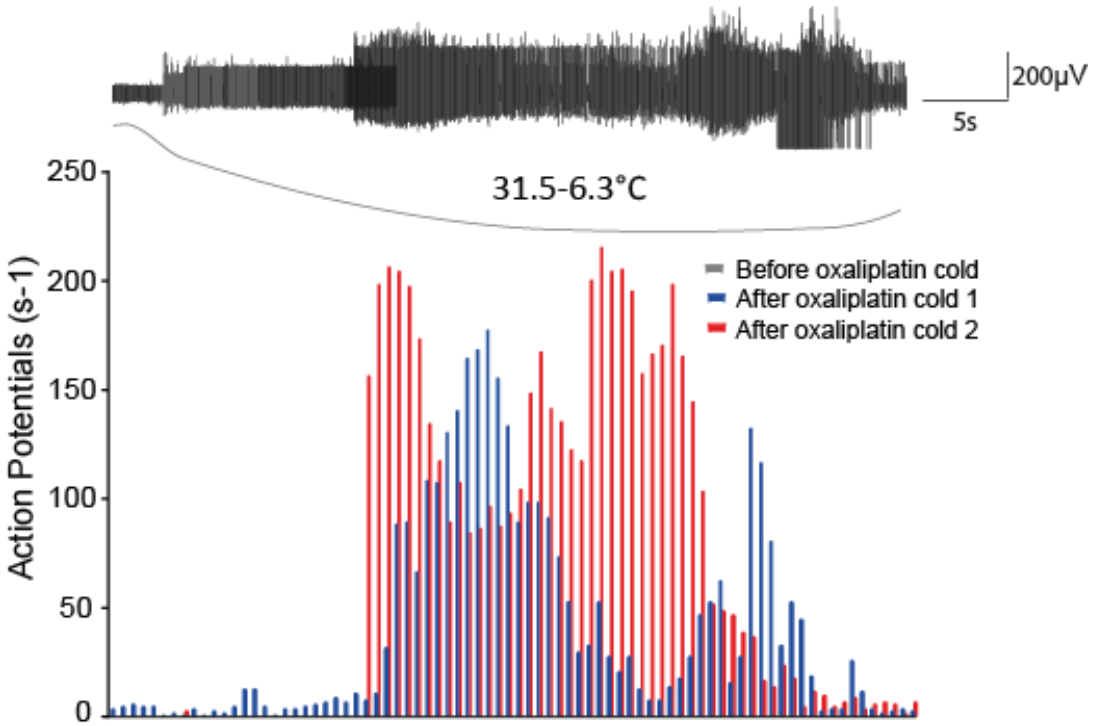

Figure 5-12 Oxaliplatin causes action potential bursts in AM fibres during cold stimulation.

Oxaliplatin sensitises AM fibres to cold ramps and causes action potential bursts. Example AM fibre trace during cold ramp shown in black. It is typical for multiple fibres to become sensitised after oxaliplatin. Histogram showing the impulse discharge rate for a single AM fibre during cold ramp 1 (blue) and cold ramp 2 (red) after oxaliplatin. The example AM fibre trace shown matches the impulse discharge rate during the second cold ramp (red) for this fibre. Notably, another small fibre starts discharging impulses almost immediately on cooling and multiple larger fibres show action potential bursts towards the end of the ramp.

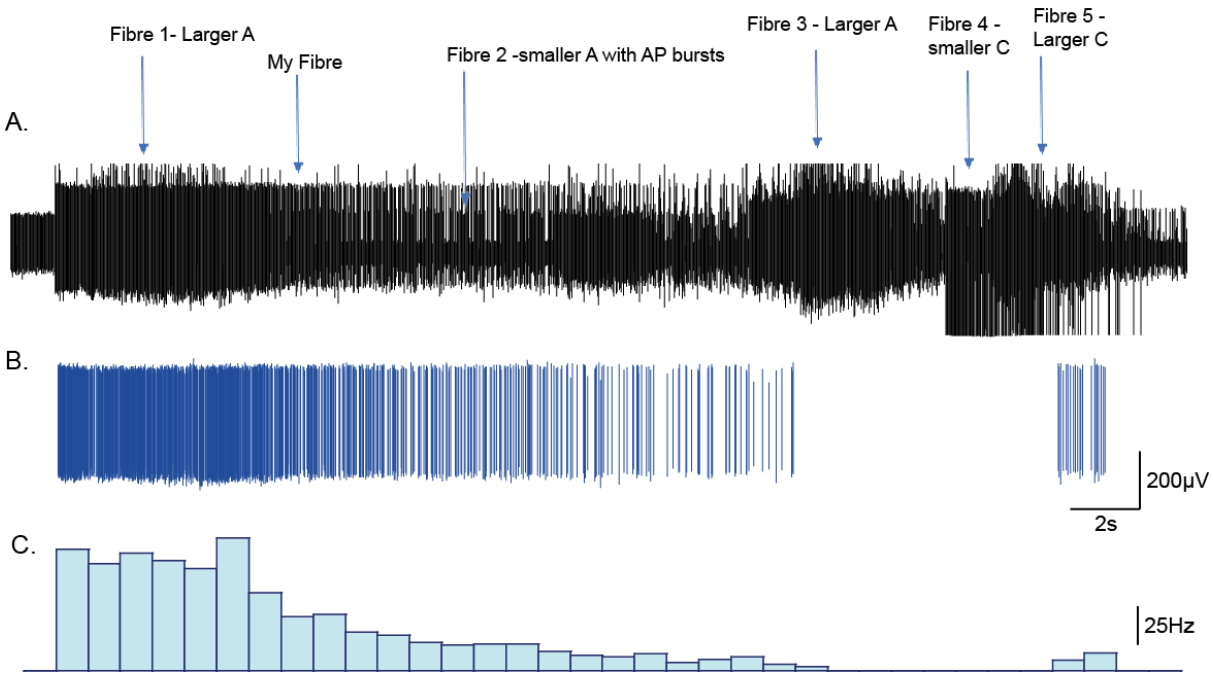

Figure 5-13 Oxaliplatin causes action potential bursts in AM fibres and sensitises multiple other fibres.

A) Expanded excerpt of the trace shown in 5-12, illustrating the activity of multiple units at 31.5 to 6.5 °C. Oxaliplatin typically sensitised multiple A and C fibres. B) Template for my AM fibre of interest. C) Histogram showing the impulse discharge rate during this period of stimulation.

5.4.7.2 DH fibres

DH fibres were very challenging to record from as many were lost throughout the recording protocol. Therefore, it is less certain whether these fibres display functional abnormalities to a similar extent as other A fibres. Oxaliplatin significantly increased the number of cold-sensitive fibres seen during the second cold ramp compared to control (control: 0/4 fibres; oxaliplatin 2: 4/4 fibres, Fisher's exact test, two-sided, $P = 0.029$, n = 4 fibres). Whilst 50 % (2/4) of DH fibres were cold-sensitive to cold ramp 1 after oxaliplatin treatment, this did not show statistical significance. Oxaliplatin caused a trend towards increased cold-evoked discharges (control: 0 APs, oxaliplatin 1: 77 ± 71 APs, oxaliplatin 2: 118 ± 71 APs, n = 2 - 4 fibres) (Figure 5-14 A). The peak discharge frequency also was not significantly altered during either cold ramp after oxaliplatin treatment when compared to control (control: 0 APs, oxaliplatin 1: 23 ± 20 APs, oxaliplatin 2: 31 ± 16 APs, n = 2 - 4 fibres) (Figure 5-14 B). Oxaliplatin significantly increased the threshold temperatures of activation towards warmer temperatures during the second cold ramp when compared to the first (oxaliplatin 1: 3.4 ± 2.0 °C; oxaliplatin 2: 18.4 ± 6.5 °C, paired *t* test, $P = 0.049$, n = 2 - 4 fibres) (Figure 5-14 C). Interestingly, DH fibres also displayed cold-evoked action potential bursts after oxaliplatin treatment (Figure 5-15), although this was substantially less than AM fibres. In DH fibres, it is apparent that there was a progressive cold sensitisation after oxaliplatin. This was a common pattern among all A fibres more broadly, excluding RA fibres.

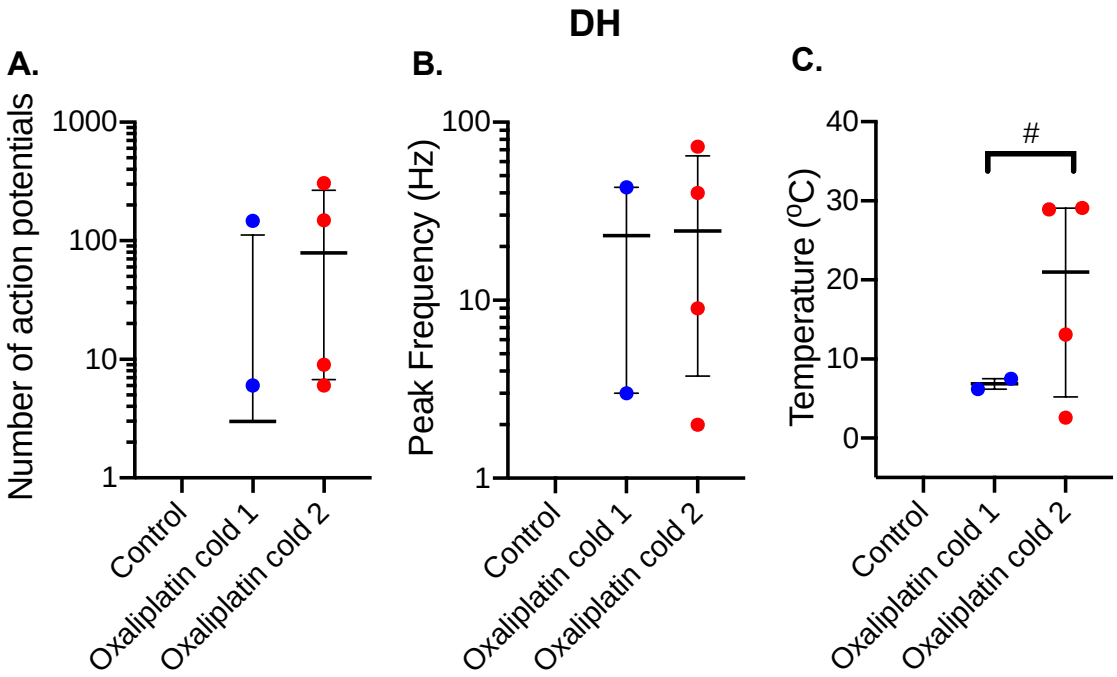

Figure 5-14 Oxaliplatin induces novel cold responses in DH fibres.

A) Oxaliplatin did not significantly alter the number of action potentials during either cold ramp when compared to control. B) Oxaliplatin did not significantly increase the peak discharge frequency during either the first (blue circles) or second (red circles) cold ramp when compared to control. C) Oxaliplatin significantly increased the average threshold temperature for DH fibres during the second (red circles) cold ramp compared to the first (blue circles) cold ramp (denoted by #) (oxaliplatin 1: 3.4 ± 2.0 °C; oxaliplatin 2: 18.4 ± 6.5 °C, paired *t* test, $P = 0.049$, n = 2 - 4 fibres).

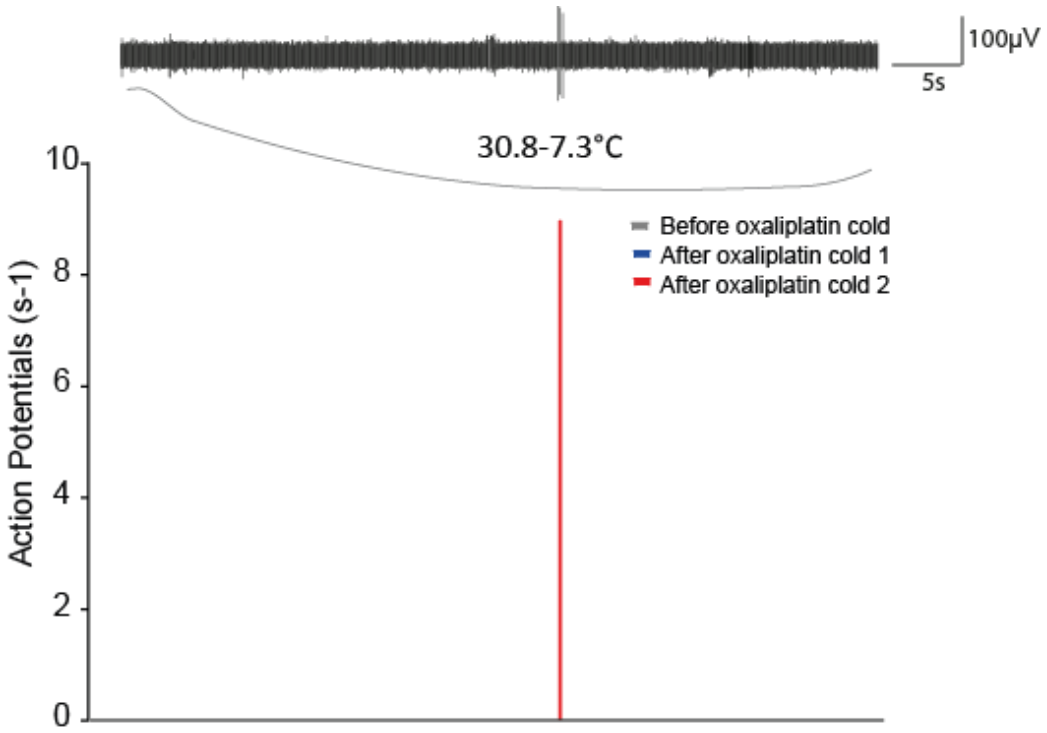

Figure 5-15 Oxaliplatin produced brief action potential bursts in DH fibres during cold stimulation.

Oxaliplatin sensitised DH fibres to cold ramps and caused brief action potential bursts. Example DH fibre trace during cold ramp shown in black. Histogram showing the impulse discharge rate for a single DH fibre during cold ramp 2 (red) after oxaliplatin. The example DH fibre trace shown matches the impulse discharge rate during the second cold ramp (red) for this fibre. There was no cold sensitivity before oxaliplatin or during the first cold ramp after oxaliplatin in this fibre.

5.4.7.3 RA fibres

In recordings with RA fibres, oxaliplatin produced a gain of cold-sensitive function in normally temperature insensitive single-units during the first and second cold ramps compared to control (control: 0/7 fibres; oxaliplatin 1 and 2: 6/7 fibres, Fisher's exact test, two-tailed, P = 0.0047, n = 7 fibres). In addition, oxaliplatin significantly increased the total number of action potentials discharged during the first and second ramps compared to control (control: 0 APs, oxaliplatin 1: 236 ± 199 APs, oxaliplatin 2: 476 ± 395 APs, Wilcoxon test, P = 0.031 for both ramps, n = 6 fibres) (Figure 5-16 A). Oxaliplatin increased the peak discharge frequency during both cold ramps when compared to control (control: 0 APs; oxaliplatin 1: 38 ± 21 APs; oxaliplatin 2: 64 ± 34 APs, Wilcoxon test, P = 0.031 for both ramps, n = 6 fibres) (Figure 5-16 B). Oxaliplatin transformed RA single-units to cold responsive fibres and progressive sensitisation was not observed with time of exposure. This is reflected in the temperature activation thresholds which were low (control: n/a, oxaliplatin 1: 8.9 ± 2.4 °C; oxaliplatin 2: 9.1 ± 2.4 °C, Wilcoxon test, P = 0.031 for both ramps, n = 6 fibres) (Figure 5-16 C, Figure 5-17). RA fibres showed dramatic changes to their firing properties, with periods of cold-evoked action potential bursts common after oxaliplatin treatment. Therefore, RA fibres lost their typical adaptation properties after oxaliplatin treatment (trace in Figure 5-17).

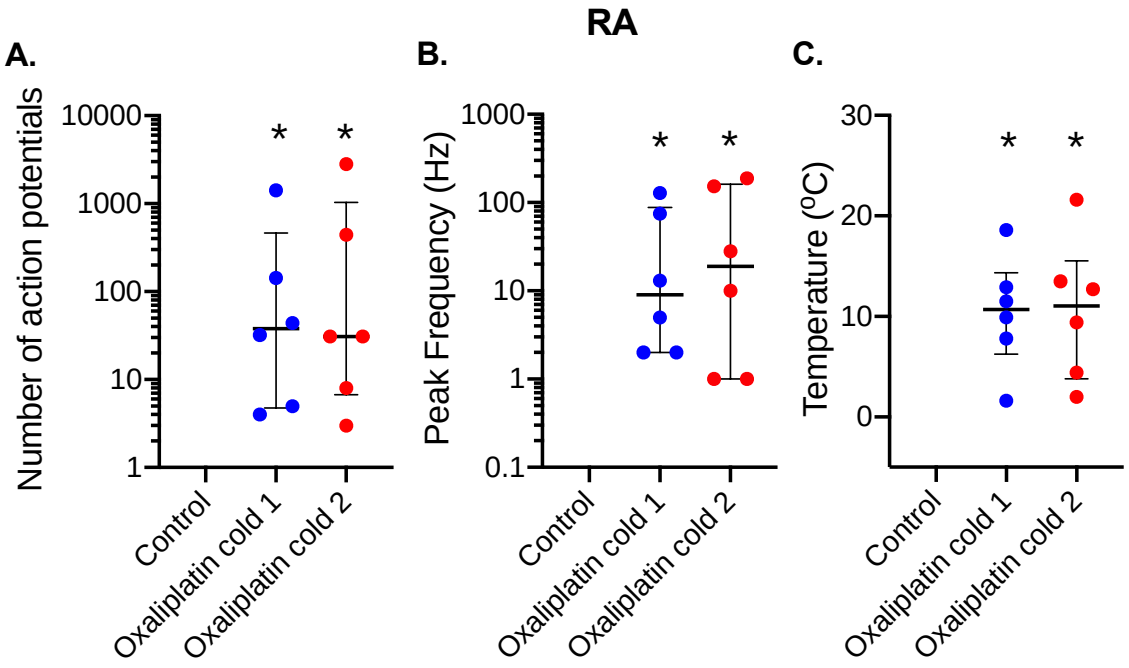

Figure 5-16 Oxaliplatin induces novel gain of cold function in normally temperature-insensitive RA fibres.

A) The number of action potentials discharged during the first (blue circles) and second (red circles) cold ramp after oxaliplatin was significantly increased when compared to control (denoted by *) (control: 0 APs, oxaliplatin 1: 236 ± 199 APs, oxaliplatin 2: 476 ± 395 APs, Wilcoxon test, *P* = 0.031 for both ramps, n = 6 fibres). B) Oxaliplatin increased the peak discharge frequency during the first (blue circles) and second (red circles) cold ramp compared to control (denoted by *) (control: 0 APs; oxaliplatin 1: 38 ± 21 APs; oxaliplatin 2: 64 ± 34 APs, Wilcoxon test, *P* = 0.031 for both ramps, n = 6 fibres). C) Oxaliplatin significantly increased the average threshold temperature for RA fibres during both cold ramps (blue and red circles) compared to control (denoted by *) (control: n/a, oxaliplatin 1: 8.9 ± 2.4 °C; oxaliplatin 2: 9.1 ± 2.4 °C, Wilcoxon test, *P* = 0.031 for both ramps, n = 6 fibres).

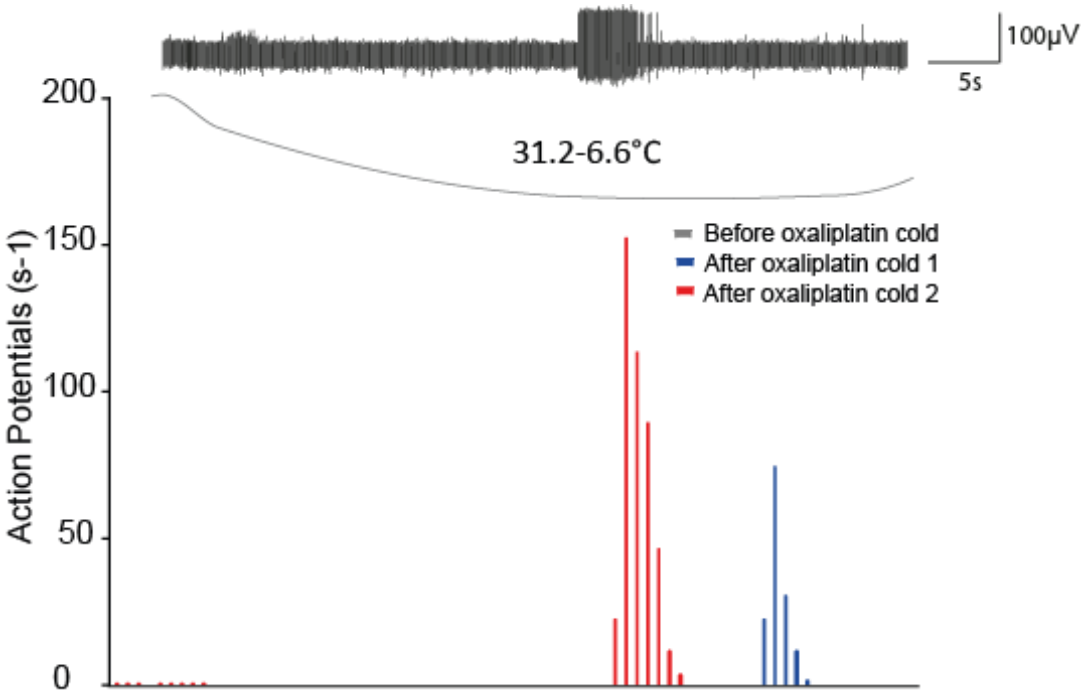

Figure 5-17 Oxaliplatin causes action potential bursts in RA fibres during cold stimulation.

Oxaliplatin sensitised RA fibres to cold ramps and caused periods of action potential bursts. Example RA fibre trace during cold ramp shown in black. Histogram showing the impulse discharge rate for a single RA fibre during cold ramp 1 (blue) and 2 (red) after oxaliplatin. The example RA fibre trace shown matches the impulse discharge rate during the second cold ramp (red) for this fibre. RA fibres changed their adaptation properties during oxaliplatin-induced cold-evoked firing.

5.4.7.4 SA fibres

In recordings of SA fibres, 3/10 fibres and 6/10 fibres became cold-sensitive during the first and second cold ramps respectively after oxaliplatin treatment. Oxaliplatin treatment significantly increased the number of cold-sensitive fibres during the second cold ramp compared to control (control: 0/10 fibres; oxaliplatin 2: 6/10 fibres, Fisher's exact test, two-sided, P = 0.002, n = 10 fibres). Since SA fibres do not normally respond to cold, the cold sensitivity generated by oxaliplatin was associated with an increased number of action potentials during the second cold ramp when compared to control (control: 0 APs; oxaliplatin 2: 668 ± 497 APs, Wilcoxon test, P = 0.031, n = 6 fibres) (Figure 5-18 A). In addition, the peak discharge frequency was significantly increased during the second cold ramp but not the first after oxaliplatin treatment when compared to control (control: 0 APs; oxaliplatin 2: 87 ± 44 APs, Wilcoxon test, P = 0.031, n = 6 fibres) (Figure 5-18 B). Intriguingly, the cold activation threshold for SAs after oxaliplatin appeared to be unchanged in response to the first cold ramp after, although the proportion of units that responded was 3/10. The temperature threshold for the second cold ramp after oxaliplatin 19.1 ± 2.0 °C, was increased compared to naïve SA (which do not respond), but also appeared higher than in RA fibres (Figure 5-18 C). There was a degree of sensitisation seen between the first and second cold ramps following oxaliplatin treatment as highlighted by increased impulse discharge patterns (Figure 5-19) and in the number of cold-sensitive fibres. Interestingly, oxaliplatin sensitised fibres to discharge impulses earlier on during cold ramps in oxaliplatin 2 compared to oxaliplatin 1 (Figure 5-19).

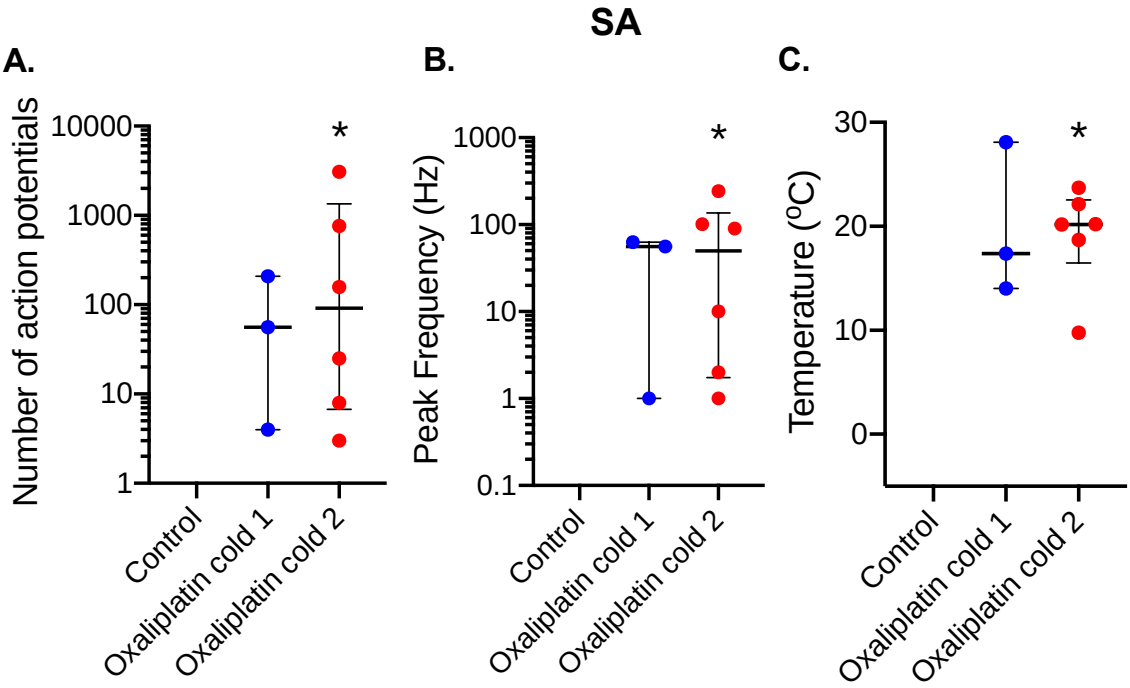

Figure 5-18 Oxaliplatin generates abnormal cold responses in SA fibres.

A) There was a significant increase in the number of action potentials discharged during the second (red circles) cold ramp after oxaliplatin when compared to control (denoted by *) (control: 0 APs; oxaliplatin 2: 668 ± 497 APs, Wilcoxon test, *P* = 0.031, n = 6 fibres). B) Oxaliplatin increased the peak discharge frequency during the second (red circles) cold ramp compared to control (denoted by *) (control: 0 APs; oxaliplatin 2: 87 ± 44 APs, Wilcoxon test, *P* = 0.031, n = 6 fibres). C) Oxaliplatin significantly increased the average threshold temperature for SA fibres during the second (red circles) cold ramp compared to control (denoted by *) (control: n/a; oxaliplatin 2: 19.1 ± 2.0 °C, Wilcoxon test, *P* = 0.031, n = 6 fibres).

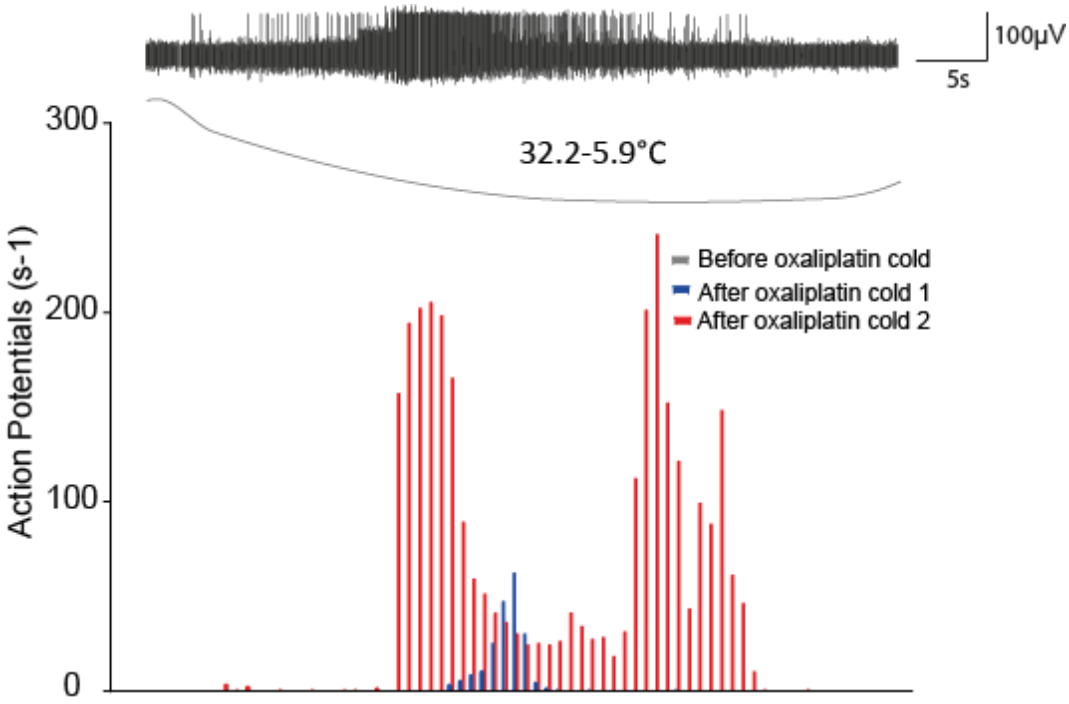

Figure 5-19 Oxaliplatin causes action potential bursts in SA fibres during cold stimulation.

Oxaliplatin sensitised SA fibres to cold ramps and caused persistent action potential discharges. Example SA fibre trace during cold ramp shown in black. Histogram showing the impulse discharge rate for a single SA fibre during cold ramp 1 (blue) and 2 (red) after oxaliplatin. The example SA fibre trace does not match either of the impulse discharge rates shown in the histogram. Instead, a cleaner recording was used.

Importantly, we observed no cold-sensitive A fibres after vehicle treatment. This shows that direct and acute application of oxaliplatin to the receptive field of these fibres is sufficient to sensitise them to generate a gain of cold-sensitivity.

5.4.8 C fibres are less affected by oxaliplatin than A fibres

Our observations from A fibres recordings show that oxaliplatin sensitised a small proportion of CM fibres and made some of these normally temperature insensitive fibres respond to cold. After oxaliplatin, 2/10 CM fibres and 3/10 CM fibres became cold responsive after the first and second cold ramps respectively. Whilst this was not significant in Fisher's exact test, the recruitment of CM fibres to cold stimulations effectively changed their phenotype to C-mechano-cold (CMC) fibres. These CM fibres had a modest number of action potentials. Oxaliplatin did not significantly change the total number of action potentials discharged (oxaliplatin 1: 8 ± 2 APs; oxaliplatin 2: 29 ± 9 APs) (Figure 5-20 A). The small number of responding units makes the conclusions uncertain, but the activation threshold appeared to move towards warmer temperatures in response to the second cold ramp after oxaliplatin (Figure 5-20 C). This was similar for other parameters including peak firing frequency (Figure 5-20 B). Furthermore, there were no novel cold-sensitive CM fibres after vehicle treatment.

In CMC fibre recordings, vehicle treatment (5 % glucose) did not increase the total number of action potentials fired during cold stimulations when compared to control (control: 56 ± 32 APs; oxaliplatin 1: 55 ± 24 APs; oxaliplatin 2: 48 ± 23 APs, n = 10 fibres) (Figure 5-21 A). The peak discharge frequency remained similar across all three cold ramps (control: 6 ± 3 APs; oxaliplatin 1: 5 ± 2 APs; oxaliplatin 2: 4 ± 2 APs, n = 10 fibres) (5- 21 B). In addition, vehicle

treatment did not change the threshold temperatures of activation in CMC fibres when compared to control (control: 19.4 ± 2.6 °C; vehicle 1: 14.7 ± 2.6 °C; vehicle 2: 17.4 ± 2.8 °C, n = 10 fibres) (Figure 5-21 C). Finally, the impulse discharge patterns remained unchanged during cold ramps with vehicle treatment (Figure 5-22 A).

Interestingly, there was a modest effect on CMC fibres after oxaliplatin treatment, when compared to some A fibre classes. Oxaliplatin significantly increased the total number of action potentials discharged during both cold ramps compared to control (control: 48 ± 34 APs; oxaliplatin 1: 113 ± 67 APs; oxaliplatin 2: 148 ± 98 APs, Wilcoxon test, $P = 0.004$ and $P = 0.012$ respectively, n = 10 fibres) (Figure 5-21 D). In addition, there was a significant increase in the peak discharge frequency (control: 3 ± 2 APs; oxaliplatin 1: 7 ± 3 APs; oxaliplatin 2: 11 ± 5 APs, paired *t* test, $P = 0.016$ for both ramps, n = 10 fibres) (Figure 5-21 E). However, oxaliplatin did not shift the threshold temperatures when compared to control (control: 15.4 ± 2.7 °C; oxaliplatin 1: 16.9 ± 2.2 °C; oxaliplatin 2: 18.2 ± 2.2 °C, n = 10 fibres) (Figure 5-21 F). Oxaliplatin sensitised the firing pattern, as fibres started firing earlier during the second cold ramp after oxaliplatin (Figure 5-22 B). Notably, there were no significant differences between the total number of action potentials, peak discharge frequencies and threshold temperatures between treatment groups.

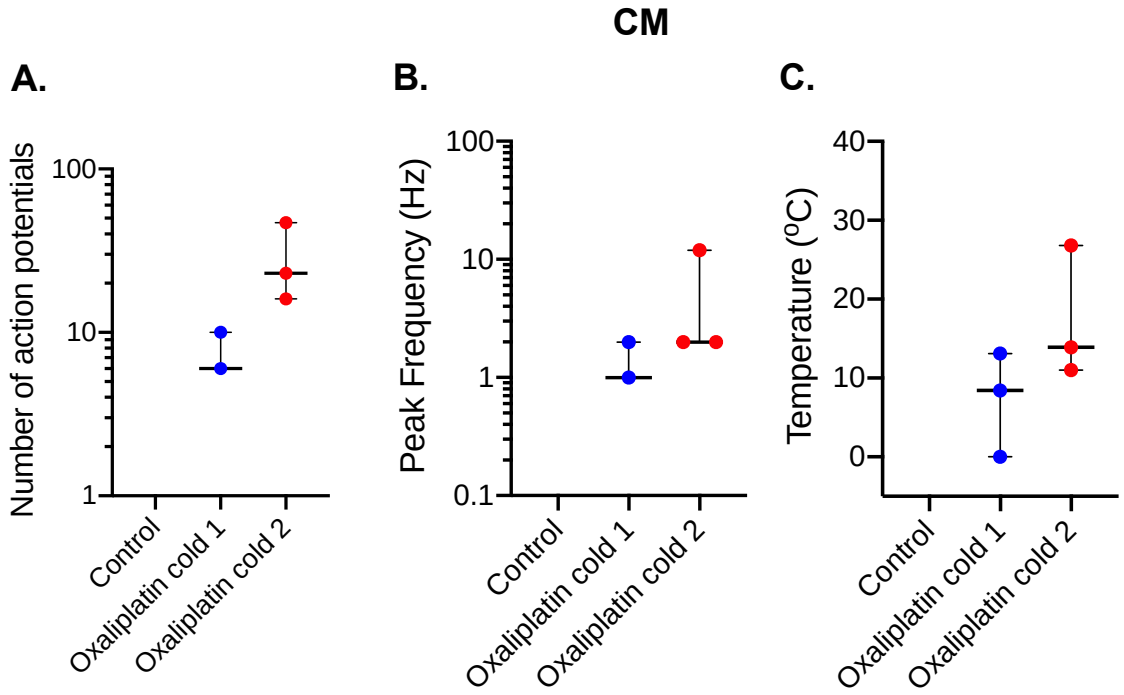

Figure 5-20 Oxaliplatin induces de novo cold responses in CM fibres.

A) A trend towards increased numbers of action potentials was evident during the first (blue circles) and second (red circles) cold ramps after oxaliplatin when compared to control. B) Oxaliplatin did not significantly increase the peak discharge frequency during cold ramps after oxaliplatin when compared to control. C) Oxaliplatin did not change the average threshold temperature for CM fibres during cold ramps when compared to control.

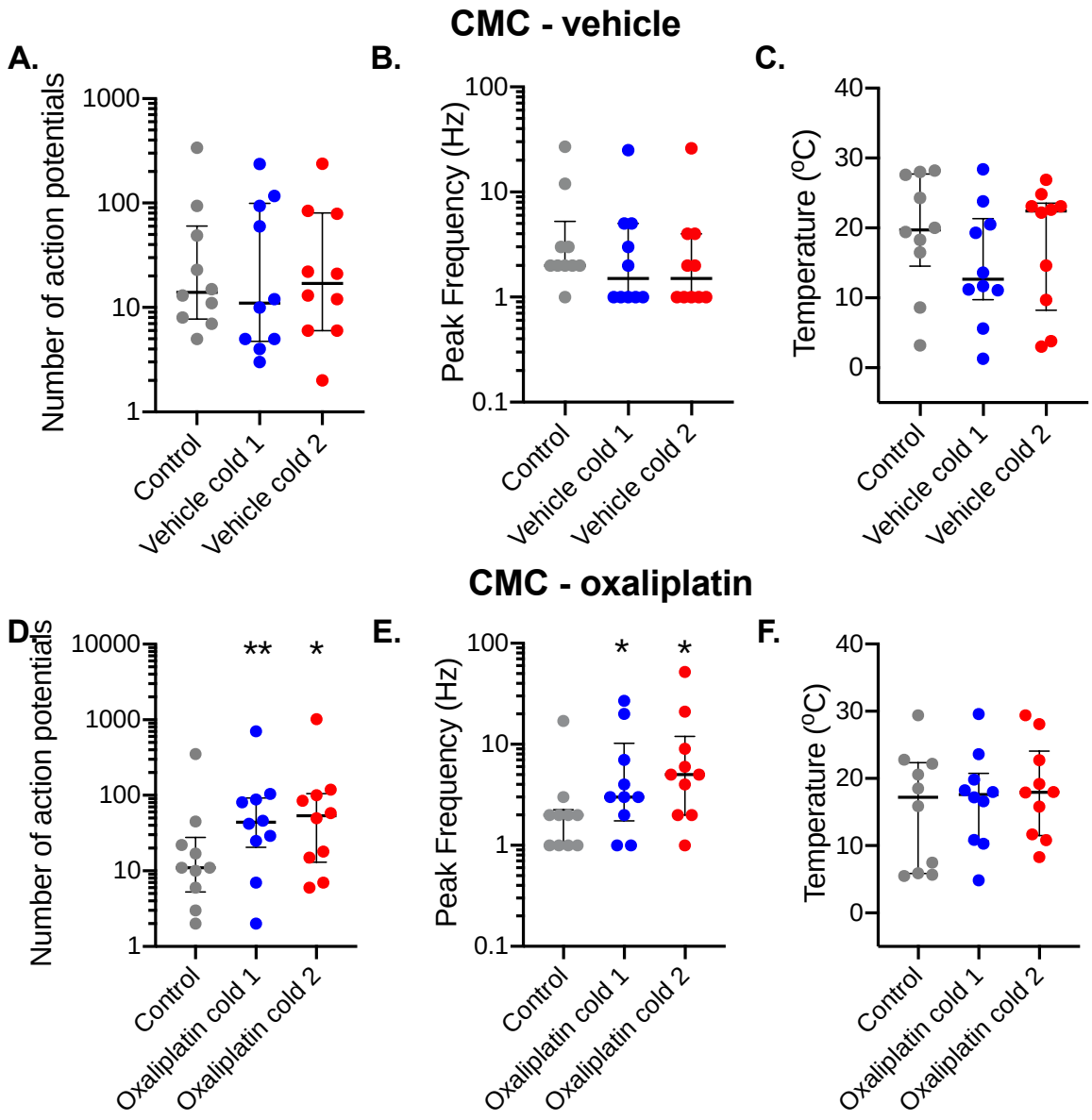

Figure 5-21 Oxaliplatin increases cold sensitivity in CMC fibres.

A) Vehicle treatment did not change the number of action potentials discharged during cold ramps compared to control. B) The peak firing frequency in CMC fibres was unchanged during cold ramps after vehicle treatment. C) Vehicle treatment did not significantly affect the threshold temperatures of activation of CMC fibres when compared to control (grey circles). D) Oxaliplatin increased (denoted by *) the number of action potentials discharged during the first (blue circles) and second (red circles) cold ramps when compared to control (grey circles) (control: 48 ± 34 APs; oxaliplatin 1: 113 ± 67 APs; oxaliplatin 2: 148 ± 98 APs, Wilcoxon test, P = 0.004 and P = 0.012 respectively, n = 10 fibres). E) Oxaliplatin significantly increased (denoted by *) the peak discharge frequency during the first (blue circles) and second (red circles) cold ramp compared to control (grey circles) (control: 3 ± 2 APs; oxaliplatin 1: 7 ± 3 APs; oxaliplatin 2: 11 ± 5 APs, paired t test, P = 0.016 for both ramps, n = 10 fibres). F) Oxaliplatin did not shift the threshold temperatures of CMC fibres during the cold ramps compared to control.

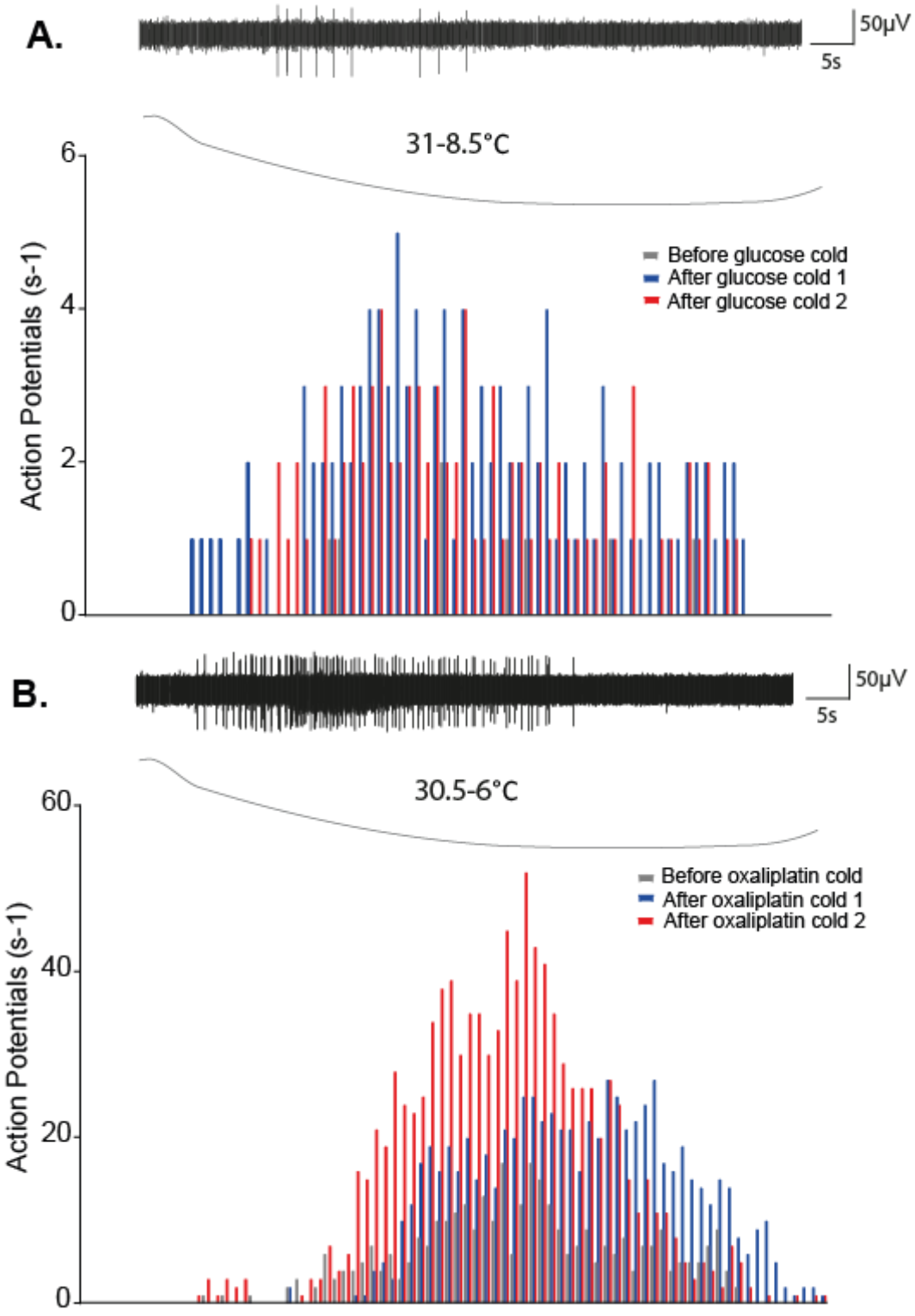

Figure 5-22 Oxaliplatin increased the cold-evoked impulse discharge rate of CMC fibres.

A) Example trace for CMC fibre response during cold ramp after vehicle (5 % glucose treatment). Histogram showing the impulse discharge rate during cold stimulation before glucose (grey) and the first (blue) and second (red) cold ramps after glucose application. B)

Oxaliplatin sensitised CMC fibres to cold ramps and caused increased firing rather than action potential bursts. Example CMC fibre trace during cold ramp shown in black. Histogram showing the impulse discharge rate for a single CMC fibre during cold ramp before oxaliplatin (grey) and the first (blue) and second (red) cold ramps after oxaliplatin. The example CMC fibre traces shown do not match any of the impulse discharge patterns shown in the respective histograms.

5.4.9 Increased cold sensitivity in fibres 4 days after oxaliplatin treatment *in vivo*

Preparations were taken on multiple days (days 1, 2 and 4) following oxaliplatin and vehicle treatment *in vivo*. Although the number of recordings conducted in treated preparations was limited, we found that the proportion of cold-sensitive fibres of any class was significant at day 4 post-injection between treatment groups (vehicle-treated 4/19 fibres; oxaliplatin-treated 11/11 fibres, Fisher's exact test, two-sided, $P < 0.0001$) (Table 5-2). We could not say with certainty whether there were changes on other days due to small sample sizes and data points. In addition, the number of spontaneously active fibres in preparations from oxaliplatin-treated mice was increased significantly compared to vehicle-treated mice 4 days after treatment (vehicle 0/19 fibres; oxaliplatin-treated 5/11 fibres, Fisher's exact test, two-sided, $P = 0.003$).

Table 5-2 Single- and multi-unit recordings made in skin-nerve preparations from mice treated with either 5 % glucose or 6 mg/kg oxaliplatin i.p.

Preparation treatment and time post dosing	Fibre class	Total number of recordings	Total number of cold-sensitive fibres	Fibre type when known	Spontaneous activity seen
Vehicle Day 4	A	16 (2 multi-unit)	4/19 fibres	5 Ab (2 RA, 3 SA)	0/19 fibres
				9 Ad (6 AM, 2 AMC, 1 Ad)	
	C	3		2 CMC, 1 CC	
Oxaliplatin Day 4	A	5	11 (all)	1 Ab (1 SA)	5/11 fibres
				1 Ad (1 DH)	
	C	6 (3 multi-unit)		3 C, 3 multi-unit	
Oxaliplatin Day 2	A	2 (1 multi-unit)	4 (all)	0 Ab	2/4 fibres
				1 Ad (1 DH)	
	C	2		1 CMC, 1 CC	
Oxaliplatin Day 1	A	1	10 (all)	1 Ab (1 SA)	4/11 fibres
				0 Ad	
	C	9		6 CMC, 2 CC, 1 C	

5.4.10 Increased activity in C fibres in preparations from oxaliplatin-treated mice

In contrast to the results from earlier recordings in naïve preparations, oxaliplatin treatment *in vivo* increased activity of C fibres in *ex vivo* recordings. The number of action potentials was increased ~10 fold during the first and second cold ramps in C fibres recorded from oxaliplatin-treated mouse preparations when compared to vehicle-treated preparations. There was an increase in the number of action potentials discharged by C fibres during the first and second ramps (Figure 5-23 B). In addition, there was a trend towards increased peak discharge frequencies in C fibres from oxaliplatin-treated preparations when compared to vehicle-treated preparations (Figure 5-23 D). Furthermore, the threshold temperatures in the same fibres showed a trend towards activation at warmer temperatures compared to vehicle counterparts (Figure 5-23 F). Interestingly, A fibres did not show similar patterns of sensitisation (Figure 5-23 A, 5-23 C, 5-23 E). A fibres were less responsive to cold stimulation in recordings from treated mice-skin preparations when compared to naïve preparations. This may indicate a difference in the mechanisms for acute and long-term oxaliplatin treatment at the level of peripheral nerve terminals. However, the small number of data points makes conclusions uncertain.

5.4.11 C fibres increased activity compared to than A fibres in small sample size

Interestingly, single and multi-unit recordings from oxaliplatin-treated mouse skin-nerve preparations showed increased responsiveness in C fibres, but not A fibres (Figure 5-23). Given the small sample sizes from both fibre classes in these experiments, firm conclusions cannot be drawn. However, it is evident from these few recordings that A fibres were not affected as dramatically as in the experiments with naïve preparations with application of oxaliplatin directly to the corium. These pilot studies might indicate that oxaliplatin affects different fibre types in different ways over time and is dependent on level and duration of exposure.

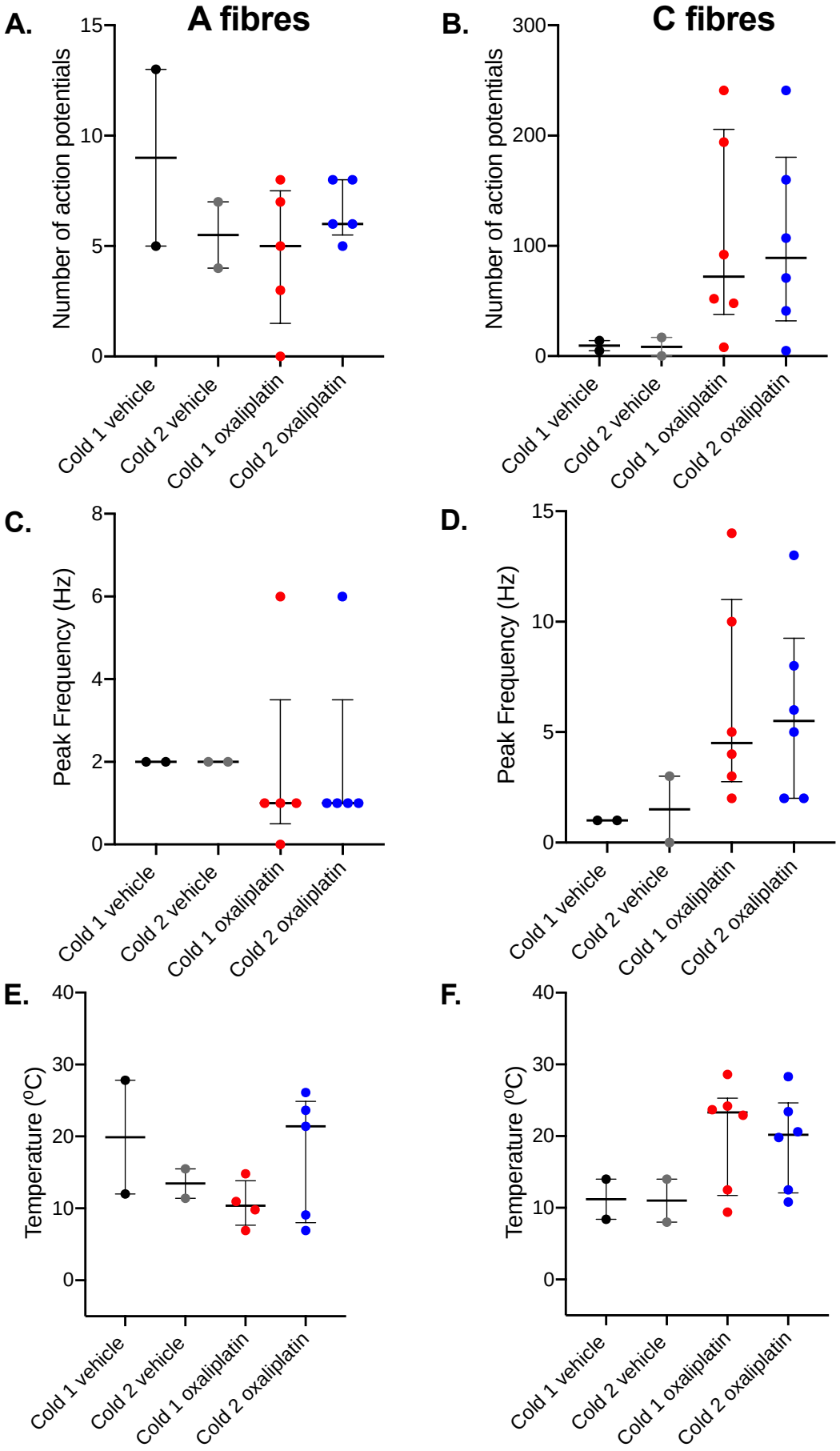
A.
A fibres
Number of action potentials
15
10
5
0
Cold 1 vehicle
Cold 2 vehicle
Cold 1 oxaliplatin
Cold 2 oxaliplatin
B.
C fibres
Number of action potentials
300
200
100
0
Cold 1 vehicle
Cold 2 vehicle
Cold 1 oxaliplatin
Cold 2 oxaliplatin
C.
Peak Frequency (Hz)
8
6
4
2
0
Cold 1 vehicle
Cold 2 vehicle
Cold 1 oxaliplatin
Cold 2 oxaliplatin
D.
Peak Frequency (Hz)
15
10
5
0
Cold 1 vehicle
Cold 2 vehicle
Cold 1 oxaliplatin
Cold 2 oxaliplatin
E.
Temperature (°C)
40
30
20
10
0
Cold 1 vehicle
Cold 2 vehicle
Cold 1 oxaliplatin
Cold 2 oxaliplatin
F.
Temperature (°C)
40
30
20
10
0
Cold 1 vehicle
Cold 2 vehicle
Cold 1 oxaliplatin
Cold 2 oxaliplatin

Figure 5-23 Oxaliplatin-treatment in vivo increases responsiveness to cold in C fibres.

A) Oxaliplatin (red and blue circles) treatment *in vivo* did not affect the number of action potentials discharged in A fibres when compared to vehicle (black and grey circles) treatment *in vivo*. B) Oxaliplatin treatment *in vivo* increased the number of action potentials ~10 fold during cold ramps when compared to vehicle treatment. C) Oxaliplatin treatment *in vivo* did not alter the peak discharge frequency during cold raps in A fibres when compared to vehicle treatment *in vivo*. D) A trend towards increased peak discharge frequencies during cold ramps was seen in C fibres from oxaliplatin treatment *in vivo* compared to vehicle treatment *in vivo*. E) Oxaliplatin treatment *in vivo* did not alter the threshold temperatures of activation in A fibres when compared to vehicle treatment *in vivo*. F) A trend towards warmer threshold temperatures of activation were seen in C fibres from oxaliplatin treated mice compared to those from vehicle treated mice.

5.4.12 Fewer impulses discharged during cold stimulations in preparations from treated mice

In all experiments from treated mouse skin-nerve preparations, ice-cold SIF was used to identify the receptive fields of cold-sensitive fibres, before applying cold ramps. It was common for fibres to respond more dramatically to ice-cold SIF than to time-controlled cold ramps (Figure 5-24 A, B). This is likely to be due to the fact that the temperature that reaches the receptive field not being the same as the ice-cold SIF. Whilst there was increased spontaneous activity in preparations from treated mice, the general responsiveness to cold was lower than in naïve preparations (Figure 5-24 A). This may be due to fibres being exposed to lower concentrations of oxaliplatin than in direct application experiments. In addition, there may be longer term adaptation to increased activity.

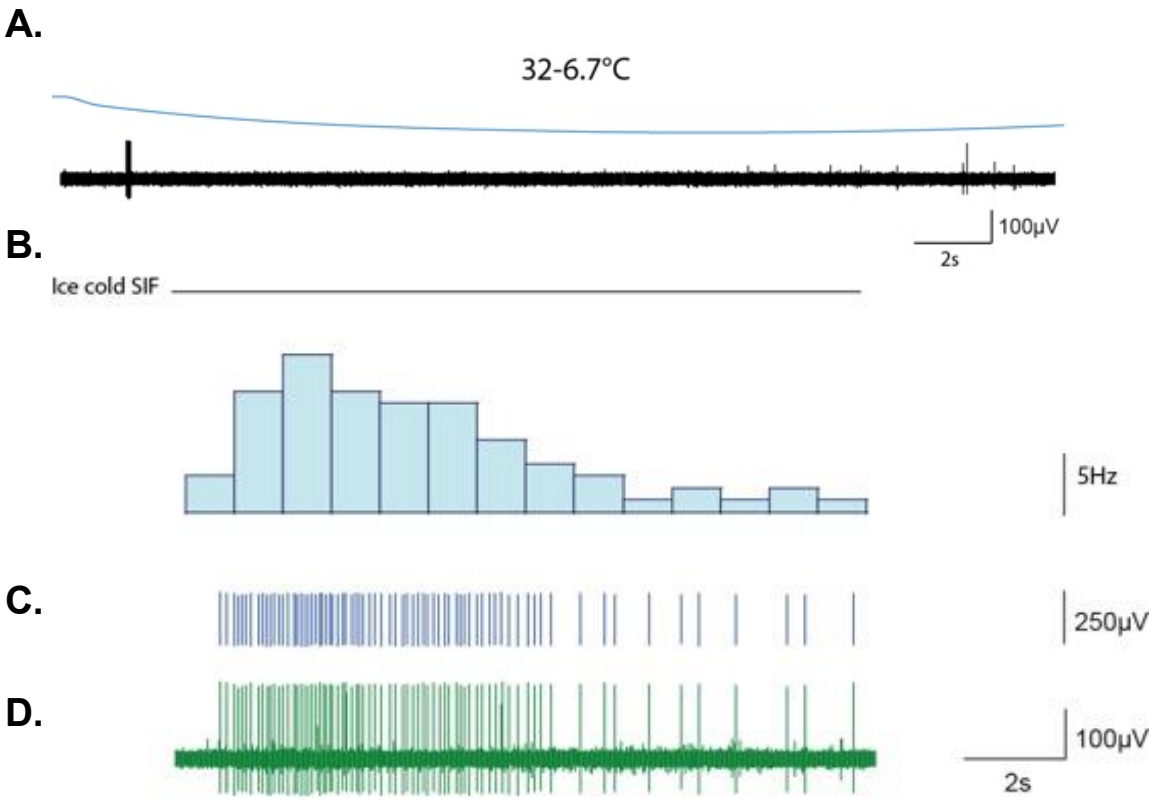

Figure 5-24 Example A fibre response to cold ramp and ice-cold SIF from an oxaliplatin-treated mouse preparation.

A) Typically, there were a few impulses discharged by A fibres during cold ramps (DH shown in above example). This was a striking difference from cold-evoked responses seen in A fibres after acute application of oxaliplatin. B) Example DH fibre response to ice cold SIF shown. There was an increased rate of impulse discharges seen during this period. This response is similar to the action potential bursts that were observed in A fibres after direct and acute oxaliplatin application. The histogram shows the rate of impulses discharged (Hz). C) The blue fibre is the template created which is necessary for quantitative analysis. D) The green trace shows the action potentials seen during the recording.

5.5 Discussion

In this results chapter, we successfully identified the subpopulations of sensory afferent fibre classes that are modulated by acute and direct application of oxaliplatin in skin-saphenous nerve preparations. First, we show that acute application of oxaliplatin to the receptive field of single fibres alters the adaptation properties in all fibre classes tested, particularly Aβ fibres. For A fibres, oxaliplatin substantially increased the number of action potentials discharged during mechanical stimulation periods. In addition, impulses discharged outlasted the mechanical stimulation window in AM, SA and RA fibre recordings. In contrast, oxaliplatin decreased the number of action potentials discharged during a ramp stimulus in C fibres. This shows an effect on the encoding properties of these fibres. Notably, we show for the first time that acute local application of oxaliplatin induces novel cold sensitivity in all subpopulations of A fibres. Often, oxaliplatin induced action potential bursts in these cold-sensitive fibres. Oxaliplatin also made normally cold-insensitive C fibres become cold-sensitive, although the magnitude of this effect was less marked than in A fibres. This is likely to be very important to the pathophysiology of oxaliplatin-induced neuropathic pain. Oxaliplatin is able to cause both small and large fibre neuropathy (Barbosa et al., 2014; Krøigård et al., 2014). However, intraepidermal nerve fibre density (IENFD) studies have revealed that large myelinated A fibres are affected first and to a greater extent (Kang et al., 2020). This supports our findings here. Furthermore, we report that C fibres show increased responsiveness to cold compared to A fibres in preparations taken from oxaliplatin-treated mice. This could suggest different mechanisms involved between the acute and direct effects of the drug versus longer term treatment *in vivo*.

Acute oxaliplatin treatment caused functional changes in all A fibre responses to mechanical and cold stimuli. This provides evidence of a cellular mechanism for the acute effects of oxaliplatin in the clinic. Our results are in agreement with a recent *in vivo* calcium imaging study conducted by MacDonald and colleagues, who showed that oxaliplatin sensitises previously cold-insensitive large-diameter neurons to cold (MacDonald et al., 2021). However, the authors report that these fibres did not express molecular markers for Aβ or Aδ fibres. This contrasts with the functional characterisation of these fibres in our study. Up to 90 % of all patients treated with oxaliplatin report paraesthesias and cold-evoked dysaesthesias (Saif and Reardon, 2005). We report that acute oxaliplatin application to the receptive field of nerve terminals sensitises Aβ-LTMRs. Oxaliplatin greatly increases the number of action potentials discharged during mechanical force applications in both RA and SA fibres. The adaptation properties of RA fibres are altered at low and high forces. It is particularly striking that some RA fibres display slow adaptation properties to 15 g forces, resembling SA fibres. Oxaliplatin also sensitised SA fibres to innocuous forces and significantly increased the impulse discharge frequency during the mechanical stimulation periods. In addition to high frequency discharges, both RA and SA fibres displayed post-stimulus discharges which lasted for seconds to minutes. This level of spontaneous discharge has been reported previously in severed nerves (Govrin-Lippmann and Devor, 1978). This is usually preceded by a period of action potential bursts and quiescent periods. The fingertips and other locations characterised by a high level of tactile acuity are densely innervated by RA and SA fibres (Bensmaïa et al., 2006). RA fibres are important for the detection and scaling of low-frequency vibrations (Torebjörk and Ochoa, 1980). They also sense changes to grip function e.g. when objects slip (Abraira and Ginty, 2013). In comparison, SA-LTMRs are important for acute spatial acuity and imaging of tactile stimuli (Johnson, 2001), as well as

stretch detection (Abraira and Ginty, 2013). Oxaliplatin-induced changes of the impulse discharge rates and patterns of firing produced in these *ex vivo* experiments might underlie patient symptoms. The changes to Aβ fibre properties can explain the paraesthesias experienced by patients after a single treatment cycle. Furthermore, QST studies have shown that long term treatment of oxaliplatin causes deficits in Aβ fibre functions, by increasing detection thresholds the bumps test and to von Frey filaments (Barbosa et al., 2014). Over time, patients experience mechanical and tactile allodynia (Kawashiri et al., 2011) and this may in part be explained by the sensitisation of Aβ-LTMRs (Shir and Seltzer, 1990).

Although we cannot make conclusions with certainty for DH fibres due to the very small sample size, oxaliplatin did not appear to sensitise DH fibres to mechanical stimuli. This may, in part, be due to the inability of these low threshold-mechanoreceptors to sustain high frequency patterns due to their sensitivity to even the finest of movements (Schütze et al., 2016). However, the other class of Aδ fibres recorded, AM nociceptors, were strongly sensitised to mechanical forces after oxaliplatin treatment. Importantly, oxaliplatin significantly increased the number of action potentials discharged by AM fibres at innocuous forces (4 g). This, along with the sensitisation of Aβ-LTMRs provides a mechanism for oxaliplatin-induced mechanical allodynia. There were also a greater number of action potentials discharged in response to higher mechanical forces. This may explain the mechanical hyperalgesia which is a common side effect of the drug (Boyette-Davis and Dougherty, 2011). In addition, AM fibres displayed post-stimulus discharges, which sometimes appeared as action potential bursts that lasted for seconds to minutes after the stimulation period. AM fibres are responsible for detecting acute and sharp pain (Basbaum et al., 2009; Purves et al., 2001). Therefore, the changes to the adaptation properties of AM-HTMRs are likely to cause sharp, burning pain, mechanical hyperalgesia and allodynia, which

are all reported in the clinic (Boyette-Davis and Dougherty, 2011; Kawashiri et al., 2011; Nassini et al., 2011; Pachman et al., 2015; Tofthagen et al., 2013b).

In contrast to A fibres, direct applications of oxaliplatin desensitised C fibre responses to high mechanical forces. In both CM and CMC recordings, oxaliplatin significantly decreased the number of action potentials discharged during 20 g ramp forces. Again, this change to the encoding and adaptation properties of C fibres may be important in explaining clinical symptoms. Paraesthesias have actually been reported to be more bothersome to patients than sharp pain over the course of treatment (Pachman et al., 2015). Therefore, C fibre abnormalities may be less impactful than A fibres in causing acute oxaliplatin-induced symptomatology. This is supported by other studies which report that oxaliplatin affects myelinated A fibres more than unmyelinated C fibres (Adelsberger et al., 2000; Deuis et al., 2013, 2014; Forstenpointner et al., 2018; Kagiava et al., 2008; Sittl et al., 2010, 2012). In addition, oxaliplatin-induced cold hyperalgesia can be alleviated by preferential A fibre blockade (Forstenpointner et al., 2018). This is likely to occur due to the differential expression of ion channels in medium- and large-diameter A fibres when compared to small-diameter C fibres. Fibre types, such as RA, SA and AM fibres, are more prone to oxaliplatin-induced action potential bursts and spontaneous discharges in response to cold and mechanical stimuli when compared to other A fibres, such as DH fibres. It would also explain why only a subset of these fibres are more amenable to oxaliplatin-induced hyperexcitability to mechanical and cold stimuli. The differential expression pattern of ion channels is likely to explain this. Not all AM, RA or SA fibres were affected by oxaliplatin. It is possible that these fibre classes are functionally heterogeneous (Lopes et al., 2017), and it cannot be ruled out that oxaliplatin application achieved different levels of exposure to different receptive fields.

Notably, acute oxaliplatin application recruited cold sensitivity in all A fibre classes. This may provide a cellular mechanism for the basis of cold hypersensitivity and cold-evoked paraesthesias, a hallmark symptom of oxaliplatin treatment (Attal et al., 2009; Descoeur et al., 2011; Deuis et al., 2013; Wilson et al., 2002). Importantly, A fibres displayed oxaliplatin-induced cold-evoked action potential bursts. The maintenance of high frequency and repetitive firing during and after cold ramps may indicate a mechanism for the oxaliplatin-induced neuropathic pain. The acute effects of oxaliplatin are likely to be mediated by voltage-gated ion channels (Adelsberger et al., 2000). The effects of the anticancer drug on A fibres may be explained by the exclusive expression of $Na_v1.6$ in medium- to large-diameter sensory neurons (Cummins et al., 2005). Indeed, a study by Sittl *et al.* also reported that oxaliplatin treatment induced action potential bursts to cold stimuli in A fibres, but not C fibres. This was absent in preparations taken from *Scn8a*$^{med/med}$ mice which lacked functional $Na_v1.6$ channels (Sittl et al., 2012). Oxaliplatin also directly influences the kinetics of $Na_v1.6$ channels, which prolonged the opening time of the channel and results in resurgent and persistent currents (Cummins et al., 2005; Sittl et al., 2012). In addition, selective inhibition of $Na_v1.6$ was able to reverse the acute oxaliplatin-induced cold and mechanical allodynia in mice (Deuis et al., 2013, 2014). Another potential target in driving increased excitability in A fibres after oxaliplatin treatment is axonal K_v7 channels. Acute treatment with the anticancer drug increased the duration and amplitude of A fibre compound action potentials (Sittl et al., 2010). This was suppressed in the presence of flupirtine, which activates axonal K_v7 channels, and may indicate a possible analgesic strategy (Sittl et al., 2010). Therefore, the ability to increase and enhance currents of channels which negatively regulate neuronal hyperexcitability, particularly K^+ channels is important. An example of this includes increasing

leak current from voltage-gated potassium channels which may act as excitability brakes in neurons. $Na_v1.6$ is a potential target as it can be modulated directly by oxaliplatin and blockade of it can reverse the acute effects of the drug which fit the clinical time course. This is in contrast to other mechanisms with have proposed expressional changes and altered function of ion channels expressed in C fibres (Descoeur et al., 2011; Gauchan et al., 2009; Nassini et al., 2011; Zhao et al., 2012).

We also report a gain of cold sensitivity in CM fibres, which were previously insensitive to cold. In addition, CMC fibres showed increased impulse discharges after oxaliplatin treatment. This is likely to be important to the pathophysiological mechanism involved in cold-evoked dysaesthesias after oxaliplatin treatment (Pachman et al., 2015; Tofthagen et al., 2013b). The majority of AM and CM nociceptors do have the ability to detect and respond to noxious cold temperatures (Basbaum et al., 2009; Purves et al., 2001). However, oxaliplatin sensitised both fibre types to cause novel cold sensitivity and for afferent fibres to discharge action potentials at cool, innocuous temperatures. The latter phenomenon was more common in AM fibres compared to CM fibres, shown by increased threshold temperatures of activation towards warmer temperatures. Gain of cold sensitivity in CM fibres also suggests that there may be ion channels that are commonly expressed in A and C fibres which can be modulated by oxaliplatin. This is most likely to be ion channels that govern excitability in neurons such as Na_v or K_v channels (Adelsberger et al., 2000). Two K_v channels which are expressed in both A and C fibres are $K_v1.1$ and $K_v2.1$ (Usoskin et al., 2015; Zeisel et al., 2018). However, there is greater expression of both channels in myelinated, large-diameter A fibres when compared to unmyelinated, small-diameter C fibres (Rasband et al., 2001; Tsantoulas et al., 2014). Shaker-like $K_v1.1$ and $K_v1.2$ channels form the molecular counterpart underlying the excitability brake current, I_{KD}. These channels have been shown to have a significant role

in driving cold sensitivity and allodynia in peripheral sensory neurons (González et al., 2017). In fact, a reduction in the I_{KD} current in response to neuronal damage was able to induce cold sensitivity in previously cold-insensitive neurons and to decrease threshold temperatures in cold-sensitive neurons, providing a strong molecular basis for cold hypersensitivity (González et al., 2017). $K_v2.1$ is a delayed rectifier channel which is important in regulating neuronal excitability (Liu and Bean, 2014; Speca et al., 2014). Although it has not previously been implicated in oxaliplatin-induced hyperexcitability, it may play an important role when activated or inhibited in the maintenance of oxaliplatin-induced repetitive firing. The increased expression in A fibres compared to C fibres may enable greater sensitivity to cold and mechanical treatment after acute oxaliplatin treatment. This channel is important for hyperexcitability states as discussed in detail in Chapters 6 and 7.

In addition, another study has reported oxaliplatin-induced repetitive firing and bursting discharges in sensory neurons using the phrenic nerve hemi-diaphragm preparation (Webster et al., 2005). A single stimulus after oxaliplatin was able to evoke multiple abnormal potentials. This pattern of action potential bursts and post-discharge stimulus highlights the irreversible actions of oxaliplatin to peripheral sensory afferent axons or ion channels. The ability of oxaliplatin to interact directly with and alter Na_v channel kinetics is important in increasing depolarised current and hyperexcitability (Adelsberger et al., 2000; Webster et al., 2005). Use of tetrodotoxin (TTX) in the presence of oxaliplatin abolishes action potential bursts, further implicating Na_v channels (Webster et al., 2005). However, TTX does block most, if not all activity. $Na_v1.6$ has been shown to be a particularly important isoform in generating persistent currents which results in oxaliplatin-induced action potential bursts (Sittl et al., 2012). In addition, oxaliplatin has been shown to induce spontaneous bursts of rapid whole

nerve terminal calcium transients (Webster et al., 2005). Activation of voltage-gated calcium channels are thought to underlie action potential bursts in hippocampal, thalamic and cerebral Purkinje neurons (Williams and Stuart, 1999). However, this would have to be assessed in sensory neurons to see whether it is also likely to be the case here. Overall, it is likely that there is more than one mechanism to explain oxaliplatin-induced action potential bursts.

In recordings conducted in preparations taken from treated mice, we report increased spontaneous discharges in fibres. This may be a correlate for oxaliplatin-induced paraesthesias and pain. In addition, we show increased cold sensitivity in fibres from oxaliplatin-treated mice compared to vehicle-treated mice 4 days after treatment. This was expected as the behavioural phenotype was apparent in mice in the days prior to the dissection. Interestingly, we observed a greater sensitivity to cold in single- and multi-unit C fibres compared to A fibres in these preparations. This does not align with results in naïve preparations treated acutely with oxaliplatin, suggesting different mechanisms. One possibility could be that A fibres are more susceptible to activity-induced block. Indeed, cold has been reported to block Aδ, Aβ and then C fibres (Douglas and Malcolm, 1955; Nathan and Sears, 1963). In addition, irreversible differential A fibre block has been achieved by local heating to the nerve (Klumpp and Zimmermann, 1980). In our study, oxaliplatin blocked the activity of some A fibres after acute treatment as shown by the silencing of AM and RA fibres to mechanical stimulation when compared to vehicle. One study has reported K^+-dependent excitation block in myelinated A fibres in response to repetitive stimulation (Brazhe et al., 2011). Periods of repetitive activity result in potassium ion channel accumulation under the myelin. This results in an osmotic gradient, so water follows and causes swelling of the myelin.

Permanent reorganisation of the myelin can occur if the efflux of K^+ ions doesn't occur fast enough (Brazhe et al., 2011). This eventually can result in lower myelin resistance, which in turn leads to more pronounced depolarisations in the paranodal axonal membranes. The compromised resistance from the rearranged myelin can increase K^+ efflux, which in turn will raise the excitation threshold (Brazhe et al., 2011). However, most studies in the literature report that reversible block and recovery is faster in C fibres compared to A fibres as shown by parameters including electrical stimulation (Campero et al., 2009; Serra et al., 1999), analgesics (Nathan and Sears, 1963) and pressure (Gasser and Erlanger, 1929b). It may be possible that oxaliplatin also blocks C fibres but they recover faster than large-diameter A fibres, which has been reported previously (Klumpp and Zimmermann, 1980; Nygaard et al., 1998).

Furthermore, transcriptional changes and immune changes are likely to have occurred in the days following oxaliplatin treatment in mice and dissection. This provides another mechanism to explain the greater cold sensitivity in C fibres when compared to A fibres. Many studies have reported upregulation of TRPM8, TRPA1 and potassium channels including TREK-1 and TRAAK after oxaliplatin treatment (Anand et al., 2010; Descoeur et al., 2011; Gauchan et al., 2009; Kono et al., 2012; Nassini et al., 2011; Noël et al., 2009b; Zhao et al., 2012). These channels are all expressed primarily on small-diameter C fibres (Deuis et al., 2013; Usoskin et al., 2015). Therefore, they are likely to contribute to C fibre functional sensitivity to cold stimuli. It may be possible that oxaliplatin-induced hyperalgesia is mediated by C fibres in the longer term, but A fibres following acute treatment.

In summary, we report the effects of acute and direct oxaliplatin treatment in naïve skin-saphenous nerve preparations. We investigated the changes elicited to the functional properties of six different classes of A and C fibres in response to mechanical and cold stimuli. Acute oxaliplatin treatment to the receptive field of individual fibres sensitised all fibre types to cold ramps. A fibres also displayed functional abnormalities in response to mechanical stimulation. Oxaliplatin-induced gain-of-function cold sensitivity often resulted in action potential bursts in A fibres. It is likely that the acute cold hypersensitivity and paraesthesias reported in the clinic after oxaliplatin treatment are primarily mediated by A fibres, since the changes to the adaptation properties of these fibres would reflect symptoms such as cold-evoked paraesthesias. In contrast, datasets from longer term treatment of oxaliplatin *in vivo* remain incomplete and conclusions cannot be made with certainty. From the data presented here, oxaliplatin treatment *in vivo* affected C fibres more than A fibres in single- and multi-unit recordings. The greater cold sensitivity in C fibres after oxaliplatin treatment may be due to indirect changes such as transcription of ion channels, and treatment timings would enable this. Alternatively, it is possible that different fibres have different concentration response relationships for oxaliplatin.

6. Screening of potential ion channel targets for interventions

6.1 Introduction

Many ion channel candidates have been proposed or shown to underpin peripheral oxaliplatin-induced hyperexcitability. The direct and indirect role of ion channels has been studied extensively, particularly with respect to the mechanisms oxaliplatin-induced cold hypersensitivity. Previously identified targets of oxaliplatin-induced hyperexcitability included voltage-gated sodium (Na_v), potassium (K_v) and calcium channels (Ca_v), as well as hyperpolarisation-activated and cyclic nucleotide-gated (HCN) channels (Deuis et al., 2013; Han et al., 2017a; Lolignier et al., 2015; Luiz et al., 2019; Resta et al., 2018; Sittl et al., 2010, 2012; Young et al., 2014), all of which regulate, influence and act as effectors in the excitability of neurons. In addition, other targets such as TRPA1 and TRPM8 have been demonstrated to be important for oxaliplatin-induced hyperexcitability (Descoeur et al., 2011; Gauchan et al., 2009; Kono et al., 2012; Nassini et al., 2011; Zhao et al., 2012). In some cases, these ion channels are directly modulated by the oxaliplatin molecule in naïve tissues e.g. Na_v and K_v channels in dorsal root ganglia (DRG) neurons and at the terminal level of primary afferent neurons (Adelsberger et al., 2000; Lolignier et al., 2015; Sittl et al., 2012). Other targets were defined based on antagonism *in vivo* (Descoeur et al., 2011; Deuis et al., 2013; Resta et al., 2018) or upregulation of the target in sensory neurons (Descoeur et al., 2011; Gauchan et al., 2009; Nassini et al., 2011). We sought to confirm and consolidate the list of existing targets as well as identify novel targets using a medium-throughput screening (MTS) technique.

Oxaliplatin does not cross the blood-brain barrier (Branca et al., 2018), the side effects of oxaliplatin are almost exclusively restricted to the peripheral nervous system. Consequently, any direct effects on neurons of the central nervous system (CNS) are less studied as they are not likely to be responsible for the specific side effects such as cold allodynia seen in patients

treated with oxaliplatin. Given this, using isolated neurons of the peripheral nervous system would be the ideal candidate for HTS for ion channel targets *in vitro.* This would also be additive to the findings from the Ca^{2+} imaging results chapter (Chapter 3), where we assessed the role of TRP channels in oxaliplatin-induced hyperexcitability. However, mice have too few DRG neurons for these to be used for high and medium throughput screening (HTS/MTS) that require high densities of cells. By contrast, the abundance of cortical neurons makes them attractive for plate assays and MTS/HTS.

Transcriptomic analysis has determined the relative expression levels of ion channels commonly involved in nociception in sensory neurons (Table 6-1) (Parisien et al., 2017; Roth et al., 2006; Zeisel et al., 2018). Roth *et al.* provide a direct comparison of the gene expression between DRG neurons and cortical neurons (Roth et al., 2006). The expression of ion channels such as $Na_v1.9$ is absent in the CNS. However, many, if not most other channel types and isoforms are expressed at similar or equal levels (summarised in Table 1). Therefore, cortical neurons serve as an appropriate model system for high-throughput investigations of the mechanisms underlying oxaliplatin-induced hyperexcitability.

The multielectrode array system (MEA) is designed to study the synaptic activity of cortical neurons *in vitro*. MEA systems overcome the significant time required for single-cell recording and behavioural assays and can record activity of many cells at one time (Liu et al., 2012; Massobrio et al., 2015). MEA systems have been developed and refined as tools for drug discovery and design as they are considered to be a high-throughput technique (Massobrio et al., 2015). Therefore, we designed and refined a method for MTS of oxaliplatin-induced hyperexcitability using murine cortical neurons *in vitro*. We show that oxaliplatin causes

robust hyperexcitability of cortical neurons. Finally, we found that the oxaliplatin-induced hyperexcitability was sufficient to test the effect of several ion channel blockers and gating modifiers *in vitro*. We show for the first time, a reduction in oxaliplatin-induced hyperexcitability by the $K_v2.1$ gating modifier guangxitoxin-1E.

6.2 Aims

The aims of this chapter were to use a medium throughput technique to screen ion channels as targets involved in oxaliplatin-induced hyperexcitability. Some of the targets that were chosen as they have already been proposed to play a role in oxaliplatin-induced hyperexcitability, others were novel targets. The cortical neuron culture served as a good model of sensory neurons as there is commonality in the expression of key ion channels (Table 6-1) that have been implicated in oxaliplatin-induced hyperexcitability. By reducing the number of possible targets in this mechanism using pharmacological intervention of a candidate channels, it was possible to later evaluate their/its importance in sensory neurons.

Table 6-1: Transcriptomic analysis for the expression of ion channels involved in nociception in DRG and cortical neurons

N.B. the darker the shade of green, the greater the expression level of the ion channel.

Ion channel	Species	Hs	Hs	Hs
	Platform	Affymetrix	Affymetrix	Affymetrix
	Protocol	hta_20	hgu133plus2	hgu133plus2
	Study	(Parisien et al., 2017)	(Roth et al., 2006)	(Roth et al., 2006)
	Specimen	**Dorsal root ganglia**	**Dorsal root ganglia**	**Cerebral cortex**
$Na_v1.1$	**SCN1A**	25.1	14.1	81.5
$Na_v1.6$	**SCN8A**	40.9	36.6	87.6
$Na_v1.7$	**SCN9A**	168.8	21.1	2.4
$Na_v1.8$	**SCN10A**	90.2	20.4	8.6
$Na_v1.9$	**SCN11A**	210.2	33.4	2.6
$K_v1.1$	**KCNA1**	119.8	109.1	74.9
$K_v1.2$	**KCNA2**	126.6	87.9	102.4
$K_v2.1$	**KCNB1**	48.4	63.4	204.5
$K_v2.2$	**KCNB2**	83.6	22.5	24.1
$K_v7.2$	**KCNQ2**	33.1	22.2	134.3
$K_v7.3$	**KCNQ3**	56.4	32.8	62.7
$Ca_v2.1$	**CACNA1A**	49.1	62.1	279.8
$Ca_v2.2$	**CACNA1B**	42.1	29.6	58.8
$Ca_v3.1$ (T type)	**CACNA1G**	16.6	19.9	26.9
$Ca_v3.2$ (T type)	**CACNA1H**	26.1	19.9	20.6
$Ca_v3.3$ (T type)	**CACNA1I**	19.3	19.6	23.6
HCN1	**HCN1**	172.2	20.3	18.3
HCN2	**HCN2**	73.7	15.7	29.8
HCN3	**HCN3**	21.0	13.5	19.3
HCN4	**HCN4**	84.5	15.1	16.6
TWIK-1	**KCNK1**	15.4	58.1	169.6
TREK-1	**KCNK2**	21.2	5.8	5.5
TASK-1	**KCNK3**	47.6	60.2	58.2
TRAAK-1	**KCNK4**	0	8.7	10.1
TASK-2	**KCNK5**	20.1	9.2	6.0
TWIK-2	**KCNK6**	51.4	9.2	8.1
TWIK-3	**KCNK7**	34.2	10.1	12.3
TASK-3	**KCNK9**	13.4	12.4	16.9
TREK-2	**KCNK10**	13.2	17.1	44.8
THIK-2	**KCNK12**	50.8	84.6	29.1
THIK-1	**KCNK13**	23.7	6.6	6.4
TALK-1	**KCNK16**	19.9	16.5	19.0
TALK-2	**KCNK17**	20.9	11.3	9.9
TRESK-2	**KCNK18**	20.8	0	0
TRPC5	**TRPC5**	12.2	2.8	3.1
TRPA1	**TRPA1**	12.0	7.8	4.7
TRPM8	**TRPM8**	10.3	10.1	11.0

6.3 Methods

6.3.1 Animals

All studies were carried out in strict accordance with Evotec AG policies, AAALAC guidelines, the European Directive 2010/63/EU and the German Animal Welfare Act. The protocol was approved by the Hamburg Animal Care and Use committee. Female mice were kept on a 12 hour light-dark cycle and given food and water ad libitum. 8 - 13 week old C57BL/6J female mice were mated with age matched C57BL/6J male mice. The breeding pairs were set up (Zenti2 breeding facility at UKE) in the afternoon and a vaginal plug check was conducted the next morning in female mice. Mice with vaginal plugs were assumed to be pregnant and plug day was calculated as E0.5 (embryonic stage 0/0.5). Embryos were dissected at the E16 stage and approximately 7 - 9 embryos were used per dissection.

6.3.2 Compounds and solutions

Dissociation buffer (used when dissecting cortical neurons) containing kynurenic acid (1 M, Sigma), HEPES (5 mM, Sigma), $MgCl_2$ (10 mM, Sigma), D-Glucose (17 mM, Sigma) in Hanks' balanced salt solution with phenol red (HBSS, Gibco) adjusted to pH 7.4 using 1 M NaOH (Merck) was prepared and frozen as 25 ml aliquots. One aliquot was used per dissection and diluted 1:10 with HBSS. Preparation medium, required for astrocyte dissection (Earle's balanced salt solution, Sigma) containing penicillin-streptomycin (10,000 U/ml, Gibco), 45 % glucose stock for final concentration of 0.1 % (Sigma) and 1 M HEPES stock for final concentration of 10 mM (Gibco) was used.

Serum-free medium composed of minimum essential medium (MEM +L-Glu, -HEPES, Gibco) containing penicillin-streptomycin and glutamax (Gibco) and growth medium composed of

Dulbecco's minimum essential medium (DMEM + 1 g/l glucose, glutamax and pyruvate, Gibco) containing penicillin-streptomycin and fetal bovine serum (FBS), heat inactivated (10 %, Gibco) were used during cell isolation after dissection.

Neurobasal medium (Invitrogen) with addition of 2 % B-27 supplement, 2 mM L-Glutamine (Invitrogen) and 10,000 U/mL penicillin-streptomycin (PS) (Invitrogen) was used for cortical neuron and astrocyte seeding and medium change in the MEA plates. Astrocyte growth medium was used for the maintenance of astrocyte flasks in culture using DMEM (+ 1 g/l glucose, glutamax and pyruvate, Gibco) with 10 % heat inactivated fetal bovine serum (FBS) (Gibco) and 10,000 U/ml (100X) PS.

Compounds used for MEA experiments included: oxaliplatin (Sigma-Aldrich), A-803467 (Alomone labs), guangxitoxin-1E (Alomone labs), 4,9-Anhydrotetrodotoxin (Alomone labs), Mibefradil dihydrochloride hydrate (Alomone labs), Tetrodotoxin citrate (Tocris), 4-Aminopyridine (Sigma), Ivabradine hydrochloride (Sigma), Spadin (Phoenix pharmaceuticals), Amitriptyline (Sigma) and Retigabine (Sigma).

Table 6-2: Ion channel modulators and their EC/IC_{50} values

Ion channel target	*Compound name*	*EC/IC_{50}*
Na_v	Tetrodotoxin citrate	1 nM- 30 nM
K_v	4-Aminopyridine	147 μM
HCN	Ivabradine hydrochloride	2 - 3 μM
$Na_v1.8$	A-803467	8 nM
$Na_v1.6$	4,9 -anhydroTTX	5.5 nM
TREK-1	Spadin	71 nM
$K_v1.1$	Amitriptyline	22 μM
$K_v2.1$	Guangxitoxin-1E	1 nM
$K_v7.2/7.3$	Retigabine	1.6 μM
T-type Ca_v, $Na_v1.8$, $Na_v1.9$	Mibefradil	2 μM

References used for table: (Bucchi et al., 2006; Foti et al., 2011; Gunthorpe et al., 2012; Herrington, 2007; Heurteaux et al., 2011; Kasteel and Westerink, 2017; Punke and Friederich, 2007; Rosker et al., 2007; Stephens et al., 1994).

Dimethyl sulfoxide (Thermo Fisher Scientific), deionised water (Fisher chemicals) and absolute ethanol (VWR chemicals) were used as solvents for compounds as per the manufacturer's instructions.

6.3.3 Dissection

Mice were euthanised with CO_2 (80 %) using a gradient approach. The placenta with embryos attached was removed and the embryos were detached from the amniotic sac. The heads of pups were decapitated and washed using ice cold calcium and magnesium-free PBS (Gibco) and fixated to enable removal of the skin and skullcap. The brain was dissected and kept in dissociation buffer. The cerebellum was pricked to fixate the brain and the bulb, meninges and both hemispheres of the brainstem were removed. Cortices were then collected into a falcon tube containing ice cold preparation medium. Astrocytes were also dissected from the same animal as they were needed for the co-culture with cortical neurons.

6.3.4 Neuron isolation

Once all cortices were isolated, medium was removed using a vacuum pump and cortices were washed twice with 10 ml serum-free medium and once with 10 ml growth medium. The cortices were triturated to create a single cell suspension in three rounds, each round consisting of ten times using a 100 µl pipette tip in 2 ml medium. Growth medium was filled up to 35 ml and cells were centrifuged for 10 minutes at 800 revolutions per minute (rpm). Once the supernatant was removed, the cell pellet was resuspended in an appropriate volume of growth medium (10 - 20 ml). Cells were counted using the Luna-FL™ automated fluorescence cell counter (Logos Biosystems) using 18 µl cell suspension and 2 µl acridine orange/ propidium iodide stain, a nucleic acid binding dye (Cat. # F23001, Logos Biosystems).

6.3.5 Preparation of MEA plates

MEA plates were composed of 48-wells with each well containing an array of 16 embedded gold electrodes (~40 - 50 µm diameter, 350 µm centre-to-centre spacing; schematic 3), with integrated ground electrodes, for a total of 768 channels (Axion Biosystems, Atlanta, GA). MEA wells were coated with 0.07 % polyethyleneimine (PEI) solution (Sigma) which was diluted in a 1X borate buffer, made from a 20X stock (Thermo Fisher Scientific) for 1 hour at room temperature one day prior to cell plating (DIV-1). Plates were rinsed with sterile, deionised water four times after removing the PEI solution and left to air dry in a biological safety hood overnight.

6.3.6 Cell culture

6.3.6.1 Cortical neuron seeding (DIV0)

Laminin (15 µl; L2020 1 mg/ml; Sigma) droplets were dispensed onto each well and incubated for 1 hour at 37 °C, 5 % CO_2 prior to cortical neuron plating. Cortical neurons were centrifuged at 1500 rpm for 5 minutes before resuspension in the necessary volume of neurobasal medium to give a density of 75,000 cells per well. 15 µl of cell suspension was added into each well after removal of the laminin droplet. Plates were incubated for 1 hour at 37 °C, 5 % CO_2 with sterile water placed in corner to prevent evaporation before gently flooding each well with 600 µl (2x 300 µl) neurobasal medium. 50 % medium change took place every 3/4 days.

6.3.6.2 Astrocyte cell culture

Astrocytes were harvested and cultured in T175 cm^2 tissue culture flasks for 2 - 4 weeks prior to seeding. Complete media change took place weekly. Astrocytes were kept in astrocyte

growth medium. Frozen astrocytes were used in plates 1 and 5. Vials were thawed on the day of seeding and were prepared from the cell count stage.

6.3.6.3 Astrocyte preparation and seeding

Astrocytes were plated on DIV03 (3 days post cortical neuron seeding). Flasks with at least 80 % confluence were used. Medium was aspirated and cells were washed once with 10 ml calcium and magnesium-free PBS. Cells were then treated with 7 ml 0.25 % trypsin and incubated for 3 - 4 minutes at 37 °C, 5 % CO_2. Trypsinisation was stopped by addition of 14 ml astrocyte growth medium and any remaining adherent cells were loosened into a cell suspension by pipetting the solution several times. The entire volume of the cell suspension was centrifuged for 5 minutes at 1000 rpm. The supernatant was removed, and the cell pellet resuspended in 1 - 2 ml of neurobasal medium. Cells were counted using the Luna cell counter as described above. The required volume of cell suspension for a density of 30,000 astrocytes per well was removed and added to 14.4 ml neurobasal medium. 300 µl of medium from each well was removed and replaced with astrocyte-containing medium.

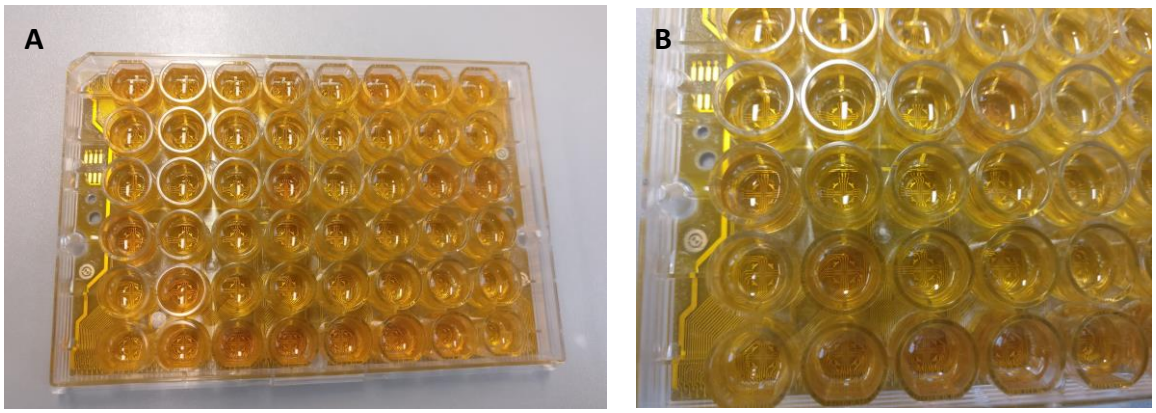

Schematic 3 48-well MEA plates.

A) All wells filled with 600 µl neurobasal medium B) zoomed in section of 48-well plate showing 16 gold embedded electrodes.

6.3.7 MEA experiment

Compound application was conducted on DIV13. The first plate was designed to generate an oxaliplatin concentration-response curve (0.2 - 100 µM) over time (0 - 27 hours). Two subsequent plates were designed to assess the effects of pharmacological inhibitors and modulators of a selection of Na^+, K^+, HCN and Ca^{2+} permeant channels. These modulators were co-applied with 100 µM oxaliplatin on one plate and alone on the other plate. Compounds dissolved in DMSO were applied to give a final DMSO concentration of 0.3 %. Once compounds were applied to each well, MEA plates were incubated at 37 °C, 5 % CO_2 and this was regarded as the starting time for all experiments. For the final plate, guangxitoxin and ivabradine stocks were dissolved in water and then dissolved in neurobasal medium when co-applied with oxaliplatin (10 - 100 µM).

6.3.8 Recordings on Axion Maestro system

Recordings for the monitoring phase were conducted between DIV05 and DIV12. All experiments were conducted at 37 °C after a 5-minute equilibration period after the MEA plate was placed into the head stage. Spontaneous activity of neuronal networks was recorded every day for 7 minutes. The monitoring period of recordings enabled the optimal day for compound application to be selected based on the mean firing rate of all wells (> 1 Hz). In all experiments, DIV13 was found to be the day of optimal electrical activity and was used as compound application day. Recordings were made on DIV13 prior to compound application (pre-treatment) and then between 0 - 27 hours after compound application.

6.3.9 Software and Analysis

The MEA set up included the Axion Maestro system (Axion Biosystems) head stage, a temperature controller, a CO_2 controller and PC with the Axion Integrated Studio Software (AxIS2.5.1) software (Axion BioSystems).

During recordings, a heat map was visible for individual wells within the 48-well plate depicting the level of activity in all wells. Activity levels increased at a steady rate during the monitoring phase and reached peak activity levels by DIV12-13. The action potentials per well and the synchrony in all wells could also be assessed in the software.

6.3.9.1 Analysis criteria

Voltages were recorded at 3 kHz and filtered at 200 Hz. A spike detection criterion of > 6 SDs above background signals was used to separate action potential spikes from noise. Active electrodes were defined as > 1 spike over a 300 second analysis period. Firing frequencies were averaged among all active electrodes from wells of the same treatment group.

6.3.9.2 Analysis and statistics

MEA data was analysed for network bursts using AxIS software (version 2.5.1, Atlanta, GA). The event time denotes the time at which network bursts occurred in individual wells for the 5-minute period. All data is presented as mean ± S.E.M. and was tested for normality and the corresponding parametric i.e. Two-way repeated measures (RM) ANOVA or non-parametric tests i.e. Mann-Whitney *U* test were conducted for statistical analysis using Prism 8 (version 8.3.0, GraphPad, San Diego, CA). *P* values were considered significant when $P < 0.05$.

6.4 Results

6.4.1 Oxaliplatin causes high frequency firing of cortical neurons

Oxaliplatin treatment (50 - 100 µM) produced high frequency and repetitive firing in cortical neurons. The impulse discharge frequency increased with increasing oxaliplatin concentrations, and the number of action potentials discharged was increased compared to vehicle. Network bursts were defined as a collection of 10 spikes from a minimum of 25 % of participating electrodes in a well, each separated with an inter-spike interval (ISI) of no more than 100 milliseconds (Cotterill et al., 2016) (Figure 6-1). Oxaliplatin increased the number of network bursts in cortical neurons in a concentration-dependent manner (Figure 6-2). Recordings were conducted at various time points after oxaliplatin addition. However, the EC_{50}, defined as the concentration of a drug required to produce 50 % of the maximal response, remained consistent and stable for up to 3 hours (Figure 6-2). The EC_{50} value was 18 ± 1 µM at 1 hour, 13 ± 1 µM at 2 hours and 20 ± 1 µM at 3 hours. In addition, the maximal response occurred after 1 hour incubation with 100 µM oxaliplatin (Figure 6-2). Maximal network burst firing was observed in response to the highest concentration used, 100 µM oxaliplatin (n = 173), after 1 hour incubation (Figure 6-1) compared to vehicle (n = 110) and closely followed by 50 µM at 2 hours (supplementary figure 6-I C). This increase in network bursts was accompanied by clusters of irregular and high frequency firing which was absent in vehicle-treated wells. In contrast, we observed a regular pattern of network bursts evoked by lower concentrations of oxaliplatin, without apparent clusters of network bursts (10 µM; supplementary figure 6-I B) and after vehicle (water; supplementary figure 6-I A). Based on these findings, 100 µM oxaliplatin was used in the subsequent pharmacological experiments, since these conditions generated a maximal activity in cortical neurons.

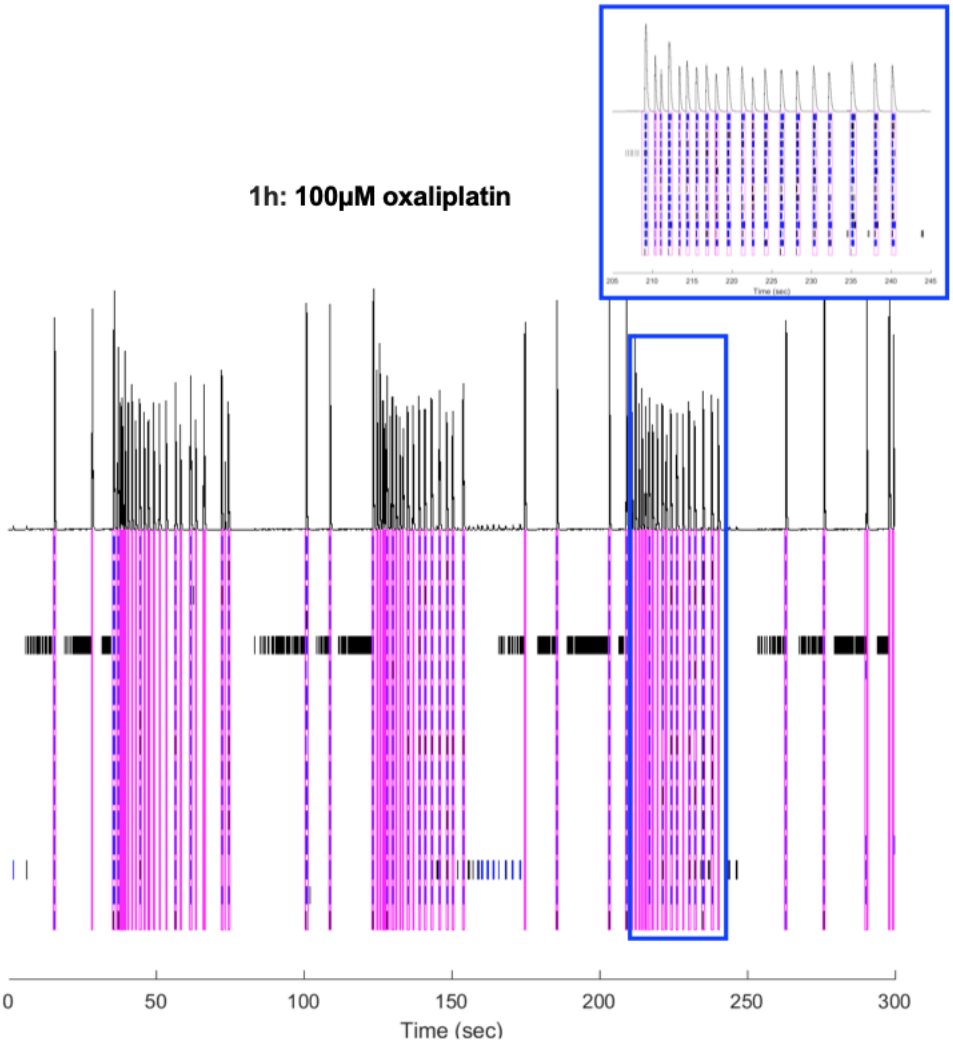

Figure 6-1 Activity of cortical neurons after 1 h incubation with 100 µM oxaliplatin.

Raster plot depicts the firing patterns of neurons across 16 electrodes after 100 µM oxaliplatin. Each black spike in the lower half of the image represents a detected spike. Blue lines represent single channel bursts – a collection of at least 5 spikes, each with ISI of no longer than 100 milliseconds. The number of network bursts (pink lines) are defined as > 10 spikes in a minimum of 25 % of electrodes in a well with the frequency histogram for network bursts (black lines at top) over 5 minutes. Inset panel shows zoom of histogram peaks representing network burst events. Blue lines can be used to calculate the total number of action potential occurring within each network burst. Oxaliplatin (100 µM, 1 h) increases network burst firing in cortical neurons (n = 173 vs n = 110 in vehicle).

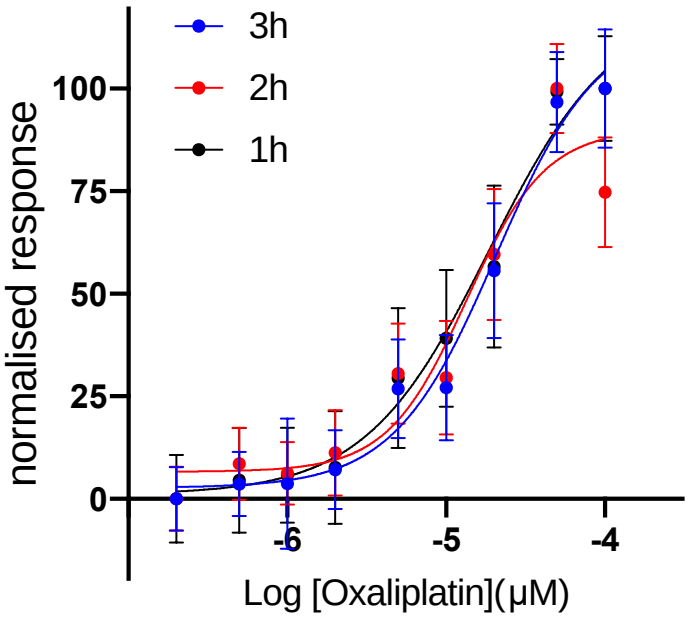

Figure 6-2 Concentration-dependent increase in network burst firing unchanged by oxaliplatin incubation duration.

Concentration-response curve of oxaliplatin-induced firing 1 - 3 h after application. Network burst events normalised to maximum network burst firing. The EC50 value was 1 h: 18 ± 1 µM, 2 h: 13 ± 1 µM and 3 h: 20 ± 1 µM, n = 3 wells, 1 plate, 1 mouse. Data presented as mean ± S.E.M.

6.4.2 Oxaliplatin acutely reduces inter-burst interval in cortical neurons

The increase in the number of network bursts was accompanied by a reduction in inter-burst intervals (IBI; time between network bursts). Therefore, the neurons treated with 100 µM oxaliplatin fired many action potentials over a shorter period of time compared to vehicle. There was no difference between the IBIs prior to treatment (Figure 6-3A) or in the vehicle treatment over time (supplementary figure 6-II A). The peak frequency for IBIs was significantly reduced after 1 hour from 6.3 ± 0.5 seconds for vehicle (n = 110) to 1.3 ± 0.5 seconds for 100 µM oxaliplatin (n = 173) (Mann-Whitney *U* test, $P < 0.05$; Figure 6-3 B). This was also seen after 2 hours where the peak frequency for IBIs was reduced for both 100 µM and 50 µM oxaliplatin to 1.8 ± 0.5 seconds compared to vehicle (6.0 ± 0.5 seconds) (Mann-Whitney *U* test, $P < 0.05$) (supplementary figure 6-II A). In contrast, the IBIs were significantly increased with 100 µM and 50 µM oxaliplatin after 24 hours (Mann-Whitney *U* test, $P < 0.05$) compared to vehicle (supplementary figure 6-II B), demonstrating reduced excitability. The frequency was reduced at both concentrations when compared to vehicle (vehicle: n = 119, 50 µM: n = 45, 100 µM: n = 19). Overall, the peak frequency of IBIs was reduced after acute treatment (1 - 2 hours) with 100 µM oxaliplatin to indicate peak oxaliplatin-induced hyperexcitability. This was reversed after 24 hours when the IBIs had increased, indicating a reduced excitability.

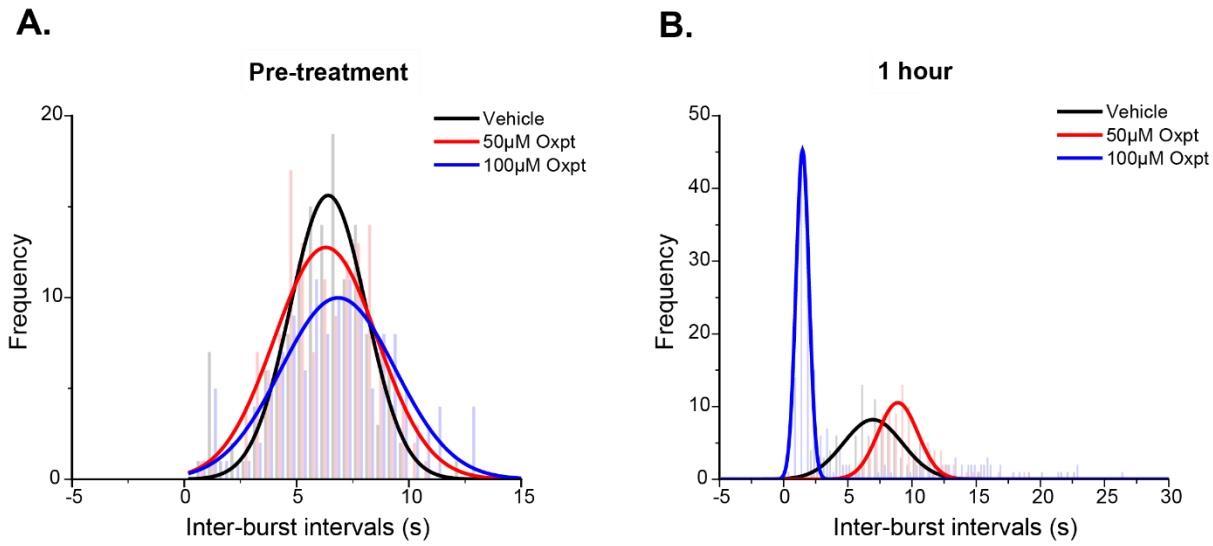

Figure 6-3 Reduction in IBIs when cortical neurons were treated with 100 µM oxaliplatin for 1 hour.

A) No difference in the peak frequency of IBIs before treatment with vehicle (water; black line), 50 µM (red line) and 100 µM (blue line) oxaliplatin. B) 100 µM (blue line) oxaliplatin significantly reduces the peak frequency of IBIs compared to vehicle at 1 h (100 µM 1.3 ± 0.5 s oxaliplatin, n = 173, vehicle 6.3 ± 0.5 s, n = 110, Mann-Whitney *U* test, $P < 0.05$).

6.4.3 Reduced oxaliplatin-induced hyperexcitability after longer incubation periods

In line with the findings with IBIs, we demonstrated that the mean firing frequency was reduced over time in the presence of 100 µM oxaliplatin (Figure 6-4). The firing frequency after 24 hours in the presence of 100 µM oxaliplatin was reduced significantly compared to vehicle (100 µM 0.68 ± 0.06 Hz; vehicle 2.62 ± 0.18 Hz) and baseline (0 hours) (100 µM at 0 h 1.97 ± 0.07 Hz, Two-way RM ANOVA, $P < 0.05$). In contrast, the mean firing frequency was increased significantly at earlier time points (Figure 6-4). There was a significant increase in the firing rate after 2 hours when 100 µM oxaliplatin was compared with vehicle (100 µM 4.76 ± 0.23 Hz; vehicle 2.13 ± 0.19 Hz) and 0 hours (100 µM at 0 h 1.97 ± 0.07 Hz, Two-way RM ANOVA, $P < 0.05$).

The number of action potentials fired during network bursts was reduced in the presence of the highest concentrations of oxaliplatin (50 and 100 µM) after 24 hours of incubation (vehicle 298 ± 10 action potentials (APs); 50 µM 113 ± 11 APs; 100 µM 289 ± 49 APs, Mann-Whitney *U* test, $P < 0.05$ (vehicle vs 50 µM)) (Figure 6-5 A). The average number of action potentials fired after 27 h was reduced compared to vehicle (vehicle 275 ± 10 APs; 50 µM 106 ± 10 APs; 100 µM 178 ± 32 APs, Mann-Whitney *U* test, $P < 0.05$) (Figure 6-5 B). To examine whether prolonged exposure to high concentrations of oxaliplatin caused cortical neuron death, the viability of cells was examined by conducting presto blue cell viability assays. Cells were viable as confirmed by their ability to perform reduction processes and did not reveal any reduced viability compared to vehicle (data not shown).

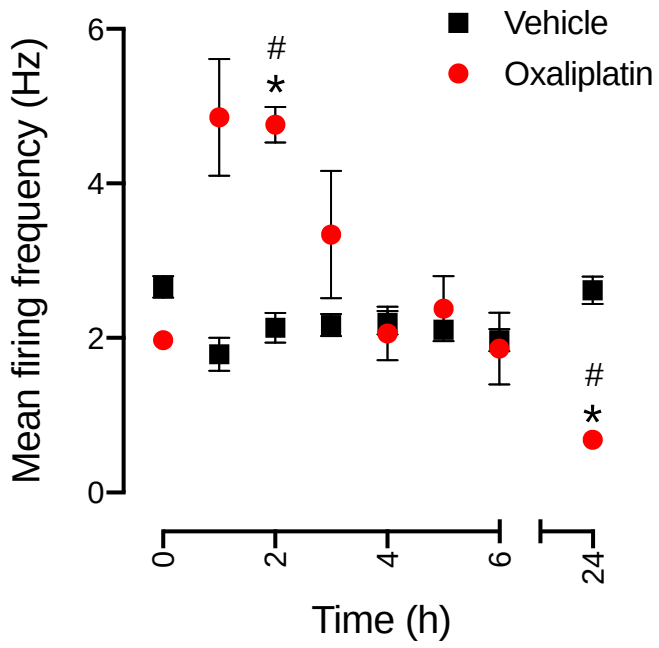

Figure 6-4 Impulse frequency over time in the presence of oxaliplatin.

100 µM (red circles) oxaliplatin significantly increased the mean firing frequency (Hz) at short incubation periods e.g. 2 hours, when compared to both the vehicle (black squares, denoted by *) and baseline (0 h, denoted by #) (100 µM 2 h 4.76 ± 0.23 Hz; vehicle 2h 2.13 ± 0.19 Hz; 100 µM 0 h 1.97 ± 0.07 Hz, Two-way RM ANOVA, $P < 0.05$). In contrast, 100 µM (red circles) oxaliplatin significantly reduced mean firing frequency (Hz) at longer incubation periods e.g. 24 hours, when compared to both the vehicle (black squares, denoted by *) and baseline (0 h, denoted by #) (100 µM at 24 h 0.68 ± 0.06 Hz; vehicle at 24 h 2.62 ± 0.18 Hz; 100 µM at 0 h 1.97 ± 0.07 Hz, Two-way RM ANOVA, $P < 0.05$).

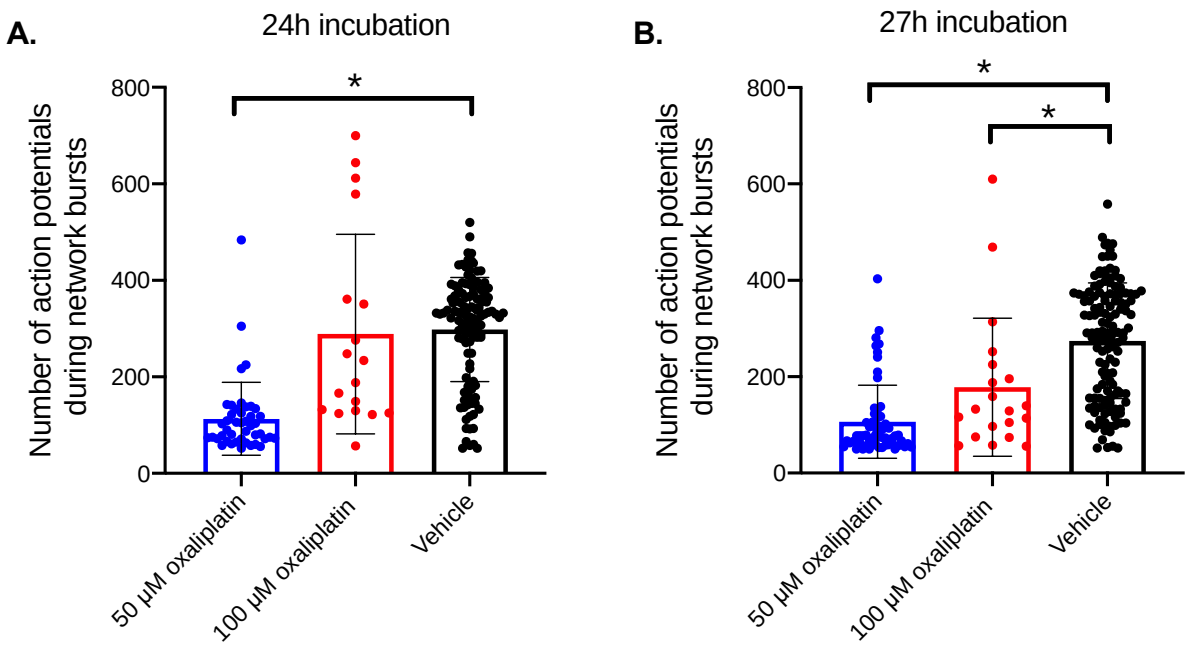

Figure 6-5 Longer incubation periods with oxaliplatin reduced the number of action potentials fired in cortical neurons.

A) 24 hours incubation of 50 (blue circles) but not 100 µM (red circles) oxaliplatin significantly decreased the number of action potentials fired by cortical neurons compared to vehicle (black circles) as measured by the MEA (50 µM 113 ± 11 APs; 100 µM 289 ± 49 APs; vehicle 298 ± 10 APs, Mann-Whitney *U* test, $P < 0.05$ (vehicle vs 50 µM)). B) 27 hours incubation of both 50 (blue circles) and 100 µM (red circles) oxaliplatin significantly decreased the number of action potentials fired by cortical neurons compared to vehicle (black circles) as measured by the MEA (50 µM 106 ± 10 APs; 100 µM 178 ± 32 APs; vehicle 275 ± 10 APs, Mann-Whitney *U* test, $P < 0.05$). Data presented as mean ± S.E.M.

6.4.4 Modulation of oxaliplatin-induced hyperexcitability by ion channel antagonists

Following assay development, outlined in sections 6.4.1 – 3, a concentration of 100 µM oxaliplatin, incubated for 1 hour was chosen for the following experiments. This concentration and time point represent the maximum oxaliplatin-induced hyperexcitability in cortical neurons.

Co-application of 4-Aminopyridine (4-AP), spadin, ivabradine, 4,9-anhydroTTX and retigabine with 100 µM oxaliplatin all significantly reduced the number of action potentials per network burst compared to vehicle control (Figure 6-6). 4-AP, a K_v channel blocker, increased the number of network burst events, as denoted by the number of dots on Figure 6-6 (oxaliplatin + 4-AP: n = 368; oxaliplatin + vehicle: n = 56), however, reduced the number of action potentials within those events (4-AP 115 ± 2 APs; vehicle 507 ± 12 APs, Mann-Whitney *U* test, $P < 0.05$). Spadin, a TREK-1 channel blocker also decreased the number of action potentials per network burst compared to oxaliplatin + vehicle (spadin 413 ± 13 APs; vehicle 507 ± 12 APs, Mann-Whitney *U* test, $P < 0.05$), but did not inhibit the number of network bursts which occurred (oxaliplatin + spadin: n = 64; oxaliplatin + vehicle: n = 56). In addition, the HCN blocker ivabradine decreased the number of action potentials per network burst compared to vehicle (ivabradine 318 ± 11 APs; vehicle 507 ± 12 APs, Mann-Whitney *U* test, $P < 0.05$). However, the number of network bursts was increased in the presence of ivabradine, compared to vehicle (oxaliplatin + ivabradine: n = 172; oxaliplatin + vehicle: n = 56).

The average number of action potentials per network burst could not be fully determined for retigabine, a $K_v7.2/7.3$ channel opener and for a reported $Na_v1.6$ antagonist 4,9-anhydroTTX (Rosker et al., 2007) (retigabine 379 APs; 4,9-anhydroTTX 119 APs; vehicle 507 ± 12 APs).

These compounds ostensibly abolished network burst firing caused by oxaliplatin after the 1 hour time point (Figure 6-6) (retigabine: n = 1; 4,9-anhydroTTX: n = 2 when compared to vehicle: n = 56). This indicates that 4,9-anhydroTTX is not specific, nor selective for $Na_v1.6$. Three other inhibitors tested in the MEA; tetrodotoxin (TTX), a general Na_v channel blocker, mibefradil, a T-type Ca_v-channel inhibitor and blocker of $Na_v1.8$ and $Na_v1.9$ channels (Coste et al., 2007), and amitriptyline, a non-selective blocker of Na_v, K_v and Ca_v channels caused total inhibition of cortical neuron activity e.g. zero network bursts and zero action potentials.

Interestingly, there was a significant increase in the number of action potentials per network burst when A-803467, a $Na_v1.8$ antagonist was co-applied with oxaliplatin when compared to the vehicle (Figure 6-6) (A-803467 494 ± 21 APs; vehicle 507 ± 12 APs, Mann-Whitney *U* test, $P < 0.05$). There was also an increase in the number of network bursts by two-fold when compared to the vehicle (A-803467: n = 112; vehicle: n = 56). It is likely that there was limited specificity of this molecule, as there appears to be a surprising prominence of this channel in cortical neurons.

Ivabradine had the most dramatic effect in reducing the number of action potentials per network burst when compared to vehicle without abolishing firing at later time points. It was taken into subsequent experiments to assess whether it could inhibit the network burst firing seen at lower concentrations of oxaliplatin, including the EC_{50} value (10 - 100µM).

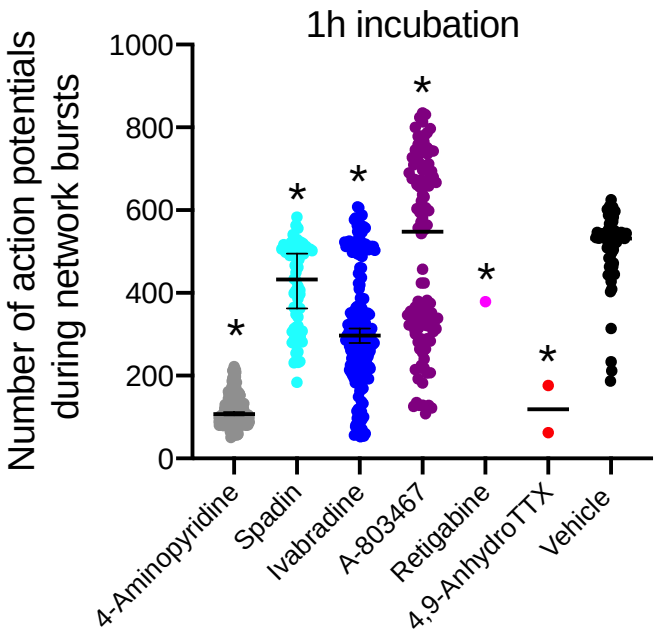

Figure 6-6 MEA screen of ion channel antagonists against oxaliplatin-induced hyperexcitability.

The number of action potentials per network burst (one dot = one network burst) after co-application of oxaliplatin and ion channel blockers: vehicle (black circles) 507 ± 12 APs; 4-AP (grey circles), 250 µM, 115 ± 2 APs, $P < 0.05$; Spadin (light blue circles), 300 nM, 413 ± 13 APs, $P < 0.05$; Ivabradine (dark blue circles), 10 µM, 318 ± 11 APs, $P < 0.05$; A-803467 (purple circles), 80 nM, 494 ± 21 APs, $P < 0.05$; Retigabine (pink circle), 10 µM, 379 APs, $P < 0.05$; 4,9-anhydroTTX (red circles), 80 nM, 119 APs, $P < 0.05$. Mann-Whitney *U* test performed. All data presented as mean ± S.E.M.

6.4.5 K_v2.1 identified as a potential target

Guangxitoxin-1E (GxTx) is a gating modifier toxin initially isolated from the venom of the tarantula *Plesiophrictus guangxiensi* (Liu and Bean, 2014). It is a potent (IC_{50} = 1 – 3 nM) and selective K_v2.1 channel antagonist (Herrington, 2007). Co-application of GxTx significantly reduced the number of action potentials per network burst (Figure 6-7 A) and also reduced the total number of network bursts (vehicle control; 507 ± 12 APs, n = 56 and GxTx 413 ± 12, n = 53, Mann-Whitney *U* test, $P < 0.05$) (Figure 6-7 A). The reduction in oxaliplatin-induced hyperexcitability was apparent when compared to experiments without GxTx co-application. An example raster plot is shown in Figure 6-7 B and may be compared to Figure 6-1 to highlight the altered firing pattern in wells after co-application of GxTx. Thus, antagonism of K_v2.1 (by GxTx) and HCN channels (by ivabradine) were most effective in reducing oxaliplatin-induced hyperexcitability in cortical neurons. Therefore, we sought to test the efficacy of these inhibitors in a wider range of oxaliplatin concentrations (10 - 100 µM) to investigate whether these antagonists could inhibit the different effects seen after oxaliplatin treatment at different concentrations.

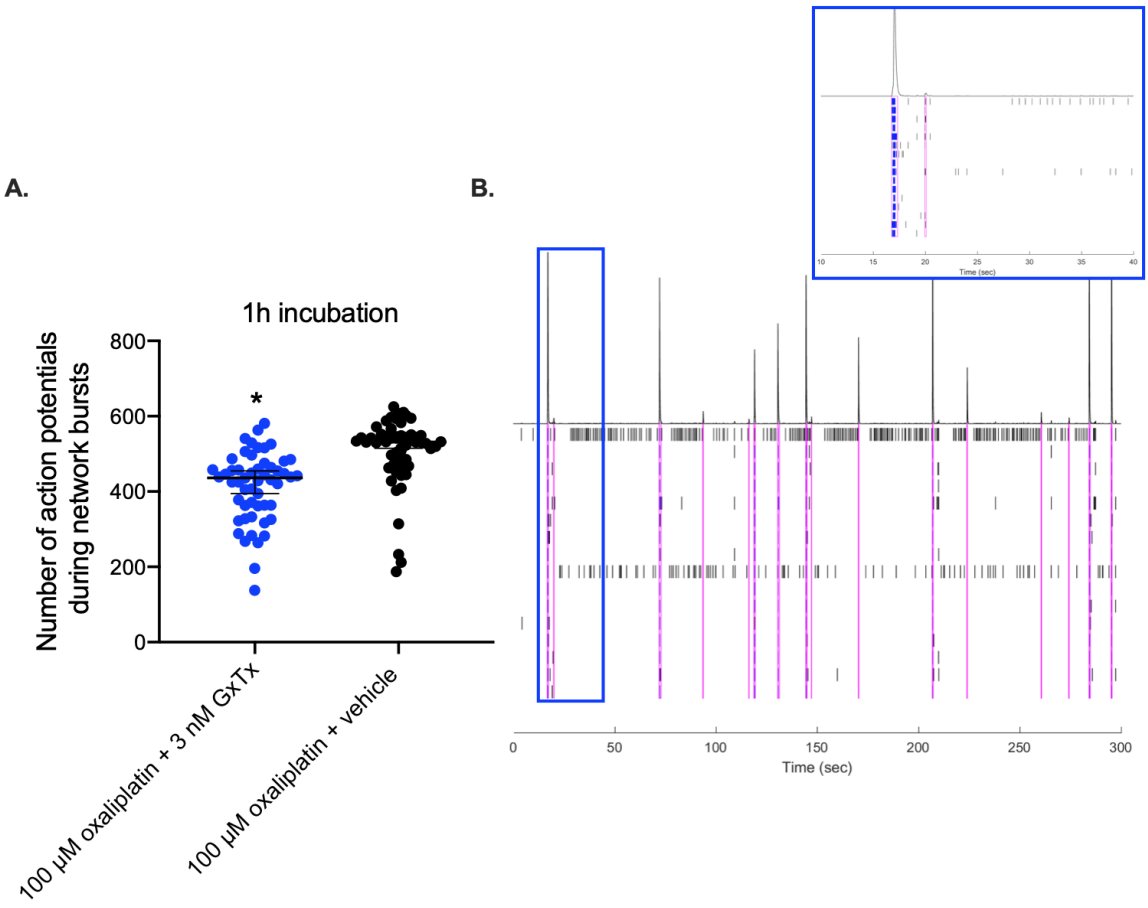

Figure 6-7 Kv2.1 block by GxTx reduces oxaliplatin-induced hyperexcitability.

A) The number of action potentials per network burst (one dot = one network burst) after co-application of oxaliplatin with GxTx: vehicle (black circles) 507 ± 12 APs; GxTx (blue circles), 3 nM, 413 ± 12 APs, Mann-Whitney *U* test, $P < 0.05$. B) Example raster plot to show a reduced number of network bursts and activity when compared to the number of network bursts fired after 100 µM oxaliplatin as shown previously.

6.4.6 Similar pattern of inhibition after GxTx and ivabradine application

In the final set of experiments, a concentration-response of oxaliplatin (10 - 100 µM) against GxTx and Ivabradine was conducted to determine whether these antagonists could inhibit oxaliplatin-induced hyperexcitability at lower concentrations. Interestingly, both GxTx (3 nM) and ivabradine (10 µM) significantly reduced the number of action potentials per network burst in just the highest concentration of oxaliplatin (100 µM) incubated for 1 hour (Figure 6-8 A, 6-9 A) (GxTx 343 ± 29 APs; ivabradine 342 ± 8 APs; vehicle 527 ± 10 APs, Mann-Whitney *U* test, $P < 0.05$). There was no effect seen with the lower concentrations of the compound. In addition, ivabradine significantly reduced oxaliplatin-induced hyperexcitability at 50 µM oxaliplatin (ivabradine; 350 ± 12 APs; vehicle 391 ± 24 APs, Mann-Whitney *U* test, $P < 0.05$). Both inhibitors reduced the number of action potentials per network burst following 100 µM oxaliplatin after 2 hours compared to vehicle (GxTx 566 ± 28 APs; ivabradine 384 ± 10 APs; vehicle 691 ± 16 APs, Mann-Whitney *U* test, $P < 0.05$) (Figure 6-8 B, 6-9 B). Ivabradine also inhibited the activity with 50 µM oxaliplatin after 2 hours (Figure 6-2). Maximal activity using 50 µM oxaliplatin was seen after 2 hours (supplementary figure 6-I C).

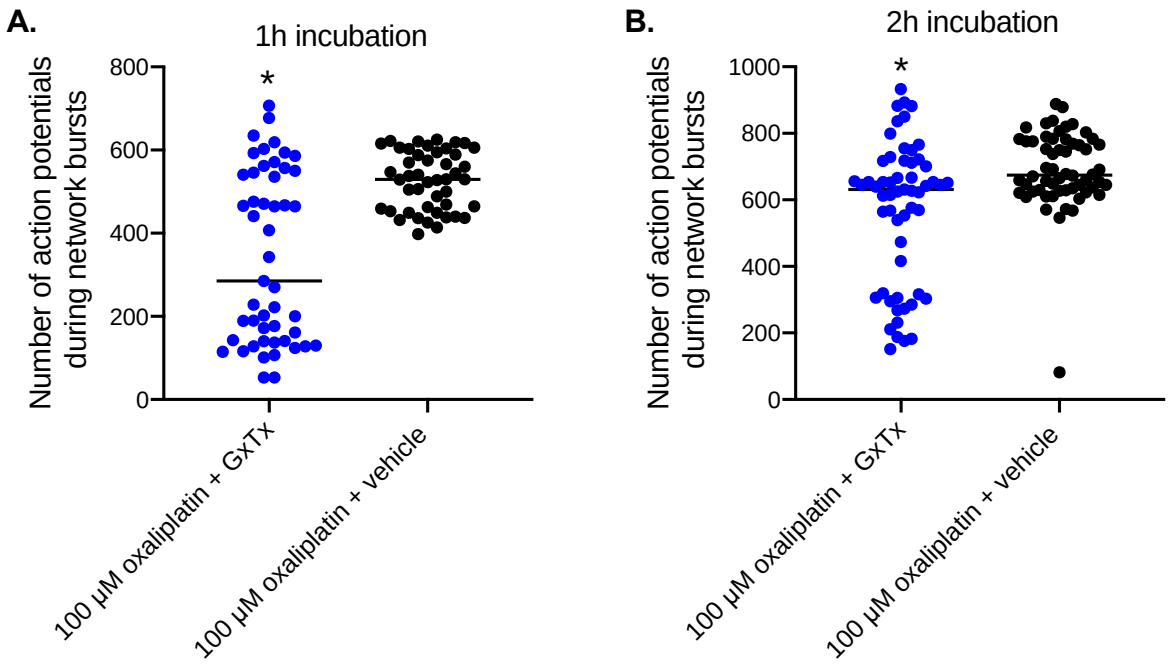

Figure 6-8 GxTx reduces oxaliplatin-induced hyperexcitability after 100 µM oxaliplatin for 2 hours.

A) The number of action potentials per network burst (one dot = one network burst) after co-application of oxaliplatin with GxTx 1 h: vehicle (black circles) 527 ± 10 APs; GxTx (blue circles), 3 nM, 343 ± 29 APs, Mann-Whitney *U* test, $P < 0.05$. B) The number of action potentials per network burst after co-application of oxaliplatin with GxTx 2 h: vehicle (black circles) 691 ± 16 APs; GxTx (blue circles), 3 nM, 566 ± 28 APs, Mann-Whitney *U* test, $P < 0.05$.

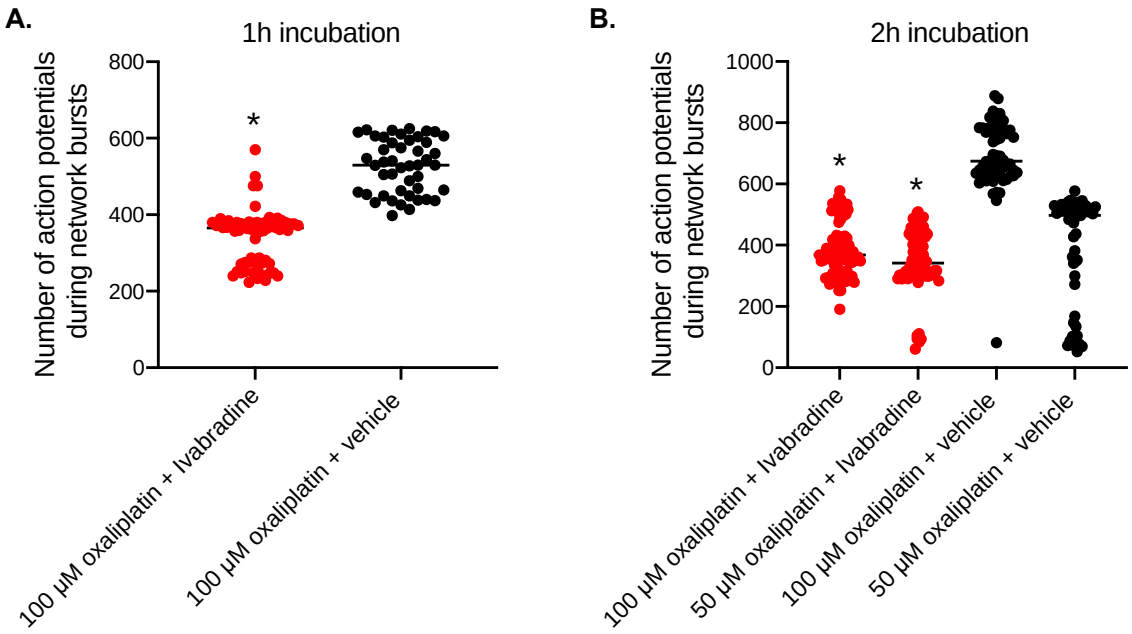

Figure 6-9 Ivabradine reduces oxaliplatin-induced hyperexcitability at different oxaliplatin concentrations for 2 hours.

A) The number of action potentials per network burst (one dot = one network burst) after co-application of oxaliplatin with ivabradine 1 h: vehicle (black circles) 527 ± 10 APs; ivabradine (red circles), 10 µM, 342 ± 8 APs, Mann-Whitney *U* test, $P < 0.05$. B) The number of action potentials per network burst after co-application of oxaliplatin with ivabradine 2 h: 100 or 50 µM oxaliplatin + vehicle (black circles) 691 ± 16 APs, and 391 ± 24 APs respectively; ivabradine (red circles), 10 µM, with 100 µM oxaliplatin 384 ± 10 APs, with 50 µM oxaliplatin 350 ± 13 APs, Mann-Whitney *U* test, $P < 0.05$.

6.5 Discussion

In this chapter, we have successfully developed a MTS method for assessing putative ion channel targets in oxaliplatin-induced hyperexcitability. To begin, we show that cortical neurons respond to oxaliplatin incubation with high frequency firing. This includes maximal firing seen at 1 hour after 100 µM oxaliplatin and stable EC_{50} values between 1 - 3 hours. There were fewer network bursts and firing after longer incubation periods. However, we confirmed using a cell viability assay that cells were still alive. Instead, we propose a depolarisation-induced block occurred at later time points. The ability to seed cortical neurons onto a MEA plate at a high density provides a much needed and adaptable platform that facilitates rapid assessment of selective ion channel antagonists. As a result, we demonstrated that multiple potassium channel modulators, including 4-AP, spadin and retigabine reduced oxaliplatin-induced hyperexcitability. This was also demonstrated after HCN channel antagonism by ivabradine. Finally, using this assay we have identified $K_v2.1$ as an ion channel of interest in oxaliplatin-induced hyperexcitability.

The major dose limiting side effects of oxaliplatin, cold and mechanical hyperalgesia are caused by sensitisation of peripheral primary afferent neurons (Binder et al., 2007; Forstenpointner et al., 2018; Sittl et al., 2012). This has been confirmed in our study (Chapter 5) and QST studies, where patients have clearly presented peripheral neuron abnormalities including decreased cold pain thresholds and greater sensitivity to light touch (Binder et al., 2007). Some of these side effects and QST parameters might be explained by the serious neurotoxicity of the platin molecule. However, preclinical models of oxaliplatin-induced peripheral excitability and *in vitro* studies implicate voltage-gated ion channels. In particular, those voltage-gated ion channels that govern the excitability of sensory neurons such as Na_v and K_v channels.

In this study, we used the Na_v pore blocker TTX which inhibits $Na_v1.1$-$Na_v1.4$, $Na_v1.6$ and $Na_v1.7$ to assess Na_v channel function. Unsurprisingly, blocking all TTX-sensitive Na_v channels in cortical neurons, even those exposed to oxaliplatin, completely abolished network burst firing. Cortical neurons do not express TTX-resistant (TTX-r) channels so there was no channel to carry the AP upstroke. Concurrently, we tested its derivative 4,9-anhydro-TTX that was initially reported to block $Na_v1.6$ selectively (Rosker et al., 2007). Deuis *et al* showed inhibition of $Na_v1.6$ by a selective μ-conotoxin reversed the effects of oxaliplatin (Deuis et al., 2013). In addition, electrophysiological studies conducted in DRG neurons from WT mice demonstrated oxaliplatin-induced action potential bursts seen during cooling. The effects of oxaliplatin to cold-evoked responses were abolished in *Scn8a*$^{med/med}$ mice, which lack functional $Na_v1.6$ channels (Sittl et al., 2012). We also showed a dramatic reduction in oxaliplatin-induced hyperexcitability after 4,9-anhydroTTX. However, the effects were similar to TTX, suggesting that 4,9-anhydroTTX is unlikely to be a selective $Na_v1.6$ blocker. This is supported by a recent study which showed that 4,9-anhydroTTX also acts on $Na_v1.1$, therefore $Na_v1.6$ currents cannot be separated from $Na_v1.1$ currents in neural networks (Denomme et al., 2020). In contrast, co-application of A-803467, a $Na_v1.8$-selective blocker (Bennett et al., 2019), did not reduce the oxaliplatin-induced network burst firing in cortical neurons. This is due to the low expression levels of $Na_v1.8$ in cortical neurons, therefore we did not detect these TTX-r channels in this model. Instead, we would require a high-throughput method using DRG neurons. $Na_v1.8$ which is primarily expressed in nociceptors have been implicated in oxaliplatin-induced cold hypersensitivity, as it is a key channel in noxious cold sensing (Luiz et al., 2019).

Voltage-gated potassium (K_v) channels regulate the resting membrane potential, control the downstroke and frequency of action potentials (Hille et al., 1999). Often, injury-induced K_v dysregulation is associated with reduction in associated current, augmented sensory neuron excitability and pain phenotypes (Chien et al., 2007; Everill and Kocsis, 1999; Tsantoulas et al., 2012). Therefore, the use of K_v blockers to DRG neurons induces neuronal firing (Kajander et al., 1992), while K_v openers reduces neuronal excitability and relieves pain symptoms (Blackburn-Munro and Jensen, 2003; Dost et al., 2004; Mishra et al., 2012). We confirmed that blocking K_v channels with 4-AP reduced the number of action potentials per network burst in the absence of changes to the total number of network bursts. 4-AP is an antagonist of Shaker-like $K_v1.1$ and $K_v1.2$ channels. These channels are the major carrier of the excitability brake current, I_{KD} which has been shown to have a significant role in driving cold sensitivity and allodynia in peripheral sensory neurons (González et al., 2017). In addition, $K_v1.1$ and $K_v1.2$ are expressed in large-diameter sensory neurons which give rise to myelinated A fibres (Rasband et al., 2001) and $K_v1.1$ transcripts have been down-regulated in mice treated with oxaliplatin (Descoeur et al., 2011). It is unlikely however, that this is a direct effect of oxaliplatin.

Finally, axonal K_v7 channels have been shown to drive increased excitability in A fibres after oxaliplatin, depicted by increased duration and amplitude of compound action potentials (Sittl et al., 2010). The K_v7 (KCNQ) channel family contribute to the resting membrane potential by maintaining the membrane potential below the threshold for sodium channel activation (Tatulian et al., 2001; Wladyka and Kunze, 2006). KCNQ2/3 subunits form the correlate for the M-current (I_{KM}) and regulates neuronal excitability in central and peripheral neurons (Passmore et al., 2003). Mutations in KCNQ2/3 subunits results in inheritable syndromes such as benign familial neonatal convulsions (Jentsch, 2000). Retigabine, a K^+

channel opener has proven effective in treatment of epilepsy and reduces inflammation-induced pain in mice (Passmore et al., 2003). It increases the number of K_v7 channels that are open at rest, which act as an excitability brake and thus decreases hyperexcitability (Brown, 1988; Gunthorpe et al., 2012). In MEA experiments, retigabine reduced the activity markedly. However, it was difficult to effectively assess the longer-term effects of this drug in our assays. This compound effectively abolished all action potentials and network bursts in cortical neurons. Therefore, it was challenging to investigate the role of the M-current any further in these experiments.

The two-pore loop potassium channels (K_{2P}) such as TREK-1, TREK-2 and TRAAK are activated by thermal, mechanical and lipid stimuli (Pereira et al., 2014). In a study which used riluzole, an activator of TREK-1, there was a reduction in oxaliplatin-induced neuropathic effects (Poupon et al., 2018). Like KCNQ channels, TREK-1 can provide increased hyperpolarizing currents this way to reverse the hyperexcitability induced by oxaliplatin. Counterintuitively, we show here that spadin, a TREK-1 channel inhibitor significantly reduced the number of action potentials per network burst after oxaliplatin treatment. However, like 4-AP it had a contradictory effect and increased the number of network bursts. It is likely that this is explained by a more depolarised membrane potential and block. TREK-1 channels are referred to as leak channels, because they are voltage-independent and important for setting the resting membrane potential (Lamas et al., 2019).

Another study reported a marked decrease in TREK-1 and TRAAK transcripts in mice that were treated with oxaliplatin (Descoeur et al., 2011), suggesting further important regulatory roles for excitability in neurons. Whilst there was robust mechanical hyperalgesia in the TREK1-TRAAK double knockout mice, oxaliplatin failed to increase tonic hypersensitivity to cold seen

in the double knockout mice, suggesting a total loss of oxaliplatin modulation of cold perception in this genotype (Descoeur et al., 2011). The effects of potassium channel blockers and openers on oxaliplatin-induced hyperexcitability in cortical neurons was not always predictable, and at times in conflict with the findings of earlier studies using sensory neurons.

In our study, co-application of 100 µM oxaliplatin with ivabradine reduced oxaliplatin-induced hyperexcitability. There was a significant reduction in the number of action potentials per network burst in the presence of ivabradine. There was also a reduction in the high frequency firing which formed 'clusters' of network bursts, although there was no reduction in the overall number of events. According to transcriptomics data above, and recent investigations by Linnarsson and colleagues, HCN channels are expressed in both DRG and cortical neurons (Parisien et al., 2017; Roth et al., 2006; Zeisel et al., 2018). Ivabradine is a pan HCN channel blocker (Berdeaux et al., 2009). HCN channels are cation channels that are activated by hyperpolarisation of the membrane potential, modulated by cyclic nucleotides and are expressed in sensory neurons (Kase and Imoto, 2012). The hyperpolarisation-activated current (I_h), generated by HCN channels promotes repetitive impulse activity and regulates the excitability of nociceptive neurons (Emery et al., 2011; Momin et al., 2008; Young et al., 2014). In addition, HCN channels are overexpressed in inflammatory and neuropathic pain states. Inhibitors of the channels blockers have been reported to reduce neuronal hyperexcitability and ameliorate painful states in animal models (Resta et al., 2018).

The role of HCN channels in oxaliplatin-induced hyperexcitability has been investigated and two isoforms, HCN1 and HCN2 are most important in the neuropathic pain. HCN1 and HCN2 are expressed in primary somatosensory neurons, albeit quite modestly (Zeisel et al., 2018).

Descoeur *et al.* reported an increase in HCN1 mRNA levels in DRG neurons from oxaliplatin-treated mice and showed that ivabradine reduced oxaliplatin-induced hyperalgesia (Descoeur et al., 2011). Ivabradine also inhibits the development of hyperexcitability in electrophysiological recordings from small nociceptive neurons isolated from oxaliplatin-treated mice (Young et al., 2014). In MEA experiments, ivabradine reduced oxaliplatin-induced hyperexcitability for up to 2 hours after co-treatment with 100 µM and 50 µM oxaliplatin. It had no effect at the later time point of 24 hours. Ivabradine was successful in reducing the effects of oxaliplatin better than other inhibitors, including GxTx. Interestingly, the mean number of action potentials discharged with ivabradine was the same after 1 and 2 hours. Thus, findings from *in vivo* and *in vitro* experiments demonstrate acute HCN channel block is effective in reducing oxaliplatin-induced hyperexcitability. Unfortunately, ivabradine cannot be used in the clinic due to the expression of HCN isoforms in the heart. However, selective HCN1 and HCN2 antagonism may be useful in reducing oxaliplatin-induced hyperexcitability.

Our MEA experiments show for the first time that antagonism of $K_v2.1$ reduces oxaliplatin-induced hyperexcitability. $K_v2.1$ is highly expressed, and commonly with $K_v2.2$ in DRG neurons and also in cortical neurons (Bocksteins et al., 2009; Tsantoulas et al., 2014; Zeisel et al., 2018). $K_v2.1$ channels are delayed rectifier channels and therefore are essential to the regulation of neuronal excitability and repetitive firing properties (Misonou et al., 2005; Speca et al., 2014). Use of GxTx, a $K_v2.1$ channel gating modifier and blocker, reduced the number of network bursts and the total number of action potentials per network burst in response to oxaliplatin. We demonstrated that there was complete inhibition of the clusters of network bursts after 100 µM oxaliplatin at 1 hour. This marked the maximal activity of oxaliplatin in cortical

neurons in the MEA system. This inhibition also extended to 2 hours after 100 µM oxaliplatin, but GxTx was not as effective. Therefore, GxTx may provide acute reversal of oxaliplatin-induced hyperexcitability only. Our results suggest that it may not be useful in long-term reversal of excitability. In line with our findings, the loss of K_v2 ion channels disrupts repetitive firing properties in many neuronal types (Du et al., 2000; Guan et al., 2013; Liu and Bean, 2014; Malin and Nerbonne, 2002; Romer et al., 2019). In a study using superior cervical ganglion (SCG) neurons, inhibition of K_v2 currents by GxTx treatment resulted in increased time between action potentials, referred to as inter-spike intervals (Liu and Bean, 2014). In addition, there was a reduction in the maximum downstroke velocity of the falling phase, which corresponds to the maximum outward current. However, the most dramatic effect of blocking K_v2 channels with GxTx was a depolarising shift of the trough after the first action potential (Liu and Bean, 2014). This has been suggested to reduce recovery of sodium channel inactivation. This in turn could limit the sodium current able to contribute to action potentials after the first spike, resulting in slowed firing over time (Guan et al., 2013; Liu and Bean, 2014).

In summary, we used a medium throughput screening assay to explore ion channel targets in oxaliplatin-induced hyperexcitability. The ion channels chosen in MEA experiments were firstly based on those that may play a role in oxaliplatin-induced hyperexcitability. Secondly, their expression levels in cortical and DRG neurons was important. The most intriguing results came from the effects of GxTx with oxaliplatin as this suggested a potential role for $K_v2.1$ in oxaliplatin-induced hyperexcitability. In order to investigate this further, we explored whether GxTx could also reduce and even reverse the effects of oxaliplatin *in vivo* and in electrophysiological recordings from single fibres. We also investigated the effects of

oxaliplatin directly on the $K_v2.1$ channel using a in a recombinant cell line expressing human $K_v2.1$ plasmid DNA (Chapter 7).

Supplementary figures for Chapter 6

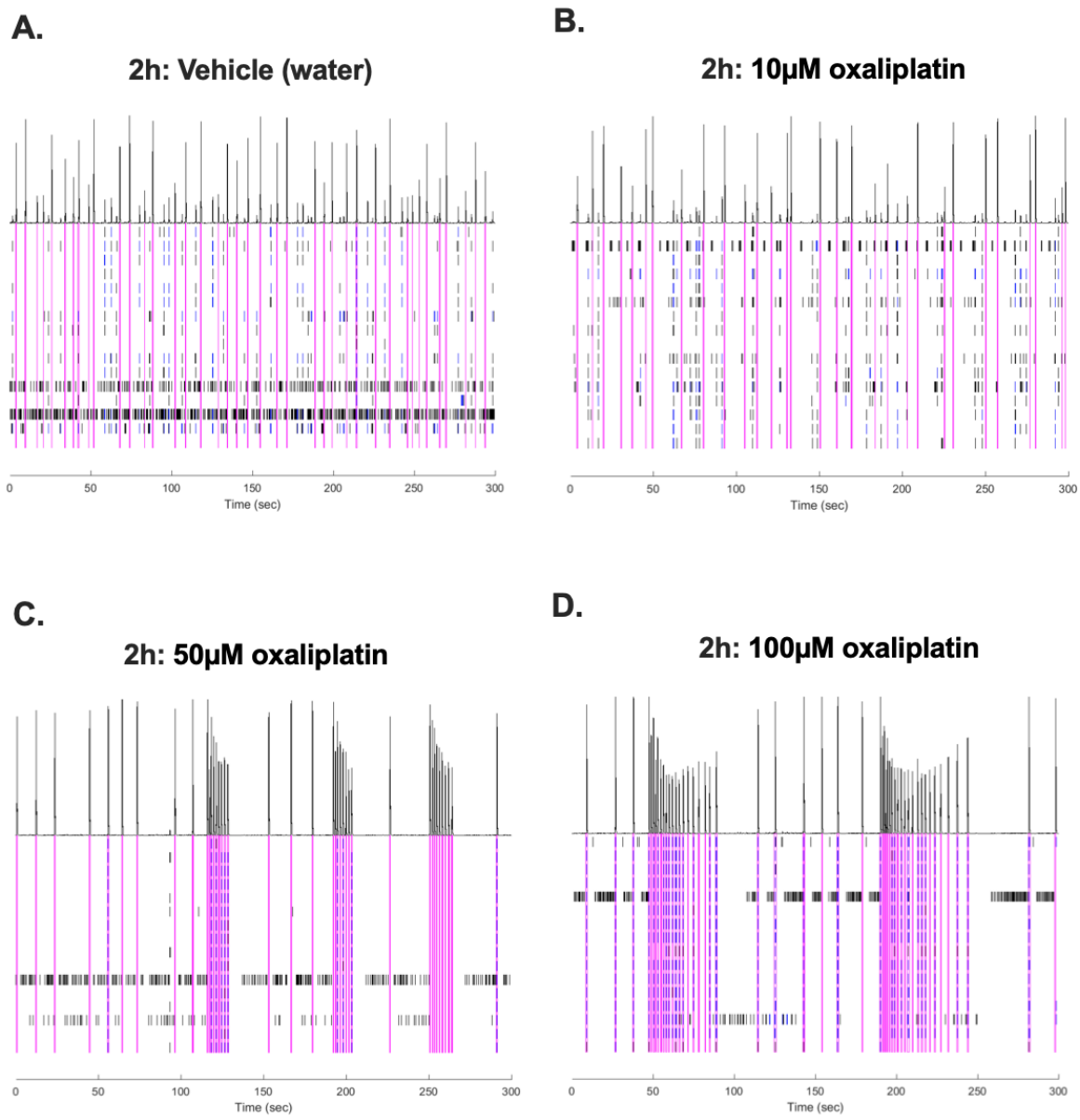

Figure 6-I Activity of cortical neurons after 2 h incubation with multiple oxaliplatin concentrations.

Raster plot depicts the firing patterns of neurons across 16 electrodes after 100 µM oxaliplatin. Each black spike in the lower half of the image represents a detected spike. Blue lines represent single channel bursts – a collection of at least 5 spikes, each with ISI of no longer than 100 ms. The number of network bursts (pink lines) are defined as > 10 spikes in a minimum of 25 % of electrodes in a well with the frequency histogram for network bursts (black lines at top) over 5 minutes. Inset panel shows zoom of histogram peaks representing network burst events. Blue lines can be used to calculate the total number of action potential occurring within each network burst. A) vehicle (water) B) 10 µM oxaliplatin C) 50 µM

oxaliplatin D) 100 µM oxaliplatin. Oxaliplatin (50-100 µM, 2 h) increases clusters of network burst firing in cortical neurons (n = 104 and 174 respectively vs n = 138 in vehicle).

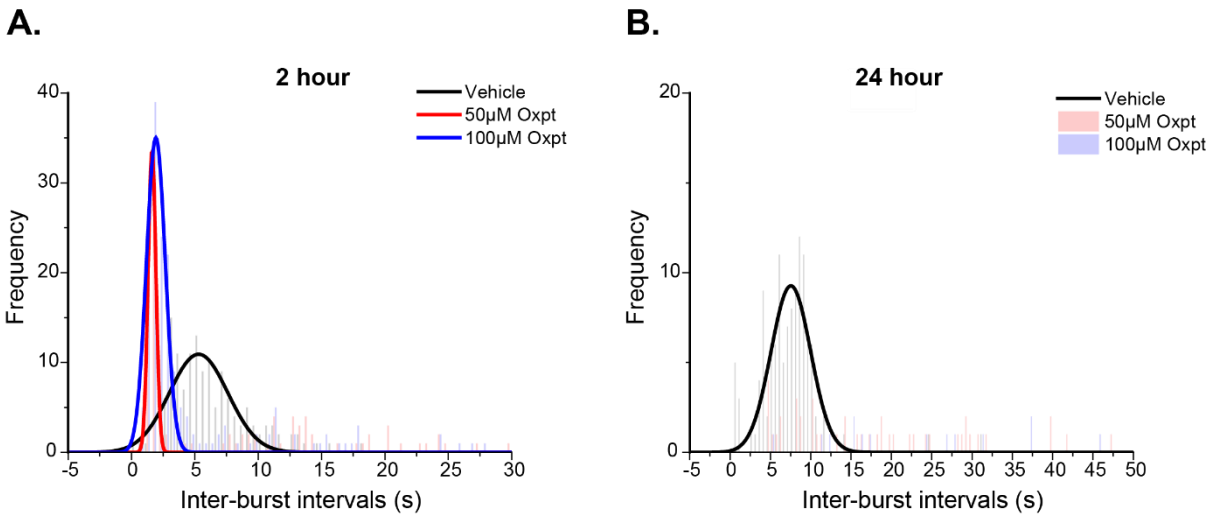

Figure 6-II IBIs increased over time when cortical neurons were treated with 50-100µM oxaliplatin

A) 100 µM (blue line) and 50 µM (red line) oxaliplatin significantly reduces the peak frequency of IBIs compared to vehicle at 2h (100 µM 1.75 ± 0.5s, n = 174, 50 µM 1.75 ± 0.5s, n = 104, vehicle 6.0 ± 0.5s, n = 110, Mann-Whitney *U* test, $P < 0.05$). B) 100 µM (blue line) and 50 µM (red line) oxaliplatin significantly increases the peak frequency of IBIs compared to vehicle at 24h (100 µM n = 19, 50 µM n = 45, vehicle 7.5 ± 0.5s, n = 119, Mann-Whitney *U* test, $P < 0.05$).

7. $K_V2.1$ as a potential candidate in oxaliplatin-induced hyperexcitability

7.1 Introduction

In chapter 6, we defined a putative role for various ion channels in oxaliplatin-induced neuronal hyperexcitability using the medium-throughput multi-electrode array (MEA). This included the reversal of oxaliplatin-induced action potential burst firing in cortical neurons by inhibition of $K_v2.1$ channels with guangxitoxin (GxTx) (Chapter 6, Figures 6-7, 6-8). In this chapter, we aim to extend those findings to study the role of $K_v2.1$ in oxaliplatin-induced neuropathy *in vivo* and *ex vivo*, and to assess whether oxaliplatin alters the kinetics of the $K_v2.1$ channel.

Voltage-dependent K^+ (K_v) channels are important regulators of neuronal excitability and have remained attractive candidates for therapeutic modulation of neuronal activity, including hyperexcitability that occurs in epilepsy and in response to chemotherapy treatment (Speca et al., 2014). The K_v2 family are important in regulating somatodendritic excitability (Liu and Bean, 2014; Misonou et al., 2005; Speca et al., 2014) and are integral to forming the delayed rectifier K_v currents (I_K). Delayed rectifier potassium channels allow a sustained K^+ efflux following membrane depolarisation. The outward movement of K^+ ions leads to rapid repolarisation of the membrane (Baloh, 2012). $K_v2.1$ is amply expressed in DRG neurons of all sizes (Tsantoulas et al., 2014; Zeisel et al., 2018), is a key mediator of I_K and has been shown to be important in action potential repolarisation kinetics in nociceptors (Du and Gamper, 2013; Speca et al., 2014). It is also highly expressed in hippocampal and cortical neurons, where it displays slow activation and inactivation kinetics. This has led to suggestions that $K_v2.1$ regulates repetitive firing. The I_K current would result in a greater number of $K_v2.1$ channels to open over time, causing increased outward K^+ conductance and making it difficult for the generation of further action potentials (Misonou et al., 2005). This is confirmed by a

study which investigated neuronal excitability in hippocampal slices from WT and $K_v2.1$ knockout (*Kcnb1*$^{-/-}$) mice and demonstrated that *Kcnb1*$^{-/-}$ neurons were hyperexcitable. In addition, the same study found that *Kcnb1*$^{-/-}$ mice were hyperactive, with greater jumping behaviour in cages, and showed more severe seizure-like behaviours when treated with convulsant therapeutics compared to *Kcnb1*$^{+/+}$ mice (Speca et al., 2014).

Previous studies have demonstrated a role for potassium channels in oxaliplatin-induced hyperexcitability. Kagiava and colleagues showed that oxaliplatin application for 300-700 minutes in rat sciatic nerve preparations *in vitro* dramatically distorted the compound action potential (CAP) waveform. This included the broadening of repolarisation kinetics, afterhyperpolarisation and repetitive firing, all of which are related to the malfunction of K_v channels (Kagiava et al., 2008). Other K_v channels underlying oxaliplatin-induced neuropathy include members from the K_v1 and K_v7 families (Descoeur et al., 2011; Madrid et al., 2009; Sittl et al., 2010). In all cases, direct oxaliplatin application induces repetitive firing, alter K^+ and Na^+ currents or interfere with potassium channels that act as excitability brakes (Adelsberger et al., 2000; Benoit et al., 2006; Descoeur et al., 2011). In addition, non-voltage gated potassium channels including the background hyperpolarising two-pore loop (K_{2P}) family are affected by oxaliplatin, as shown by the down-regulation of TREK-1, TREK-2 and TRAAK mRNA in oxaliplatin-treated mice (Descoeur et al., 2011; Pereira et al., 2014). Furthermore, TREK-1 and TRAAK double knockout mice have failed to develop increased cold sensitivity after oxaliplatin treatment. This is a phenomenon also demonstrated in TREK-2 knockout mice, suggesting a role for this family of potassium channels in cold sensitivity (Pereira et al., 2014). Thus, exploring the effects of oxaliplatin on a new potassium channel, $K_v2.1$ could possibly provide a novel and additional mechanism of oxaliplatin-induced hyperexcitability and cold sensitivity.

7.2 Aims

The aims of this chapter were to further interrogate the molecular mechanism(s) of oxaliplatin-induced cold hypersensitivity and paraesthesias. We first assess whether the $K_v2.1$ selective antagonist, GxTx reverses the behavioural phenotype induced by oxaliplatin in mice. Next, we test whether acute application of GxTx to the receptive field of single fibres causes a reduction in the proportion of cold-sensitive fibres. These experiments were conducted both in naïve preparations, where GxTx was co-applied with oxaliplatin acutely and in treated animal preparations. In addition, we assess whether $K_v2.1$ is directly modulated by oxaliplatin *in vitro*. Finally, we investigate oxaliplatin-induced modifications to human serum albumin to identify amino acid residues that may be covalently modified by the compound.

7.3 Methods

7.3.1 Drugs and reagents

The dosage and concentration of oxaliplatin (in 5 % glucose) used for the following experiments was as reported in previous experimental chapters (Chapters 2 and 5). To reduce adsorbance to plastics, guangxitoxin (100 μM, GxTx; Alomone Labs, Jerusalem, Israel) was reconstituted using 0.1 % bovine serum albumin (BSA) and water. For behavioural experiments, three different concentrations (10, 30 and 100 nM in 0.1 % BSA) of GxTx were used. In single fibre experiments, 100 nM GxTx was used.

7.3.2 Behaviour

8-12 week old adult female C57BL/6J mice were injected i.p. with a single dose (6 mg/kg) oxaliplatin as before (Chapter 2). Baseline readings for cold sensitivity and paw pressure were taken for all mice before oxaliplatin administration on the cold plate (Ugo Basile, Italy) and Randall-Siletto set up respectively. Mice developed hypersensitivity to both cold and mechanical stimuli as shown before (Chapter 2) and we tested whether intra-plantar administration of GxTx at day 4 post-oxaliplatin injection could reverse all hypersensitivities. All oxaliplatin-treated mice were split into four different treatment groups (n = 6 per group) – 0.1 % BSA (vehicle control), 10 nM, 30 nM and 100 nM GxTx. Each mouse was administered a 10 μl intra-plantar (i.pl) injection of either BSA or GxTx and cold and mechanical sensitivity was monitored using cold plate and Randall-Siletto assays at 15, 30 and 60 minutes after drug administration.

All behavioural experiments presented in this chapter were conducted by Clive Gentry. The experimenter was unblinded to all treatment groups, however, all experiments were performed in a randomised manner.

7.3.3 Skin-saphenous nerve recordings

The skin-saphenous nerve was dissected from the hind paw of C57BL/6J mice as previously described (Chapters 4 and 5). The protocol in recordings was similar to previous experiments and included three cold stimulations (schematic 4); one before drug application (control) and two after oxaliplatin (600 μM) and GxTx (100 nM) co-application (20 minutes). A total of 6 AM fibres were characterised and used in this study and compared with the 7/10 AM fibres that became novel cold responders after oxaliplatin (Chapter 5). In a second set of experiments, the skin- saphenous nerve preparation was dissected from oxaliplatin-treated mice 4 days post-injection. Cold-sensitive fibres were identified using a cold search stimulus as described in Chapter 5. A 60 second cold ramp was applied once a cold-sensitive fibre was discovered. Subsequently, GxTx (100 nM) or vehicle (0.1 % BSA) was directly applied to the receptive field (isolated by metal ring) in the skin and incubated for 15 minutes. Following this, a second stimulus (60 s) was applied (schematic 5).

7.3.4 Human embryonic kidney cells

Un-transfected human embryonic kidney (HEK293) cells were grown in DMEM AQ supplemented with penicillin (100 U/ml), streptomycin (100 μg/ml) and foetal bovine serum (10 %). Cells were plated ~48 hours before experimentation onto poly-D-lysine coated (10 μg/ml) glass 13 mm coverslips at a low density (~30 %). Cultures were maintained at 37 °C in a humidified incubator gassed with 5 % CO_2. Plated HEK cells were transfected with a human $K_v2.1$ plasmid (h$K_v2.1$-pEGFP-N1, plasmid #111532; Addgene) DNA using Lipofectamine® 2000 transfection reagent (Invitrogen) ~12 - 24 hours before experimentation. The optimal concentration of h$K_v2.1$ plasmid DNA used for transfections was 500 ng. This allowed the

largest proportion of cells to remain healthy before subsequent electrophysiology experiments.

Naïve preparations

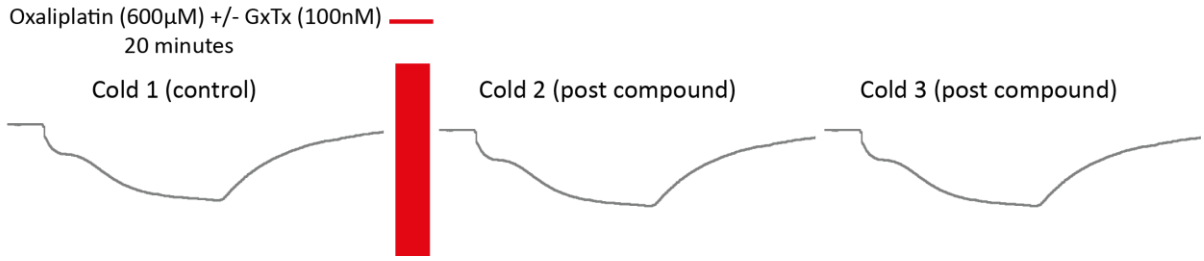

Schematic 4 protocol used in experiments using preparations from naïve mice.

Preparations from oxaliplatin-treated mice

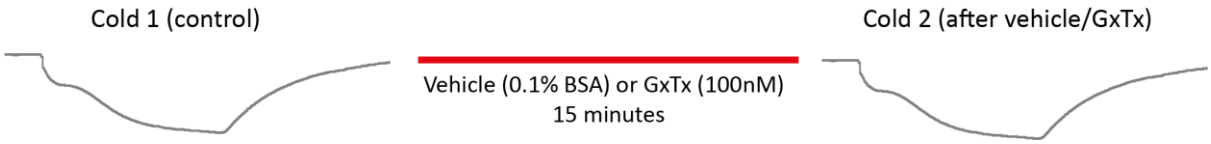

Schematic 5 protocol used in experiments using preparations from oxaliplatin-treated mice.

7.3.5 Patch-clamp recordings

All patch clamp experiment were performed using a Axopatch 200B amplifier (Molecular Devices, Sunnyvale, CA, USA) and Multiclamp 1550B series digitizer. Recordings were acquired at 25 kHz and filtered with a low-pass Bessel filter at 2.9 kHz. Experiments were performed at 20 ± 3 °C. Boroscillate glass pipettes (Warner Instruments, CT, USA) were pulled using a Narashige PC-10 to a resistance of 1-2 mΩ and filled with internal solution (ICS) that contained (in mM) 10 NaCl, 50 KCl, 60 KF, 1 $MgCl_2$, 10 EGTA and 10 HEPES to a pH of 7.2 using KOH, osmolarity was buffered to 300-305 mOsm. The external (ECS) solution contained (in mM) 140 Choline-Cl, 5 KCl, 1 $MgCl_2$, 2 $CaCl_2$, 10 HEPES to a pH of 7.2 using NaOH, osmolarity was buffered to 315-320 mOsm using sucrose. hK_v2.1 HEK cells were incubated with 100 µM oxaliplatin (MEM ± oxaliplatin or buffer control) for 30-45 minutes prior to recording. Coverslips with HEK293 cells were then placed in a bath of ECS ± oxaliplatin 100 µM or buffer control. Cells were chosen based on GFP expression, and after whole cell configuration was achieved cells were held at -80 mV for all voltage-clamp experiments and > 60 % series resistance compensation to reduce voltage errors. To obtain whole K_v2.1 currents a conditioning prepulse to -100 for 500 ms was used, following this outward current was obtained from 10 mV increasing steps to + 60 mV. To confirm that the outward current was K_v2.1 specific, cells that did not have expressed GFP were also tested for outward current. Conductance-voltage curves were generated using the Boltzmann equation $G_{Na} = \frac{GNa,max}{1+e^{\left[\left(Vm-V\frac{1}{2}\right)\right]/k}}$ with a reversal potential of -85 mV.

All patch-clamp recordings were conducted by Dr. Mathilde Israel.

7.3.6 Mass spectrometry

All mass spectrometry experiments and analysis were conducted at the core facility (James Black Centre, King's College London, UK) by Stephen Lynham.

7.3.6.1 Sample preparation

Human serum albumin (HSA) was used as a model protein in the following mass spectrometry experiments. A final HSA concentration of 100 µM was used and incubated with oxaliplatin in a 5-fold molar excess (500 µM). Oxaliplatin was first made up in 5 % glucose and then dissolved in a physiological extracellular solution (ECS) to reach the final concentration of 500 µM. The ECS contained (in mM) 140 NaCl, 5 KCl, 10 glucose, 10 HEPES, 2 $CaCl_2$ and 1 $MgCl_2$. The HSA and oxaliplatin mixture were incubated for either 2 hours or 24 hours. The samples were then trypsinised at a 1:4 dilution of trypsin to substrate. Following this, they were placed on a heat block set at 37 °C for 2 hours before being snap frozen.

7.3.6.2 Liquid chromatography-Mass spectrometry/Mass spectrometry (LC-MS/MS)

The peptide sample was resuspended in 30 µl of resuspension buffer (2 % ACN in 0.05 % FA), 10 µl of which was injected to be analysed by LC-MS/MS. Chromatographic separation was performed using a U 3000 UHPLC NanoLC system (Thermo Fisher Scientific, UK). Peptides were resolved by reversed phase chromatography on a 75 µm C 18 Pepmap column (50 cm length) using a three-step linear gradient of 80 % acetonitrile in 0.1 % formic acid. The gradient was delivered to elute the peptides at a flow rate of 250 nl/min over 60 minutes starting at 5 % B (0 - 5 minutes) and increasing solvent to 40 % B (5 - 40 minutes) prior to a wash step at 99 % B (40 - 45 minutes) followed by an equilibration step at 5 % B (45 - 60 minutes). The eluate was ionised by electrospray ionisation using an Orbitrap Fusion Lumos

(Thermo Fisher Scientific, UK) operating under Xcalibur v 4.1.5. The instrument was first programmed to acquire using an Orbitrap-Ion Trap method by defining a 3 second cycle time between a full MS scan and MS/MS fragmentation. Orbitrap spectra (FTMS1) were collected at a resolution of 120,000 over a scan range of m/z 375-1500 with an automatic gain control (AGC) setting of 4.0 e5 with a maximum injection time of 35 milliseconds. Monoisotopic precursor ions were filtered using charge state (+ 2 to + 7) with an intensity threshold set between 5.0 e3 to 1.0 e20 and a dynamic exclusion window of 35 second ± 10 ppm. MS2 precursor ions were isolated in the quadrupole set to a mass width filter of 1.6 m/z. Ion trap fragmentation spectra (ITMS2) were collected with an AGC target setting of 1.0e4 with a maximum injection time of 35 ms with CID collision energy set at 35 %. This method takes advantage of multiple analysers in the Orbitrap Fusion Lumos and drives the system to use all available parallelizable time, resulting in decreasing dependence on method parameters.

7.3.6.3 Database Searching

Raw mass spectrometry data were processed into peak list files using Proteome Discoverer (ThermoScientific; v2.2) (schematic 6). The raw data file was processed and searched using the Mascot search algorithm (v2.6.0; www.matrixscience.com) and the Sequest search algorithm (Eng *et al*; PMID 24226387) against a bespoke database containing the sequence for human albumin (Accession number P02768) alone. The search allowed for variable modifications of cysteine including: di oxidation (32 Da), tri oxidation (48 Da) and cysteinyl (119 Da). The database output file was uploaded into Scaffold software (version 4.11.1; www.proteomesoftware.com) for visualisation and manual verification.

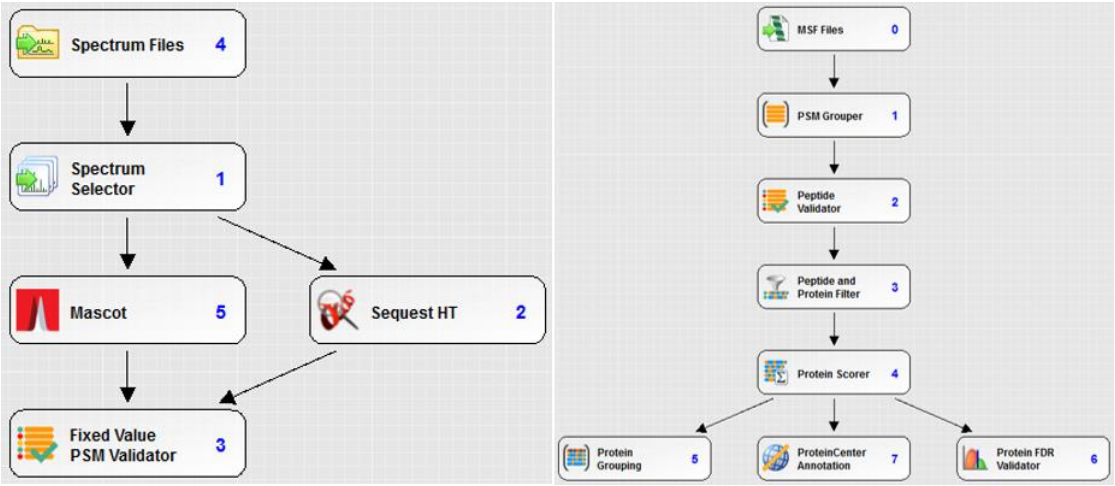

Schematic 6 Proteome discoverer nodal workflow for raw data processing.

7.3.7 Statistical analysis

All *in vivo* data was analysed using Two-way repeated measures (RM) ANOVA. Sidak's *post-hoc* when comparing between treatments and Dunnett's *post-hoc* when comparing to pre-dose values. All single fibre data was first analysed for normality. When comparing between treatment groups, an unpaired *t* test or Mann-Whitney *U* test were conducted based on the results from the normality test. When comparing within treatment groups, a paired *t* test or Wilcoxon test were conducted based on results from the normality test. Categorical data was analysed using Fisher's exact test, two-sided. All data is presented as mean ± S.E.M.

7.4 Results

7.4.1 GxTx reverses oxaliplatin-induced mechanical and cold hypersensitivity *in vivo*

We again confirm that oxaliplatin (6 mg/kg, i.p) causes a reduction in the paw withdrawal threshold to mechanical stimulus (Figure 7-1 A, black squares) and withdrawal latency to cold stimulus (Figure 7-1 B, black squares). GxTx (i.pl) causes a concentration dependent increase in the paw withdrawal thresholds of mice administered oxaliplatin (Figure 7-1A). Both 30 nM (1.2 mg/ml; pink squares) and 100 nM (3.9 mg/ml; red triangles) GxTx reverse oxaliplatin-induced reduction in withdrawal threshold at 30 minutes (vehicle 91 ± 2 g; 30 nM 102 ± 1 g; 100 nM 105 ± 3 g, Two-way RM ANOVA, Sidak's *post-hoc*, $P < 0.05$, n = 6). This reversal was maintained after 60 minutes (30 nM 105 ± 1 g; 100 nM 106 ± 2 g, Two-way RM ANOVA, Sidak's *post-hoc*, $P < 0.05$, n = 6) following 30 nM and 100 nM GxTx. We observed a partial reversal in mechanical hypersensitivity after 10 nM GxTx at 30 minutes (vehicle 91 ± 2 g; 10 nM 95 ± 5 g, $P > 0.05$, n = 6) although not to the level as higher concentrations of the toxin. In addition, 30 nM and 100 nM GxTx reversed oxaliplatin-induced mechanical hypersensitivity at all time points when compared to pre-dose (Figure 7-1A). GxTx reversed oxaliplatin-induced reduction in withdrawal thresholds at 15 minutes when compared to pre-dose (pre-dose 91 ± 2 g; 30 nM 98 ± 2 g; 100 nM 99 ± 2 g, Two-way RM ANOVA, Dunnett's *post-hoc*, $P < 0.05$, n = 6). This was maintained at 30 minutes (30 nM 102 ± 1 g; 100 nM 105 ± 3 g, Two-way RM ANOVA, Dunnett's *post-hoc*, $P < 0.05$, n = 6) and 60 minutes (30 nM 105 ± 1 g; 100 nM 106 ± 2 g, Two-way RM ANOVA, Dunnett's *post-hoc*, $P < 0.05$, n = 6) after 30 nM and 100 nM GxTx.

Similarly, GxTx causes a concentration-dependent increase in paw withdrawal latencies to a cold plate (10 °C) in mice treated with oxaliplatin (Figure 7-1 B). Both 30 nM (pink squares) and 100 nM (red triangles) GxTx reversed oxaliplatin-induced reduction in paw withdrawal

latencies by 30 minutes (vehicle 9.7 ± 0.3 s; 30 nM 12.0 ± 0.7 s; 100 nM 12.2 ± 0.5 s, Two-way RM ANOVA, Sidak's *post-hoc*, $P < 0.05$, n = 6). The antihyperalgesic effect was maintained at both concentrations of GxTx at 60 minutes (vehicle 9.3 ± 0.5 s; 30 nM 12.2 ± 0.5 s; 100 nM 11.9 ± 0.4 s, Two-way RM ANOVA, Sidak's *post-hoc*, $P < 0.05$, n = 6). In addition, this GxTx-induced reversal in paw withdrawal latencies was significant at all time points compared to pre-dose values. Paw withdrawal latencies were increased at 15 minutes (pre-dose 9.6 ± 0.6 s; 30 nM 11.8 ± 0.6 s; 100 nM 10.8 ± 0.7 s), 30 minutes (30 nM 12.0 ± 0.7 s; 100 nM 12.2 ± 0.5 s) and 60 minutes (30 nM 12.2 ± 0.5 s; 100nM 11.9 ± 0.4 s, Two-way RM ANOVA, Dunnett's *post-hoc*, $P < 0.05$, n = 6) after 30 nM and 100 nM GxTx.

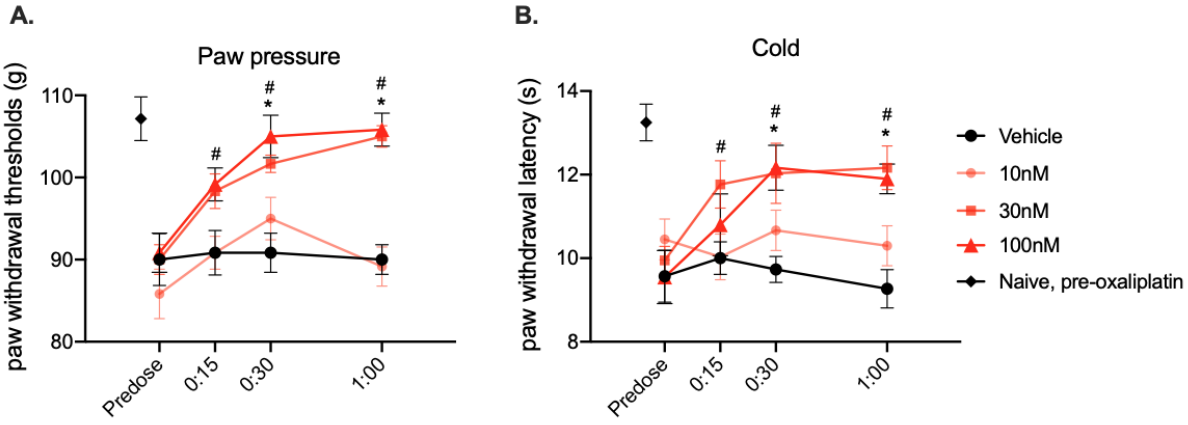

Figure 7-1 GxTx reverses oxaliplatin-induced hypersensitivity *in vivo*.

Female C57BL/6J mice injected with oxaliplatin show a reduction in paw pressure (Randall-Selitto), and paw withdrawal latencies to a cold plate (10 °C), that is reversed by GxTx. A) 30 nM (pink squares) and 100 nM (red triangles) GxTx reverse oxaliplatin induced reduction in paw withdrawal thresholds at 30 and 60 minutes. There was also a in after 30 nM and 100 nM GxTx significantly increased paw withdrawal thresholds when compared to pre-dose values at 15, 30 and 60 minutes. B) 30 nM and 100 nM GxTx reversed oxaliplatin induced reduction in paw withdrawal latencies to cold (10 °C) at 30 and 60 minutes. This increased in paw withdrawal threshold was also observed after 30 nM and 100 nM GxTx compared to pre-dose values at 15, 30 and 60 minutes.

7.4.2 GxTx reduced recruitment of novel cold-sensitive AM fibres

Direct and acute application of oxaliplatin (600 µM) to the skin causes novel cold sensitivity in AM fibres innervating the skin (Chapter 5, Figure 5-10, 5-11). We therefore co-applied GxTx with oxaliplatin to AM receptive fields to test whether $K_v2.1$ antagonism reduced the recruitment of de novo cold-sensitive fibres. GxTx (100 nM) co-application with oxaliplatin reduced the number of cold-sensitive AM fibres identified in the skin-saphenous nerve set-up (oxaliplatin alone 7/10 cold-sensitive AM fibres; oxaliplatin + GxTx 2/6 cold-sensitive AM fibres, Fisher's exact test, $P < 0.05$, n = 10 and 6 fibres respectively).

All AM fibres responded to cold ramps with action potential bursts after oxaliplatin application (Figure 7-3 A). This was not seen after GxTx application. Therefore, GxTx co-application with oxaliplatin inhibited the gain of novel cold sensitivity in AM fibres (Figure 7-3 B).

7.4.2 GxTx reduces cold evoked responses

GxTx co-application with oxaliplatin to the receptive fields of fibres, reduced the total number of action potentials evoked by cold, compared to responses in AM fibre treated with oxaliplatin only (Figure 7-2 B) (oxaliplatin 1801 ± 1004 action potentials (APs); oxaliplatin + GxTx 4 ± 3 APs; Mann-Whitney *U* test, $P < 0.05$). There was a trend towards a reduction in the mean number of action potentials after the first cold ramp after GxTx application, although this was not statistically significant (Figure 7-2 A) (oxaliplatin 789 ± 473 APs; oxaliplatin + GxTx 99 ± 89 APs, Mann-Whitney *U* test, $P > 0.05$).

Furthermore, GxTx treatment shifted the average threshold temperature significantly towards colder temperatures compared to oxaliplatin treatment alone (Figure 7-2 D) (oxaliplatin 26.4 ± 1.2 °C; oxaliplatin + GxTx 11.6 ± 4.4 °C; unpaired *t* test, $P < 0.05$). This shift was also seen in cold ramp 1 after GxTx but was not significant (Figure 7-2 C) (oxaliplatin 19.6 ± 3.5 °C; oxaliplatin + GxTx 10.4 ± 4.3 °C, unpaired *t* test, $P < 0.05$).

Naïve preparations

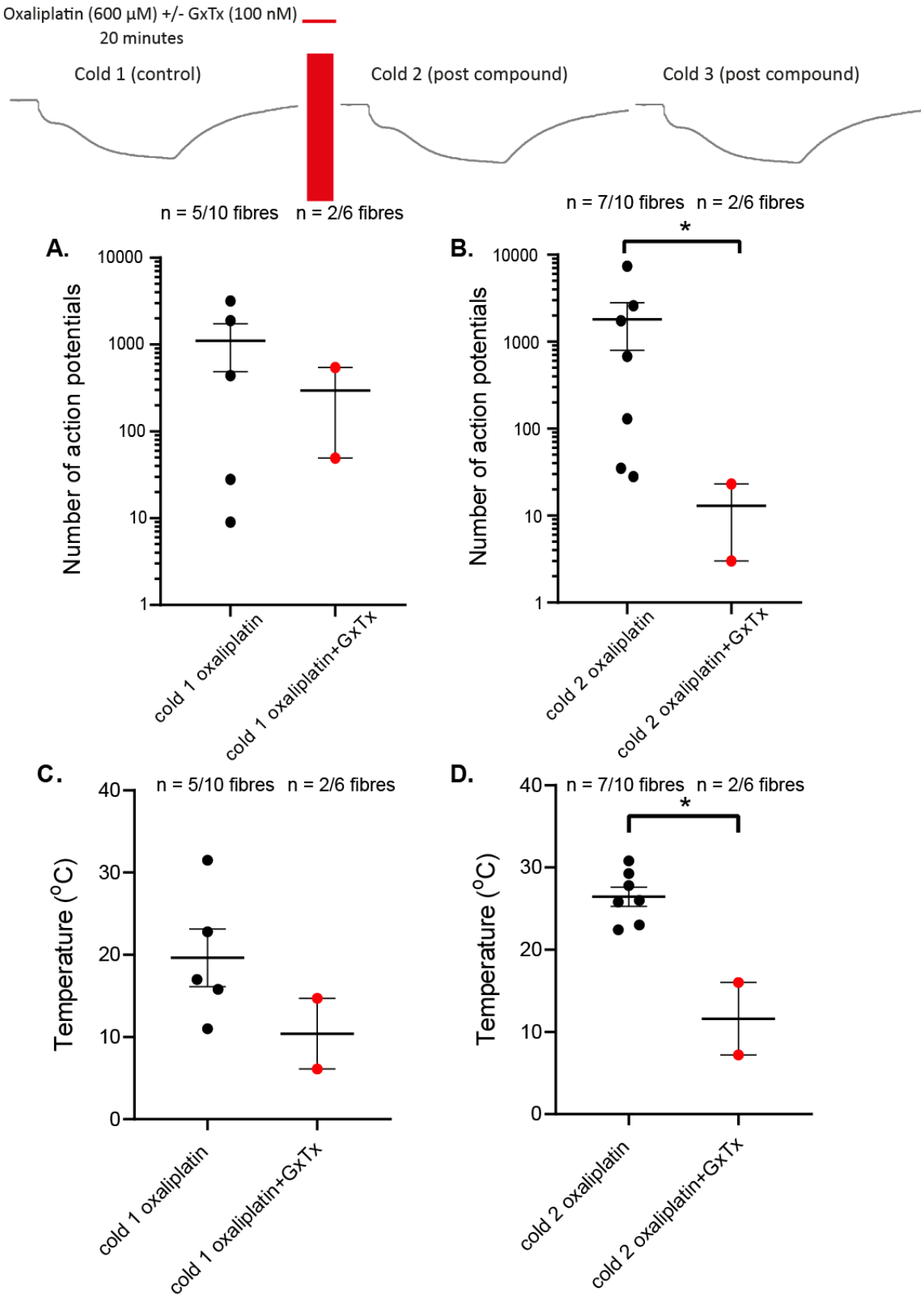

Figure 7-2 GxTx inhibits cold-evoked responses in AM fibres.

GxTx reduced the cold-evoked activity in AM fibres from naïve skin-nerve preparations. A) GxTx (red circles) reduced the mean number of action potentials compared to oxaliplatin alone (black circles) during cold stimulation 1 (oxaliplatin 789 ± 473 action potentials (APs), n = 5/7 fibres; oxaliplatin + GxTx 99 ± 89 APs, n = 2/6 fibres). B) GxTx significantly reduced the mean number of action potentials compared to oxaliplatin alone during cold stimulation 2 (oxaliplatin 1801 ± 1004 APs, n = 7/7 fibres; oxaliplatin + GxTx 4 ± 3 APs, n = 2/6 fibres; Mann-Whitney *U* test, $P < 0.05$). C) GxTx shifted threshold temperatures of activation towards colder temperatures after cold stimulation 1 (oxaliplatin 19.6 ± 3.5 °C, n = 5/7 fibres; oxaliplatin + GxTx 10.4 ± 4.3 °C, n = 2/6 fibres) and D) cold stimulation 2 (oxaliplatin 26.4 ± 1.2 °C, n = 7/7 fibres; oxaliplatin + GxTx 11.6 ± 4.4 °C, n = 2/6 fibres; unpaired *t* test, $P < 0.05$).

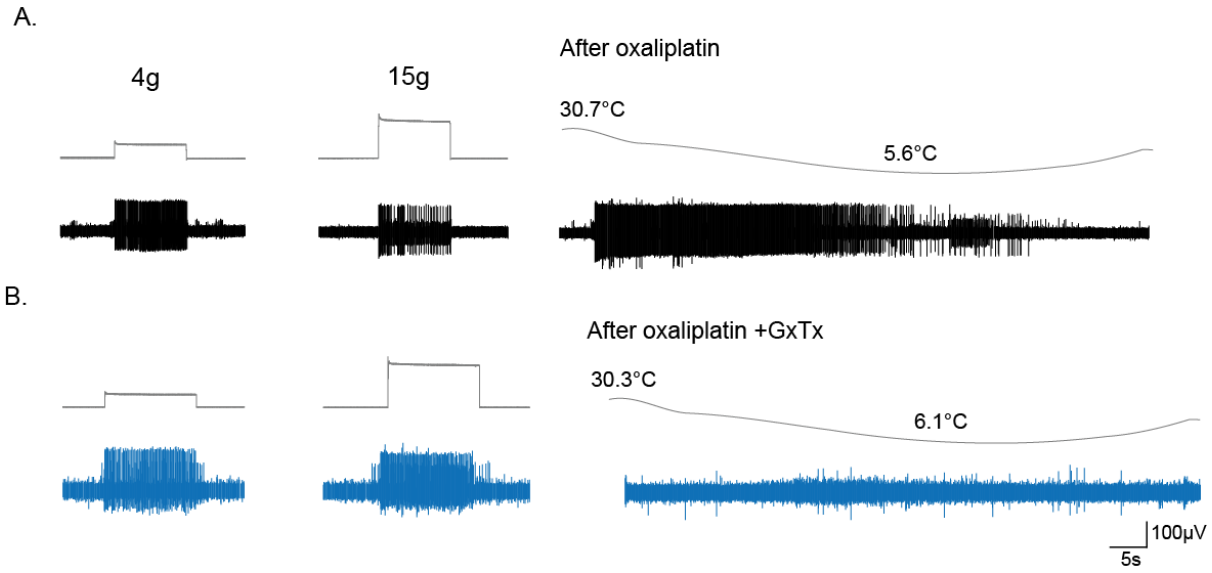

Figure 7-3 GxTx (100 nM), when co-applied with oxaliplatin (600 µM) inhibited the abnormal cold sensitivity in AM fibres.

A) Direct application of oxaliplatin (black traces) leads to novel cold sensitivity in AM fibres. This is commonly seen as action potential bursts during cold stimulations. B) GxTx co-application with oxaliplatin (blue traces) inhibits de novo cold-sensitive AM fibres. In both sets of experiments, suprathreshold forces at 4 g and 15 g were applied to correctly characterise the fibres as AM units.

7.4.4 GxTx treated fibres from oxaliplatin-treated mice remain hyperexcitable

In the second set of skin-saphenous nerve experiments, GxTx was applied (15 minutes) to preparations taken from oxaliplatin-treated mice.

In line with earlier experiments (Chapter 5, Figure 5-23), the effect of oxaliplatin is less marked in preparations from treated mice, compared to direct application of the drug to the receptive fields of single-units. GxTx application showed a trend towards increasing the mean number of action potentials discharged in A fibres during a cold ramp (Figure 7-4 A). The opposite effect was seen in C fibres (Figure 7-4 B). However, no certain conclusions can be drawn from these preliminary findings due to the small sample sizes. In addition, GxTx treatment showed a trend towards reducing the mean number of action potentials when compared to pre-GxTx and vehicle impulse discharges. More recordings are required to assess the veracity of this effect.

In addition, GxTx treatment did not affect the threshold temperatures of activation of cold-sensitive fibres when compared to vehicle. This was also true when compared to cold-sensitive fibres in recordings from oxaliplatin-treated mice. The average threshold temperature for cold-sensitive fibres was 18.3 ± 2.8 °C and 21.6 ± 3.7 °C (n = 3 - 5) in fibres treated with vehicle control and GxTx respectively. This was within error of the threshold temperature in cold-sensitive fibres found in preparations from oxaliplatin-treated mice (18.4 ± 2.2 °C).

Preparations from oxaliplatin-treated mice

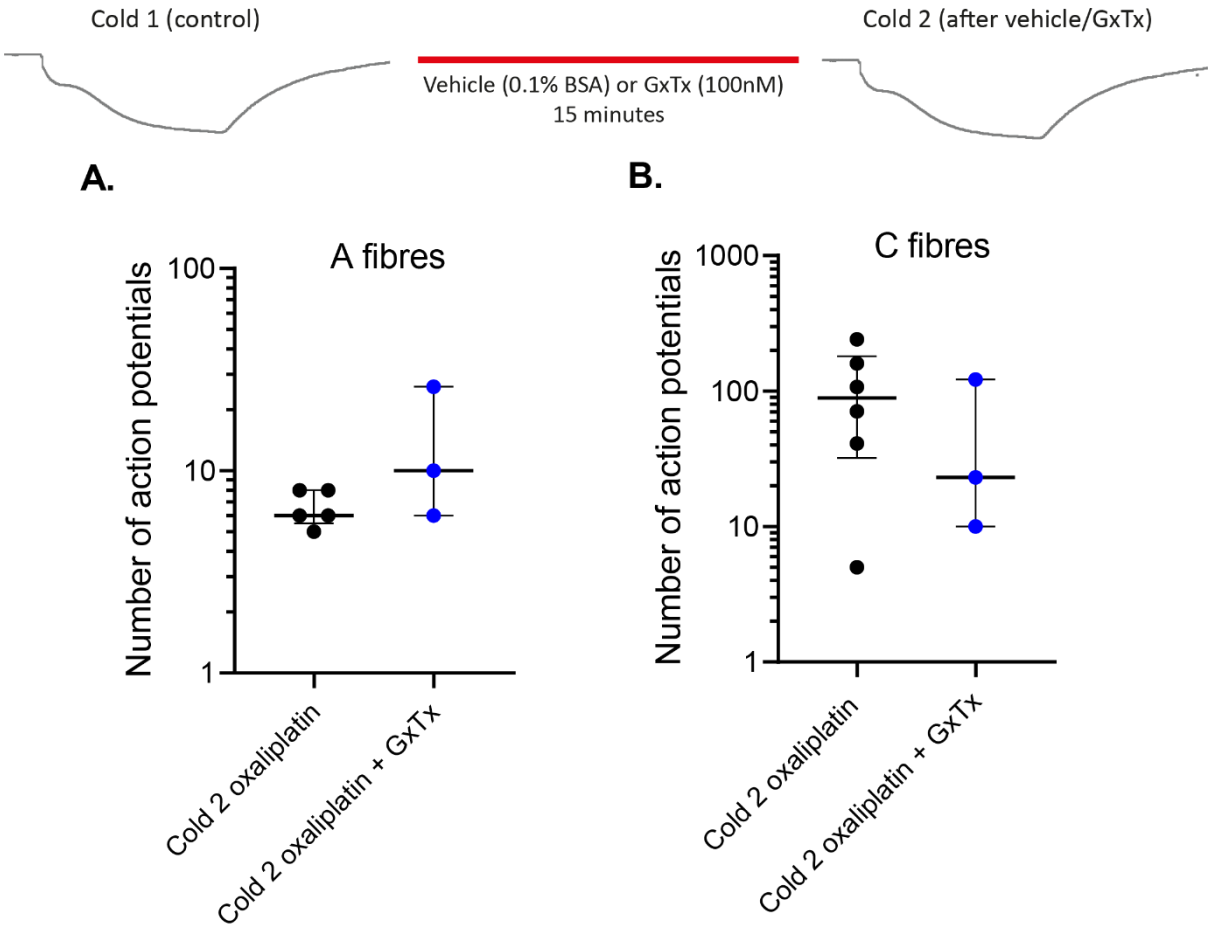

Figure 7-4 No effect of GxTx on cold-evoked responses in fibres from treated mice.

A) GxTx (blue circles) increased the mean number of action potentials in A fibres compared to oxaliplatin alone (black circles) during cold stimulation 2 (cold 2 without GxTx 7 ± 1 APs, n = 5; cold 2 with GxTx 14 ± 6 APs, n = 3, unpaired *t* test, $P > 0.05$). B) GxTx reduced the mean number of action potentials in C fibres compared to oxaliplatin alone during cold stimulation 2 (cold 2 without GxTx 104 ± 35 APs, n = 6; cold 2 with GxTx 52 ± 35 APs, n = 3, unpaired *t* test, $P > 0.05$).

7.4.5 Oxaliplatin alters the activation kinetics of $K_v2.1$

Finally, given that intra-plantar injection of GxTx caused a concentration dependent reversal of oxaliplatin-induced hypersensitivity to mechanical and cold stimuli *in vivo* (Figure 7-1) and cold ramps *ex vivo* (Figure 7-2-4); we asked whether oxaliplatin directly modulates the activity of the $K_v2.1$ when expressed in HEK293 cells. Voltage-clamp experiments from HEK293-$K_v2.1$ cells display a non-inactivating outward current which resembled that of previously reported $K_v2.1$ kinetics (Figure 7-5 B). The V_{50} activation of control treated cells (0.5 % glucose in ECS) was slightly more positive than reported values ~ 10 – 20 mV for $K_v2.1$ (Baver and O'Connell, 2012; Mohapatra et al., 2008). Incubation of HEK293-$K_v2.1$ cells with oxaliplatin (100 µM in 5 % glucose) causes a D 8.2 mV leftward shift in the voltage-dependence of activation curve (Figure 7-5 C, control 27.6 ± 0.7 mV ; oxaliplatin 19.3 ± 1.9 mV, n = 9; 10, $p > 0.05$, unpaired *t* test). The leftward shift in the activation kinetics causes a a small non-significant increase in current density in oxaliplatin treated cells compared to vehicle control. Fitting of the fast component of $K_v2.1$ activation curves with a single exponential function gives an approximation of the time constant (t). There was no significant change in the t activation at peak current sweeps (Figure 7-5 E). The apparent decrease in the t activation at more hyperpolarised potentials reflects the early channel opening observed in Figure 7-5 C. The late current, taken from the final 50 ms of the test pulse and normalised to the peak current value is unchanged in oxaliplatin treated cells compared to control (Figure 7-5 F)

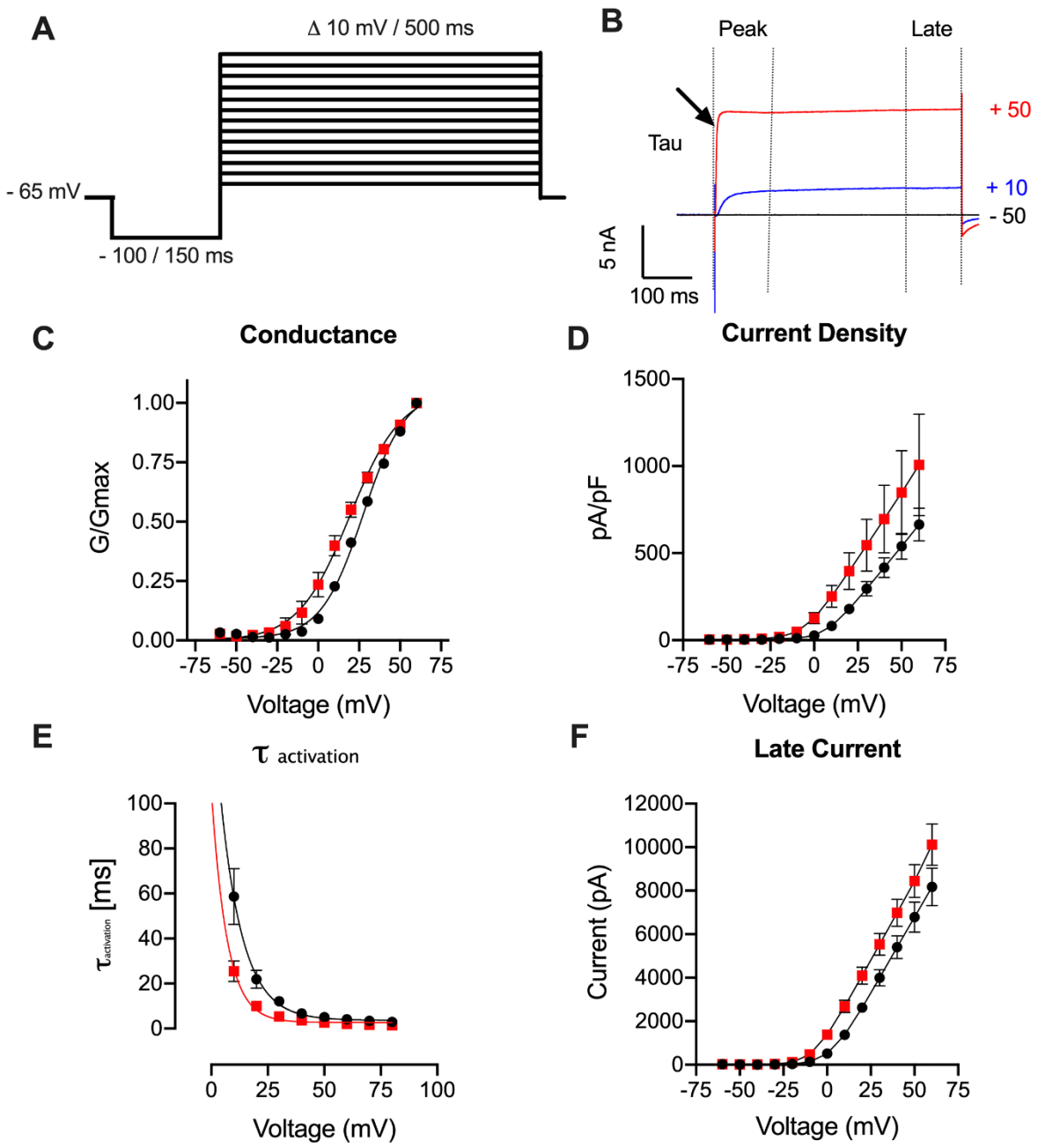

Figure 7-5 The effect of oxaliplatin on Kv2.1 kinetics.

Whole-cell manual voltage-clamp experiments on $K_v2.1$ transfected HEK293 cells. Cells incubated with oxaliplatin 100 µM 1 hr prior to recording (red squares) show altered kinetics compared to those incubated with vehicle control (5 % glucose, black circles). A) The protocol used for obtaining voltage-dependent data for the $K_v2.1$ channel included a 150 ms pre-pulse to -100 mV to inactivate the channel followed by 500 ms test pulses from -60 to +60 mV. B) Representative trace of non-inactivating $K_v2.1$ current at -50 (black), +10 (blue) and +50 mV (red) sweeps from a transfected HEK293 cell. Dotted lines indicate the regions from the test pulse from which graphs 7 C-G was obtained. C) Normalised conductance (G) -voltage (mV) relationship showing an 8.3 mV leftward shift in the voltage-dependence of activation of $K_v2.1$ for cells incubated with oxaliplatin 100 mM (V_{50} 19.3 ± 1.9 mV, n = 10) compared to vehicle

control (V_{50} 27.6 ± 0.7 mV, n = 8) (*P* < 0.05, unpaired *t* test). Calculated with a Boltzmann equation assuming a K^+ internal of [140] mM and a reversal potential of -85 mV. D) Current-density (pA/pF) is not significantly increased in cells incubated with oxaliplatin compared to control (peak pA/pF, 60 mV = control, 664.1 ± 93.4 and oxaliplatin, 1007 ± 291.7). E) The tau of activation (t) was calculated by fitting a single exponential to the fast rising phase of the activation curve. t significantly altered by oxaliplatin incubation at oxaliplatin 7-5 E, control at 10 mV 58.6 ± 12.4; oxaliplatin at 10 mV 25.5 ± 4.6, n = 8; 10, *P* > 0.05. F) The late current, at the end of the 500 ms test pulse, is unchanged in oxaliplatin treated cells compared to control.

7.4.6 Oxaliplatin causes irreversible covalent modification of human serum albumin

Oxaliplatin is known to bind to plasma proteins with high affinity (Kato et al., 2019). Like other platinum agents, it has been reported to have high protein binding rates (PBR) which is affected by slight changes in plasma albumin concentrations (Larsen et al., 1985). The PBR of oxaliplatin, like cisplatin is 98 %, and both agents bind irreversibly to proteins (Bell et al., 2008; Benedetti et al., 2011). Previous studies have shown that platinum drugs bind to the thiol and methionine groups in albumin. Oxaliplatin has been reported to interfere with redox signalling and cause oxidative stress. We therefore used mass spectrometry to assess whether oxaliplatin modified the model protein human serum albumin (HSA). We found that oxaliplatin modifies multiple residues of HSA after 2 hours and 24 hours incubation. Oxaliplatin caused HSA modifications by reversible and irreversible di- and tri-oxidation of cysteine residues (Figure 7-6). An example of a cysteine modified peptide with m/z 498.25 after 2 hours incubation with oxaliplatin is shown (Figure 7-6). This was assigned to Cysteine 99 (Cys99) on this peptide sequence. In these experiments, a substantial part of the sequence remained unresolved (figure 7-6A), which raises the possibility that residues central for trypsin cleavage may have undergone covalent modification. It is also possible that oxaliplatin generated peptides with modifications of previously unreported mass that may have escaped identification.

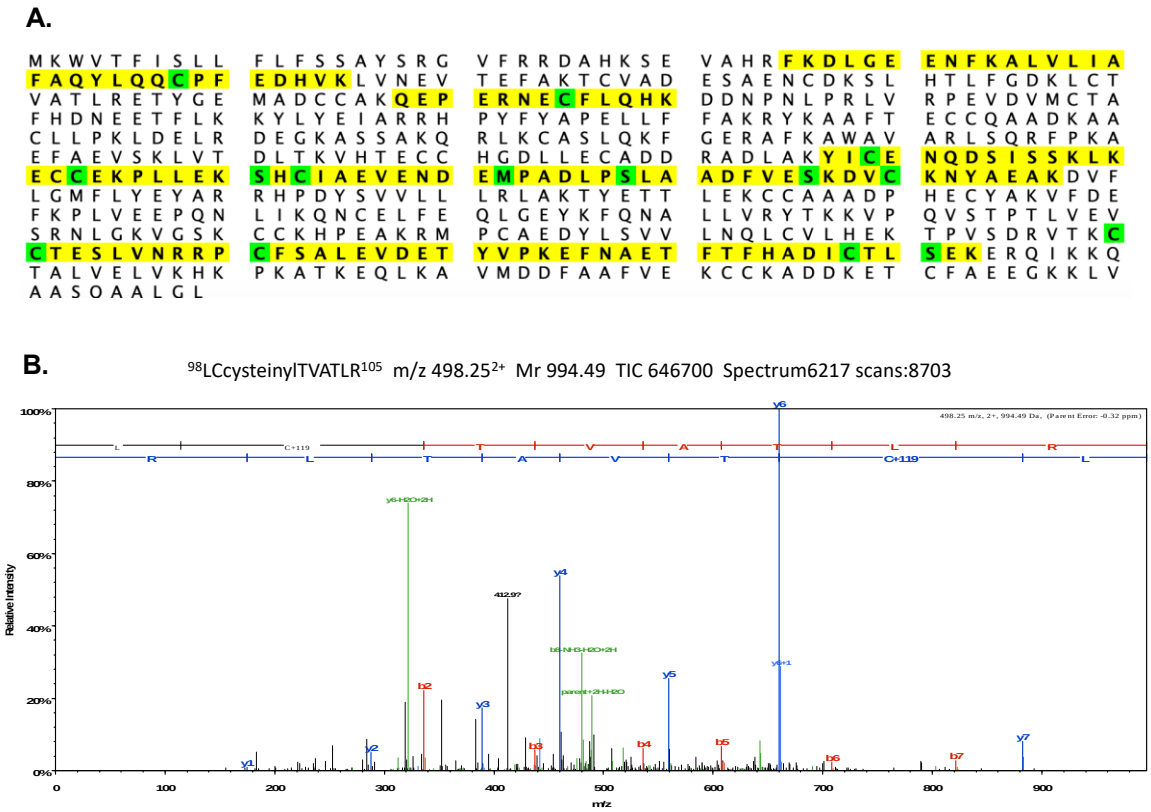

Figure 7-6 oxaliplatin treatment causes cysteinyl modifications in human serum albumin.

Following a 2-hour incubation period of oxaliplatin with human serum albumin (HSA), there were covalent modifications which occurred in multiple amino acid residues. This was particularly prominent at cysteine residues which showed irreversible oxidative modification. A) Snapshot of amino acid residues in HSA sample. Yellow fields indicate the percentage of coverage of the amino acid sequence using trypsin. Green fields indicate covalent modifications occurring at the highlighted residues. B) Evidence of a cysteinyl modified peptide with m/z 498.25^{2+}. A well-matched sequence tag from b1-y8 correctly determine the peptide assignment. The database assignment of the 119 Da modification is detected at the y11-ion in the spectra. Although the modification was not detected at the corresponding b2-ion, the ions matched from b3-b8 after the modification event gives added evidence for correct assignment at Cys99.

7.5 Discussion

We show for the first time that $K_v2.1$ can be added to the list of candidate channels that are modulated by oxaliplatin. The blockade of $K_v2.1$ using guangxitoxin (GxTx) was able to reverse the effects of oxaliplatin *in vivo* and in single-fibre recordings. In addition, oxaliplatin treatment in $K_v2.1$-expressing HEK cells showed a slight shift towards hyperpolarised currents in the voltage dependence of activation.

$K_v2.1$ is a delayed rectifier channel and is ubiquitously expressed in the brain and sensory neurons, where it regulates excitability (Du et al., 2000; Misonou et al., 2005; Speca et al., 2014; Tsantoulas et al., 2014). Typically, the use of K_v blockers in DRG neurons induces neuronal firing (Kajander et al., 1992), while K_v openers reduces neuronal excitability and relieves pain symptoms (Blackburn-Munro and Jensen, 2003; Dost et al., 2004; Mishra et al., 2012). However, we demonstrated that antagonism of $K_v2.1$, using GxTx reduced oxaliplatin-induced hyperexcitability in cortical neurons (Chapter 6), *in vivo* and in single-fibre recordings as demonstrated in this chapter. In behavioural studies, acute application of GxTx reversed oxaliplatin-induced mechanical and cold hypersensitivity. GxTx was injected locally into the paw of mice at the peak of the oxaliplatin-induced behavioural hypersensitivity and showed a dose-dependent reversal in the pain phenotype exhibited by mice. The greatest effects of GxTx *in vivo* were at 30 and 100 nM, and the same effects were seen by both concentrations between 30-60 minutes, suggesting maximal reversal had been achieved. At these low dosages, both $K_v2.1$ and $K_v2.2$ antagonism is achieved (Herrington, 2007). Therefore, there could have been off-target effects involving the blockade of other K_v or accessory subunits.

$K_v2.1$ is commonly associated with $K_v2.2$ and other modulatory K_v subunits including $K_v9.1$, $K_v4.3$ and $K_v6.1$ (Aimond Franck et al., 2005; McCrossan et al., 2009; Montalbetti et al., 2019).

K_v2.1 and K_v2.2 are expressed in cells of all sizes at the level of DRG neurons (Zeisel et al., 2018). Expression levels of K_v2 channels are particularly high in medium- to large-diameter sensory neurons (Tsantoulas et al., 2014). However, the majority of the sustained, delayed rectifier K_v conductance in nociceptors is modulated by stromatoxin (ScTx), a K_v2.1 inhibitor (Bocksteins et al., 2009). In this study, antagonism of K_v2.1 at the terminal level of primary afferent neurons reduced the number of *de novo* cold AM fibres. Direct co-application of GxTx with oxaliplatin inhibited the novel oxaliplatin-induced cold sensitivity demonstrated in AM fibres. In contrast, we did not detect a phenotype of GxTx on cold sensitivity of A or C fibres found in preparations from treated animals. Further study is required to reach a clear conclusion. This suggests that there are two differing mechanisms; one may involve the acute oxaliplatin-induced hyperexcitability that is blocked by GxTx, and the other driven by long term administration *in vivo*. The latter being more inclined to modification at the level of mRNA/ transcriptional modification. Acute application of oxaliplatin to the receptive fields of single-units had a very striking effect on A fibres, conferring an abnormal cold sensitivity on these normally temperature insensitive classes of fibres (Chapter 5). This was not the case in preparations taken from oxaliplatin-treated animals. Both the total number of cold-sensitive fibres and impulse discharge during cold stimulation was dramatically lower when compared to oxaliplatin application in naïve preparations.

In contrast to our findings, antagonism of K_v2 channels has been demonstrated to increase neuronal hyperexcitability in some studies (Romer et al., 2019; Tsantoulas et al., 2014). Inhibition of K_v2.1 currents in DRG neurons and spinal motoneurons shortened inter-spike intervals and increased repetitive firing rates (Romer et al., 2019; Tsantoulas et al., 2014). However, other studies have reported that use of GxTx increased the duration of inter-spike

intervals and reduced the maximal outward current (Liu and Bean, 2014). This, in combination with a depolarising shift of the trough after the first action potential, resulted in slowed firing over time (Liu and Bean, 2014). In our study, acute application of oxaliplatin induced repetitive firing in single fibres. Co-application of GxTx with oxaliplatin inhibited this phenomenon and may be explained by the depolarising shift in the trough of action potentials after the initial firing. A similar finding is reported in another study which demonstrated that blocking K_v2 / $K_v9.1$ subunits with GxTx during sustained electrical stimulation, inhibits repetitive firing of sensitised IB4- bladder sensory neurons (Montalbetti et al., 2019). K_v2 / $K_v9.1$ channels were activated during the first action potential evoked by the electrical stimulus, and were therefore able to maintain excitability during repetitive firing (Montalbetti et al., 2019). This notion is consistent with K_v2 channels playing a major role in regulating neuronal excitability during periods of high-frequency firing (Malin and Nerbonne, 2002; Misonou et al., 2005; Speca et al., 2014). Due to the slow deactivation kinetics of K_v2 subunits, there is cumulative activation during periods of high frequency firing (Guan et al., 2007; Malin and Nerbonne, 2002). This cumulative recruitment of activated K_v2 channels is critical for producing a sufficient negative inter-spike potential that allows Na_v channels to recover faster from inactivation, making them available to generate subsequent action potentials (Liu and Bean, 2014).

In addition, we show that oxaliplatin caused a leftward shift of activation in $K_v2.1$-expressing HEK cells. The conductance and current density were increased at negative potentials after oxaliplatin treatment when compared to vehicle treatment. The shift towards negative potentials has been reported previously in GxTx-sensitive currents in sensitised bladder sensory neurons (Montalbetti et al., 2019). When $K_v9.1$ was co-expressed with $K_v2.2$ subunits,

the voltage dependence of activation, but not inactivation was shifted towards more negative potentials (Montalbetti et al., 2019). This phenomenon is likely to occur during sensitised states as K_v2 currents are important in maintaining neuronal excitability during periods of repetitive firing. In this study, we demonstrate a shift of 8 mV towards more negative potentials after oxaliplatin treatment. $K_v2.1$ channel pores being open at negative potentials might facilitate periods of high frequency firing, which is caused by oxaliplatin in sensory neurons (Adelsberger et al., 2000; Sittl et al., 2012). Small changes in channel kinetics can bring about profound changes in neuronal firing and underlie pain states in humans. One example is $Na_v1.7$ inherited erythromelalgia mutations (Stadler et al., 2015). Therefore, any small changes brought about by oxaliplatin, in conjunction with the changes which have already been identified in other ion channels, such as $Na_v1.6$ (Deuis et al., 2013; Sittl et al., 2012), could reasonably explain the symptoms seen in patients.

Further investigations into how oxaliplatin might modulate ion channels was conducted using mass spectrometry. We hypothesised that it was through oxidation of particularly important channel residues. We show that oxaliplatin irreversibly modifies cysteine residues by di- and tri-oxidation in HSA peptides. Other studies have also reported the irreversible binding of oxaliplatin to plasma proteins such as albumin (Kato et al., 2019), and that oxaliplatin evokes reactive oxygen species (ROS) mediated cysteine oxidation (Miyake et al., 2016). Cysteine oxidation is possible due to the presence of a thiol group and can produce reversible and irreversible products. The simplest oxyacid of sulfur, sulfenic acid, is produced by oxidation of thiol groups by hydroperoxides (Poole, 2015). This is a reversible product. Irreversible oxidation of sulfur produces sulfinic and sulfonic acid (Poole, 2015). These are not commonly formed under normal physiological processes. This makes our findings for the effects of

oxaliplatin on albumin more striking. In our mass spectrometry findings, oxaliplatin failed to form reversible products from cysteine oxidation, and instead caused advanced oxidation to form irreversible products. This provides a molecular mechanism for how the anticancer drug can modulate ion channels. Cysteine oxidation by oxaliplatin-induced ROS formation has been shown to activate TRPA1 (Miyake et al., 2016). In addition, K_v2.1 is regulated by oxidative modulation (Sahoo et al., 2014; Sesti, 2016). Cysteine oxidation in K_v2.1 channels has been reported to be linked to the progression of Alzheimer's and other neurodegenerative diseases (Sahoo et al., 2014; Sesti, 2016). Therefore, oxidative modulation of K_v2.1 may be important in pain states in the peripheral nervous system.

In conclusion, K_v2.1 is a potential target in oxaliplatin-induced hyperexcitability *in vivo* and *in vitro*. Co-application of oxaliplatin with a K_v2.1 inhibitor may provide a therapeutic opportunity for pain management in oxaliplatin-treated patients. In addition, we show that oxaliplatin directly alters K_v2.1 kinetics of activation. Finally, we show that oxaliplatin can irreversibly oxidise cysteine residues in human serum albumin. Based on these findings, we expect that oxaliplatin can also oxidise K_v2.1 and modulate its activity. Other channels important in pain mechanisms such as TRPA1, are known to affected by oxidation. Thus, oxidation of K_v2.1 by oxaliplatin may provide another molecular mechanism for oxaliplatin-induced hyperexcitability.

8. General discussion and conclusions

Oxaliplatin is an effective platinum-based anticancer drug used in the treatment of colorectal, ovarian, breast and lung cancers (Descoeur et al., 2011; Lehky et al., 2004; McWhinney et al., 2009; Saif and Reardon, 2005; Wilson et al., 2002). However, it has dose-limiting effects which manifest as cold hypersensitivity and paraesthesias. Acute cold hypersensitivity has a rapid onset and symptoms can occur during or straight after infusions in the clinic, but takes days to be resolved (Argyriou et al., 2008). Other side effects include paraesthesias, which develop into functional impairments over time. Patients have reported being unable to fasten buckles and buttons and use zippers (Grothey et al., 2011; Tofthagen et al., 2013b). Chronic neuropathy develops over many treatment cycles (Saif and Reardon, 2005). The mechanisms of acute oxaliplatin-induced cold hypersensitivity have been studied extensively and it is likely that it occurs in a different way to chronic neuropathy. The acute phase of hypersensitivity occurs due to oxaliplatin directly interacting with voltage-gated ion channels. The main classes of ion channels that have been proposed to play a role are important in regulating and determining excitability in neurons such as Na_v, K_v and HCN channels (Adelsberger et al., 2000; Deuis et al., 2014; Resta et al., 2018; Sittl et al., 2010, 2012; Young et al., 2014). TRP channels have also been implicated in the mechanism (Anand et al., 2010; Gauchan et al., 2009; Kawashiri et al., 2012; Kono et al., 2012; Nassini et al., 2011; Zhao et al., 2012). It is important to note that in all models of pain behaviour, TRPA1 or TRPV1 inhibition will produce analgesia (Koivisto et al., 2018; Premkumar and Sikand, 2008). Thus, it does not necessarily indicate a direct role for these channels in oxaliplatin evoked hyperexcitability mechanisms. The aims of this project were to investigate the neuronal and ionic mechanisms of acute oxaliplatin-induced cold hypersensitivity and paraesthesias using methodology that could enable the potential discovery of novel and alternative/additional mechanisms.

In the first results chapter (Chapter 2), we confirmed the effects of oxaliplatin *in vivo* and demonstrated a robust pain phenotype to mechanical and cold stimuli in these behavioural studies in mice. Our findings were aligned to those from previous studies that have reported oxaliplatin-induced mechanical and cold hypersensitivity (Descoeur et al., 2011; Deuis et al., 2013; Gauchan et al., 2009; Sittl et al., 2012; Young et al., 2014; Zhao et al., 2012). We also observed a delayed onset of oxaliplatin-induced cold hypersensitivity in *Trpm8*$^{-/-}$ mice. The behavioural phenotype in WT mice recapitulated some of the patient side effects reported in the clinic and offered opportunities to explore the mechanisms in greater detail. *Ex vivo* experiments for Ca^{2+}-imaging and single fibre recordings were made possible using the DRG neurons and skin-saphenous nerve preparations from the hind paw of oxaliplatin-treated mice (Chapters 3 and 5 respectively). In addition, the role of $K_v2.1$ in oxaliplatin-induced cold and mechanical hypersensitivity was investigated *in vivo* using this model (Chapter 7).

Oxaliplatin-induced hyperexcitability in DRG neurons has been investigated extensively (Adelsberger et al., 2000; Anand et al., 2010; Descoeur et al., 2011; Sittl et al., 2012; Young et al., 2014; Zhao et al., 2012). We showed that acute and longer-term oxaliplatin treatment in DRG neurons resulted in a significant, but small increase in cold sensitivity (Chapter 3). There was a significant reduction in the proportion of cold-sensitive neurons isolated from oxaliplatin-treated *Trpm8*$^{-/-}$ mice. This may show a role for TRPM8 in oxaliplatin-induced cold hypersensitivity as proposed by previous studies (Gauchan et al., 2009; Kawashiri et al., 2012; Kono et al., 2012). However, TRPM8 is also the principal mammalian cold sensor and previous knockout studies have shown deficits in cold sensitivity and thermal preference in mice (Colburn et al., 2007; Dhaka et al., 2007; Knowlton et al., 2010). Therefore, it is unclear whether this reduction is oxaliplatin-dependent. We also reported that oxaliplatin directly

activated a small proportion of DRG neurons. These neurons often showed an oscillatory response over time. The limited functional effects of oxaliplatin that we detected in isolated DRG neurons, suggest that other approaches may be more appropriate for studies of oxaliplatin-induced hyperexcitability. The addition of skin-nerve investigations provided a possible strategy for more in-depth studies into the subsets of sensory afferent fibres which are affected by oxaliplatin.

We conducted comprehensive single fibre electrophysiological recordings using the skin-saphenous nerve preparation, to identify which functional classes of sensory afferents are affected by oxaliplatin. We first started off by characterising the normal physiological responses of each class of A and C fibres to mechanical and cold stimuli (Chapter 4). The fibre classes were divided further into LTMRs and HTMRs according to their adaptation properties to different levels and types of forces. In these studies, we observed no response to cold stimulation amongst any class of A fibres as expected and there was a subpopulation of C fibres, referred to as CMC which were responsive during cold stimulations. Acute oxaliplatin produced a gain of cold sensitivity in all A fibre classes and one in type of C fibres (Chapter 5). In addition, oxaliplatin resulted in cold-evoked action potential bursts and impulse discharges that outlasted mechanical and cold stimulation periods. Oxaliplatin changed the adaptation properties of all classes of fibres. The changes to the properties of Aβ fibres may explain the cellular basis of oxaliplatin-induced cold-evoked paraesthesias. In addition, altered adaptation properties of Aβ, AM and C fibres are likely to explain cold-evoked allodynia, a hallmark symptom of oxaliplatin-induced hyperexcitability. Oxaliplatin treatment *in vivo* increased spontaneous discharges in single and multi-unit fibres. We also noted that C fibres

appeared more affected than A fibres in these preparations. It is possible that the apparent differences were produced by the duration of exposure and effective concentrations reached.

For a long time, the molecular mechanisms of oxaliplatin-induced hyperexcitability have been explained by the sensitisation and increased expression of ion channels such as TRP channels, Na_v and K_v channels in C nociceptors (Descoeur et al., 2011; Deuis et al., 2013; Gauchan et al., 2009; Kono et al., 2012; Zhao et al., 2012). However, our experiments identified a prominent role of A fibres, highlighting other cellular and molecular mechanisms for oxaliplatin-induced hyperexcitability. These findings are in line with more recent studies, where oxaliplatin has been shown to sensitise A fibres (Deuis et al., 2013; Forstenpointner et al., 2018; MacDonald et al., 2021; Sittl et al., 2012). Oxaliplatin-induced cold-evoked bursting in A fibres is explained by the direct effects of the drug on $Na_v1.6$ channels, which is exclusively expressed in A fibres (Deuis et al., 2013, 2014; Sittl et al., 2012). The duration of oxaliplatin treatment influences the mechanism by which the drug exerts its effects. It is likely that there are additional mechanisms involved for oxaliplatin-induced hyperexcitability.

We used cortical neurons as a model system in a higher throughput multielectrode array to explore the potential involvement of different ion channels (Chapter 6). Over the years, many ion channels have been proposed to be candidates for a role in oxaliplatin-induced hyperexcitability, some of which were chosen for investigation in our own studies and others that have not been explored previously. We discovered that oxaliplatin rapidly produced hyperexcitability in cortical neurons, which may be a tractable model for mechanistic studies, since they are available in far larger numbers. In these experiments, we demonstrated that

the oxaliplatin-induced hyperexcitability could be prevented either by an HCN blocker or a specific K_v2.1 toxin inhibitor.

In the final chapter (Chapter 7), we investigated a putative role for K_v2.1 in oxaliplatin-induced cold hypersensitivity in greater detail. We demonstrated that K_v2.1 antagonism *in vivo* reversed oxaliplatin-induced cold and mechanical hypersensitivity in mice, 4 days after oxaliplatin treatment. In addition, we found that co-application of the specific K_v2.1 inhibitor guangxitoxin (GxTx) together with oxaliplatin inhibited the abnormal cold sensitivity of AM fibres in skin-saphenous nerve experiments. Furthermore, oxaliplatin produced a hyperpolarising shift of the voltage-dependent activation (~9 mV) of K_v2.1, demonstrating that oxaliplatin facilitates opening of this channel. Taken together, our results strongly suggest that oxaliplatin evoked hypersensitivity and hyperexcitability rely on an enhanced activity of K_v2.1. Furthermore, interventions that target the increased activity of K_v2.1 may represent therapeutic opportunities. Preliminary mass spectrometry investigations of human albumin suggest that oxaliplatin oxidises cysteine residues in proteins. Future studies will determine whether K_v2.1 is covalently modified by oxaliplatin, and its potential impact on the properties of the channel. In addition, further studies should be conducted to assess whether the onset of cold and mechanical hypersensitivity can be prevented or delayed by co-application of GxTx with oxaliplatin *in vivo*. Furthermore, it would be practical to know what the expression levels of K_v2.1 (or indeed other ion channels of interest) are in primary afferent neurons at the level of the terminal. This may provide an explanation for the different effects of oxaliplatin in sensory neuron populations.

Oxaliplatin-induced cold hypersensitivity and paraesthesias are caused by hyperexcitability of ion channels in sensory neurons. We have demonstrated that positive modulation of K_v2.1 is

required for oxaliplatin-induced hypersensitivity *in vivo* and neuronal hyperexcitability *in vitro*. Further exploration of this channel's role will establish whether it represents a tractable avenue for possible adjuvant therapies that may be used in conjunction with oxaliplatin to reduce its dose-limiting effects.

In summary, we show which subpopulations of sensory neurons are affected at the level of the terminal for the first time, using the skin-nerve preparation. We also identified an additional and novel ion channel target for oxaliplatin-induced hyperexcitability and cold hypersensitivity. Taken together, this sheds further light into this research area.

References

Abdo, H., Calvo-Enrique, L., Lopez, J.M., Song, J., Zhang, M.-D., Usoskin, D., Manira, A.E., Adameyko, I., Hjerling-Leffler, J., and Ernfors, P. (2019). Specialized cutaneous Schwann cells initiate pain sensation. Science *365*, 695–699.

Abraira, V.E., and Ginty, D.D. (2013). The Sensory Neurons of Touch. Neuron *79*.

Ackerley, R., Saar, K., McGlone, F., and Backlund Wasling, H. (2014). Quantifying the sensory and emotional perception of touch: differences between glabrous and hairy skin. Front. Behav. Neurosci. *8*.

Adelsberger, H., Quasthoff, S., Grosskreutz, J., Lepier, A., Eckel, F., and Lersch, C. (2000). The chemotherapeutic oxaliplatin alters voltage-gated Na(+) channel kinetics on rat sensory neurons. Eur. J. Pharmacol. *406*, 25–32.

Adriaensen, H., Gybels, J., Handwerker, H.O., and Van Hees, J. (1983). Response properties of thin myelinated (A-delta) fibers in human skin nerves. J. Neurophysiol. *49*, 111–122.

Adrian, E.D., and Zotterman, Y. (1926). The impulses produced by sensory nerve endings. J. Physiol. *61*, 465–483.

Aimond Franck, Kwak Seung P., Rhodes Kenneth J., and Nerbonne Jeanne M. (2005). Accessory Kvβ1 Subunits Differentially Modulate the Functional Expression of Voltage-Gated K+ Channels in Mouse Ventricular Myocytes. Circ. Res. *96*, 451–458.

Akopian, A.N., Souslova, V., England, S., Okuse, K., Ogata, N., Ure, J., Smith, A., Kerr, B.J., McMahon, S.B., Boyce, S., et al. (1999). The tetrodotoxin-resistant sodium channel SNS has a specialized function in pain pathways. Nat. Neurosci. *2*, 541–548.

Alkhatib, O., Costa, R. da, Gentry, C., Quallo, T., Mannebach, S., Weissgerber, P., Freichel, M., Philipp, S.E., Bevan, S., and Andersson, D.A. (2019). Promiscuous G-Protein-Coupled Receptor Inhibition of Transient Receptor Potential Melastatin 3 Ion Channels by Gβγ Subunits. J. Neurosci. *39*, 7840–7852.

Alloui, A., Zimmermann, K., Mamet, J., Duprat, F., Noël, J., Chemin, J., Guy, N., Blondeau, N., Voilley, N., Rubat-Coudert, C., et al. (2006). TREK-1, a K+ channel involved in polymodal pain perception. EMBO J. *25*, 2368–2376.

Anand, U., Otto, W.R., and Anand, P. (2010). Sensitization of capsaicin and icilin responses in oxaliplatin treated adult rat DRG neurons. Mol. Pain *6*, 82.

Andersson, D.A., Gentry, C., Moss, S., and Bevan, S. (2008). Transient receptor potential A1 is a sensory receptor for multiple products of oxidative stress. J. Neurosci. Off. J. Soc. Neurosci. *28*, 2485–2494.

Andersson, D.A., Gentry, C., Moss, S., and Bevan, S. (2009). Clioquinol and pyrithione activate TRPA1 by increasing intracellular Zn2+. Proc. Natl. Acad. Sci. U. S. A. *106*, 8374–8379.

Andersson, D.A., Gentry, C., Light, E., Vastani, N., Vallortigara, J., Bierhaus, A., Fleming, T., and Bevan, S. (2013). Methylglyoxal Evokes Pain by Stimulating TRPA1. PLoS ONE *8*.

Andersson, D.A., Filipović, M.R., Gentry, C., Eberhardt, M., Vastani, N., Leffler, A., Reeh, P., and Bevan, S. (2015). Streptozotocin Stimulates the Ion Channel TRPA1 Directly. J. Biol. Chem. *290*, 15185–15196.

Andrews, M.D., af Forselles, K., Beaumont, K., Galan, S.R.G., Glossop, P.A., Grenie, M., Jessiman, A., Kenyon, A.S., Lunn, G., Maw, G., et al. (2015). Discovery of a Selective TRPM8 Antagonist with Clinical Efficacy in Cold-Related Pain. ACS Med. Chem. Lett. *6*, 419–424.

Argyriou, A.A., Polychronopoulos, P., Iconomou, G., Chroni, E., and Kalofonos, H.P. (2008). A review on oxaliplatin-induced peripheral nerve damage. Cancer Treat. Rev. *34*, 368–377.

Attal, N., Bouhassira, D., Gautron, M., Vaillant, J.N., Mitry, E., Lepère, C., Rougier, P., and Guirimand, F. (2009). Thermal hyperalgesia as a marker of oxaliplatin neurotoxicity: A prospective quantified sensory assessment study. PAIN® *144*, 245–252.

Avan, A., Postma, T.J., Ceresa, C., Avan, A., Cavaletti, G., Giovannetti, E., and Peters, G.J. (2015). Platinum-induced neurotoxicity and preventive strategies: past, present, and future. The Oncologist *20*, 411–432.

Bade, H., Braun, H.A., and Hensel, H. (1979). Parameters of the static burst discharge of lingual cold receptors in the cat. Pflüg. Arch. - Eur. J. Physiol. *382*, 1–5.

Baloh, R.W. (2012). Chapter 42 - Episodic ataxias 1 and 2. In Handbook of Clinical Neurology, S.H. Subramony, and A. Dürr, eds. (Elsevier), pp. 595–602.

Bandell, M., Story, G.M., Hwang, S.W., Viswanath, V., Eid, S.R., Petrus, M.J., Earley, T.J., and Patapoutian, A. (2004). Noxious cold ion channel TRPA1 is activated by pungent compounds and bradykinin. Neuron *41*, 849–857.

Banik, R.K., and Brennan, T.J. (2008). Sensitization of primary afferents to mechanical and heat stimuli after incision in a novel in vitro mouse glabrous skin-nerve preparation. Pain *138*, 380–391.

Barbosa, M. de C., Kosturakis, A.K., Eng, C., Wendelschafer-Crabb, G., Kennedy, W.R., Simone, D.A., Wang, X.S., Cleeland, C.S., and Dougherty, P.M. (2014). A Quantitative Sensory Analysis of Peripheral Neuropathy in Colorectal Cancer and Its Exacerbation by Oxaliplatin Chemotherapy. Cancer Res. *74*, 5955–5962.

Barclay, J., Patel, S., Dorn, G., Wotherspoon, G., Moffatt, S., Eunson, L., Abdel'al, S., Natt, F., Hall, J., Winter, J., et al. (2002). Functional Downregulation of P2X3 Receptor Subunit in Rat Sensory Neurons Reveals a Significant Role in Chronic Neuropathic and Inflammatory Pain. J. Neurosci. *22*, 8139–8147.

Baron, R. (2006). Mechanisms of Disease: neuropathic pain—a clinical perspective. Nat. Clin. Pract. Neurol. *2*, 95–106.

Basbaum, A.I., Bautista, D.M., Scherrer, G., and Julius, D. (2009). Cellular and Molecular Mechanisms of Pain. Cell *139*, 267–284.

Bautista, D.M., Movahed, P., Hinman, A., Axelsson, H.E., Sterner, O., Högestätt, E.D., Julius, D., Jordt, S.-E., and Zygmunt, P.M. (2005). Pungent products from garlic activate the sensory ion channel TRPA1. Proc. Natl. Acad. Sci. U. S. A. *102*, 12248–12252.

Bautista, D.M., Jordt, S.-E., Nikai, T., Tsuruda, P.R., Read, A.J., Poblete, J., Yamoah, E.N., Basbaum, A.I., and Julius, D. (2006). TRPA1 Mediates the Inflammatory Actions of Environmental Irritants and Proalgesic Agents. Cell *124*, 1269–1282.

Bautista, D.M., Siemens, J., Glazer, J.M., Tsuruda, P.R., Basbaum, A.I., Stucky, C.L., Jordt, S.-E., and Julius, D. (2007). The menthol receptor TRPM8 is the principal detector of environmental cold. Nature *448*, 204–208.

Baver, S.B., and O'Connell, K.M.S. (2012). The C-terminus of neuronal Kv2.1 channels is required for channel localization and targeting but not for NMDA-receptor mediated regulation of channel function. Neuroscience *217*, 56–66.

Bell, D.N., Liu, J.J., Tingle, M.D., Rattel, B., Meyer, T.U., and McKeage, M.J. (2008). COMPARATIVE PROTEIN BINDING, STABILITY AND DEGRADATION OF SATRAPLATIN, JM118 AND CISPLATIN IN HUMAN PLASMA *IN VITRO*. Clin. Exp. Pharmacol. Physiol. ???-???

Belmonte, C., and Gallar, J. (2011). Cold Thermoreceptors, Unexpected Players in Tear Production and Ocular Dryness Sensations. Invest. Ophthalmol. Vis. Sci. *52*, 3888–3892.

Belmonte, C., and Viana, F. (2008). Molecular and cellular limits to somatosensory specificity. Mol. Pain *4*, 14.

Benedetti, B.T., Peterson, E.J., Kabolizadeh, P., Martínez, A., Kipping, R., and Farrell, N.P. (2011). Effects of Noncovalent Platinum Drug–Protein Interactions on Drug Efficacy: Use of Fluorescent Conjugates as Probes for Drug Metabolism. Mol. Pharm. *8*, 940–948.

Bennett, G.J., and Xie, Y.K. (1988). A peripheral mononeuropathy in rat that produces disorders of pain sensation like those seen in man. Pain *33*, 87–107.

Bennett, D.L., Clark, A.J., Huang, J., Waxman, S.G., and Dib-Hajj, S.D. (2019). The Role of Voltage-Gated Sodium Channels in Pain Signaling. Physiol. Rev. *99*, 1079–1151.

Benoit, E., Brienza, S., and Dubois, J.M. (2006). Oxaliplatin, an anticancer agent that affects both Na+ and K+ channels in frog peripheral myelinated axons. Gen. Physiol. Biophys. *25*, 263–276.

Bensmaïa, S.J., Craig, J.C., Yoshioka, T., and Johnson, K.O. (2006). SA1 and RA Afferent Responses to Static and Vibrating Gratings. J. Neurophysiol. *95*, 1771–1782.

Berdeaux, A., Tissier, R., Couvreur, N., Salouage, I., and Ghaleh, B. (2009). [Heart rate reduction: beneficial effects in heart failure and post-infarcted myocardium]. Therapie *64*, 87–91.

Bessou, P., and Perl, E.R. (1969). Response of cutaneous sensory units with unmyelinated fibers to noxious stimuli. J. Neurophysiol. *32*, 1025–1043.

Bevan, S., and Szolcsányi, J. (1990). Sensory neuron-specific actions of capsaicin: mechanisms and applications. Trends Pharmacol. Sci. *11*, 331–333.

Bevan, S., and Winter, J. (1995). Nerve growth factor (NGF) differentially regulates the chemosensitivity of adult rat cultured sensory neurons. J. Neurosci. *15*, 4918–4926.

Bevan, S., Quallo, T., and Andersson, D.A. (2014). TRPV1. In Mammalian Transient Receptor Potential (TRP) Cation Channels: Volume I, B. Nilius, and V. Flockerzi, eds. (Berlin, Heidelberg: Springer), pp. 207–245.

Binder, A., Stengel, M., Maag, R., Wasner, G., Schoch, R., Moosig, F., Schommer, B., and Baron, R. (2007). Pain in oxaliplatin-induced neuropathy – Sensitisation in the peripheral and central nociceptive system. Eur. J. Cancer *43*, 2658–2663.

Binshtok, A.M., Bean, B.P., and Woolf, C.J. (2007). Inhibition of nociceptors by TRPV1-mediated entry of impermeant sodium channel blockers. Nature *449*, 607–610.

Blackburn-Munro, G., and Jensen, B.S. (2003). The anticonvulsant retigabine attenuates nociceptive behaviours in rat models of persistent and neuropathic pain. Eur. J. Pharmacol. *460*, 109–116.

Bocksteins, E., Raes, A.L., Van de Vijver, G., Bruyns, T., Van Bogaert, P.-P., and Snyders, D.J. (2009). Kv2.1 and silent Kv subunits underlie the delayed rectifier K+ current in cultured small mouse DRG neurons. Am. J. Physiol.-Cell Physiol. *296*, C1271–C1278.

Bond, C.T., Herson, P.S., Strassmaier, T., Hammond, R., Stackman, R., Maylie, J., and Adelman, J.P. (2004). Small Conductance Ca2+-Activated K+ Channel Knock-Out Mice Reveal the Identity of Calcium-Dependent Afterhyperpolarization Currents. J. Neurosci. *24*, 5301–5306.

Boughattas, N.A., Hecquet, B., Fournier, C., Bruguerolle, B., Trabelsi, H., Bouzouita, K., Omrane, B., and Lévi, F. (1994). Comparative pharmacokinetics of oxaliplatin (L-OHP) and carboplatin (CBDCA) in mice with reference to circadian dosing time. Biopharm. Drug Dispos. *15*, 761–773.

Boyette-Davis, J., and Dougherty, P.M. (2011). Protection against oxaliplatin-induced mechanical hyperalgesia and intraepidermal nerve fiber loss by minocycline. Exp. Neurol. *229*, 353–357.

Boyette-Davis, J.A., Cata, J.P., Zhang, H., Driver, L.C., Wendelschafer-Crabb, G., Kennedy, W.R., and Dougherty, P.M. (2011). Follow-up psychophysical studies in bortezomib-related chemoneuropathy patients. J. Pain Off. J. Am. Pain Soc. *12*, 1017–1024.

Boyette-Davis, J.A., Cata, J.P., Driver, L.C., Novy, D.M., Bruel, B.M., Mooring, D.L., Wendelschafer-Crabb, G., Kennedy, W.R., and Dougherty, P.M. (2013). Persistent

chemoneuropathy in patients receiving the plant alkaloids paclitaxel and vincristine. Cancer Chemother. Pharmacol. *71*, 619–626.

Boyette-Davis, J.A., Walters, E.T., and Dougherty, P.M. (2015). Mechanisms involved in the development of chemotherapy-induced neuropathy. Pain Manag. *5*, 285–296.

Brain, S.D., and Williams, T.J. (1985). Inflammatory oedema induced by synergism between calcitonin gene-related peptide (CGRP) and mediators of increased vascular permeability. Br. J. Pharmacol. *86*, 855–860.

Brain, S.D., and Williams, T.J. (1988). Substance P regulates the vasodilator activity of calcitonin gene-related peptide. Nature *335*, 73–75.

Branca, J.J.V., Maresca, M., Morucci, G., Becatti, M., Paternostro, F., Gulisano, M., Ghelardini, C., Salvemini, D., Di Cesare Mannelli, L., and Pacini, A. (2018). Oxaliplatin-induced blood brain barrier loosening: a new point of view on chemotherapy-induced neurotoxicity. Oncotarget *9*, 23426–23438.

Brazhe, A.R., Maksimov, G.V., Mosekilde, E., and Sosnovtseva, O.V. (2011). Excitation block in a nerve fibre model owing to potassium-dependent changes in myelin resistance. Interface Focus *1*, 86–100.

Brock, J.A., McLachlan, E.M., and Belmonte, C. (1998). Tetrodotoxin-resistant impulses in single nociceptor nerve terminals in guinea-pig cornea. J. Physiol. *512*, 211–217.

Brown, D.A. (1988). M currents. Ion Channels *1*, 55–94.

Brown, A.G., and Iggo, A. (1967). A quantitative study of cutaneous receptors and afferent fibres in the cat and rabbit. J. Physiol. *193*, 707–733.

Bucchi, A., Tognati, A., Milanesi, R., Baruscotti, M., and DiFrancesco, D. (2006). Properties of ivabradine-induced block of HCN1 and HCN4 pacemaker channels. J. Physiol. *572*, 335–346.

Burakgazi, A.Z., Messersmith, W., Vaidya, D., Hauer, P., Hoke, A., and Polydefkis, M. (2011). Longitudinal assessment of oxaliplatin-induced neuropathy. Neurology *77*, 980–986.

Burgess, P.R., and Perl, E.R. (1967). Myelinated afferent fibres responding specifically to noxious stimulation of the skin. J. Physiol. *190*, 541–562.

Burgess, P.R., Petit, D., and Warren, R.M. (1968). Receptor types in cat hairy skin supplied by myelinated fibers. J. Neurophysiol. *31*, 833–848.

Burnstock, G. (2000). P2X receptors in sensory neurones. Br. J. Anaesth. *84*, 476–488.

Burnstock, G., and Wood, J.N. (1996). Purinergic receptors: their role in nociception and primary afferent neurotransmission. Curr. Opin. Neurobiol. *6*, 526–532.

Cain, D.M., Khasabov, S.G., and Simone, D.A. (2001). Response Properties of Mechanoreceptors and Nociceptors in Mouse Glabrous Skin: An In Vivo Study. J. Neurophysiol. *85*, 1561–1574.

Cameron, N.E., Eaton, S.E., Cotter, M.A., and Tesfaye, S. (2001). Vascular factors and metabolic interactions in the pathogenesis of diabetic neuropathy. Diabetologia *44*, 1973–1988.

Campero, M., Serra, J., and Ochoa, J.L. (1996). C-polymodal nociceptors activated by noxious low temperature in human skin. J. Physiol. *497*, 565–572.

Campero, M., Serra, J., Bostock, H., and Ochoa, J.L. (2001). Slowly conducting afferents activated by innocuous low temperature in human skin. J. Physiol. *535*, 855–865.

Campero, M., Baumann, T.K., Bostock, H., and Ochoa, J.L. (2009). Human cutaneous C fibres activated by cooling, heating and menthol. J. Physiol. *587*, 5633–5652.

Carlton, S.M., and Hargett, G.L. (2007). Colocalization of metabotropic glutamate receptors in rat dorsal root ganglion cells. J. Comp. Neurol. *501*, 780–789.

Carozzi, V.A., Canta, A., and Chiorazzi, A. (2015). Chemotherapy-induced peripheral neuropathy: What do we know about mechanisms? Neurosci. Lett. *596*, 90–107.

Carr, R.W., Pianova, S., and Brock, J.A. (2002). The Effects of Polarizing Current on Nerve Terminal Impulses Recorded from Polymodal and Cold Receptors in the Guinea-pig Cornea. J. Gen. Physiol. *120*, 395–405.

Carr, R.W., Pianova, S., Fernandez, J., Fallon, J.B., Belmonte, C., and Brock, J.A. (2003). Effects of Heating and Cooling on Nerve Terminal Impulses Recorded from Cold-sensitive Receptors in the Guinea-pig Cornea. J. Gen. Physiol. *121*, 427–439.

Caterina, M.J., Schumacher, M.A., Tominaga, M., Rosen, T.A., Levine, J.D., and Julius, D. (1997). The capsaicin receptor: a heat-activated ion channel in the pain pathway. Nature *389*, 816–824.

Caterina, M.J., Rosen, T.A., Tominaga, M., Brake, A.J., and Julius, D. (1999). A capsaicin-receptor homologue with a high threshold for noxious heat. Nature *398*, 436–441.

Caterina, M.J., Leffler, A., Malmberg, A.B., Martin, W.J., Trafton, J., Petersen-Zeitz, K.R., Koltzenburg, M., Basbaum, A.I., and Julius, D. (2000). Impaired Nociception and Pain Sensation in Mice Lacking the Capsaicin Receptor. Science *288*, 306–313.

Cavanaugh, D.J., Lee, H., Lo, L., Shields, S.D., Zylka, M.J., Basbaum, A.I., and Anderson, D.J. (2009). Distinct subsets of unmyelinated primary sensory fibers mediate behavioral responses to noxious thermal and mechanical stimuli. Proc. Natl. Acad. Sci. *106*, 9075–9080.

Chambers, M.R., Andres, K.H., Duering, M. v, and Iggo, A. (1972). The Structure and Function of the Slowly Adapting Type Ii Mechanoreceptor in Hairy Skin. Q. J. Exp. Physiol. Cogn. Med. Sci. *57*, 417–445.

Chao, M.V. (2003). Neurotrophins and their receptors: A convergence point for many signalling pathways. Nat. Rev. Neurosci. *4*, 299–309.

Chaplan, S.R., Bach, F.W., Pogrel, J.W., Chung, J.M., and Yaksh, T.L. (1994). Quantitative assessment of tactile allodynia in the rat paw. J. Neurosci. Methods *53*, 55–63.

Chemin, J., Girard, C., Duprat, F., Lesage, F., Romey, G., and Lazdunski, M. (2003). Mechanisms underlying excitatory effects of group I metabotropic glutamate receptors via inhibition of 2P domain K+ channels. EMBO J. *22*, 5403–5411.

Chen, C., Nenov, A., Norris, C.H., and Bobbin, R.P. (1995). ATP modulation of L-type calcium channel currents in guinea pig outer hair cells. Hear. Res. *86*, 25–33.

Cheng, L.E., Song, W., Looger, L.L., Jan, L.Y., and Jan, Y.N. (2010). The role of the TRP channel NompC in Drosophila larval and adult locomotion. Neuron *67*, 373–380.

Chesler, A.T., Szczot, M., Bharucha-Goebel, D., Čeko, M., Donkervoort, S., Laubacher, C., Hayes, L.H., Alter, K., Zampieri, C., Stanley, C., et al. (2016). The Role of PIEZO2 in Human Mechanosensation. N. Engl. J. Med. *375*, 1355–1364.

Chien, L.-Y., Cheng, J.-K., Chu, D., Cheng, C.-F., and Tsaur, M.-L. (2007). Reduced Expression of A-Type Potassium Channels in Primary Sensory Neurons Induces Mechanical Hypersensitivity. J. Neurosci. *27*, 9855–9865.

Cho, H., Yang, Y.D., Lee, J., Lee, B., Kim, T., Jang, Y., Back, S.K., Na, H.S., Harfe, B.D., Wang, F., et al. (2012). The calcium-activated chloride channel anoctamin 1 acts as a heat sensor in nociceptive neurons. Nat. Neurosci. *15*, 1015–1021.

Chung, M.-K., Lee, H., Mizuno, A., Suzuki, M., and Caterina, M.J. (2004). TRPV3 and TRPV4 Mediate Warmth-evoked Currents in Primary Mouse Keratinocytes. J. Biol. Chem. *279*, 21569–21575.

Cockayne, D.A., Dunn, P.M., Zhong, Y., Rong, W., Hamilton, S.G., Knight, G.E., Ruan, H.-Z., Ma, B., Yip, P., Nunn, P., et al. (2005). P2X2 knockout mice and P2X2/P2X3 double knockout mice reveal a role for the P2X2 receptor subunit in mediating multiple sensory effects of ATP. J. Physiol. *567*, 621–639.

Colbert, H.A., Smith, T.L., and Bargmann, C.I. (1997). OSM-9, A Novel Protein with Structural Similarity to Channels, Is Required for Olfaction, Mechanosensation, and Olfactory Adaptation inCaenorhabditis elegans. J. Neurosci. *17*, 8259–8269.

Colburn, R.W., Lubin, M.L., Stone, D.J., Wang, Y., Lawrence, D., D'Andrea, M.R., Brandt, M.R., Liu, Y., Flores, C.M., and Qin, N. (2007). Attenuated Cold Sensitivity in TRPM8 Null Mice. Neuron *54*, 379–386.

Colloca, L., Ludman, T., Bouhassira, D., Baron, R., Dickenson, A.H., Yarnitsky, D., Freeman, R., Truini, A., Attal, N., Finnerup, N.B., et al. (2017). Neuropathic pain. Nat. Rev. Dis. Primer *3*, 17002.

Coste, B., Crest, M., and Delmas, P. (2007). Pharmacological dissection and distribution of NaN/Nav1.9, T-type Ca2+ currents, and mechanically activated cation currents in different populations of DRG neurons. J. Gen. Physiol. *129*, 57–77.

Coste, B., Mathur, J., Schmidt, M., Earley, T.J., Ranade, S., Petrus, M.J., Dubin, A.E., and Patapoutian, A. (2010). Piezo1 and Piezo2 are essential components of distinct mechanically-activated cation channels. Science *330*, 55–60.

Coste, B., Houge, G., Murray, M.F., Stitziel, N., Bandell, M., Giovanni, M.A., Philippakis, A., Hoischen, A., Riemer, G., Steen, U., et al. (2013). Gain-of-function mutations in the mechanically activated ion channel PIEZO2 cause a subtype of Distal Arthrogryposis. Proc. Natl. Acad. Sci. U. S. A. *110*, 4667–4672.

Cotterill, E., Hall, D., Wallace, K., Mundy, W.R., Eglen, S.J., and Shafer, T.J. (2016). Characterization of Early Cortical Neural Network Development in Multiwell Microelectrode Array Plates. J. Biomol. Screen. *21*, 510–519.

Culy, C.R., Clemett, D., and Wiseman, L.R. (2000). Oxaliplatin. Drugs *60*, 895–924.

Cummins, T.R., Dib-Hajj, S.D., and Waxman, S.G. (2004). Electrophysiological Properties of Mutant Nav1.7 Sodium Channels in a Painful Inherited Neuropathy. J. Neurosci. *24*, 8232–8236.

Cummins, T.R., Dib-Hajj, S.D., Herzog, R.I., and Waxman, S.G. (2005). Nav1.6 channels generate resurgent sodium currents in spinal sensory neurons. FEBS Lett. *579*, 2166–2170.

Cummins, T.R., Sheets, P.L., and Waxman, S.G. (2007). The roles of sodium channels in nociception: implications for mechanisms of pain. Pain *131*, 243–257.

Damann, N., Voets, T., and Nilius, B. (2008). TRPs in Our Senses. Curr. Biol. *18*, R880–R889.

Daniels, R.L., Takashima, Y., and McKemy, D.D. (2009). Activity of the Neuronal Cold Sensor TRPM8 Is Regulated by Phospholipase C via the Phospholipid Phosphoinositol 4,5-Bisphosphate. J. Biol. Chem. *284*, 1570–1582.

Davis, J.B., Gray, J., Gunthorpe, M.J., Hatcher, J.P., Davey, P.T., Overend, P., Harries, M.H., Latcham, J., Clapham, C., Atkinson, K., et al. (2000). Vanilloid receptor-1 is essential for inflammatory thermal hyperalgesia. Nature *405*, 183–187.

Dawes, J.M., and McMahon, S.B. (2013). Chemokines as peripheral pain mediators. Neurosci. Lett. *557*, 1–8.

Dawes, J.M., Weir, G.A., Middleton, S.J., Patel, R., Chisholm, K.I., Pettingill, P., Peck, L.J., Sheridan, J., Shakir, A., Jacobson, L., et al. (2018). Immune or Genetic-Mediated Disruption of CASPR2 Causes Pain Hypersensitivity Due to Enhanced Primary Afferent Excitability. Neuron *97*, 806-822.e10.

Decosterd, I., and Woolf, C.J. (2000). Spared nerve injury: an animal model of persistent peripheral neuropathic pain. Pain *87*, 149–158.

Delfini, M.-C., Mantilleri, A., Gaillard, S., Hao, J., Reynders, A., Malapert, P., Alonso, S., François, A., Barrere, C., Seal, R., et al. (2013). TAFA4, a Chemokine-like Protein, Modulates Injury-Induced Mechanical and Chemical Pain Hypersensitivity in Mice. Cell Rep. *5*, 378–388.

Delmas, P., Hao, J., and Rodat-Despoix, L. (2011). Molecular mechanisms of mechanotransduction in mammalian sensory neurons. Nat. Rev. Neurosci. *12*, 139–153.

Denomme, N., Lukowski, A.L., Hull, J.M., Jameson, M.B., Bouza, A.A., Narayan, A.R.H., and Isom, L.L. (2020). The voltage-gated sodium channel inhibitor, 4,9-anhydrotetrodotoxin, blocks human Nav1.1 in addition to Nav1.6. Neurosci. Lett. *724*, 134853.

Descoeur, J., Pereira, V., Pizzoccaro, A., Francois, A., Ling, B., Maffre, V., Couette, B., Busserolles, J., Courteix, C., Noel, J., et al. (2011). Oxaliplatin-induced cold hypersensitivity is due to remodelling of ion channel expression in nociceptors. EMBO Mol. Med. *3*, 266–278.

Deuis, J.R., Zimmermann, K., Romanovsky, A.A., Possani, L.D., Cabot, P.J., Lewis, R.J., and Vetter, I. (2013). An animal model of oxaliplatin-induced cold allodynia reveals a crucial role for Nav1.6 in peripheral pain pathways. Pain *154*, 1749–1757.

Deuis, J.R., Lim, Y.L., Rodrigues de Sousa, S., Lewis, R.J., Alewood, P.F., Cabot, P.J., and Vetter, I. (2014). Analgesic effects of clinically used compounds in novel mouse models of polyneuropathy induced by oxaliplatin and cisplatin. Neuro-Oncol. *16*, 1324–1332.

Dhaka, A., Murray, A.N., Mathur, J., Earley, T.J., Petrus, M.J., and Patapoutian, A. (2007). TRPM8 Is Required for Cold Sensation in Mice. Neuron *54*, 371–378.

Dhaka, A., Earley, T.J., Watson, J., and Patapoutian, A. (2008). Visualizing Cold Spots: TRPM8-Expressing Sensory Neurons and Their Projections. J. Neurosci. *28*, 566–575.

Di Cesare Mannelli, L., Zanardelli, M., Failli, P., and Ghelardini, C. (2012). Oxaliplatin-Induced Neuropathy: Oxidative Stress as Pathological Mechanism. Protective Effect of Silibinin. J. Pain *13*, 276–284.

Di Francia, R., Siesto, R.S., Valente, D., Del Buono, A., Pugliese, S., Cecere, S., Cavaliere, C., Nasti, G., Facchini, G., and Berretta, M. (2013). Current strategies to minimize toxicity of oxaliplatin: selection of pharmacogenomic panel tests. Anticancer. Drugs *24*, 1069–1078.

Dib-Hajj, S.D., Rush, A.M., Cummins, T.R., Hisama, F.M., Novella, S., Tyrrell, L., Marshall, L., and Waxman, S.G. (2005). Gain-of-function mutation in Nav1.7 in familial erythromelalgia induces bursting of sensory neurons. Brain *128*, 1847–1854.

Dib-Hajj, S.D., Cummins, T.R., Black, J.A., and Waxman, S.G. (2007). From genes to pain: Nav1.7 and human pain disorders. Trends Neurosci. *30*, 555–563.

Dorn, G., Patel, S., Wotherspoon, G., Hemmings-Mieszczak, M., Barclay, J., Natt, F.J.C., Martin, P., Bevan, S., Fox, A., Ganju, P., et al. (2004). siRNA relieves chronic neuropathic pain. Nucleic Acids Res. *32*, e49.

Dost, R., Rostock, A., and Rundfeldt, C. (2004). The anti-hyperalgesic activity of retigabine is mediated by KCNQ potassium channel activation. Naunyn. Schmiedebergs Arch. Pharmacol. *369*, 382–390.

Douglas, W.W., and Malcolm, J.L. (1955). The effect of localized cooling on conduction in cat nerves. J. Physiol. *130*, 53–71.

Drew, L.J., Rohrer, D.K., Price, M.P., Blaver, K.E., Cockayne, D.A., Cesare, P., and Wood, J.N. (2004). Acid-sensing ion channels ASIC2 and ASIC3 do not contribute to mechanically activated currents in mammalian sensory neurones. J. Physiol. *556*, 691–710.

Du, X., and Gamper, N. (2013). Potassium Channels in Peripheral Pain Pathways: Expression, Function and Therapeutic Potential. Curr. Neuropharmacol. *11*, 621–640.

Du, J., Haak, L.L., Phillips-Tansey, E., Russell, J.T., and McBain, C.J. (2000). Frequency-dependent regulation of rat hippocampal somato-dendritic excitability by the K+ channel subunit Kv2.1. J. Physiol. *522*, 19–31.

Dubin, A.E., and Patapoutian, A. (2010). Nociceptors: the sensors of the pain pathway. J. Clin. Invest. *120*, 3760–3772.

Duclaux, R., Schafer, K., and Hensel, H. (1980). Response of cold receptors to low skin temperatures in nose of the cat. J. Neurophysiol. *43*, 1571–1577.

Eberhardt, M., Dux, M., Namer, B., Miljkovic, J., Cordasic, N., Will, C., Kichko, T.I., de la Roche, J., Fischer, M., Suárez, S.A., et al. (2014). H 2 S and NO cooperatively regulate vascular tone by activating a neuroendocrine HNO–TRPA1–CGRP signalling pathway. Nat. Commun. *5*, 4381.

Ehrsson, H., Wallin, I., and Yachnin, J. (2002). Pharmacokinetics of oxaliplatin in humans. Med. Oncol. Northwood Lond. Engl. *19*, 261–265.

Emery, E.C., Young, G.T., Berrocoso, E.M., Chen, L., and McNaughton, P.A. (2011). HCN2 Ion Channels Play a Central Role in Inflammatory and Neuropathic Pain. Science *333*, 1462–1466.

Esteban-Fernández, D., Moreno-Gordaliza, E., Cañas, B., Palacios, M.A., and Gómez-Gómez, M.M. (2010). Analytical methodologies for metallomics studies of antitumor Pt-containing drugs. Met. Integr. Biometal Sci. *2*, 19–38.

Everill, B., and Kocsis, J.D. (1999). Reduction in Potassium Currents in Identified Cutaneous Afferent Dorsal Root Ganglion Neurons After Axotomy. J. Neurophysiol. *82*, 700–708.

Faucherre, A., Nargeot, J., Mangoni, M.E., and Jopling, C. (2013). piezo2b Regulates Vertebrate Light Touch Response. J. Neurosci. *33*, 17089–17094.

Forstenpointner, J., Oberlojer, V.C., Naleschinski, D., Höper, J., Helfert, S.M., Binder, A., Gierthmühlen, J., and Baron, R. (2018). A-Fibers Mediate Cold Hyperalgesia in Patients with Oxaliplatin-Induced Neuropathy. Pain Pract. *18*, 758–767.

Foti, R.S., Rock, D.A., Pearson, J.T., Wahlstrom, J.L., and Wienkers, L.C. (2011). Mechanism-Based Inactivation of Cytochrome P450 3A4 by Mibefradil through Heme Destruction. Drug Metab. Dispos. *39*, 1188–1195.

Foulkes, T., and Wood, J. (2007). Mechanisms of Cold Pain. Channels *1*, 154–160.

Gamelin, E., Gamelin, L., Bossi, L., and Quasthoff, S. (2002). Clinical aspects and molecular basis of oxaliplatin neurotoxicity: Current management and development of preventive measures. Semin. Oncol. *29*, 21–33.

Gamelin, L., Boisdron-Celle, M., Delva, R., Guérin-Meyer, V., Ifrah, N., Morel, A., and Gamelin, E. (2004). Prevention of Oxaliplatin-Related Neurotoxicity by Calcium and Magnesium Infusions. Clin. Cancer Res. *10*, 4055–4061.

Gasser, H.S., and Erlanger, J. (1922). A STUDY OF THE ACTION CURRENTS OF NERVE WITH THE CATHODE RAY OSCILLOGRAPH. Am. J. Physiol.-Leg. Content *62*, 496–524.

Gasser, H.S., and Erlanger, J. (1927). THE RÔLE PLAYED BY THE SIZES OF THE CONSTITUENT FIBERS OF A NERVE TRUNK IN DETERMINING THE FORM OF ITS ACTION POTENTIAL WAVE. Am. J. Physiol.-Leg. Content *80*, 522–547.

Gasser, H.S., and Erlanger, J. (1929a). The Action Potential in Fibers of Slow Conduction in Spinal Roots and Somatic Nerves. Proc. Soc. Exp. Biol. Med. *26*, 647–649.

Gasser, H.S., and Erlanger, J. (1929b). THE RÔLE OF FIBER SIZE IN THE ESTABLISHMENT OF A NERVE BLOCK BY PRESSURE OR COCAINE. Am. J. Physiol.-Leg. Content *88*, 581–591.

Gauchan, P., Andoh, T., Kato, A., and Kuraishi, Y. (2009). Involvement of increased expression of transient receptor potential melastatin 8 in oxaliplatin-induced cold allodynia in mice. Neurosci. Lett. *458*, 93–95.

Gentry, C., Stoakley, N., Andersson, D.A., and Bevan, S. (2010). The roles of iPLA2, TRPM8 and TRPA1 in chemically induced cold hypersensitivity. Mol. Pain *6*, 4.

Genzen, J.R., Van Cleve, W., and McGehee, D.S. (2001). Dorsal Root Ganglion Neurons Express Multiple Nicotinic Acetylcholine Receptor Subtypes. J. Neurophysiol. *86*, 1773–1782.

Gold, M.S., and Gebhart, G.F. (2010). Nociceptor sensitization in pain pathogenesis. Nat. Med. *16*, 1248–1257.

Gold, M.S., Shuster, M.J., and Levine, J.D. (1996). Characterization of six voltage-gated K+ currents in adult rat sensory neurons. J. Neurophysiol. *75*, 2629–2646.

González, A., Ugarte, G., Restrepo, C., Herrera, G., Piña, R., Gómez-Sánchez, J.A., Pertusa, M., Orio, P., and Madrid, R. (2017). Role of the Excitability Brake Potassium Current IKD in Cold Allodynia Induced by Chronic Peripheral Nerve Injury. J. Neurosci. *37*, 3109–3126.

Govrin-Lippmann, R., and Devor, M. (1978). Ongoing activity in severed nerves: source and variation with time. Brain Res. *159*, 406–410.

Grolleau, F., Gamelin, L., Boisdron-Celle, M., Lapied, B., Pelhate, M., and Gamelin, E. (2001). A Possible Explanation for a Neurotoxic Effect of the Anticancer Agent Oxaliplatin on Neuronal Voltage-Gated Sodium Channels. J. Neurophysiol. *85*, 2293–2297.

Grothey, A. (2003). Oxaliplatin-safety profile: neurotoxicity. Semin. Oncol. *30*, 5–13.

Grothey, A., Nikcevich, D.A., Sloan, J.A., Kugler, J.W., Silberstein, P.T., Dentchev, T., Wender, D.B., Novotny, P.J., Chitaley, U., Alberts, S.R., et al. (2011). Intravenous Calcium and Magnesium for Oxaliplatin-Induced Sensory Neurotoxicity in Adjuvant Colon Cancer: NCCTG N04C7. J. Clin. Oncol. *29*, 421–427.

Guan, D., Tkatch, T., Surmeier, D.J., Armstrong, W.E., and Foehring, R.C. (2007). Kv2 subunits underlie slowly inactivating potassium current in rat neocortical pyramidal neurons. J. Physiol. *581*, 941–960.

Guan, D., Armstrong, W.E., and Foehring, R.C. (2013). Kv2 channels regulate firing rate in pyramidal neurons from rat sensorimotor cortex. J. Physiol. *591*, 4807–4825.

Güler, A.D., Lee, H., Iida, T., Shimizu, I., Tominaga, M., and Caterina, M. (2002). Heat-Evoked Activation of the Ion Channel, TRPV4. J. Neurosci. *22*, 6408–6414.

Gunthorpe, M.J., Large, C.H., and Sankar, R. (2012). The mechanism of action of retigabine (ezogabine), a first-in-class K+ channel opener for the treatment of epilepsy. Epilepsia *53*, 412–424.

Halata, Z. (1993). Sensory innervation of the hairy skin (light-and electronmicroscopic study). J. Invest. Dermatol. *101*, S75–S81.

Han, C.H., Khwaounjoo, P., Hill, A.G., Miskelly, G.M., and McKeage, M.J. (2017a). Predicting effects on oxaliplatin clearance: in vitro , kinetic and clinical studies of calcium- and magnesium-mediated oxaliplatin degradation. Sci. Rep. *7*, 4073.

Han, C.H., Khwaounjoo, P., Hill, A.G., Miskelly, G.M., and McKeage, M.J. (2017b). Predicting effects on oxaliplatin clearance: in vitro , kinetic and clinical studies of calcium- and magnesium-mediated oxaliplatin degradation. Sci. Rep. *7*, 4073.

Hatem, S., Attal, N., Willer, J.-C., and Bouhassira, D. (2006). Psychophysical study of the effects of topical application of menthol in healthy volunteers: Pain *122*, 190–196.

Hensel, H., and Boman, K.K.A. (1960). AFFERENT IMPULSES IN CUTANEOUS SENSORY NERVES IN HUMAN SUBJECTS. J. Neurophysiol. *23*, 564–578.

Hensel, H., and Schäfer, K. (1982). Static and dynamic activity of cold receptors in cats after long-term exposure to various temperatures. Pflüg. Arch. *392*, 291–294.

Hensel, H., and Schafer, K. (1984). Thermoreception and Temperature Regulation in Man. In Recent Advances in Medical Thermology, E.F.J. Ring, and B. Phillips, eds. (Boston, MA: Springer New York), pp. 51–64.

Hensel, H., Iggo, A., and Witt, I. (1960). A quantitative study of sensitive cutaneous thermoreceptors with C afferent fibres. J. Physiol. *153*, 113–126.

Herrington, J. (2007). Gating modifier peptides as probes of pancreatic β-cell physiology. Toxicon *49*, 231–238.

Heurteaux, C., Mazella, J., and Borsotto, M. (2011). Spadin, a Sortilin-derived peptide: a new concept in the antidepressant drug design. Ol. Corps Gras Lipides *18*, 202–207.

Hille, B., Armstrong, C.M., and MacKinnon, R. (1999). Ion channels: From idea to reality. Nat. Med. *5*, 1105–1109.

Hjerling-Leffler, J., AlQatari, M., Ernfors, P., and Koltzenburg, M. (2007). Emergence of Functional Sensory Subtypes as Defined by Transient Receptor Potential Channel Expression. J. Neurosci. *27*, 2435–2443.

Ho Kim, S., and Mo Chung, J. (1992). An experimental model for peripheral neuropathy produced by segmental spinal nerve ligation in the rat. PAIN *50*, 355–363.

Holzer, P. (1998). Neurogenic vasodilatation and plasma leakage in the skin. Gen. Pharmacol. Vasc. Syst. *30*, 5–11.

Huang, J., Estacion, M., Zhao, P., Dib-Hajj, F.B., Schulman, B., Abicht, A., Kurth, I., Brockmann, K., Waxman, S.G., and Dib-Hajj, S.D. (2019). A Novel Gain-of-Function Nav1.9 Mutation in a Child With Episodic Pain. Front. Neurosci. *13*.

Huang, S.M., Li, X., Yu, Y., Wang, J., and Caterina, M.J. (2011). TRPV3 and TRPV4 ion channels are not major contributors to mouse heat sensation. Mol. Pain *7*, 37.

Iggo, A. (1960). Cutaneous mechanoreceptors with afferent C fibres. J. Physiol. *152*, 337–353.

Iggo, A. (1969). Cutaneous thermoreceptors in primates and sub-primates. J. Physiol. *200*, 403–430.

Iggo, A. (1984). Cutaneous Thermoreceptors. In Somatosensory Mechanisms: Proceedings of an International Symposium Held at The Wenner-Gren Center, Stockholm, June 8–10, 1983, C. von Euler, O. Franzén, U. Lindblom, and D. Ottoson, eds. (London: Palgrave Macmillan UK), pp. 261–272.

Iggo, A., and Muir, A.R. (1969). The structure and function of a slowly adapting touch corpuscle in hairy skin. J. Physiol. *200*, 763-796.4.

Ikeda, R., Cha, M., Ling, J., Jia, Z., Coyle, D., and Gu, J.G. (2014). Merkel cells transduce and encode tactile stimuli to drive Aβ-afferent impulses. Cell *157*, 664–675.

Jankowski, M.P., Rau, K.K., and Koerber, H.R. (2017). Cutaneous TRPM8-expressing sensory afferents are a small population of neurons with unique firing properties. Physiol. Rep. *5*.

Jeffry, J.A., Yu, S.-Q., Sikand, P., Parihar, A., Evans, M.S., and Premkumar, L.S. (2009). Selective Targeting of TRPV1 Expressing Sensory Nerve Terminals in the Spinal Cord for Long Lasting Analgesia. PLoS ONE *4*.

Jentsch, T.J. (2000). Neuronal KCNQ potassium channels:physislogy and role in disease. Nat. Rev. Neurosci. *1*, 21–30.

Jerremalm, E., Wallin, I., and Ehrsson, H. (2009). New insights into the biotransformation and pharmacokinetics of oxaliplatin. J. Pharm. Sci. *98*, 3879–3885.

Ji, R.-R., Xu, Z.-Z., and Gao, Y.-J. (2014). Emerging targets in neuroinflammation-driven chronic pain. Nat. Rev. Drug Discov. *13*, 533–548.

Johansson, R.S., and Vallbo, A.B. (1979). Detection of tactile stimuli. Thresholds of afferent units related to psychophysical thresholds in the human hand. J. Physiol. *297*, 405–422.

Johnson, K.O. (2001). The roles and functions of cutaneous mechanoreceptors. Curr. Opin. Neurobiol. *11*, 455–461.

Johnston, I.N., Tan, M., Cao, J., Matsos, A., Forrest, D.R.L., Si, E., Fardell, J.E., and Hutchinson, M.R. (2017). Ibudilast reduces oxaliplatin-induced tactile allodynia and cognitive impairments in rats. Behav. Brain Res. *334*, 109–118.

Jordt, S.-E., Bautista, D.M., Chuang, H., McKemy, D.D., Zygmunt, P.M., Högestätt, E.D., Meng, I.D., and Julius, D. (2004). Mustard oils and cannabinoids excite sensory nerve fibres through the TRP channel ANKTM1. Nature *427*, 260–265.

Joseph, E.K., Chen, X., Bogen, O., and Levine, J.D. (2008). Oxaliplatin Acts on IB4-Positive Nociceptors to Induce an Oxidative Stress-Dependent Acute Painful Peripheral Neuropathy. J. Pain *9*, 463–472.

Julius, D., and Basbaum, A.I. (2001). Molecular mechanisms of nociception. Nature *413*, 203–210.

Juster-Switlyk, K., and Smith, A.G. (2016). Updates in diabetic peripheral neuropathy. F1000Research *5*.

Kagiava, A., Tsingotjidou, A., Emmanouilides, C., and Theophilidis, G. (2008). The effects of oxaliplatin, an anticancer drug, on potassium channels of the peripheral myelinated nerve fibres of the adult rat. Neurotoxicology *29*, 1100–1106.

Kajander, K.C., Wakisaka, S., and Bennett, G.J. (1992). Spontaneous discharge originates in the dorsal root ganglion at the onset of a painful peripheral neuropathy in the rat. Neurosci. Lett. *138*, 225–228.

Kang, L., Tian, Y., Xu, S., and Chen, H. (2020). Oxaliplatin-induced peripheral neuropathy: clinical features, mechanisms, prevention and treatment. J. Neurol.

Karashima, Y., Talavera, K., Everaerts, W., Janssens, A., Kwan, K.Y., Vennekens, R., Nilius, B., and Voets, T. (2009). TRPA1 acts as a cold sensor in vitro and in vivo. Proc. Natl. Acad. Sci. U. S. A. *106*, 1273–1278.

Kase, D., and Imoto, K. (2012). The Role of HCN Channels on Membrane Excitability in the Nervous System (Hindawi).

Kasteel, E.E.J., and Westerink, R.H.S. (2017). Comparison of the acute inhibitory effects of Tetrodotoxin (TTX) in rat and human neuronal networks for risk assessment purposes. Toxicol. Lett. *270*, 12–16.

Kato, R., Sato, T., Iwamoto, A., Yamazaki, T., Nakashiro, S., Yoshikai, S., Fujimoto, A., Imano, H., Ijiri, Y., Mino, Y., et al. (2019). Interaction of platinum agents, cisplatin, carboplatin and oxaliplatin against albumin in vivo rats and in vitro study using inductively coupled plasma-mass spectrometory. Biopharm. Drug Dispos. *40*, 242–249.

Kawashiri, T., Egashiral, N., Watanabe, H., Ikegami, Y., Hirakawa, S., Mihara, Y., Yano, T., Ikesue, H., and Oishi, R. (2011). Prevention of oxaliplatin-induced mechanical allodynia and neurodegeneration by neurotropin in the rat model. Eur. J. Pain *15*, 344–350.

Kawashiri, T., Egashira, N., Kurobe, K., Tsutsumi, K., Yamashita, Y., Ushio, S., Yano, T., and Oishi, R. (2012). L type Ca2+ channel blockers prevent oxaliplatin-induced cold hyperalgesia and TRPM8 overexpression in rats. Mol. Pain *8*, 7.

Kirschstein, T., Büsselberg, D., and Treede, R.-D. (1997). Coexpression of heat-evoked and capsaicin-evoked inward currents in acutely dissociated rat dorsal root ganglion neurons. Neurosci. Lett. *231*, 33–36.

Klement, W., and Arndt, J.O. (1991). Pain but no temperature sensations are evoked by thermal stimulation of cutaneous veins in man. Neurosci. Lett. *123*, 119–122.

Klement, W., and Arndt, J.O. (1992). The role of nociceptors of cutaneous veins in the mediation of cold pain in man. J. Physiol. *449*, 73.

Klumpp, D., and Zimmermann, M. (1980). Irreverisble differential block of A- and C-fibres following local nerve heating in the cat. J. Physiol. *298*, 471–482.

Knowlton, W.M., Fisher, A., Bautista, D.M., and McKemy, D.D. (2010). TRPM8, but not TRPA1, is required for neural and behavioral responses to acute noxious cold temperatures and cold-mimetics in vivo. Pain *150*, 340–350.

Koivisto, A., Jalava, N., Bratty, R., and Pertovaara, A. (2018). TRPA1 Antagonists for Pain Relief. Pharmaceuticals *11*.

Koltzenburg, M., Stucky, C.L., and Lewin, G.R. (1997). Receptive Properties of Mouse Sensory Neurons Innervating Hairy Skin. J. Neurophysiol. *78*, 1841–1850.

Kono, T., Satomi, M., Suno, M., Kimura, N., Yamazaki, H., Furukawa, H., and Matsubara, K. (2012). Oxaliplatin-induced neurotoxicity involves TRPM8 in the mechanism of acute hypersensitivity to cold sensation. Brain Behav. *2*, 68–73.

Krøigård, T., Schrøder, H.D., Qvortrup, C., Eckhoff, L., Pfeiffer, P., Gaist, D., and Sindrup, S.H. (2014). Characterization and diagnostic evaluation of chronic polyneuropathies induced by oxaliplatin and docetaxel comparing skin biopsy to quantitative sensory testing and nerve conduction studies. Eur. J. Neurol. *21*, 623–629.

Krøigård, T., Svendsen, T.K., Wirenfeldt, M., Schrøder, H.D., Qvortrup, C., Pfeiffer, P., Gaist, D., and Sindrup, S.H. (2020). Early changes in tests of peripheral nerve function during oxaliplatin treatment and their correlation with chemotherapy-induced polyneuropathy symptoms and signs. Eur. J. Neurol. *27*, 68–76.

Kruger, L., Perl, E.R., and Sedivec, M.J. (1981). Fine structure of myelinated mechanical nociceptor endings in cat hairy skin. J. Comp. Neurol. *198*, 137–154.

Kwan, K.Y., Allchorne, A.J., Vollrath, M.A., Christensen, A.P., Zhang, D.-S., Woolf, C.J., and Corey, D.P. (2006). TRPA1 Contributes to Cold, Mechanical, and Chemical Nociception but Is Not Essential for Hair-Cell Transduction. Neuron *50*, 277–289.

Lamas, J.A., Rueda-Ruzafa, L., and Herrera-Pérez, S. (2019). Ion Channels and Thermosensitivity: TRP, TREK, or Both? Int. J. Mol. Sci. *20*.

Larsen, F.G., Larsen, C.G., Jakobsen, P., and Brodersen, R. (1985). Interaction of warfarin with human serum albumin. A stoichiometric description. Mol. Pharmacol. *27*, 263–270.

Lauria, G., Ziegler, D., Malik, R., Merkies, I.S.J., Waxman, S.G., Faber, C.G., and On behalf of the PROPANE Study group (2014). The Role of Sodium Channels in Painful Diabetic and Idiopathic Neuropathy. Curr. Diab. Rep. *14*, 538.

Lechner, S.G., and Lewin, G.R. (2013). Hairy Sensation. Physiology *28*, 142–150.

Lehky, T. j., Leonard, G. d., Wilson, R. h., Grem, J. l., and Floeter, M. k. (2004). Oxaliplatin-induced neurotoxicity: Acute hyperexcitability and chronic neuropathy. Muscle Nerve *29*, 387–392.

Lennertz, R.C., Medler, K.A., Bain, J.L., Wright, D.E., and Stucky, C.L. (2011). Impaired sensory nerve function and axon morphology in mice with diabetic neuropathy. J. Neurophysiol. *106*, 905–914.

Levinson, S.R., Luo, S., and Henry, M.A. (2012). THE ROLE OF SODIUM CHANNELS IN CHRONIC PAIN. Muscle Nerve *46*, 155–165.

Li, L., Rutlin, M., Abraira, V.E., Cassidy, C., Kus, L., Gong, S., Jankowski, M.P., Luo, W., Heintz, N., Koerber, H.R., et al. (2011). The functional organization of cutaneous low-threshold mechanosensory neurons. Cell *147*, 1615–1627.

Li, L., Shao, J., Wang, J., Liu, Y., Zhang, Y., Zhang, M., Zhang, J., Ren, X., Su, S., Li, Y., et al. (2019). MiR-30b-5p attenuates oxaliplatin-induced peripheral neuropathic pain through the voltage-gated sodium channel Nav1.6 in rats. Neuropharmacology *153*, 111–120.

Liang, Z., Hore, Z., Harley, P., Stanley, F.U., Michrowska, A., Dahiya, M., LaRussa, F., Jager, S.E., Villa, S., and Denk, F. (2019). A transcriptional toolbox for exploring peripheral neuro-immune interactions. BioRxiv 813980.

Liedtke, W., and Friedman, J.M. (2003). Abnormal osmotic regulation in trpv4-/- mice. Proc. Natl. Acad. Sci. *100*, 13698–13703.

Liu, M., and Wood, J.N. (2011). The roles of sodium channels in nociception: implications for mechanisms of neuropathic pain. Pain Med. Malden Mass *12 Suppl 3*, S93-99.

Liu, P.W., and Bean, B.P. (2014). Kv2 Channel Regulation of Action Potential Repolarization and Firing Patterns in Superior Cervical Ganglion Neurons and Hippocampal CA1 Pyramidal Neurons. J. Neurosci. *34*, 4991–5002.

Liu, M.-G., Chen, X.-F., He, T., Li, Z., and Chen, J. (2012). Use of multi-electrode array recordings in studies of network synaptic plasticity in both time and space. Neurosci. Bull. *28*, 409–422.

Lolignier, S., Bonnet, C., Gaudioso, C., Noël, J., Ruel, J., Amsalem, M., Ferrier, J., Rodat-Despoix, L., Bouvier, V., Aissouni, Y., et al. (2015). The Nav1.9 Channel Is a Key Determinant of Cold Pain Sensation and Cold Allodynia. Cell Rep. *11*, 1067–1078.

Lolignier, S., Gkika, D., Andersson, D., Leipold, E., Vetter, I., Viana, F., Noël, J., and Busserolles, J. (2016). New Insight in Cold Pain: Role of Ion Channels, Modulation, and Clinical Perspectives. J. Neurosci. *36*, 11435–11439.

Lopes, D.M., Denk, F., and McMahon, S.B. (2017). The Molecular Fingerprint of Dorsal Root and Trigeminal Ganglion Neurons. Front. Mol. Neurosci. *10*.

Luiz, A.P., MacDonald, D.I., Santana-Varela, S., Millet, Q., Sikandar, S., Wood, J.N., and Emery, E.C. (2019). Cold sensing by NaV1.8-positive and NaV1.8-negative sensory neurons. Proc. Natl. Acad. Sci. *116*, 3811–3816.

Lumpkin, E.A., Marshall, K.L., and Nelson, A.M. (2010). The cell biology of touch. J. Cell Biol. *191*, 237–248.

Lynn, B. (1971). The form and distribution of the receptive fields of Pacinian corpuscles found in and around the cat's large foot pad. J. Physiol. *217*, 755–771.

MacDonald, D.I., Luiz, A.P., Millet, Q., Emery, E.C., and Wood, J.N. (2020a). Silent cold-sensing neurons drive cold allodynia in neuropathic pain states (Neuroscience).

MacDonald, D.I., Wood, J.N., and Emery, E.C. (2020b). Molecular mechanisms of cold pain. Neurobiol. Pain *7*, 100044.

MacDonald, D.I., Luiz, A.P., Iseppon, F., Millet, Q., Emery, E.C., and Wood, J.N. (2021). Silent cold-sensing neurons contribute to cold allodynia in neuropathic pain. Brain J. Neurol.

Madrid, R., de la Peña, E., Donovan-Rodriguez, T., Belmonte, C., and Viana, F. (2009). Variable Threshold of Trigeminal Cold-Thermosensitive Neurons Is Determined by a Balance between TRPM8 and Kv1 Potassium Channels. J. Neurosci. *29*, 3120–3131.

Maeda, T., Ochi, K., Nakakura-Ohshima, K., Youn, S.H., and Wakisaka, S. (1999). The Ruffini Ending as the Primary Mechanoreceptor in the Periodontal Ligament: Its Morphology, Cytochemical Features, Regeneration, and Development. Crit. Rev. Oral Biol. Med. *10*, 307–327.

Maksimovic, S., Nakatani, M., Baba, Y., Nelson, A.M., Marshall, K.L., Wellnitz, S.A., Firozi, P., Woo, S.-H., Ranade, S., Patapoutian, A., et al. (2014). Epidermal Merkel cells are mechanosensory cells that tune mammalian touch receptors. Nature *509*, 617–621.

Malin, S.A., and Nerbonne, J.M. (2002). Delayed Rectifier K+ Currents,IK, Are Encoded by Kv2 α-Subunits and Regulate Tonic Firing in Mammalian Sympathetic Neurons. J. Neurosci. *22*, 10094–10105.

Marmiroli, P., Riva, B., Pozzi, E., Ballarini, E., Lim, D., Chiorazzi, A., Meregalli, C., Distasi, C., Renn, C.L., Semperboni, S., et al. (2017). Susceptibility of different mouse strains to oxaliplatin peripheral neurotoxicity: Phenotypic and genotypic insights. PLoS ONE *12*.

Massaad, C.A., Safieh-Garabedian, B., Poole, S., Atweh, S.F., Jabbur, S.J., and Saadé, N.E. (2004). Involvement of substance P, CGRP and histamine in the hyperalgesia and cytokine upregulation induced by intraplantar injection of capsaicin in rats. J. Neuroimmunol. *153*, 171–182.

Massobrio, P., Tessadori, J., Chiappalone, M., and Ghirardi, M. (2015). In Vitro Studies of Neuronal Networks and Synaptic Plasticity in Invertebrates and in Mammals Using Multielectrode Arrays. Neural Plast. *2015*.

McCrossan, Z.A., Roepke, T.K., Lewis, A., Panaghie, G., and Abbott, G.W. (2009). Regulation of the Kv2.1 potassium channel by MinK and MiRP1. J. Membr. Biol. *228*, 1–14.

McGlone, F., and Reilly, D. (2010). The cutaneous sensory system. Neurosci. Biobehav. Rev. *34*, 148–159.

McKemy, D.D. (2007). TRPM8: The Cold and Menthol Receptor. In TRP Ion Channel Function in Sensory Transduction and Cellular Signaling Cascades, W.B. Liedtke, and S. Heller, eds. (Boca Raton (FL): CRC Press/Taylor & Francis), p.

McKemy, D.D. (2013). The Molecular and Cellular Basis of Cold Sensation. ACS Chem. Neurosci. *4*, 238–247.

McKemy, D.D., Neuhausser, W.M., and Julius, D. (2002). Identification of a cold receptor reveals a general role for TRP channels in thermosensation. Nature *416*, 52–58.

McNamara, F.N., Randall, A., and Gunthorpe, M.J. (2005). Effects of piperine, the pungent component of black pepper, at the human vanilloid receptor (TRPV1). Br. J. Pharmacol. *144*, 781–790.

McWhinney, S.R., Goldberg, R.M., and McLeod, H.L. (2009). Platinum neurotoxicity pharmacogenetics. Mol. Cancer Ther. *8*, 10–16.

Mishra, S., Bhatnagar, S., Goyal, G.N., Rana, S.P.S., and Upadhya, S.P. (2012). A Comparative Efficacy of Amitriptyline, Gabapentin, and Pregabalin in Neuropathic Cancer Pain: A Prospective Randomized Double-Blind Placebo-Controlled Study. Am. J. Hosp. Palliat. Med. *29*, 177–182.

Misonou, H., Mohapatra, D.P., and Trimmer, J.S. (2005). Kv2.1: A Voltage-Gated K+ Channel Critical to Dynamic Control of Neuronal Excitability. NeuroToxicology *26*, 743–752.

Miyake, T., Nakamura, S., Zhao, M., So, K., Inoue, K., Numata, T., Takahashi, N., Shirakawa, H., Mori, Y., Nakagawa, T., et al. (2016). Cold sensitivity of TRPA1 is unveiled by the prolyl hydroxylation blockade-induced sensitization to ROS. Nat. Commun. *7*, ncomms12840.

Mizuno, K., Kono, T., Suzuki, Y., Miyagi, C., Omiya, Y., Miyano, K., Kase, Y., and Uezono, Y. (2014). Goshajinkigan, a traditional Japanese medicine, prevents oxaliplatin-induced acute peripheral neuropathy by suppressing functional alteration of TRP channels in rat. J. Pharmacol. Sci. *125*, 91–98.

Mohapatra, D.P., Siino, D.F., and Trimmer, J.S. (2008). Interdomain Cytoplasmic Interactions Govern the Intracellular Trafficking, Gating, and Modulation of the Kv2.1 Channel. J. Neurosci. *28*, 4982–4994.

Momin, A., Cadiou, H., Mason, A., and McNaughton, P.A. (2008). Role of the hyperpolarization-activated current Ih in somatosensory neurons. J. Physiol. *586*, 5911–5929.

Montalbetti, N., Rooney, J.G., Rued, A.C., and Carattino, M.D. (2019). Molecular determinants of afferent sensitization in a rat model of cystitis with urothelial barrier dysfunction. J. Neurophysiol. *122*, 1136–1146.

Moqrich, A., Hwang, S.W., Earley, T.J., Petrus, M.J., Murray, A.N., Spencer, K.S.R., Andahazy, M., Story, G.M., and Patapoutian, A. (2005). Impaired Thermosensation in Mice Lacking TRPV3, a Heat and Camphor Sensor in the Skin. Science *307*, 1468–1472.

Morenilla-Palao, C., Luis, E., Fernández-Peña, C., Quintero, E., Weaver, J.L., Bayliss, D.A., and Viana, F. (2014). Ion channel profile of TRPM8 cold receptors reveals a novel role of TASK-3 potassium channels in thermosensation. Cell Rep. *8*, 1571–1582.

Munns, C., AlQatari, M., and Koltzenburg, M. (2007). Many cold sensitive peripheral neurons of the mouse do not express TRPM8 or TRPA1. Cell Calcium *41*, 331–342.

Nagasaka, K., Yamanaka, K., Ogawa, S., Takamatsu, H., and Higo, N. (2017). Brain activity changes in a macaque model of oxaliplatin-induced neuropathic cold hypersensitivity. Sci. Rep. *7*, 4305.

Nakatani, M., Maksimovic, S., Baba, Y., and Lumpkin, E.A. (2015). Mechanotransduction in epidermal Merkel cells. Pflugers Arch. *467*, 101–108.

Namer, B., Kleggetveit, I.P., Handwerker, H., Schmelz, M., and Jorum, E. (2008). Role of TRPM8 and TRPA1 for cold allodynia in patients with cold injury: Pain *139*, 63–72.

Nandigama, R., Bonitz, M., Papadakis, T., Schwantes, U., Bschleipfer, T., and Kummer, W. (2010). Muscarinic acetylcholine receptor subtypes expressed by mouse bladder afferent neurons. Neuroscience *168*, 842–850.

Nassini, R., Gees, M., Harrison, S., De Siena, G., Materazzi, S., Moretto, N., Failli, P., Preti, D., Marchetti, N., Cavazzini, A., et al. (2011). Oxaliplatin elicits mechanical and cold allodynia in rodents via TRPA1 receptor stimulation. PAIN® *152*, 1621–1631.

Nathan, P.W., and Sears, T.A. (1963). The susceptibility of nerve fibres to analgesics. Anaesthesia *18*, 467–476.

Neeper, M.P., Liu, Y., Hutchinson, T.L., Wang, Y., Flores, C.M., and Qin, N. (2007). Activation Properties of Heterologously Expressed Mammalian TRPV2: EVIDENCE FOR SPECIES DEPENDENCE *. J. Biol. Chem. *282*, 15894–15902.

Noël, J., Zimmermann, K., Busserolles, J., Deval, E., Alloui, A., Diochot, S., Guy, N., Borsotto, M., Reeh, P., Eschalier, A., et al. (2009a). The mechano-activated K+ channels TRAAK and TREK-1 control both warm and cold perception. EMBO J. *28*, 1308–1318.

Noël, J., Zimmermann, K., Busserolles, J., Deval, E., Alloui, A., Diochot, S., Guy, N., Borsotto, M., Reeh, P., Eschalier, A., et al. (2009b). The mechano-activated K+ channels TRAAK and TREK-1 control both warm and cold perception. EMBO J. *28*, 1308–1318.

Norrsell, U., Finger, S., and Lajonchere, C. (1999). Cutaneous sensory spots and the “law of specific nerve energies”: history and development of ideas. Brain Res. Bull. *48*, 457–465.

Nygaard, O., Kloster, R., and Mellgren, S. (1998). Recovery of sensory nerve fibres after surgical decompression in lumbar radiculopathy: use of quantitative sensory testing in the exploration of different populations of nerve fibres. J. Neurol. Neurosurg. Psychiatry *64*, 120–123.

Oakes, S.G., Martin, W.J., Lisek, C.A., and Powis, G. (1988). Incomplete hydrolysis of the calcium indicator precursor fura-2 pentaacetoxymethyl ester (fura-2 AM) by cells. Anal. Biochem. *169*, 159–166.

Ogawa, H. (1996). The merkel cell as a possible mechanoreceptor cell. Prog. Neurobiol. *49*, 317–334.

Olausson, H., Wessberg, J., Morrison, I., McGlone, F., and Vallbo, Å. (2010). The neurophysiology of unmyelinated tactile afferents. Neurosci. Biobehav. Rev. *34*, 185–191.

Owens, D.M., and Lumpkin, E.A. (2014). Diversification and Specialization of Touch Receptors in Skin. Cold Spring Harb. Perspect. Med. *4*.

Pachman, D.R., Qin, R., Seisler, D.K., Smith, E.M.L., Beutler, A.S., Ta, L.E., Lafky, J.M., Wagner-Johnston, N.D., Ruddy, K.J., Dakhil, S., et al. (2015). Clinical Course of Oxaliplatin-Induced Neuropathy: Results From the Randomized Phase III Trial N08CB (Alliance). J. Clin. Oncol. *33*, 3416–3422.

Page, A.J., Brierley, S.M., Martin, C.M., Martinez-Salgado, C., Wemmie, J.A., Brennan, T.J., Symonds, E., Omari, T., Lewin, G.R., Welsh, M.J., et al. (2004). The ion channel ASIC1 contributes to visceral but not cutaneous mechanoreceptor function. Gastroenterology *127*, 1739–1747.

Page, A.J., Brierley, S.M., Martin, C.M., Price, M.P., Symonds, E., Butler, R., Wemmie, J.A., and Blackshaw, L.A. (2005). Different contributions of ASIC channels 1a, 2, and 3 in gastrointestinal mechanosensory function. Gut *54*, 1408–1415.

Parisien, M., Khoury, S., Chabot-Doré, A.-J., Sotocinal, S.G., Slade, G.D., Smith, S.B., Fillingim, R.B., Ohrbach, R., Greenspan, J.D., Maixner, W., et al. (2017). Effect of Human Genetic Variability on Gene Expression in Dorsal Root Ganglia and Association with Pain Phenotypes. Cell Rep. *19*, 1940–1952.

Park, J.-H., Chae, J., Roh, K., Kil, E.-J., Lee, M., Auh, C.-K., Lee, M.-A., Yeom, C.-H., and Lee, S. (2015). Oxaliplatin-Induced Peripheral Neuropathy via TRPA1 Stimulation in Mice Dorsal Root Ganglion Is Correlated with Aluminum Accumulation. PloS One *10*, e0124875.

Park, S.B., Goldstein, D., Lin, C.S.-Y., Krishnan, A.V., Friedlander, M.L., and Kiernan, M.C. (2009). Acute Abnormalities of Sensory Nerve Function Associated With Oxaliplatin-Induced Neurotoxicity. J. Clin. Oncol. *27*, 1243–1249.

Park, S.B., Davare, M., Falla, M., Kennedy, W.R., Selim, M.M., Wendelschafer-Crabb, G., and Koltzenburg, M. (2016). Fast-adapting mechanoreceptors are important for force control in precision grip but not for sensorimotor memory. J. Neurophysiol. *115*, 3156–3161.

Park, U., Vastani, N., Guan, Y., Raja, S.N., Koltzenburg, M., and Caterina, M.J. (2011). TRP Vanilloid 2 Knock-Out Mice Are Susceptible to Perinatal Lethality But Display Normal Thermal and Mechanical Nociception. J. Neurosci. *31*, 11425–11436.

Parra, A., Madrid, R., Echevarria, D., del Olmo, S., Morenilla-Palao, C., Acosta, M.C., Gallar, J., Dhaka, A., Viana, F., and Belmonte, C. (2010). Ocular surface wetness is regulated by TRPM8-dependent cold thermoreceptors of the cornea. Nat. Med. *16*, 1396–1399.

Passmore, G.M., Selyanko, A.A., Mistry, M., Al-Qatari, M., Marsh, S.J., Matthews, E.A., Dickenson, A.H., Brown, T.A., Burbidge, S.A., Main, M., et al. (2003). KCNQ/M Currents in Sensory Neurons: Significance for Pain Therapy. J. Neurosci. *23*, 7227–7236.

Peier, A.M., Reeve, A.J., Andersson, D.A., Moqrich, A., Earley, T.J., Hergarden, A.C., Story, G.M., Colley, S., Hogenesch, J.B., McIntyre, P., et al. (2002a). A Heat-Sensitive TRP Channel Expressed in Keratinocytes. Science *296*, 2046–2049.

Peier, A.M., Moqrich, A., Hergarden, A.C., Reeve, A.J., Andersson, D.A., Story, G.M., Earley, T.J., Dragoni, I., McIntyre, P., Bevan, S., et al. (2002b). A TRP channel that senses cold stimuli and menthol. Cell *108*, 705–715.

Pereira, V., Busserolles, J., Christin, M., Devilliers, M., Poupon, L., Legha, W., Alloui, A., Aissouni, Y., Bourinet, E., Lesage, F., et al. (2014). Role of the TREK2 potassium channel in cold and warm thermosensation and in pain perception. Pain *155*, 2534–2544.

Perl, E.R. (1968). Myelinated afferent fibres innervating the primate skin and their response to noxious stimuli. J. Physiol. *197*, 593–615.

Pierau, F.-K., Torrey, P., and Carpenter, D.O. (1974). Mammalian cold receptor afferents: role of an electrogenic sodium pump in sensory transduction. Brain Res. *73*, 156–160.

Poole, L.B. (2015). The Basics of Thiols and Cysteines in Redox Biology and Chemistry. Free Radic. Biol. Med. *0*, 148–157.

Poole, K., Herget, R., Lapatsina, L., Ngo, H.-D., and Lewin, G.R. (2014). Tuning Piezo ion channels to detect molecular-scale movements relevant for fine touch. Nat. Commun. *5*, 3520.

Poupon, L., Lamoine, S., Pereira, V., Barriere, D.A., Lolignier, S., Giraudet, F., Aissouni, Y., Meleine, M., Prival, L., Richard, D., et al. (2018). Targeting the TREK-1 potassium channel via riluzole to eliminate the neuropathic and depressive-like effects of oxaliplatin. Neuropharmacology *140*, 43–61.

Premkumar, L.S., and Sikand, P. (2008). TRPV1: A Target for Next Generation Analgesics. Curr. Neuropharmacol. *6*, 151–163.

Price, M.P., McIlwrath, S.L., Xie, J., Cheng, C., Qiao, J., Tarr, D.E., Sluka, K.A., Brennan, T.J., Lewin, G.R., and Welsh, M.J. (2001). The DRASIC Cation Channel Contributes to the Detection of Cutaneous Touch and Acid Stimuli in Mice. Neuron *32*, 1071–1083.

Proudfoot, C.J., Garry, E.M., Cottrell, D.F., Rosie, R., Anderson, H., Robertson, D.C., Fleetwood-Walker, S.M., and Mitchell, R. (2006). Analgesia Mediated by the TRPM8 Cold Receptor in Chronic Neuropathic Pain. Curr. Biol. *16*, 1591–1605.

Punke, M.A., and Friederich, P. (2007). Amitriptyline is a potent blocker of human Kv1.1 and Kv7.2/7.3 channels. Anesth. Analg. *104*, 1256–1264, tables of contents.

Purves, D., Augustine, G.J., Fitzpatrick, D., Katz, L.C., LaMantia, A.-S., McNamara, J.O., and Williams, S.M. (2001). Nociceptors. Neurosci. 2nd Ed.

Quallo, T., Vastani, N., Horridge, E., Gentry, C., Parra, A., Moss, S., Viana, F., Belmonte, C., Andersson, D.A., and Bevan, S. (2015). TRPM8 is a neuronal osmosensor that regulates eye blinking in mice. Nat. Commun. *6*, 7150.

Quasthoff, S., and Hartung, H.P. (2002). Chemotherapy-induced peripheral neuropathy. J. Neurol. *249*, 9–17.

Ramirez, G.A., Coletto, L.A., Sciorati, C., Bozzolo, E.P., Manunta, P., Rovere-Querini, P., and Manfredi, A.A. (2018). Ion Channels and Transporters in Inflammation: Special Focus on TRP Channels and TRPC6. Cells *7*.

Randall, L.O., and Selitto, J.J. (1957). A method for measurement of analgesic activity on inflamed tissue. Arch. Int. Pharmacodyn. Ther. *111*, 409–419.

Rasband, M.N., Park, E.W., Vanderah, T.W., Lai, J., Porreca, F., and Trimmer, J.S. (2001). Distinct potassium channels on pain-sensing neurons. Proc. Natl. Acad. Sci. U. S. A. *98*, 13373–13378.

Reeh, P.W. (1986). Sensory receptors in mammalian skin in an in vitro preparation. Neurosci. Lett. *66*, 141–146.

Reeh, P.W. (1994). Chemical Excitation and Sensitization of Nociceptors. In Cellular Mechanisms of Sensory Processing, L. Urban, ed. (Berlin, Heidelberg: Springer), pp. 119–131.

Reichling, D.B., and Levine, J.D. (1997). Heat transduction in rat sensory neurons by calcium-dependent activation of a cation channel. Proc. Natl. Acad. Sci. *94*, 7006–7011.

Reid, G., and Flonta, M.-L. (2001). Cold transduction by inhibition of a background potassium conductance in rat primary sensory neurones. Neurosci. Lett. *297*, 171–174.

Resta, F., Micheli, L., Laurino, A., Spinelli, V., Mello, T., Sartiani, L., Di Cesare Mannelli, L., Cerbai, E., Ghelardini, C., Romanelli, M.N., et al. (2018). Selective HCN1 block as a strategy to control oxaliplatin-induced neuropathy. Neuropharmacology *131*, 403–413.

Reynders, A., Mantilleri, A., Malapert, P., Rialle, S., Nidelet, S., Laffray, S., Beurrier, C., Bourinet, E., and Moqrich, A. (2015). Transcriptional Profiling of Cutaneous MRGPRD Free Nerve Endings and C-LTMRs. Cell Rep. *10*, 1007–1019.

Ringkamp, M., Peng, Y.B., Wu, G., Hartke, T.V., Campbell, J.N., and Meyer, R.A. (2001). Capsaicin Responses in Heat-Sensitive and Heat-Insensitive A-Fiber Nociceptors. J. Neurosci. *21*, 4460–4468.

Robertson, B., and Bevan, S. (1991). Properties of 5-hydroxytryptamine3 receptor-gated currents in adult rat dorsal root ganglion neurones. Br. J. Pharmacol. *102*, 272–276.

Rolke, R., Baron, R., Maier, C., Tölle, T.R., Treede, R.-D., Beyer, A., Binder, A., Birbaumer, N., Birklein, F., Bötefür, I.C., et al. (2006). Quantitative sensory testing in the German Research Network on Neuropathic Pain (DFNS): standardized protocol and reference values. Pain *123*, 231–243.

Romer, S.H., Deardorff, A.S., and Fyffe, R.E.W. (2019). A molecular rheostat: Kv2.1 currents maintain or suppress repetitive firing in motoneurons. J. Physiol. *597*, 3769–3786.

Rosker, C., Lohberger, B., Hofer, D., Steinecker, B., Quasthoff, S., and Schreibmayer, W. (2007). The TTX metabolite 4,9-anhydro-TTX is a highly specific blocker of the Nav1.6 voltage-dependent sodium channel. Am. J. Physiol.-Cell Physiol. *293*, C783–C789.

Roth, R.B., Hevezi, P., Lee, J., Willhite, D., Lechner, S.M., Foster, A.C., and Zlotnik, A. (2006). Gene expression analyses reveal molecular relationships among 20 regions of the human CNS. Neurogenetics *7*, 67–80.

Roza, C., Puel, J.-L., Kress, M., Baron, A., Diochot, S., Lazdunski, M., and Waldmann, R. (2004). Knockout of the ASIC2 channel in mice does not impair cutaneous mechanosensation, visceral mechanonociception and hearing. J. Physiol. *558*, 659–669.

Rutlin, M., Ho, C.-Y., Abraira, V.E., Cassidy, C., Woodbury, C.J., and Ginty, D.D. (2014). The Cellular and Molecular Basis of Direction Selectivity of Aδ-LTMRs. Cell *159*, 1640–1651.

Sahoo, N., Hoshi, T., and Heinemann, S.H. (2014). Oxidative Modulation of Voltage-Gated Potassium Channels. Antioxid. Redox Signal. *21*, 933–952.

Saif, M.W., and Reardon, J. (2005). Management of oxaliplatin-induced peripheral neuropathy. Ther. Clin. Risk Manag. *1*, 249–258.

Sakurai, M., Egashira, N., Kawashiri, T., Yano, T., Ikesue, H., and Oishi, R. (2009). Oxaliplatin-induced neuropathy in the rat: involvement of oxalate in cold hyperalgesia but not mechanical allodynia. Pain *147*, 165–174.

Sato, K., Kiyama, H., Park, H.T., and Tohyama, M. (1993). AMPA, KA and NMDA receptors are expressed in the rat DRG neurones. Neuroreport *4*, 1263–1265.

Schlake, T. (2007). Determination of hair structure and shape. Semin. Cell Dev. Biol. *18*, 267–273.

Schulze, C., McGowan, M., Jordt, S.-E., and Ehrlich, B.E. (2011). Prolonged oxaliplatin exposure alters intracellular calcium signaling: a new mechanism to explain oxaliplatin-associated peripheral neuropathy. Clin. Colorectal Cancer *10*, 126–133.

Schütze, S., Orozco, I.J., and Jentsch, T.J. (2016). KCNQ Potassium Channels Modulate Sensitivity of Skin Down-hair (D-hair) Mechanoreceptors. J. Biol. Chem. *291*, 5566–5575.

Screnci, D., McKeage, M., Galettis, P., Hambley, T., Palmer, B., and Baguley, B. (2000). Relationships between hydrophobicity, reactivity, accumulation and peripheral nerve toxicity of a series of platinum drugs. Br. J. Cancer 7.

Seal, R.P., Wang, X., Guan, Y., Raja, S.N., Woodbury, C.J., Basbaum, A.I., and Edwards, R.H. (2009). Unmyelinated Low Threshold Mechanoreceptors are Required for Injury-induced Mechanical Hypersensitivity. Nature *462*, 651–655.

Seltzer, Z., Dubner, R., and Shir, Y. (1990). A novel behavioral model of neuropathic pain disorders produced in rats by partial sciatic nerve injury. Pain *43*, 205–218.

Serra, J., Campero, M., Ochoa, J., and Bostock, H. (1999). Activity-dependent slowing of conduction differentiates functional subtypes of C fibres innervating human skin. J. Physiol. *515*, 799–811.

Sesti, F. (2016). Oxidation of K+ Channels in Aging and Neurodegeneration. Aging Dis. *7*, 130–135.

Sexton, J.E., Vernon, J., and Wood, J.N. (2014). TRPs and Pain. In Mammalian Transient Receptor Potential (TRP) Cation Channels: Volume II, B. Nilius, and V. Flockerzi, eds. (Cham: Springer International Publishing), pp. 873–897.

Shir, Y., and Seltzer, Z. (1990). A-fibers mediate mechanical hyperesthesia and allodynia and C-fibers mediate thermal hyperalgesia in a new model of causalgiform pain disorders in rats. Neurosci. Lett. *115*, 62–67.

Sittl, R., Carr, R.W., Fleckenstein, J., and Grafe, P. (2010). Enhancement of axonal potassium conductance reduces nerve hyperexcitability in an in vitro model of oxaliplatin-induced acute neuropathy. Neurotoxicology *31*, 694–700.

Sittl, R., Lampert, A., Huth, T., Schuy, E.T., Link, A.S., Fleckenstein, J., Alzheimer, C., Grafe, P., and Carr, R.W. (2012). Anticancer drug oxaliplatin induces acute cooling-aggravated neuropathy via sodium channel subtype Na(V)1.6-resurgent and persistent current. Proc. Natl. Acad. Sci. U. S. A. *109*, 6704–6709.

Smith, E.St.J., and Lewin, G.R. (2009). Nociceptors: a phylogenetic view. J. Comp. Physiol. A Neuroethol. Sens. Neural. Behav. Physiol. *195*, 1089–1106.

Smith, A.K., O'Hara, C.L., and Stucky, C.L. (2013). Mechanical sensitization of cutaneous sensory fibers in the spared nerve injury mouse model. Mol. Pain *9*, 61.

Smith, G.D., Gunthorpe, M.J., Kelsell, R.E., Hayes, P.D., Reilly, P., Facer, P., Wright, J.E., Jerman, J.C., Walhin, J.-P., Ooi, L., et al. (2002). TRPV3 is a temperature-sensitive vanilloid receptor-like protein. Nature *418*, 186–190.

Speca, D.J., Ogata, G., Mandikian, D., Bishop, H.I., Wiler, S.W., Eum, K., Wenzel, H.J., Doisy, E.T., Matt, L., Campi, K.L., et al. (2014). Deletion of the Kv2.1 delayed rectifier potassium channel leads to neuronal and behavioral hyperexcitability. Genes Brain Behav. *13*, 394–408.

Sprowl, J.A., Ciarimboli, G., Lancaster, C.S., Giovinazzo, H., Gibson, A.A., Du, G., Janke, L.J., Cavaletti, G., Shields, A.F., and Sparreboom, A. (2013). Oxaliplatin-induced neurotoxicity is dependent on the organic cation transporter OCT2. Proc. Natl. Acad. Sci. U. S. A. *110*, 11199–11204.

Stadler, T., O'Reilly, A.O., and Lampert, A. (2015). Erythromelalgia Mutation Q875E Stabilizes the Activated State of Sodium Channel Nav1.7. J. Biol. Chem. *290*, 6316–6325.

Starobova, H., and Vetter, I. (2017). Pathophysiology of Chemotherapy-Induced Peripheral Neuropathy. Front. Mol. Neurosci. *10*.

Stephens, G.J., Garratt, J.C., Robertson, B., and Owen, D.G. (1994). On the mechanism of 4-aminopyridine action on the cloned mouse brain potassium channel mKv1.1. J. Physiol. *477*, 187–196.

Story, G.M., Peier, A.M., Reeve, A.J., Eid, S.R., Mosbacher, J., Hricik, T.R., Earley, T.J., Hergarden, A.C., Andersson, D.A., Hwang, S.W., et al. (2003). ANKTM1, a TRP-like channel expressed in nociceptive neurons, is activated by cold temperatures. Cell *112*, 819–829.

Streng, T., Axelsson, H.E., Hedlund, P., Andersson, D.A., Jordt, S.-E., Bevan, S., Andersson, K.-E., Högestätt, E.D., and Zygmunt, P.M. (2008). Distribution and Function of the Hydrogen Sulfide–Sensitive TRPA1 Ion Channel in Rat Urinary Bladder. Eur. Urol. *53*, 391–400.

Stucky, C.L., Koltzenburg, M., Schneider, M., Engle, M.G., Albers, K.M., and Davis, B.M. (1999). Overexpression of Nerve Growth Factor in Skin Selectively Affects the Survival and Functional Properties of Nociceptors. J. Neurosci. *19*, 8509–8516.

Szolcsányi, J. (1977). A pharmacological approach to elucidation of the role of different nerve fibres and receptor endings in mediation of pain. J. Physiol. (Paris) *73*, 251–259.

Ta, L.E., Bieber, A.J., Carlton, S.M., Loprinzi, C.L., Low, P.A., and Windebank, A.J. (2010). Transient Receptor Potential Vanilloid 1 is essential for cisplatin-induced heat hyperalgesia in mice. Mol. Pain *6*, 15.

Tajino, K., Hosokawa, H., Maegawa, S., Matsumura, K., Dhaka, A., and Kobayashi, S. (2011). Cooling-Sensitive TRPM8 Is Thermostat of Skin Temperature against Cooling. PLoS ONE *6*.

Tan, C.-H., and McNaughton, P.A. (2016). The TRPM2 ion channel is required for sensitivity to warmth. Nature *536*, 460–463.

Tatulian, L., Delmas, P., Abogadie, F.C., and Brown, D.A. (2001). Activation of Expressed KCNQ Potassium Currents and Native Neuronal M-Type Potassium Currents by the Anti-Convulsant Drug Retigabine. J. Neurosci. *21*, 5535–5545.

Themistocleous, A.C., Ramirez, J.D., Shillo, P.R., Lees, J.G., Selvarajah, D., Orengo, C., Tesfaye, S., Rice, A.S.C., and Bennett, D.L.H. (2016). The Pain in Neuropathy Study (PiNS): a cross-sectional observational study determining the somatosensory phenotype of painful and painless diabetic neuropathy. Pain *157*, 1132–1145.

Tofthagen, C., Gonzalez, L., Visovsky, C., and Akers, A. (2013a). Self-Management of Oxaliplatin-Related Peripheral Neuropathy in Colorectal Cancer Survivors (Hindawi).

Tofthagen, C., Donovan, K.A., Morgan, M.A., and Shibata, D. (2013b). Oxaliplatin-Induced Peripheral Neuropathy's Effects on Health-Related Quality of Life of Colorectal Cancer Survivors. Support. Care Cancer Off. J. Multinatl. Assoc. Support. Care Cancer *21*, 3307–3313.

Togashi, K., Hara, Y., Tominaga, T., Higashi, T., Konishi, Y., Mori, Y., and Tominaga, M. (2006). TRPM2 activation by cyclic ADP-ribose at body temperature is involved in insulin secretion. EMBO J. *25*, 1804–1815.

Togashi, K., Inada, H., and Tominaga, M. (2008). Inhibition of the transient receptor potential cation channel TRPM2 by 2-aminoethoxydiphenyl borate (2-APB). Br. J. Pharmacol. *153*, 1324–1330.

Tominaga, M. (2007). Nociception and TRP Channels. In Transient Receptor Potential (TRP) Channels, V. Flockerzi, and B. Nilius, eds. (Berlin, Heidelberg: Springer), pp. 489–505.

Torebjörk, E., and Schmelz, M. (2005). Chapter 38 - Single-Unit Recordings of Afferent Human Peripheral Nerves by Microneurography. In Peripheral Neuropathy (Fourth Edition), P.J. Dyck, and P.K. Thomas, eds. (Philadelphia: W.B. Saunders), pp. 1003–1014.

Torebjörk, H.E., and Ochoa, J.L. (1980). Specific sensations evoked by activity in single identified sensory units in man. Acta Physiol. Scand. *110*, 445–447.

Torebjörk, H.E., Vallbo, A.B., and Ochoa, J.L. (1987). Intraneural microstimulation in man. Its relation to specificity of tactile sensations. Brain J. Neurol. *110 (Pt 6)*, 1509–1529.

Tsai, Y.-J., Lin, J.-K., Chen, W.-S., Jiang, J.-K., Teng, H.-W., Yen, C.-C., Lin, T., and Yang, S.-H. (2016). Adjuvant FOLFOX treatment for stage III colon cancer: how many cycles are enough? SpringerPlus *5*.

Tsantoulas, C., and McMahon, S.B. (2014). Opening paths to novel analgesics: the role of potassium channels in chronic pain. Trends Neurosci. *37*, 146–158.

Tsantoulas, C., Zhu, L., Shaifta, Y., Grist, J., Ward, J.P.T., Raouf, R., Michael, G.J., and McMahon, S.B. (2012). Sensory Neuron Downregulation of the Kv9.1 Potassium Channel Subunit Mediates Neuropathic Pain following Nerve Injury. J. Neurosci. *32*, 17502–17513.

Tsantoulas, C., Zhu, L., Yip, P., Grist, J., Michael, G.J., and McMahon, S.B. (2014). Kv2 dysfunction after peripheral axotomy enhances sensory neuron responsiveness to sustained input. Exp. Neurol. *251*, 115–126.

Usoskin, D., Furlan, A., Islam, S., Abdo, H., Lönnerberg, P., Lou, D., Hjerling-Leffler, J., Haeggström, J., Kharchenko, O., Kharchenko, P.V., et al. (2015). Unbiased classification of sensory neuron types by large-scale single-cell RNA sequencing. Nat. Neurosci. *18*, 145–153.

Vallbo, A., Olausson, H., Wessberg, J., and Norrsell, U. (1993). A system of unmyelinated afferents for innocuous mechanoreception in the human skin. Brain Res. *628*, 301–304.

Vallbo, Å.B., Olausson, H., and Wessberg, J. (1999). Unmyelinated Afferents Constitute a Second System Coding Tactile Stimuli of the Human Hairy Skin. J. Neurophysiol. *81*, 2753–2763.

Vastani, N., Guenther, F., Gentry, C., Austin, A.L., King, A.J., Bevan, S., and Andersson, D.A. (2018). Impaired Nociception in the Diabetic Ins2+/Akita Mouse. Diabetes *67*, 1650–1662.

Vetter, I., Hein, A., Sattler, S., Hessler, S., Touska, F., Bressan, E., Parra, A., Hager, U., Leffler, A., Boukalova, S., et al. (2013). Amplified Cold Transduction in Native Nociceptors by M-Channel Inhibition. J. Neurosci. *33*, 16627–16641.

Viana, F., and Voets, T. (2020). Heat Pain and Cold Pain.

Viana, F., de la Peña, E., and Belmonte, C. (2002a). Specificity of cold thermotransduction is determined by differential ionic channel expression. Nat. Neurosci. *5*, 254–260.

Viana, F., de la Peña, E., and Belmonte, C. (2002b). Specificity of cold thermotransduction is determined by differential ionic channel expression. Nat. Neurosci. *5*, 254–260.

Vinik, A.I., Nevoret, M.-L., Casellini, C., and Parson, H. (2013). Diabetic neuropathy. Endocrinol. Metab. Clin. North Am. *42*, 747–787.

Volkers, L., Mechioukhi, Y., and Coste, B. (2015). Piezo channels: from structure to function. Pflüg. Arch. - Eur. J. Physiol. *467*, 95–99.

Vriens, J., Owsianik, G., Hofmann, T., Philipp, S.E., Stab, J., Chen, X., Benoit, M., Xue, F., Janssens, A., Kerselaers, S., et al. (2011). TRPM3 Is a Nociceptor Channel Involved in the Detection of Noxious Heat. Neuron *70*, 482–494.

Wagner, T.F.J., Loch, S., Lambert, S., Straub, I., Mannebach, S., Mathar, I., Düfer, M., Lis, A., Flockerzi, V., Philipp, S.E., et al. (2008). Transient receptor potential M3 channels are ionotropic steroid receptors in pancreatic β cells. Nat. Cell Biol. *10*, 1421–1430.

Walker, R.G., Willingham, A.T., and Zuker, C.S. (2000). A Drosophila Mechanosensory Transduction Channel. Science *287*, 2229–2234.

Wasner, G., Schattschneider, J., Binder, A., and Baron, R. (2004). Topical menthol—a human model for cold pain by activation and sensitization of C nociceptors. Brain *127*, 1159–1171.

Watanabe, H., Vriens, J., Suh, S.H., Benham, C.D., Droogmans, G., and Nilius, B. (2002). Heat-evoked Activation of TRPV4 Channels in a HEK293 Cell Expression System and in Native Mouse Aorta Endothelial Cells. J. Biol. Chem. *277*, 47044–47051.

Waxman, S.G., and Zamponi, G.W. (2014). Regulating excitability of peripheral afferents: emerging ion channel targets. Nat. Neurosci. *17*, 153–163.

Waxman, S.G., Dib-Hajj, S., Cummins, T.R., and Black, J.A. (1999). Sodium channels and pain. Proc. Natl. Acad. Sci. *96*, 7635–7639.

Webster, R.G., Brain, K.L., Wilson, R.H., Grem, J.L., and Vincent, A. (2005). Oxaliplatin induces hyperexcitability at motor and autonomic neuromuscular junctions through effects on voltage-gated sodium channels. Br. J. Pharmacol. *146*, 1027–1039.

Wei, E.T. (2018). United States Patent: 9895382 - Di-isopropyl-phosphinoyl-alkanes as topical agents for the treatment of sensory discomfort.

Wellnitz, S.A., Lesniak, D.R., Gerling, G.J., and Lumpkin, E.A. (2010). The Regularity of Sustained Firing Reveals Two Populations of Slowly Adapting Touch Receptors in Mouse Hairy Skin. J. Neurophysiol. *103*, 3378–3388.

Willcockson, H., and Valtschanoff, J. (2008). AMPA and NMDA glutamate receptors are found in both peptidergic and non-peptidergic primary afferent neurons in the rat. Cell Tissue Res. *334*, 17–23.

Williams, S.R., and Stuart, G.J. (1999). Mechanisms and consequences of action potential burst firing in rat neocortical pyramidal neurons. J. Physiol. *521*, 467–482.

Wilson, R.H., Lehky, T., Thomas, R.R., Quinn, M.G., Floeter, M.K., and Grem, J.L. (2002). Acute Oxaliplatin-Induced Peripheral Nerve Hyperexcitability. J. Clin. Oncol. *20*, 1767–1774.

Winchester, W.J., Gore, K., Glatt, S., Petit, W., Gardiner, J.C., Conlon, K., Postlethwaite, M., Saintot, P.-P., Roberts, S., Gosset, J.R., et al. (2014). Inhibition of TRPM8 Channels Reduces Pain in the Cold Pressor Test in Humans. J. Pharmacol. Exp. Ther. *351*, 259–269.

Winter, Z., Gruschwitz, P., Eger, S., Touska, F., and Zimmermann, K. (2017). Cold Temperature Encoding by Cutaneous TRPA1 and TRPM8-Carrying Fibers in the Mouse. Front. Mol. Neurosci. *10*.

Wladyka, C.L., and Kunze, D.L. (2006). KCNQ/M-currents contribute to the resting membrane potential in rat visceral sensory neurons. J. Physiol. *575*, 175–189.

Woo, S.-H., Ranade, S., Weyer, A.D., Dubin, A.E., Baba, Y., Qiu, Z., Petrus, M., Miyamoto, T., Reddy, K., Lumpkin, E.A., et al. (2014). Piezo2 is required for Merkel-cell mechanotransduction. Nature *509*, 622–626.

Wood, J.N., and Docherty, R. (1997). Chemical Activators of Sensory Neurons. Annu. Rev. Physiol. *59*, 457–482.

Wood, J., Winter, J., James, I., Rang, H., Yeats, J., and Bevan, S. (1988a). Capsaicin-induced ion fluxes in dorsal root ganglion cells in culture. J. Neurosci. *8*, 3208–3220.

Wood, J.N., Winter, J., James, I.F., Rang, H.P., Yeats, J., and Bevan, S. (1988b). Capsaicin-induced ion fluxes in dorsal root ganglion cells in culture. J. Neurosci. *8*, 3208–3220.

Wood, J.N., Boorman, J.P., Okuse, K., and Baker, M.D. (2004). Voltage-gated sodium channels and pain pathways. J. Neurobiol. *61*, 55–71.

Woodbury, C.J., and Koerber, H.R. (2007). Central and peripheral anatomy of slowly adapting type I low-threshold mechanoreceptors innervating trunk skin of neonatal mice. J. Comp. Neurol. *505*, 547–561.

Woodworth, R.S., and Sherrington, C.S. (1904). A pseudaffective reflex and its spinal path. J. Physiol. *31*, 234–243.

Woolf, C.J., and Ma, Q. (2007). Nociceptors—Noxious Stimulus Detectors. Neuron *55*, 353–364.

Wooten, M., Weng, H.-J., Hartke, T.V., Borzan, J., Klein, A.H., Turnquist, B., Dong, X., Meyer, R.A., and Ringkamp, M. (2014). Three functionally distinct classes of C-fibre nociceptors in primates. Nat. Commun. *5*, 4122.

Xu, H., Ramsey, I.S., Kotecha, S.A., Moran, M.M., Chong, J.A., Lawson, D., Ge, P., Lilly, J., Silos-Santiago, I., Xie, Y., et al. (2002). TRPV3 is a calcium-permeable temperature-sensitive cation channel. Nature *418*, 181–186.

Yam, M.F., Loh, Y.C., Tan, C.S., Khadijah Adam, S., Abdul Manan, N., and Basir, R. (2018). General Pathways of Pain Sensation and the Major Neurotransmitters Involved in Pain Regulation. Int. J. Mol. Sci. *19*.

Yamamoto, S., Egashira, N., Tsuda, M., and Masuda, S. (2018). Riluzole prevents oxaliplatin-induced cold allodynia via inhibition of overexpression of transient receptor potential melastatin 8 in rats. J. Pharmacol. Sci. *138*, 214–217.

Yang, J.M., Wei, E.T., Kim, S.J., and Yoon, K.C. (2018). TRPM8 Channels and Dry Eye. Pharmaceuticals *11*.

Young, G.T., Emery, E.C., Mooney, E.R., Tsantoulas, C., and McNaughton, P.A. (2014). Inflammatory and neuropathic pain are rapidly suppressed by peripheral block of hyperpolarisation-activated cyclic nucleotide-gated ion channels. PAIN® *155*, 1708–1719.

Zakrzewska, J.M., Palmer, J., Morisset, V., Giblin, G.M., Obermann, M., Ettlin, D.A., Cruccu, G., Bendtsen, L., Estacion, M., Derjean, D., et al. (2017). Safety and efficacy of a Nav1.7 selective sodium channel blocker in patients with trigeminal neuralgia: a double-blind, placebo-controlled, randomised withdrawal phase 2a trial. Lancet Neurol. *16*, 291–300.

Zeisel, A., Hochgerner, H., Lönnerberg, P., Johnsson, A., Memic, F., van der Zwan, J., Häring, M., Braun, E., Borm, L.E., La Manno, G., et al. (2018). Molecular Architecture of the Mouse Nervous System. Cell *174*, 999-1014.e22.

Zhang, Q., Martin-Caraballo, M., and Hsia, S.V. (2020). Pathophysiological roles and therapeutic potential of voltage-gated ion channels (VGICs) in pain associated with herpesvirus infection. Cell Biosci. *10*, 70.

Zhao, M., Isami, K., Nakamura, S., Shirakawa, H., Nakagawa, T., and Kaneko, S. (2012). Acute cold hypersensitivity characteristically induced by oxaliplatin is caused by the enhanced responsiveness of TRPA1 in mice. Mol. Pain *8*, 55.

Zimmerman, A., Bai, L., and Ginty, D.D. (2014). The gentle touch receptors of mammalian skin. Science *346*, 950–954.

Zimmermann, K., Leffler, A., Babes, A., Cendan, C.M., Carr, R.W., Kobayashi, J., Nau, C., Wood, J.N., and Reeh, P.W. (2007). Sensory neuron sodium channel Na v 1.8 is essential for pain at low temperatures. Nature *447*, 856–859.

Zimmermann, K., Hein, A., Hager, U., Kaczmarek, J.S., Turnquist, B.P., Clapham, D.E., and Reeh, P.W. (2009). Phenotyping sensory nerve endings in vitro in the mouse. Nat. Protoc. *4*, 174–196.

Zimmermann, K., Lennerz, J.K., Hein, A., Link, A.S., Kaczmarek, J.S., Delling, M., Uysal, S., Pfeifer, J.D., Riccio, A., and Clapham, D.E. (2011). Transient receptor potential cation channel, subfamily C, member 5 (TRPC5) is a cold-transducer in the peripheral nervous system. Proc. Natl. Acad. Sci. *108*, 18114–18119.

Zotterman, Y. (1939). Touch, pain and tickling: an electro-physiological investigation on cutaneous sensory nerves. J. Physiol. *95*, 1–28.

Zygmunt, P.M., and Högestätt, E.D. (2014). TRPA1. In Mammalian Transient Receptor Potential (TRP) Cation Channels: Volume I, B. Nilius, and V. Flockerzi, eds. (Berlin, Heidelberg: Springer), pp. 583–630.

Zygmunt, P.M., Petersson, J., Andersson, D.A., Chuang, H., Sørgård, M., Di Marzo, V., Julius, D., and Högestätt, E.D. (1999). Vanilloid receptors on sensory nerves mediate the vasodilator action of anandamide. Nature *400*, 452–457.

Zygmunt, P.M., Andersson, D.A., and Högestätt, E.D. (2002). Δ9-Tetrahydrocannabinol and Cannabinol Activate Capsaicin-Sensitive Sensory Nerves via a CB1 and CB2 Cannabinoid Receptor-Independent Mechanism. J. Neurosci. *22*, 4720–4727.

Zygmunt, P.M., Ermund, A., Movahed, P., Andersson, D.A., Simonsen, C., Jönsson, B.A.G., Blomgren, A., Birnir, B., Bevan, S., Eschalier, A., et al. (2013). Monoacylglycerols Activate TRPV1 – A Link between Phospholipase C and TRPV1. PLOS ONE *8*, e81618.

Di-isopropyl-phosphinoyl-alkanes as topical agents for the treatment of sensory discomfort - Patent US-9895382-B2 - PubChem.